EXPERIMENTAL DETERMINATION OF THE STRUCTURE OF SHOCK WAVES IN FLUID FLOW THROUGH COLLAPSIBLE TUBES WITH APPLICATION TO THE DESIGN OF A FLOW REGULATOR

by

IFIYENIA KECECIOGLU

B.S.,University of Arizona, Tucson
(1975)

M.S., University of Michigan, Ann Arbor
(1976)

SUBMITTED IN PARTIAL FULFILLMENT
OF THE REQUIREMENTS FOR THE
DEGREE OF

MECHANICAL ENGINEER

at the

MASSACHUSETTS INSTITUTE OF TECHNOLOGY

January, 1979

Signature redacted

Signature of Author . . . . . .
Department of Mechanical Engineering, January 19, 1979

Signature redacted

Certified by . . . . . .
Thesis Supervisor

Signature redacted

Accepted by . . . . . .
Chairman, Department Committee on Graduate Students

EXPERIMENTAL DETERMINATION OF THE STRUCTURE OF SHOCK WAVES IN FLUID FLOW THROUGH COLLAPSIBLE TUBES WITH APPLICATION TO THE DESIGN OF A FLOW REGULATOR

by

IFIYENIA KECECIOGLU

Submitted to the Department of Mechanical Engineering
on January 19, 1979 in partial fullfilment
of the requirements for the degree of Mechanical Engineer

ABSTRACT

Shock-like transitions in area, similar to gas-dynamic shocks and free-surface hydraulic jumps may be formed during fluid flow within compliant elastic tubes when the mean speed of flow exceeds the speed of propagation of small amplitude area waves. Such transitions are believed to occur in the human body and are of physiological importance.

Area and pressure distributions were measured within standing shock waves and the associated precursor wave train by means of a translatable, catheter-mounted pressure-area probe. An approximate theoretical model was developed to interpret the experimental data. The theoretical predictions are in satisfactory agreement with the experimental results.

A subsequent objective was the application of the flow limitation behavior of compliant tubes to the design of a novel flow regulator employing a collapsible tube as its active element. Criteria for the design of a collapsible tube flow regulator were established and a comparison of cost and performance between such a regulator and a standard diaphragm type flow regulator was made.

Thesis Supervisor: A.H. Shapiro
Title: Institute Professor, M.I.T.

ACKNOWLEDGEMENTS

I would like to express my appreciation for the advice that I have received from Professor A.H. Shapiro throughout the duration of this research. Working under his guidance has been a memorable learning experience.

Dr. L.R. Glicksman's suggestions have helped make this thesis a more complete piece of research and are gratefully acknowledged.

I wish to thank all my friends who have made my studies pleasant and intellectually rewarding. I especially wish to thank my talented colleague and dear friend Ananda M. Wijesinghe for having helped during the many hours of experimentation and for having been a source of inspiration and encouragement.

Financial assistance from the NHLBI under HEW Grant 5-R01-HL17974 and from NSF Grant ENG-7608924 made this research possible and is gratefully acknowledged.

I thank Cindy Polansky and Sandy Williams for having typed this thesis skillfully and enthusiastically.

Finally, I wish to express my deep gratitude to my parents for having helped me obtain a fuller sense of the paradoxes of life and for having instilled in me the appreciation for honesty, kindness, and hard work. Therefore, I dedicate this thesis to my father Chrysostomos Kececioglu and my mother Thalia Kececioglu for having been a source of motivation and moral support.

TABLE OF CONTENTS

LIST OF TABLES

LIST OF FIGURES

NOMENCLATURE

A	Cross-sectional area of the collapsible tube at the area probe location
A_0	Resting area, or initial area, or area of the collapsible tube at zero transmural pressure. Also, area of exit pipe of standard flow regulator
A_1, A_2 or A_1', A_2'	Tube area at inlet and exit to shock (Fig. 14)
A_D	Effective diaphragm area (Standard Flow Regulator)
A_L	Tube cross-sectional area at line contact initiation
A_R	Known cross-sectional area of rigid reference section in the experimental apparatus
A_v	Area at valve throat for standard flow regulator
$\bar{A}$	Throat area when valve fully open for standard flow regulator. Also, area at base point of perturbation analysis
a, b	Major and minor semiaxes of elliptical tube
a, b, r, ε	Definitions given by Eqs. 4.74 in section 4.5
a	Amplitude of precursor wave
C_p	Pressure recovery coefficient; $C_p \equiv \dfrac{p_2' - p_1}{\frac{1}{2}\rho u_1^2}$ (See Fig.5)
C_p'	Pressure recovery coefficient; $C_p' \equiv \dfrac{p_2' - p_1'}{\frac{1}{2}\rho u_1'^2}$ (See Fig.5)
C_{p_c}	Carnot pressure recovery (Eq. 4.41; Fig.14)
C_{p_c}'	Carnot pressure recovery; $C_{p_c}' \equiv 2\dfrac{\alpha_1'}{\alpha_2'}\left(1 - \dfrac{\alpha_1'}{\alpha_2'}\right)$
C_{p_o}	Oates pressure recovery (Eqs. 4.49 and 4.50 ; Fig.14)
C_{p_o}'	Oates pressure recovery with α_1 and α_2 in Eqs. 4.49 and 4.50 replaced by α_1' and α_2' respectively
c	Speed of propagation of small-amplitude inviscid waves

D_0 Diameter corresponding to resting area A_0

D_h Hydraulic diameter for tube ; $D_h \equiv 4A/P$

d Distance travelled by area probe

E Young's Modulus

$\hat{EI}$ Bending stiffness for tube ; $\hat{EI} \equiv \frac{Et^3}{12(1-\nu^2)}$

f Friction factor ($\tau_w \equiv \frac{1}{2}\rho u^2 f$). Also, frequency of A.C. carrier voltage

G Gain of pilot valve in standard flow regulator

h Height of fluid in free-surface open-channel flow

K_E Extensional stiffness of tube wall; $K_E \equiv \frac{E}{2(1+\nu)} \left(\frac{t}{R_0}\right)$

K_B Bending stiffness of tube wall ; $K_B \equiv \frac{E}{12(1-\nu^2)} \left(\frac{t}{R_0}\right)^3$.
Also, equivalent diaphragm stiffness in standard flow regulator; $K_B \equiv k\Delta/A_D$

K_c Contraction loss coefficient

K_e Expansion loss coefficient

K_L Loss coefficient related to K_e by Eq. (7.10)

K_v Loss coefficient due to existence of valve (standard flow regulator)

k Spring constant (standard flow regulator)

L_R Length between two electrodes in reference section of experiment

L_p Length between two electrodes mounted on the pressure-area catheter probe

ℓ Travel of valve (standard flow regulator)

M Bending moment

M^* Normalized bending moment (Eq. 2.13)

N Normal shear

N^* Normalized shear force (Eq. 2.13)

p_e	External pressure
$\hat{p}_e$	Effective external pressure
p	Pressure inside the collapsible tube
p_1, p_2 or p_1, p_2	Upstream and downstream pressures at the two ends of the flexible tube (experiments done on the so called " Starling resistors ")
$p-p_e$	Transmural pressure
p_{atm}	Atmospheric pressure
$(p-p_e)_x$	Effective contribution to $(p-p_e)$ from the wall stresses due to longitudinal deformations of the tube wall
p_i	Inlet pressure to flow regulator
p_o	Outlet pressure to flow regulator
p_c	Pressure at constriction
$(p_o-p_e)^{**}$	Value of outlet transmural pressure at which the tube buckles and the flow starts to oscillate
$(p_o-p_e)^{*}$	Value of the outlet transmural pressure at which the shock is located at the exit to the constriction
p_2-p_r	Orifice pressure differential (standard flow regulator)
$p_2'-p_r'$	Differential pressure delivered by pilot valve
P	Length of wetted perimeter
P_0	Stagnation pressure
P_{0i}	Stagnation pressure at inlet to flow regulator
Q	Flow rate
$\hat{Q}$	Normalized flow rate; $\hat{Q} \equiv \dfrac{Q}{A_0\sqrt{2K_B/\rho}}$
R	Current radius of tube (positive transmural pressure). Also, radius of curvature of tube wall in the longitudinal direction (Fig.9)

R_0	Initial radius of tube (positive transmural pressures). Also, tube circumference divided by 2π for negative and zero transmural pressures
R_c	In-plane radius of curvature of tube wall (i.e., radius of curvature of the wall in the plane of the cross-sectional area)
Re_{D_h}	Reynolds Number based on hydraulic diameter for the tube
r	Specific resistivity of the ionic solution
S	Speed index (Mean flow speed/ speed of propagation of small-amplitude inviscid area waves)
s	Arclength referred to the tube circumference (Figs. 6 and 7). Also, length of wall element in the longitudinal direction (Fig. 9)
s^*	Normalized arclength (Eq. 2.13)
s_1, s_2	Definitions given by Eq.$(4.77)_3$ (perturbation analysis section)
T_θ	Hoop tension per unit length (positive transmural pressure)
T	In-plane tension (Fig. 6)
T^*	Normalized in-plane tension
t	Thickness of collapsible tube. Also, time.
$\tilde{u}$	Fluid flow velocity
u	Mean fluid flow velocity
V_p	Voltage measured across area probe. Also, speed of translation of probe
V_R	Voltage measured across two electrodes in the reference section
V_w	Speed of propagation of finite amplitude waves
x,y	Tube wall coordinates
x	Distance along tube (Fig. 9)
x^*, y^*	Normalized tube wall coordinates (Eq. 2.13)
$\bar{x}$	Location about which the perturbation analysis is performed with $\bar{\alpha}$, $\bar{S}$, $\bar{f}$, $\bar{c}$, $\bar{\tau}_w$, $\bar{T}$ as the base quantities

$(x_1'-x_1)^{**}$ Futhest stable shock position when $(p_o-p_e) = (p_o-p_e)^{**}$

$(\ )'$ Perturbation quantity

Script Symbols

a Area of catheter probe

$\mathcal{P}$ Normalized transmural pressure ($\mathcal{P} \equiv (p-p_e)/K_B$)

$\mathcal{P}_B$ Normalized buckling transmural pressure

$\mathcal{P}_P$ Normalized transmural pressure at point contact initiation

$\mathcal{P}_L$ Normalized transmural pressure at line contact initiation

M Parameter that determines the nonlinear steepening or broadening of the propagating waves of finite amplitude

$$\left(M \equiv 3 + \frac{\alpha \, d^2\mathcal{P}/d\alpha^2}{d\mathcal{P}/d\alpha} \right)$$

Greek Symbols

α Area ratio; $\alpha \equiv A/A_0$

α_B Area ratio at initiation of buckling

α_c Area ratio at constriction

α_P Area ratio at initiation of point contact

α_L Area ratio at initiation of line contact

$\hat{\alpha}$ Mean component of area prturbation quantity

$\tilde{\alpha}$ Oscillatory component of area perturbation quantity

α_1 or α_1 Area ratio at exit to constriction

α_1' or α_1' Minimum area ratio at inlet to shock proper

α_1'' or α_1'' Hypothetical shock inlet area obtained by projecting the mean area curve on the shock proper (See Fig. 16)

α_2' Area ratio at maximum pressure location at exit of shock

α_2 Area ratio far downstream of shock

α_i Area ratio at inlet to flow regulator

α_o Area ratio at outlet to flow regulator

β_1, β_2 Definitions given in section 4.5, Eq.(4.82)

$\overline{\gamma}$ Definition given by $\text{Eq.}(4.67)_2$

Δ Difference symbol. Also, initial compression of spring for standard flow regulator

Δp_f Total stagnation pressure loss due to fluid friction Eq.(4.101). ($\Delta \tilde{p}_f$: Eq.(4.107); $\Delta \hat{p}_f$: Eq.(4.106))

ε_{xx} Longitudinal strain

ζ Nondimensional longitudinal distance ($\zeta \equiv x/D_0$)

η Height of tube wall for idealized cross-sectional shape of Fig. 8 for collapsed tube

θ Angle; see Fig.6 and Fig.7

λ Wavelength of precursor waves

ν Poisson's Ratio

ρ Fluid density

σ Hydraulic conductance of tube ($\sigma \equiv - \dfrac{Q}{dp/dx}$)

σ_L Hydraulic conductance at inception of line contact

τ_w Wall shear stress or fluid friction force per unit wall area (Fig. 9)

CHAPTER I:

INTRODUCTION

1.1 Fluid Flow in Collapsible Tubes

The flow of fluids in thin-walled highly compliant tubes is very strongly coupled to the structural mechanics of the tube, especially when the tube is partially collapsed by reason of an internal pressure less than that acting externally. This strong coupling is the central feature underlying many diverse phenomena observed in flows through collapsible tubes. They include a wide variety of steady and unsteady flows of both incompressible and compressible fluids. They span the whole range from friction-dominated, low Reynolds number flows to inertia-dominated, high Reynolds number flows which may be either stable or unstable.

Collapsible tube flows exhibit many phenomena analogous to those found in gas-dynamics and free-surface gravity flows such as wave propagation, flow limitation, transition from subcritical to supercritical flow, frictional choking, and shock-like transitions. Unlike gas-dynamic and free-surface flows, collapsible tube flows exhibit wall flutter and negative resistance limit cycle oscillations.

Collapsible tube flows are of great importance in physiology, in medical diagnostic practice, and in the design of therapeutic procedures and devices. A wide variety of physiological, diagnostic, and therapeutic applications as examples of flow in collapsible tubes have been

identified and described by Shapiro.[1,2] Physiological applications in the venous, arterial, pulmonary and urinary systems, and the vocal cords are among those cited. The existing physiologic and medical literature on these phenomena is extensive but lacks coherence and often seems to be contradictory. Consequently, there is a need to gain a better fundamental understanding of collapsible tube flow phenomena from a unified point of view supported by well-organized and controlled experiments.

Collapsible tube flow behavior may also be exploited for engineering applications such as fluidic switching, logic operations, amplification,[3,4] and flow regulation. One of the objectives of this thesis is to investigate the flow limitation characteristics of uniform collapsible tubes with a view to designing a relatively uncomplicated and reliable fluid flow regulator.

Thin-walled, highly compliant tubes collapse very easily under small negative transmural pressures (transmural pressure ≡ internal pressure minus external pressure) of the order of a few centimeters of water. The static pressure-area relationship for uniformly deformed tubes is highly nonlinear and for negative transmural pressures, small changes in transmural pressure result in large changes in cross-sectional area (see Fig. 1). Consequently, the speed of propagation of small-amplitude area waves based on the inviscid, one-dimensional fluid flow equations is very small in the collapsed state and rises abruptly to much larger values for positive transmural pressures (Fig. 2). As a result, in many physiological situations and in experiments

on thin-walled latex tubes, the mean speed of fluid flow may reach and even exceed the speed of propagation of small-amplitude area waves.

As in gas-dynamic flows and in free-surface open-channel flows, no disturbances can travel upstream beyond the critical point at which mean flow speed and the wave speed are equal. As a result, conditions downstream of this point can have no influence on the flow rate. Further, the flow rate cannot exceed the maximum flow rate which is equal to the product of the cross-sectional area and the local wave speed at the critical point, and thus flow limitation occurs.

In a steady flow within a collapsible tube, when the mean flow speed is greater than the speed of propagation of area waves, the tubes may suffer a sharp change in cross-sectional area and other flow variables. This sharp change can be explained on the basis of propagation and steepening of area waves. As the area gradients become steeper, wall curvature effects not accounted for in the uniform collapse static tube law, and fluid mechanical effects such as flow separation not accounted for in the one-dimensional inviscid fluid flow equations, come into play. These effects prevent further steepening leading to a stable flow at a different and larger cross-sectional area downstream of the shock. The occurrence of such rapid changes in flow variables over relatively short distances is analogous to the formation of gas-dynamic shocks in supersonic flows when the Mach number is greater than unity, and to the formation of hydraulic jumps in free-surface channel flows when the Froude number is greater than unity. The corresponding dimensionless speed

parameter in collapsible tube flows is the speed index, S ≡ (mean flow speed)/(speed of propagation of small-amplitude area waves). Due to the complex nature of the coupling between the mechanics of the flow and the mechanics of the tube wall, the problem of shock-like transitions in collapsible tubes can, in principle, exhibit a "wider" range of phenomena.

1.2 Previous Work on Fluid Flow Through Collapsible Tubes

In this section a brief survey of the literature on fluid flow through collapsible tubes is presented. The first part deals primarily with fluid mechanical studies of collapsible tube flow phenomena. The second and third parts deal with physiological phenomena and therapeutic applications of collapsible tube flows.

A. Fluid Mechanical Studies

The earliest investigations of flow in compliant tubes were the experiments performed by Knowlton and Starling[5] for the purpose of simulating the resistance of the vascular system. Since then, many physiological phenomena, such as the occurrence of Korotkoff sounds, have been studied on similar experimental configurations. Experiments on these so-called "Starling resistors" have subsequently been performed by Holt,[6,7,8] Brecher,[18] Rodbard and Saiki,[9] Rodbard,[10,11,12] Rodbard and Takacs,[13] and Bradley.[14] In these experiments, a segment of flexible tube is supported between two lengths of rigid tube and is mounted within a chamber as shown in Fig. 3 . The chamber pressure p_e

can be varied independently of the upstream and downstream pressures p_1 and p_2 at the two ends of the flexible tube. Typical experimental curves of p_1, p_2, $(p_1 - p_2)$ vs. the flow rate Q that are obtained from such an experiment are given in Fig. 4 and they exhibit the following salient features.

(a) When $(p_1 - p_e)$ is maintained constant and $(p_2 - p_e)$ is progressively reduced, the flow rate Q increases with increasing $(p_1 - p_2)$ as long as $(p_2 - p_e)$ is positive and the tube is distended at the exit. However, if $(p_2 - p_e)$ becomes negative and the tube collapses at the exit end, the flow rate Q becomes virtually independent of the driving pressure difference $(p_1 - p_2)$.[17] The reason for this behavior is the fact that for negative $(p_2 - p_e)$, progressive decrease of $(p_2 - p_e)$ results in reduced cross-sectional area at the exit and higher frictional resistance to flow. This in turn affects any increase in flow due to the increased driving pressure difference $(p_1 - p_2)$. This "flow limitation" phenomenon has been proposed as the mechanism of flow regulation in many physiological situations.

(b) In a certain range of negative values of $(p_2 - p_e)$, with the tube at the exit partially collapsed, the $(p_1 - p_2)$ vs. Q curve has a negative slope. This negative resistance promotes the growth of flow disturbances, leading to limit cycle relaxation oscillations at a characteristic frequency.[15,34] Such oscillations of the arterial wall have been accepted in the recent years as the source of Korotkoff sounds, which are detected during the measurement of blood pressure using a

pressurizing cuff.

Although the Starling resistor concept has been extensively studied, the failure to consider its essential features from a fluid mechanical point of view has made the interpretation of its behavior difficult and unnecessarily confusing. Brower and Noordergraaf[16] were the first to realize that although three distinct pressures were present, only the pressure differences $(p_1 - p_2)$ and $(p_2 - p_e)$ controlled the tube-flow behavior. Further, the inclusion of the resistances due to the flow control valves at the inlet and the exit in the models, and the failure to perceive the dominance of end effects at large negative pressures $(p_2 - p_e)$, has hindered interpretation. More recently, Wild, Pedley, and Riley[19] have considered viscous dominated flows in collapsible tubes. In such flows, due to the absence of inertia, no self-excited oscillations can develop.

Many theoretical and experimental studies of a fundamental nature have been undertaken in the past on the propagation of small and finite amplitude waves in compliant tubes under positive transmural pressures, especially with regard to arterial hemodynamics (Olsen and Shapiro;[20] Lambert;[21] Streeter, Keitzer, and Bohr;[22] Anliker, Rockwell, and Ogden;[23] Maxwell and Anliker;[24] Rudinger;[25] Kivity and Collins;[26,27] King;[28] and Beam[29]). However, for partially collapsed, compliant tubes under negative transmural pressures, very few fundamental studies have been reported in the literature.

Griffiths[30-34] was the first to identify the speed index S as the

controlling parameter of steady, one-dimensional flows. Griffiths discovered that, analogous to gas-dynamic flows, friction has the effect of decreasing area and pressure in the direction of flow when $S < 1$ and that it has the opposite effect for $S > 1$. He also demonstrated, by means of a simple experiment, the transition from supercritical to subcritical flow and the occurrence of flow limitation. Oates[37] extended the work of Griffiths by showing how the changes in flow variables depend on the simultaneous effects of wall friction, wall properties, resting area, and elevation in the gravity field. Oates also considered shock-like transitions and the propagation of finite amplitude waves. He identified the property of the tube law that governs the steepening or broadening of compression waves. This parameter was also identified by Shapiro[2] as M, the determinant of nonlinear steepening or broadening of propagating waves of finite amplitude. It also appears quite naturally in the equation developed by him to describe the change of speed index S in the direction of fluid flow.

Rubinow and Keller[38] formulated a theory for inertia-free, locally Poiseuille flow within a collapsible tube which exhibits flow limitation quite independent of the wave speed type flow limitation mentioned previously.

B. Physiological Flows in Collapsible Tubes

Many phenomena associated with fluid flow through collapsible tubes are of importance in physiology, in medical diagnostics, and in therapeutic procedures and devices. In particular, in physiological flows it may

be expected that whenever flow limitation occurs, the flow downstream of the flow-limiting location will be supercritical. Consequently, transition to subcritical flow and the formation of shocks can be expected downstream of such locations.

Pulmonary Airways. An important feature of lung structure is its extreme mechanical compliance. The airways are easily collapsed by a negative transmural pressure and the resulting decreased cross-sectional area leads to increased airflow speeds. The expiratory flow reaches a maximum at some value of the driving pleural pressure. Hyatt *et al.* showed that MEFR (maximum expiratory flow rate) at any point in the vital capacity was independent of effort, once flows reached their maximum value. The MEFR was uninfluenced by the addition of external resistances and it was highly reproducible from day to day. This insensitivity of the MEFR to either effort or exit conditions may be explained in terms of flow limitation due to the creation of supercritical flow and/or shocks in collapsed airways. Experimental observations indicate that people with lung disease have lower MEFR's than people in good health. This may be explained in terms of the increased stiffness of the lung structure.

The Male Urethra. In males, the urethra behaves like a thin-walled elastic tube; the urine flow rate is controlled by a "sonic" constriction near the bladder, while the diameter and the speed of the external urine stream are controlled by a second "sonic" constriction near the

external meatus with a "hydraulic jump" between the two sonic sites.

It has been shown experimentally by Griffiths[30,31,33] that the existence of shocks in the male urethra is an indication of normal micturition function. It is conjectured that the shock formation is a natural way of autoregulation according to which, when the bladder pressure is high, the sphincter allows for the creation of a shock, thus creating a loss in stagnation pressure. Hence, the flow rate through the urethra decreases compared to the flow rate in the absence of a sphincter, thus preventing possible damage by effectively decreasing the wall shear.

Cervical Venous Hums. The cervical venous hum may be explained by the existence of shock in the internal jugulars, the hum being due to the vibrations that are inherent in a shock occurring within a collapsible tube (Danahy *et al.*[35] Groom *et al.*[36]). This hum is a prominent finding in hyperdynamic circulatory states such as thyrotoxicosis and anemia. People suffering from these conditions have higher rates of blood flow and the likelihood of supercritical flow and shock formation is correspondingly greater.

A quarter to one half of the normal adult population has venous hums. The murmurs become of higher intensity when the chin is raised or the head is rotated leftward.

Extrathoracic Venous Flow. Shock wave formation can be the cause for flow limitation due to inspiratory collapse of the inferior vena

cava below the diaphragm and above the renal veins.

Extrathoracic veins collapse at their entry into the chest and except for abnormal and pathological conditions, "the negative pressure in the thorax and its variations are incapable of influencing venous return directly" (Brecher[18]). Flow studies in physical models and in direct evidence from mean venous pressure measurements support the view that resistance to flow increases in the collapsed portion of the veins and the volume flow cannot increase with greater suction (flow limitation).

C. Diagnostic and Therapeutic Devices

A variety of procedures used clinically for diagnosis and therapy involve flow in collapsible tubes. The understanding of phenomena observed in fluid flow through compliant tubes contributes to the design, improvement, and the most effective application of these procedures.

Intermittent Compression as Prophylaxis Against Deep Vein Thrombosis (EPC). In patients who have undergone surgery and were confined to bed for an extended period of time, thrombus formation most commonly originated in the deep veins of the leg. Angiographic studies have shown that blood will remain stationary in the veins of the lower extremities for minutes and even hours while the patient is in the recumbent position. When the veins are compressed externally blood flows preferably through the heart due to the relatively high resistance of the arterioles

and the capillary bed.

"Venous stasis" is thought to be a major cause of deep vein thrombosis in patients confined to bed. External physical means to overcome stasis have been used as a prophylaxis for recumbent patients against venous thromboembolism.

Currently the most promising physical approach to prophylaxis against deep veinous thrombosis is intermittent external pneumatic compression. This is accomplished with a cuff around the leg. Air pressure in the range of 20-50 mm Hg is applied intermittently and then relieved. The typical cycle period is one minute.

Experiments in our laboratory on a hydraulic model of vein collapse by external pressure show that the tube tends to collapse first near its exit end. This establishes a reduced area which acts as a flow-limiting mechanism (supercritical flow is established). The discharge flow rate, after reaching a maximum, quickly diminishes with time and the maximum flow rate no longer increases with applied pressure after the latter reaches certain values.

Severe pressurization of the cuff can result in the creation of supercritical flow and the formation of a shock downstream of the exit from the pressurizing boot. Under these conditions, in addition to the flow limitation, there is also a loss in stagnation pressure across the shock. Both of these effects lead to reduction in the blood volume that can be displaced in a given time and they result in impairment of the effectiveness of the EPC procedure.

External Counterpulsation for Temporary Cardiac Assistance (ECA). A counterpulsation scheme requires that the impedance against which the heart pumps during natural systole (the period during which the left ventricle ejects blood) be reduced, thus reducing the aortic pressure against which the heart works; and that during natural diastole (left ventricle relaxed, and refilling), the aortic pressure be increased by some external energy source, thus providing the necessary pressure for perfusing the various organs in the circulatory system, including the heart itself via the coronary arteries.

In external counterpulsation, boots are put around the legs and pressurized with high enough pressures so that the blood volume in the veins and arteries of the legs is displaced in the proper time sequence to achieve the above-mentioned goal.

In both EPC and EPA, the formation of shocks and flow limitation will impair the effectiveness of the procedures. Therefore, knowledge of the structure of shock waves and conditions under which they may be created is highly desirable.

1.3 Objectives and Scope of This Investigation

A. Introduction

The formation of shock waves in collapsible tubes has been experimentally observed (Griffiths[31,39]) and theoretically partially explained on the basis of propagation and steepening of area waves (Oates,[36,37] Shapiro[2]). However, no quantitative measurements have been made to

adequately characterize either the trans-shock jump conditions or the detailed structure of such waves. In the experiments conducted in this investigation, certain hitherto unobserved new features, such as the existence of a standing wave-train preceding a steady shock, have come to light.

By analogy to gas-dynamic shock waves and open-channel hydraulic jumps, and also by undertaking a heavy experimental program, certain conclusions have been drawn about the prominent features of standing shock waves in collapsible tubes. These features are listed below:

(1) The wave speed that is relevant to the problem is the speed of small-amplitude inviscid waves, c. The controlling parameter of the one-dimensional flow problem is the speed index, S :

$$c^2 = \frac{A}{\rho} \frac{d(p - p_e)}{dA} \tag{1.1}$$

$$S = \frac{\text{Mean Flow Speed}}{\text{Wave Speed}} = \frac{u}{c} \quad . \tag{1.2}$$

(2) The inlet flow is supercritical ($S > 1$) (this is also confirmed experimentally).

(3) A large change in cross-sectional area is achieved in a relatively short distance (e.g., exit area/inlet area $\simeq 5$ over a distance of three tube diameters).

(4) Large longitudinal wall curvatures are prevalent.

(5) Large losses in stagnation pressure across the shock have been measured. This is probably due to flow separation and conversion of

mean flow energy into turbulent eddy energy (current experimental finding).

(6) Standing precursor area and pressure waves of substantial amplitudes are observed to precede the shock; see Figs. (30) - (48s) (current experimental finding).

(7) Once a shock is established in the tube, the upstream conditions, including flow rate, become independent of changes in downstream conditions (current experimental finding consistent with the flow limitation behavior observed in gas dynamic shocks and hydraulic jumps in free-surface channel flows).

(8) Vibrations originating at the shock propagate both upstream and downstream of the shock, along the tube wall (current experimental finding).

B. Objectives and Scope

The research reported in this thesis has two distinct objectives and the work leading to these is reported in Parts A and B.

The first objective was the measurement and interpretation of the trans-shock or jump conditions as well as the determination of the detailed structure of standing shock waves in collapsible tubes. Specifically, the cross-sectional area and fluid pressure distributions within the collapsible tube over a range of upstream speed indices were measured. The principal instrumentation was in the form of a translatable catheter which was connected to a pressure transducer and which

also supported two electrodes. With these electrodes, the local cross-sectional area was determined by means of electrical impedance measurements. The catheter was drawn through the test section at a uniform rate and provided curves of pressure and area as a function of axial distance.

Since computation of the speed index requires knowledge of the speed of propagation of small-amplitude area waves, it was also necessary to experimentally determine to a high degree of accuracy the transmural pressure/cross-sectional area relationship (i.e., the tube law) for the static, uniformly-collapsed tube. The cross-sectional area in this experiment was also measured by the electrical impedance technique.

The principal thrust of the work reported in Part A of this thesis was to accumulate a body of experimental data which would give insight, guidance, and a firm basis for comparison for detailed analytical modeling in the future.

The second objective of this research was the experimental determination of the flow limitation behavior of collapsible tubes and the application of this knowledge to the design of a novel flow regulator employing a collapsible tube as its active element. The flow regulator envisaged is one which, when connected to an upstream constant head reservoir, would provide a constant flow rate of fluid irrespective of downstream pressure variations. In such a design, it is necessary to be able to specify the regulation characteristic of flow rate as a function of downstream pressure.

CHAPTER II:

STRUCTURAL MECHANICS OF UNIFORM COLLAPSIBLE TUBES

2.1 The Tube Law for Uniformly Collapsed Tubes

In the one-dimensional treatment of collapsible tube flows, the coupling between the deformation of the tube wall and the mechanics of the fluid flow take place through a constitutive relationship or "tube law." The tube law is a property of the tube alone and is an expression which relates the transmural pressure across the tube wall to the cross-sectional area of the tube. For a uniformly-collapsed tube with constant, non-retarded wall properties, the tube law provides a unique relationship between the two variables. In this sense, it is analogous to the equation of state for gases in gas-dynamics and to the relationship between fluid pressure and the depth below the surface in open-channel flows.

The manner in which a thin-walled compliant tube resists deformation in the distended state under positive transmural pressures is very different from that in the collapsed state under negative transmural pressures. When distended, the cross-sectional area of the tube is circular, and its size is determined by a balance between the membrane hoop stresses and the in-plane extensional stiffness of the tube wall. When collapsed, the shape of the cross-section is usually oval or twin-lobed, depending upon the degree of collapse. Its shape and size is then determined primarily by a balance between the bending moment exerted on each wall element by the negative transmural pressure and

the bending stiffness of the tube wall. Since the bending stiffness is much smaller than the extensional stiffness of the tube wall, the tube suffers very large changes in cross-sectional area under relatively small negative transmural pressures as indicated in Fig. 1 . As the degree of collapse increases, the opposite sides of the tube wall first come into point contact and subsequently make line contact.

A comparison of the accuracy of pressure-radius relationships for thin-walled, long elastic tubes under positive transmural pressures has been made by Taylor and Gerrard.[45] A relationship for the hoop tension per unit length T_θ by Treloar[46] which has been experimentally shown by him to valid for both large and small deformations is

$$T_\theta = \frac{Et}{2(1+\nu)} \left[\left(\frac{R}{R_0} \right) - \left(\frac{R_0}{R} \right)^3 \right] , \qquad (2.1)$$

where R and R_θ are the current and initial radii, respectively, and t is the thickness of the wall. The Young's modulus E and Poisson's ratio ν characterize the elastic properties of the wall. The balance between the hoop tension and the positive transmural pressure $(p - p_e)$ yields

$$T_\theta = (p - p_e)R \quad . \qquad (2.2)$$

If A and A_0 are the current and initial areas the area ratio α is defined by

$$\alpha \equiv \frac{A}{A_0} \quad . \qquad (2.3)$$

Equations (2.1), (2.2), and the above definition yield expression (2.4)

for the pressure-area relationship for a uniformly distended, thin elastic tube, where K_E is the extensional stiffness of the tube wall:

$$(p - p_e) = K_E \left(1 - \frac{1}{\alpha^2}\right) \tag{2.4}$$

$$K_E \equiv \frac{E}{2(1+\nu)} \left(\frac{t}{R_0}\right) \quad . \tag{2.5}$$

The speed of propagation of small area waves as given by Eq. (1.1) is therefore equal to

$$c = \sqrt{\frac{2K_E}{\rho}} \left(\frac{1}{\alpha}\right) \quad \text{for} \quad \alpha > 1 \quad . \tag{2.6}$$

As the transmural pressure is progressively reduced and becomes negative, a critical value is reached at which the tube begins to buckle. The buckling pressure for an initially circular tube for the oval mode has been calculated by Tadjbakhsh and Odeh[40] to be equal to

$$|P_B| \equiv \frac{|(p - p_e)|}{K_B} = 3 \tag{2.7}$$

$$K_B \equiv \frac{E}{12(1-\nu^2)} \left(\frac{t}{R_0}\right)^3 \quad . \tag{2.8}$$

where K_B is the bending stiffness of the tube wall.

The post-buckling deformation of compliant tubes has been considered by many authors[40-43] with various degrees of success. All of these analyses employ the constraint of inextensionality of the tube wall. This is a valid assumption as the in-plane strains are small

in the collapsed state and the deformation of the cross-section is primarily due to rotations. However, this assumption would break down at the very smallest area ratios when curvatures are large and the in-plane stresses may again become significant. The analysis of Flaherty, Keller, and Rubinow[41] is the most complete. They consider the effect of normal forces created when the opposing walls come in contact. The work of Kresh and Noordergraaf neglects these forces and is thus incorrect for this configuration.

The equations governing the deformation of the tube are obtained by considering the equilibrium of a small element of the tube wall under the action of the transmural pressure $(p - p_e)$, in-plane tension T, normal shear N, and the bending moments M as shown in Fig.6 . The equilibrium equations are

Normal force equilibrium:

$$\frac{dN^*}{ds^*} - T^* \frac{d\theta}{ds^*} + P = 0 \quad . \tag{2.9}$$

Tangential force equilibrium:

$$\frac{dT^*}{ds^*} + N^* \frac{d\theta}{ds^*} = 0 \quad . \tag{2.10}$$

Moment equilibrium:

$$\frac{dM^*}{ds^*} + N^* = 0 \quad . \tag{2.11}$$

The bending moment M^* is related to the change in curvature $d\theta/ds^*$ by

$$M^* = \left(\frac{d\theta}{ds^*}\right)_{P=0} - \frac{d\theta}{ds^*} = 1 - \frac{d\theta}{ds^*} \quad . \tag{2.12}$$

In the above expressions, the variables have been normalized according to

$$P \equiv \frac{p - p_e}{K_B} \qquad M^* \equiv \frac{M}{R_0^2 K_B}$$

$$T^* \equiv \frac{T}{R_0 K_B} \qquad N^* \equiv \frac{N}{R_0 K_B} \tag{2.13}$$

$$s^* \equiv \frac{s}{R_0} \qquad x^* \equiv \frac{x}{R_0} \qquad y^* \equiv \frac{y}{R_0} \quad .$$

The coordinates x and y in Fig.7 are related to the arc length s by

$$x = \int_0^s \cos\,\theta(s)\, ds \quad ; \qquad y = \int_0^s \sin\,\theta(s)\, ds \quad . \tag{2.14}$$

The inextensionality condition is imposed by requiring that

$$\theta(s + 2\pi R_0) = \theta(s) + 2\pi \quad . \tag{2.15}$$

The boundary conditions of the problem vary depending on whether the walls are in contact and on the manner in which they make contact at various transmural pressures P.

(1) <u>Tube walls not in contact</u>: $|P_B| < |P| < |P_P|$

$$\theta(0) = 0 \qquad \theta\left(\frac{\pi}{2}\right) = \frac{\pi}{2}$$

$$N^*(0) = 0 \qquad N^*\left(\frac{\pi}{2}\right) = 0 \quad . \tag{2.16}$$

Conditions $(2.16)_{3,4}$ are obtained from symmetry considerations.

(2) Tube walls in point contact: $|P_P| < |P| < |P_L|$

$$\begin{aligned} \theta(0) &= 0 \qquad & \theta\left(\frac{\pi}{2}\right) &= \frac{\pi}{2} \\ N^*(0) &= 0 \qquad & T^*\left(\frac{\pi}{2}\right) &= 0 \ . \end{aligned} \tag{2.17}$$

The condition $(2.17)_4$ is now different from $(2.16)_4$, and is obtained by considering the equilibrium of the tube cross-section at $\theta = \pi/2$. Point contact first begins at $|P| = |P_P|$ and continues until $|P| = |P_L|$ when the curvature at the point of contact becomes zero and line contact beings.

(3) Tube walls in line contact: $|P_L| < |P|$

$$\begin{aligned} \theta(0) &= 0 \qquad & \theta(s_L) &= \frac{\pi}{2} \\ N^*(0) &= 0 \qquad & T^*(s_L) &= 0 \ . \end{aligned} \tag{2.18}$$

For all negative transmural pressures larger than $|P_L|$ the governing equations and the boundary conditions remain the same while s_L and $|P_L|$ vary. Consequently, the solutions of the problem for any $|P| > |P_L|$ can be found from that for $|P| = |P_L|$ by a similarity transformation.[41] Thus, the cross-section A can be expressed in terms of A_L by

$$A = A_L \left(\frac{P_L}{P}\right)^{2/3} , \tag{2.19}$$

or, equivalently,

$$\frac{P}{P_L} = \left(\frac{\alpha}{\alpha_L}\right)^{-3/2} . \tag{2.20}$$

From the calculations of Flaherty *et al.*,

$$P_P = -5.247 \qquad P_L = -10.34$$

$$\alpha_P \simeq 0.27 \qquad \alpha_L \simeq 0.21 \ .$$

Using these values, the similarity tube law becomes

$$P = -0.995\ \alpha^{-3/2} \simeq -\alpha^{-3/2} \ . \tag{2.21}$$

The functional relationship in (2.21) can also be obtained through dimensional arguments and from the fact that there is no characteristic length for the problem in the similarity range.[47] The length of the contacting region will adjust itself to accommodate the balance between bending moments and bending stiffness. As $|P|$ is increased, the successive configurations assume self-similar shapes as long as the radius of the wall curvature is large compared to the wall thickness.

The radius of curvature R_c at any typical location is a function of only the bending stiffness $Et^3/12(1-\nu^2)$ and $(p - p_e)$. Thus,

$$R_c = R_c[Et^3/12(1-\nu^2), (p - p_e)] \ . \tag{2.22}$$

For dimensional homogeneity,

$$\frac{R_c^{\,3}\,(p - p_e)}{[Et^3/12(1-\nu^2)]} = \text{numerical constant.} \tag{2.23}$$

Further, the cross-sectional area A_c must vary as $R_c^{\,2}$. Thus,

$$\frac{A_c^{3/2}\,(p - p_e)}{[Et^3/12(1-\nu^2)]} = \text{numerical constant.} \tag{2.24}$$

Equivalently, using the previous definitions,

$$P = \text{(numerical constant)}\ \alpha^{-3/2} \quad . \tag{2.25}$$

This result is the same as (2.21) if the numerical constant is taken to be equal to (-1).

No simple closed-form expressions exist for the range $1 \leq \alpha \leq \alpha_L$ and the solution must be obtained by numerical solution of Eqs. (2.9) through (2.18) as it was done by Flaherty *et al.*[41] Another method would be to curve-fit the experimentally obtained pressure-area relationship. Since the character of the solution changes between $\alpha \leq \alpha_B$, $\alpha_P \leq \alpha \leq \alpha_B$ and $\alpha \leq \alpha_P$, it may be necessary to use three separate functional approximations.

In the similarity range $\alpha \leq 0.21$, the wave speed can be obtained from (2.21) using the definition of Eq. (1.1):

$$c = \sqrt{\frac{3}{2}\frac{K_B}{\rho}}\ \alpha^{-3/4} \quad . \tag{2.26}$$

Within the range $0.21 \leq \alpha \leq 1$, the wave speed would have to be obtained either by numerical solution of the governing equations or by numerical differentiation of the experimentally determined pressure-area relationship. The wave speed at various degrees of collapse has been directly determined experimentally by Brower and Scholten.[48] However, those measurements were obtained for a collapsible tube lying on a rigid surface and the transmural pressure was not uniform around the periphery of the tube.

2.2 Influence of Longitudinal Curvature

The tube law discussed in the preceding section is strictly valid only if the following assumptions are satisfied. The elastic properties of the wall must be isotropic and the elastic properties, wall thickness, resting area, and the applied transmural pressure must be constant along the tube wall at any given cross-section and also along its length. Under these conditions, the tube will collapse uniformly and without twist, when subjected to a negative transmural pressure. However, when these quantities do vary along its length, the uniform collapse tube law will be approximately valid if their gradients in the longitudinal direction are small. For example, in the case of a uniform tube along which an area wave is propagating, this tube law is valid only if the ratio of the wave amplitude to the wavelength is small.

In this section the necessary modifications to the uniform collapse tube law, for a tube of uniform properties that suffers significant longitudinal area gradients, will be considered. The pressure-area relationship at a particular section will then not be a unique function of the area alone but will also reflect its variations in the longitudinal direction through its longitudinal derivatives.

Such modifications to the tube law will play a crucial role in the establishment of the structure of shock waves in collapsible tubes.

Consider a partially-collapsed uniform tube which is subject to longitudinal transmural pressure variations. For the approximate analysis that is attempted here, the cross-section will be assumed to be

relatively flat and symmetrical about the centerline as indicated in Fig. 8 . The height $\eta(x)$ of the tube wall will be taken to represent the overall deformation of the cross-section. The gradients in $\eta(x)$ will be considered to be sufficiently small so that nonlinearities in the derivatives of η can be neglected. The conditions described here would be approximately satisfied in the collapsed region upstream of a standing shock wave of the type experimentally observed. However, these assumptions will break down within the shock itself, where large longitudinal gradients in area have been observed.

If the cross-section has the idealized geometry shown in Fig. 8 , the cross-sectional area is given by

$$A = 2\pi\eta \left[R_0 - \tfrac{1}{2}\eta\right] \quad , \tag{2.27}$$

or, equivalently,

$$\alpha \equiv \frac{A}{A_0} = \left(2 - \frac{\eta}{R_0}\right)\frac{\eta}{R_0} \quad , \tag{2.28}$$

where

$$\frac{\eta}{R_0} = 1 - \sqrt{1-\alpha} \quad .$$

It will now be assumed that the transmural fluid pressure $(p - p_e)$ is supported in part by the circumferential bending stresses as reflected in the uniform collapse tube law and in part by the stresses induced in the tube wall due to longitudinal curvature. Thus,

$$(p - p_e) = K_B P(\alpha) + (p - p_e)_x \quad , \tag{2.29}$$

where $(p - p_e)_x$ is the part of the transmural pressure supported by stresses due to the longitudinal deformations of the tube wall. Consider

the equilibrium of a wall element of length ds as shown in Fig. 9 . Balance of forces in the normal and tangential directions and balance of bending moments yield

$$\frac{dN}{ds} - \frac{T}{R} - (p - p_e)_x = 0$$

$$\frac{dT}{ds} + \frac{N}{R} + \tau_w = 0 \qquad (2.30)$$

$$\frac{dM}{ds} + N = 0 \ ,$$

where N, T, M, and τ_w are the normal shear force per unit length, longitudinal in-plane tension per unit length, bending moment per unit length, and fluid friction stress per unit wall area, respectively.

In addition, if the gradients in $\eta(x)$ are sufficiently small, the following approximations hold:

$$\frac{d}{ds} \simeq \frac{d}{dx} \ ; \quad \frac{1}{R} \simeq -\frac{d^2\eta}{dx^2} \ . \qquad (2.31)$$

Further, an approximate constitutive relation can be written for the bending moment as

$$M = \frac{\hat{E}I}{R} \simeq -\hat{E}I \frac{d^2\eta}{dx^2} \ , \qquad (2.32)$$

where the bending stiffness $\hat{E}I$ is given by

$$\hat{E}I = \frac{Et^3}{12(1-\nu^2)} \ . \qquad (2.33)$$

Before proceeding beyond this point, three limiting cases of these equations will be considered.

Case 1: Negligible longitudinal area gradients. For negligible gradients in $\eta(x)$, Eqs. (2.30) reduce to

$$(p - p_e)_x = 0 \quad ; \qquad T = T_1 - \int_0^x \tau_w \, dx \quad , \tag{2.34}$$

where T_1 is the wall tension at $x = 0$: $N = 0$. Thus, the uniform collapse tube law is recovered. Equation $(2.34)_2$ reflects the reduction in initial wall tension due to frictional drag of the fluid.

Case 2: Normal shear forces dominate longitudinal in-plane tensions. Neglecting the terms involving longitudinal in-plane tensions in comparison to bending terms and also neglecting nonlinear terms in the gradients of $\eta(x)$ yield

$$\begin{aligned} (p - p_e)_x &= \hat{E}I \frac{d^4\eta}{dx^4} \\ T &= T_1 - \int_0^x \tau_w \, dx \\ N &= \hat{E}I \frac{d^3\eta}{dx^3} \quad . \end{aligned} \tag{2.35}$$

Substituting $(2.35)_1$ in expression (2.29) gives the following expression for the modified tube law:

$$(p - p_e) = K_p P(\alpha) + \hat{E}I \frac{d^4\eta}{dx^4} \quad . \tag{2.36}$$

Recasting (2.36),

$$p - p_e - \hat{E}I \frac{d^4\eta}{dx^4} = K_B P(\alpha) \quad . \tag{2.37}$$

Thus the effect of bending deformation is to alter the effective transmural pressure by the term $\hat{E}I \frac{d\eta^4}{dx^4}$.

Case 3: Longitudinal in-plane tensions dominate normal shear forces. Neglecting the terms involving normal shear forces yields

$$(p - p_e)_x = -\frac{d^2\eta}{dx^2}\left(T_1 - \int_0^x \tau_w \, dx\right)$$

$$T = T_1 - \int_0^x \tau_w \, dx \quad . \tag{2.38}$$

Thus the modified tube law becomes

$$(p - p_e) = K_B P(\alpha) - \frac{d^2\eta}{dx^2}\left(T_1 - \int_0^x \tau_w \, dx\right). \tag{2.39}$$

Alternatively,

$$p - p_e + \frac{d^2\eta}{dx^2}\left(T_1 - \int_0^x \tau_w \, dx\right) = K_B \, P(\alpha) \quad . \tag{2.40}$$

Hence, the effect of positive wall curvature is to increase the effective transmural pressure when the local longitudinal in-plane force T is positive. This clearly shows how the initial tension can affect the tube law.

When both normal shear (i.e., bending) and longitudinal in-plane tensions are important, Eqs. (2.30)-(2.33) yield

$$T = T_1 - \int_0^x \tau_w \, dx$$

$$(p - p_e) = K_B P(\alpha) + \hat{E}I \frac{d^4\eta}{dx^4} - \frac{d^2\eta}{dx^2}\left(T_1 - \int_0^x \tau_w \, dx\right), \tag{2.41}$$

where again a nonlinear term equal to

$$-\tfrac{1}{2}\hat{E}I\left(\frac{\partial^2\eta}{\partial x^2}\right)^2$$

has been neglected in $(2.41)_1$. In the modified tube law given by $(2.41)_2$, the bending effects in the longitudinal direction will be small compared to the effects of longitudinal in-plane tension forces if

$$\frac{\hat{E}I\,\frac{d^4\eta}{dx^4}}{T\,\frac{d^2\eta}{dx^2}} \ll 1 \quad . \tag{2.42}$$

If the characteristic distance over which longitudinal variations occur is λ, then (2.42) yields

$$\frac{\hat{E}I}{T\lambda^2} \ll 1 \, . \tag{2.43}$$

If ε_{xx} is the axial strain corresponding to T, then

$$T \simeq E\,\varepsilon_{xx}\,t \quad . \tag{2.44}$$

Thus, using definition (2.33) in (2.43) gives the condition for longitudinal in-plane tension forces to be small in comparison to bending forces as

$$\frac{1}{12(1-\nu^2)\varepsilon_{xx}}\left(\frac{t}{\lambda}\right)^2 \ll 1 \quad . \tag{2.45}$$

It is stressed at this point that this formulation is only approximately valid for cross-sections approximating the shape given in Fig. and when the gradients of η are sufficiently small. A more exact analysis of the problem would be a very difficult task which is not justified at the present time.

2.3 Experimental Determination of the Tube Law

For the purpose of determining the pressure-area relationship for a uniformly collapsed latex rubber tube (I.D. = 2.54 cm, wall thickness = 0.083 cm, length = 70 cm, Young's modulus $\simeq 1.6 \times 10^7$ dynes/cm^2), the apparatus shown in Fig. 10 was constructed. In this apparatus, the latex tube was mounted horizontally between two rigid tubes and placed under the same longitudinal strain (6%) as in the shock experiments. This was done by observing the displacement between two lines drawn 15 cm apart on the tube.

The inside of the tube was filled with salt-water and the outside chamber was filled with glycerine-water solution. The densities of the two solutions were matched to better than 1% in order to eliminate buoyancy effects. The inside and outside chambers were connected to glass manometers mounted on a vertical scale. Thus, the transmural pressure could be read directly by means of a cathetometer. The external chamber was also connected to a large movable reservoir full of glycerine-water solution. Thus, the external pressure could be varied, if required, by altering the height of the reservoir. The internal pressure was varied by withdrawing small amounts of salt water using a syringe. The area in the relatively uniformly-collapsed region in the center of the tube was measured by means of the electrical impedance method described below.

In the electrical impedance method of area measurement, an A.C. voltage is applied across a column of salt-water located inside a compliant tube and a rigid tube section which is arranged in series with

the collapsible tube. Thus, the current which passes through the cross-section where the area has to be measured passes also through this rigid reference section of known cross-section area A_R. Figure shows the basic configuration. In the reference section, the voltage V_R across two electrodes, which are placed in contact with the salt solution and which are spaced a fixed distance L_R apart, is measured. An area probe consisting of two electrodes mounted on a small-diameter catheter at a known distance apart L_P is arranged parallel to the tube axis in the salt solution inside the tube. If the area of the tube cross-section at the position of the area probe is A, the catheter cross-sectional area is a, and the voltage measured across the area probe is V_P, then the following relations hold:

$$V_P = r \frac{L_P}{A - a} I \tag{2.46}$$

$$V_R = r \frac{L_R}{A_R} I \quad , \tag{2.47}$$

where r is the specific resistivity of the ionic solution.

The basic assumption here is that the same current I passes through both the reference and probe positions. Thus, from (2.46) and (2.47),

$$A = a + \left(\frac{L_P}{L_R} A_R\right)\left(\frac{V_P}{V_R}\right) . \tag{2.48}$$

By means of relation (2.48) the area A at any cross-section can be determined. In fact, the quantity $[(L_P/L_R)A_R]$ was determined as an area-measurement constant by pulling the probe into the reference section.

2.4 Sources of Error

In the determination of the static pressure-area relationship, there are many potential sources of error. One of these sources is the presence of edge effects. When the tube is collapsing and the deviation of its cross-sectional area from that at the rigid ends becomes large, the errors due to non-uniform collapse could be significant. For this reason, the tube length has to be sufficiently long so that there is always a section of the tube located at the center which collapses uniformly. Another source of error is the change in pressure due to any air bubbles that may be trapped in the inner and outer chambers. Provisions were made in this apparatus to eliminate all air bubbles from these spaces.

Some additional potential sources of error are related to the measurement of area by the electrical impedance method. These are listed below.

A. D.C. Electrode Polarization Potentials

When a D.C. voltage is applied to an ionic solution, electrode polarization potentials develop in boundary layers around the electrodes. Thus, the D.C. voltage drop across the electrodes is no longer directly proportional to the distance between them. To avoid such errors, an A.C. excitation voltage was employed. This, however, introduced certain other sources of error not encountered with D.C. excitation.

B. Leakage Currents

The existence of leakage paths shunting off current across the tube wall would reduce the current passing through the probe area position with respect to that passing through the reference section. This would result in a larger apparent probe area as calculated from Eq. (2.48). The leakage currents are due to the finite electrical resistance of the tube wall and due to the capacitive current across it. The first of these is independent of frequency but is proportional to the tube length. The capacitive current is directly proportional to the frequency and the tube length. The electrical behavior of this system is complex and can be treated in a manner similar to that employed in the study of electrical transmission lines. Instead, in this experiment, two precautions were taken to limit and place bounds on these errors.

First, the conductivity of the external solution was kept at the minimum possible value by using distilled water for making the glycerine-water solution. Next, to determine the extent of such errors and the range of acceptable frequencies that may be employed for excitation, an experiment was performed on a latex tube with a perfectly conducting external medium. The experiment is described in Appendix A. From this experiment, it was concluded that even at 500 Hz, the errors due to the leakage currents in this very unfavorable set-up would be less than 6%.

C. Amplification of Small Probe Signals in the Presence of Noise

The signal obtained from the area probe was of the order of a few millivolts when the tube was nearly inflated and increased about tenfold

when the tube was highly collapsed. Thus, it was necessary that the signal be amplified. Electrical noise was also present in the signal, induced in the salt-water column by electrical equipment and power lines present in the laboratory. Fortunately, the noise was of the common-mode type and several precautions were taken in the design of the measurement system to eliminate these errors. First, all signal cables were shielded and connected to a stable, low-noise ground. Second, a high-quality differential amplifier of very high common-mode rejection ratio (CMRR) was used to amplify the signal.

CHAPTER III:

FRICTION FACTORS FOR COLLAPSIBLE TUBE FLOW

In the one-dimensional analysis of fluid flow within a collapsible tube, it is often necessary to include the effect of viscous fluid drag. Since the cross-sectional shape and wetted perimeter of a compliant tube varies significantly with the degree of collapse, it is necessary to modify the standard formulations or to develop new expressions for viscous drag. In this section, approximate expressions are derived for this purpose subject to the following assumptions:

(1) The flow is one-dimensional in the sense that area gradients are sufficiently small so that the flow may be considered locally fully developed.

(2) The flow is steady.

(3) The flowing fluid is essentially incompressible.

3.1 Laminar Flows

If the preceding assumptions are valid and the flow is laminar, then the flow is locally a Poiseuille flow and must satisfy the following equations:

Momentum:
$$\frac{dp}{dx} = \mu\left(\frac{\partial^2\tilde{u}}{\partial y^2} + \frac{\partial^2\tilde{u}}{\partial z^2}\right) \quad \text{in A ;} \tag{3.1}$$

Boundary Condition:
$$\tilde{u} = 0 \quad \text{on P ;}$$

Flow Rate:
$$Q = \iint_A \tilde{u}(x,y,z)\, dy\, dz = Au \quad ;$$

Wall Friction: $$\frac{\tau_w P}{A} = -\frac{dp}{dx} \quad ,$$

where P is the length of wetted perimeter, A is the area of the flow region within the collapsed tube, and u is the average velocity of flow.

Flaherty, Keller, and Rubinow[41] have solved this problem numerically for the two-lobed mode of collapse. For the similarity region of collapse ($\alpha \leq 0.21$) they have given a similarity relationship for the hydraulic conductance σ of the tube. This is given as

$$\frac{\hat{\sigma}}{\sigma_L} = \left(\frac{P}{P_L}\right)^{-4/3} \quad , \tag{3.2}$$

where

$$\sigma = \frac{R_0^4}{\mu}\hat{\sigma} \quad ; \quad \sigma \equiv \frac{Q}{-dp/dx} \quad , \tag{3.3}$$

and the subscript L refers to the conditions at the inception of line contact of the opposing walls. Using the similarity relation between P and α [Eq. (2.2)] in (3.2) gives

$$\frac{\hat{\sigma}}{\sigma_L} = \left(\frac{\alpha}{\alpha_L}\right)^2 \quad , \tag{3.4}$$

where $\hat{\sigma}_L = 0.008$ and $\alpha_L = 0.21$. Thus for $\alpha \leq 0.21$,

$$\hat{\sigma} = 0.1814\ \alpha^2 \ . \tag{3.5}$$

Using (3.5), (3.3), and $(3.1)_3$ in $(3.1)_4$ yields

$$\frac{\tau_w P}{A} = \left(\frac{8\pi\mu u}{A_0}\right)\frac{2.165}{\alpha} \quad . \tag{3.6}$$

If the constant 2.165 is changed to 2.785, then Kamm[49] reports that

the result is a reasonable approximation up to $\alpha \simeq 0.36$. Thus for $\alpha \leq 0.36$,

$$\frac{\tau_w P}{A} = \left(\frac{8\pi\mu u}{A_0}\right)\frac{2.785}{\alpha} \quad . \tag{3.7}$$

For the region $0.36 \leq \alpha \leq 1$, the cross-section of the tube is approximately elliptical and the Poiseuille flow relationship for flow through elliptical tubes[50] can be used to develop an approximate expression for the wall friction.

Now, for an elliptical tube of major and minor semi-axes a and b ,

$$A = \pi ab \tag{3.8}$$

$$P \simeq \pi[2(a^2 + b^2)]^{1/2} \tag{3.9}$$

$$Q = \frac{\pi}{4\mu}\frac{a^3b^3}{a^2 + b^2}\left(-\frac{dp}{dx}\right) \tag{3.10}$$

$$Q \simeq \frac{1}{2\mu}\frac{A^3}{p^2}\left(-\frac{dp}{dx}\right) \quad . \tag{3.11}$$

As the wetted perimeter is constant in length during deformation in this area range ($0.36 \leq \alpha \leq 1.0$) ,

$$P = \sqrt{4\pi A_0} \quad . \tag{3.12}$$

Hence, for $0.36 \leq \alpha \leq 1.0$,

$$\hat{\sigma} = \frac{\pi}{8}\alpha^3 \tag{3.13}$$

$$\frac{\tau_w P}{A} = \left(\frac{8\pi\mu u}{A_0}\right)\frac{1}{\alpha^2} \quad . \tag{3.14}$$

For area ratio $\alpha \geq 1$, the cross-section is circular and by setting

$a = b = R = \sqrt{A_0\alpha/\pi}$ in (3.10) and using $(3.1)_4$ it is possible to obtain the wall friction. Thus, for $\alpha \geq 1$,

$$\hat{\sigma} = \frac{\pi}{8}\alpha^2 \tag{3.15}$$

$$\frac{\tau_w P}{A} = \left(\frac{8\pi\mu u}{A_0}\right)\frac{1}{\alpha} \quad . \tag{3.16}$$

The influence of mild area gradients on the laminar Poiseuille flow relationship for an elliptical tube has been considered by Wild, Pedley, and Riley[19] by means of a perturbation analysis. Their solution, recast in dimensional variables, is

$$-\frac{dp}{dx} = \frac{4\mu}{\pi}\left(\frac{a^2+b^2}{a^3b^3}\right)Q - \frac{4}{A}\frac{\partial A}{\partial x}\frac{1}{2}\rho\left(\frac{Q}{A}\right)^2 \quad , \tag{3.17}$$

where the cross-sectional area is given by

$$A = \pi a(x)\, b(x) \quad . \tag{3.18}$$

This expression shows three things. First, the first term is the Poiseuille flow relationship (3.10) for fully developed flow. Second, it shows that the first-order correction to the basic solution is inertial in nature and is related to the acceleration or deceleration of the fluid. Third, it shows that this correction is directly proportional to the area gradient. Using (3.9) and estimating the ratio of inertial to viscous terms in (3.17), the inertial term can be shown to be small, if the modified Reynolds number given below is much less than unity:

$$\frac{1}{4P}\frac{\partial A}{\partial x}\,Re_{D_h} \ll 1 \quad , \tag{3.19}$$

where

$$Re_{D_h} \equiv \frac{(Q/A)D_h}{\nu} \quad ; \qquad D_h \equiv \frac{4A}{P} \quad . \tag{3.20}$$

3.2 Turbulent Flows

As in the previous section, the turbulent flow is considered to be fully developed. If the Reynolds number based on the hydraulic diameter is sufficiently high (for transition from laminar to turbulent flow to have occurred), then the viscous effects are confined to a very narrow region adjacent to the wall, and they are independent of the exact shape of the tube cross-section (Schlichting[51]). As a result, it is possible to use the correlation for the friction factor given by Schlichting for turbulent flow in smooth pipes, provided the Reynolds number is based on the appropriate hydraulic diameter. Thus,

$$\tau_w = \left(\frac{0.0791}{Re_{D_h}^{0.25}}\right)\tfrac{1}{2}\rho u^2 \quad . \tag{3.21}$$

For tubes with the whole wall perimeter exposed to the flow, the wetted perimeter, hydraulic diameter, and Reynolds number are

$$P = \sqrt{4\pi A_0}$$

$$D_h = \frac{4A}{P} = \sqrt{\frac{4A_0}{\pi}}\;\alpha \tag{3.22}$$

$$Re_{D_h} = \frac{(Q/A)D_h}{\nu} = \frac{Q}{\nu}\sqrt{\frac{4}{\pi A_0}} \quad .$$

Thus,

$$\frac{\tau_w P}{A} = \frac{0.0791}{Re_{D_h}^{0.25}} \sqrt{\frac{4\pi}{A_0}} \frac{1}{\alpha} \tfrac{1}{2} \rho u^2 \quad . \tag{3.23}$$

For tubes with cross-sections in the dumbbell shape with two fluid channels and with only part of the perimeter exposed to the flow, each channel can approximately be assumed to be circular in the computation of the wetted perimeter. Thus,

$$\begin{aligned} P &= \sqrt{8\pi A_0 \alpha} \\ D_h &\equiv \frac{4A}{P} = \sqrt{\frac{2A_0\alpha}{\pi}} \\ Re_{D_h} &= \frac{Q}{\nu} \sqrt{\frac{2}{\pi A_0 \alpha}} \quad . \end{aligned} \tag{3.24}$$

Therefore, for dumbbell-shaped cross-sections,

$$\frac{\tau_w P}{A} = \frac{0.0791}{Re_{D_h}^{0.25}} \sqrt{\frac{8\pi}{A_0\alpha}} \tfrac{1}{2} \rho u^2 \quad . \tag{3.25}$$

These results can be conveniently summarized in the following single alternative form:

$$\frac{\tau_w P}{A} = \frac{4f}{D_0} \tfrac{1}{2} \rho u^2 \ , \tag{3.26}$$

where D_0 is the diameter corresponding to the resting area A_0 and f is a friction factor tabulated in Table 1 for the various flow regimes.

The wall friction relation given for both laminar and turbulent flows can be expected to be valid only when area gradients are small. Consequently, these relations can be applied both upstream and downstream

of the shock in a collapsible tube, but they cannot be applied within the shock itself. Within the shock, the flow would be similar to that in a stalled diffuser with flow separation from the walls, the formation of eddies, and re-entrainment taking place further downstream. This will be more fully discussed in the next chapter.

CHAPTER IV:
THEORETICAL ANALYSIS OF THE SHOCK WAVE

This chapter is composed of three sections. In the first section, the analogy between gas dynamic, open-channel, and collapsible tube flows is developed. Next, the propagation of area waves in collapsible tubes and their steepening are briefly considered.

In the second section, the equations governing steady flow in a collapsible tube with constant wall properties and constant external pressure, including frictional effects, are derived and the phenomenon of flow limitation is described.

In the third and last section of this chapter, an approximate analysis of the shock wave is presented first. Subsequently, approximate expressions are developed for analyzing the experimental data. A detailed theoretical analysis of shock structure and precursor waves would involve complex modeling of the tube mechanics and the separated flow within the shock. This work is beyond the scope of this thesis and is not attempted here.

4.1 Analogs: Gas Dynamics, Open-Channel, and Collapsible Tube Flows

The analogy between gas-dynamic, open-channel, and incompressible collapsible tube flows is most clearly seen by considering unsteady, one-dimensional, frictionless flows in horizontal passages. Subject to these assumptions, the momentum equation for all three types of flow is

$$\frac{\partial u}{\partial t} + u \frac{\partial u}{\partial x} = - \frac{1}{\rho} \frac{\partial p}{\partial x} \quad , \tag{4.1}$$

where u, p, ρ, x, and t are, respectively, the flow velocity, fluid pressure, mass density, distance along the passage, and time.

The equation of continuity in each of these three cases involves a mass conservation variable [density $\rho(x,t)$, height of free surface above the bottom $h(x,t)$, or the cross-sectional area $A(x,t)$] and the velocity of flow u:

$$\begin{aligned} &\text{Gas-Dynamic Flow:} && \frac{\partial \rho}{\partial t} + \frac{\partial (\rho u)}{\partial x} = 0 \\ &\text{Open-Channel Flow:} && \frac{\partial h}{\partial t} + \frac{\partial (hu)}{\partial x} = 0 \\ &\text{Collapsible Tube Flow:} && \frac{\partial A}{\partial t} + \frac{\partial (Au)}{\partial t} = 0 \quad . \end{aligned} \tag{4.2}$$

To achieve closure of each of these problems, it is necessary to relate the force variable p to the mass conservation variable ρ, h, or A through a physical "constitutive law" or "equation of state." These are:

Gas-Dynamic Flow (isentropic pressure-density relation for adiabatic, frictionless flow):

$$\rho = \rho(p) \quad ;$$

Open-Channel Flow (hydrostatic law for pressure variation):

$$h = h(p - p_{atm}) = \frac{p - p_{atm}}{\rho g} \quad ;$$

Collapsible Tube Flow (tube law for compliant tube);

$$A = A(p - p_e) \quad .$$

It is thus seen that the mass conservation variables ρ, h, and A bear an analogous relationship to each other and can be expected to display similar physical phenomena. For example, by analogy the speed of propagation of small amplitude waves can be written as

$$\text{Gas-Dynamic Flow:} \quad c^2 = \frac{\rho}{\rho}\frac{dp}{d\rho} = \left.\frac{\partial p}{\partial \rho}\right|_{\text{constant entropy}}$$

$$\text{Open-Channel Flow:} \quad c^2 = \frac{h}{\rho}\frac{d}{dh}(p - p_{atm}) = gh \qquad (4.4)$$

$$\text{Collapsible Tube Flow:} \quad c^2 = \frac{A}{\rho}\frac{d(p - p_e)}{dA} \quad .$$

Carrying this analogy further, Shapiro[2] has listed the following features to be characteristic of such collapsible tube flows:

(1) wave propagation as the prime mechanism of steady flow;

(2) speed index $S \equiv u/c$ analogous in significance to the Mach number and Froude number;

(3) in steady flow, opposite effects in subcritical ($S < 1$) and supercritical ($S > 1$) flows (example: friction causes a pressure drop in subcritical flow but a pressure rise in supercritical flow);

(4) choking and flow limitation when S reaches unity, as at the throat of a convergent-divergent nozzle or at the overflow of a dam;

(5) the possibility of continuous transitions from subcritical to supercritical flow as in a convergent-divergent nozzle.

(6) rapid transitions from supercritical to subcritical flow, as in gas-dynamic shock waves and hydraulic jumps.

A. Propagation of Area Waves

For compressible adiabatic fluid flow in a compliant tube, the governing equations are the momentum equation (4.1), the continuity equation with the mass conservation variable taken to be ρA , and both constitutive relations $(4.3)_1$ and $(4.3)_3$. For this system of equations, a small perturbation analysis about a given steady flow condition gives the wave speed as

$$\frac{1}{c^2} = \frac{1}{c_G^2} + \frac{1}{c_T^2} \quad , \tag{4.5}$$

where c_G and c_T are equal to the wave speeds given by Eqs. $(4.4)_1$ and $(4.4)_3$, respectively. It reflects the combined influence of the two sources of compliance, namely, the gas compressibility and the tube compliance acting in parallel. It also yields the correct limiting behavior given by Eqs. $(4.4)_1$, and $(4.4)_2$ individually.

Such a perturbation analysis about a given steady flow condition leads to the classical wave equation, if viewed from a coordinate frame moving with the flow (Shapiro[52]). The solution for the area perturbation in a collapsible tube flow would have the following form when referred to the fixed coordinate frame:

$$\Delta A = \Delta A_1[x - (u+c)t] + \Delta A_2[x - (u-c)t] \quad , \tag{4.6}$$

where u and c are the fluid velocity and small amplitude wave speed, respectively. Here the term ΔA_1 represents a wave propagating downstream at a velocity of $(u+c)$. If $u > c$, then the wave ΔA_2 would also propagate downstream. Under these conditions, there would be no

mechanism whereby an alteration in downstream conditions could affect conditions upstream of the point at which the speed index $S \equiv u/c$ becomes equal to unity (i.e., becomes critical). This feature has been observed in the experiments on collapsible tubes reported here.

B. Steepening of Finite Amplitude Waves

The formation of a steady shock may be viewed as the long time limit of a transient process of steepening of a finite amplitude wave. For this reason, it is important to consider the conditions under which a finite amplitude wave could steepen. This has been considered by Nicholson,[53] Oates,[37] and Shapiro.[2]

Consider, then, a flat-topped finite amplitude wave propagating in the downstream direction. In such a wave, the additional fluid velocity induced by the wave must itself be considered. As a result, each wavelet into which the finite amplitude wave can be divided travels at a speed of $V_w = u+c$ at its front and at a speed of $V_w + dV_w = (u + du) + (c + dc)$ at its rear. This increased wave speed is due to the fact that the rear of the wavelet is at a pressure higher than the front by an amount dp. Thus,

$$\frac{dV_w}{dp} = \frac{du}{dp} + \frac{dc}{dp} \quad . \tag{4.7}$$

The change in momentum of the wavelet is given by

$$dp = \rho c \, du \quad . \tag{4.8}$$

Thus,

$$\frac{dV_w}{dp} = \frac{1}{2\rho c}\left(2 + 2\rho c \frac{dc}{dp}\right) \quad . \tag{4.9}$$

The definition of wave speed,

$$c^2 = \frac{K_B}{\rho} \alpha \frac{dP}{d\alpha} \quad , \tag{4.10}$$

yields

$$2\rho c \frac{dc}{dp} = 1 + \frac{\alpha \frac{d^2P}{d\alpha^2}}{\frac{dP}{d\alpha}} \quad . \tag{4.11}$$

Substituting from Eq. (4.11) into (4.9),

$$\frac{dV_w}{dp} = \frac{M}{2\rho c} \quad , \tag{4.12}$$

where

$$M \equiv 3 + \frac{\alpha \frac{d^2P}{d\alpha^2}}{\frac{dP}{d\alpha}} \quad . \tag{4.13}$$

Equation (4.12) gives the rate of change of wave speed with pressure, so that if M is positive a compressive wave would steepen and a rarefaction wave would flatten. The converse is true if M is negative. As seen from the static tube law in Fig. 1 , $dP/d\alpha > 0$ always and the curvature $\partial^2 P/\partial\alpha^2$ is negative over the major portion of the collapsed region and becomes positive near the region of distension. Consequently, compressive waves may steepen or flatten in collapsible tubes depending on the value taken by M, a parameter which will later be seen to play an important role in steady flows as well. The basic assumption of this analysis is that the uniform collapse tube law $P(\alpha)$ remains unchanged at the front and the rear of the finite amplitude wave. There is, then,

an implied restriction that the steepness of the wave front must be sufficiently small.

It is interesting to derive the form of the tube law for which a finite amplitude wave would propagate unchanged. Setting $M = 0$ in Eq. (4.13) gives

$$\frac{d^2P}{d\alpha^2} + \frac{3}{\alpha}\frac{dP}{d\alpha} = 0 \quad . \tag{4.14}$$

Solving for P and imposing the condition for unity area ratio at zero transmural pressure,

$$P(1) = 0 \quad , \tag{4.15}$$

gives

$$P(\alpha) = C\left(1 - \frac{1}{\alpha^2}\right) \quad , \tag{4.16}$$

where C is an arbitrary constant. This result is seen to be identical to the tube law of Eq. (2.4) derived by Treloar[46] from kinetic theory for a thin rubber tube under positive transmural pressure.

4.2 Steady Flow in Collapsible Tubes

In this section, the equations governing the steady flow of incompressible fluids in collapsible tubes under certain simplifying assumptions are derived. For a more comprehensive treatment including variations in wall properties, the resting area A_0, and the elevation of the tube, the reader is referred to the work of Shapiro.[2]

The underlying assumptions of this theory are:

(1) The flow is one-dimensional and is characterized by the mean flow speed u and the mean pressure p at any cross-section along the

tube.

(2) The flow is steady, i.e., $\frac{\partial}{\partial t} = 0$.

(3) The fluid is incompressible and all the compliance of the system is due to the compliance of the tube.

(4) The external pressure p_e is constant along the tube.

(5) The resting cross-sectional area A_0 (for zero transmural pressure) is uniform along the tube.

(6) The wall friction stress is given in terms of the formulas derived in Chapter III. They have the form

$$\frac{\tau_w P}{A} = \frac{4f}{D_0} \tfrac{1}{2} \rho u^2 \quad . \tag{4.17}$$

The friction factor f is a function of the area ratio α and the Reynolds number Re_{D_h} based on the hydraulic diameter, and is tabulated in Table 1.

(7) The tube law can be expressed as in Eq. (2.29) as

$$p - p_e = K_B P(\alpha) + (p - p_e)_x \quad , \tag{4.18}$$

where $(p - p_e)_x$ is the effective contribution to $(p - p_e)$ from the wall stresses due to longitudinal deformations of the tube wall.

The first term in Eq. (4.18), $K_B P(\alpha)$, is the contribution from the circumferential stresses. In the case of small area gradients, the tube law can be expressed as in Eq. (2.41) as the sum of bending and membrane effects. For the present purpose, it is convenient to define an effective external pressure $\hat{p}_e$ as

$$\hat{p}_e = p_e + (p - p_e)_x \quad , \tag{4.19}$$

so that the tube law (4.18) becomes

$$(p - \hat{p}_e) = K_B P(\alpha) \quad . \tag{4.20}$$

The equations governing the fluid flow subject to the preceding assumptions are the following.

Conservation of Mass: $$Q = Au = A_0 u\alpha \quad ; \tag{4.21}$$

thus,

$$\frac{1}{\alpha}\frac{d\alpha}{dx} + \frac{1}{u}\frac{du}{dx} = 0 \quad . \tag{4.22}$$

Conservation of Momentum: $$-A\,dp - \tau_w P\,dx = \rho A u\,du \quad . \tag{4.23}$$

therefore,

$$-\frac{dp}{dx} = \frac{\tau_w P}{A} + \rho u \frac{du}{dx} \quad , \tag{4.24}$$

where τ_w is given by Eq. (4.17).

In addition, there is the tube law expressed by (4.20). The speed of propagation of small amplitude waves c is given by

$$c^2 = \frac{K_B}{\rho}\,\alpha\,\frac{dP(\alpha)}{d\alpha} \quad . \tag{4.25}$$

The speed index S is defined by

$$S \equiv \frac{u}{c} \quad . \tag{4.26}$$

From Eqs. (4.25) and (4.26),

$$\frac{1}{c^2}\frac{dc^2}{dx} = \left(1 + \frac{\alpha\,\dfrac{d^2P(\alpha)}{d\alpha^2}}{\dfrac{dP(\alpha)}{d\alpha}}\right)\frac{1}{\alpha}\frac{d\alpha}{dx} \tag{4.27}$$

$$\frac{1}{S^2}\frac{dS^2}{dx} = \frac{1}{u^2}\frac{du^2}{dx} - \frac{1}{c^2}\frac{dc^2}{dx} \quad . \tag{4.28}$$

By routine manipulation of Eqs. (4.20), (4.22), (4.24), (4.26), (4.27), and (4.28), the following equations governing the spatial growth of area ratio α, fluid velocity u, pressure p, and speed index S can be obtained:

$$\frac{(1-S^2)}{\alpha}\frac{d\alpha}{dx} = -\frac{(1-S^2)}{u}\frac{du}{dx} = -L(x,S^2) \tag{4.29}$$

$$\frac{(1-S^2)}{S^2}\frac{dS^2}{dx} = H(x,S^2) = ML(x,S^2) \tag{4.30}$$

$$\frac{1-S^2}{\rho u^2}\frac{dp}{dx} = -\left(\frac{1}{2}\frac{4f}{D_0} + \frac{1}{\rho c^2}\frac{d\hat{p}_e}{dx}\right) \tag{4.31}$$

where

$$L(x,S^2) \equiv +\left(\frac{S^2}{2}\frac{4f}{D_0} + \frac{1}{\rho c^2}\frac{d\hat{p}_e}{dx}\right) \tag{4.32}$$

$$M \equiv 3 + \frac{\alpha\dfrac{d^2P(\alpha)}{d\alpha^2}}{\dfrac{dP(\alpha)}{d\alpha}} = M(\alpha) \quad . \tag{4.33}$$

The solution to the above equations is obtained by solving $(4.29)_1$ and (4.30) as two coupled highly nonlinear ordinary differential equations for the area ratio α and the speed index S. The most striking feature about these equations is the occurrence of the factor $(1-S^2)$ on the left-hand side of each equation. As a result, the flow behavior for subcritical ($S<1$) and supercritical ($S>1$) flow are fundamentally different.

For example, when the effects due to longitudinal wall deformations represented by $d\hat{p}_e/dx$ are neglected, $(4.29)_1$ and (4.31) predict decreasing cross-sectional area ratio α and fluid pressure p when the flow is subcritical. When the flow is supercritical, it predicts that they will increase. Thus the flow exhibits the opposite phenomena depending on whether the flow is supercritical or subcritical.

Now consider the case of supercritical flow in a highly collapsed tube as in the upstream region of the tubes in which shocks were experimentally formed. The parameter M is essentially positive except for a small range in the collapsed region (which could be due to errors in differentiating experimental data twice) as shown in Fig.15 . Thus, if $d\hat{p}_e/dx$ is again neglected, the function H in Eq. (4.20) is positive. Therefore, for supercritical flow, the speed index would decrease in the flow direction, whereas it would increase if the flow were subcritical. As a result, the speed index is always driven towards unity by frictional effects irrespective of whether the flow is subcritical or supercritical. This is similar to the phenomenon of frictional choking observed in gas-dynamics.

If the speed index became equal to unity, Eq. (4.29) would predict an infinite area gradient in the absence of the term $d\hat{p}_e/dx$. However, it is precisely for large area gradients that this term, which contains higher derivatives of the area [see Eqs. (4.19) and (2.41)], becomes important. As a result, a smooth transition, perhaps over a small axial distance, would replace the discontinuities that would otherwise have

occurred in the variables α, p, and S. Furthermore, if the area gradients are very large, such as those encountered within a shock, neither the tube law nor the one-dimensional fluid flow equations would be valid. Thus, these equations are valid only well upstream and well downstream of the shock.

4.3 Wave Speed Flow Limitation

As a simple illustration of flow limitation in a collapsible tube, consider flow with a local stagnation pressure P_0 defined by

$$P_0 \equiv p + \tfrac{1}{2}\rho u^2 . \tag{4.34}$$

The flow rate Q is given by

$$Q = Au = A\sqrt{\frac{2}{\rho}(P_0 - p)} = A\sqrt{\frac{2}{\rho}[(P_0 - p_e) - (p - p_e)]} . \tag{4.35}$$

Now, $Q \to 0$ both when $A \to 0$ due to $(p - p_e) \to -\infty$ and when $(p - p_e) \to (P_0 - p_e)$. Thus a turning point in Q must exist for $(p - p_e)$ between $-\infty$ and $(P_0 - p_e)$. We compute this by setting

$$\frac{dQ}{d(p - p_e)} = \frac{A}{\rho u}(S^2 - 1) = 0 . \tag{4.36}$$

This yields the maximum flow rate at $S = 1$ as

$$Q_{max} = Ac , \tag{4.37}$$

where A and c refer to the point at which $S = 1$. Thus, for a fixed value of P_0 and p_e, there is a certain value of p for which the flow Q is a maximum. A similar phenomenon of flow limitation occurs in gas-dynamics and in open-channel flow over a weir.

4.4 Simplified Analysis of Steady Shock Wave

As mentioned previously, when a steady shock wave is formed in a collapsible tube, two mechanisms not usually accounted for in the model based on one-dimensional fluid flow and the tube law for uniform collapse come into play. They are:

(1) The modification of the tube law due to (a) longitudinal wall curvature in combination with longitudinal tension; (b) bending moments induced in the wall. These effects are equivalent to a radially-directed pressure which can be interpreted as an additional transmural pressure.

(2) The rapidly increasing area and decreasing fluid velocity leads to flow separation from the wall. This results in a three-dimensional jet-like flow with eddies and subsequent re-entrainment further downstream of the area expansion. This would result in large stagnation pressure losses by the conversion of mean flow energy into rotational energy of the eddies.

A. Model 1

A simplified analysis which embodies the essential features of such a shock-like transition was put forward by Shapiro.[2] As shown in Fig. 14, the flow is assumed to be essentially one-dimensional at cross-sections (1) and (2) sufficiently upstream and downstream of the shock, respectively. It is assumed that the jet separation is so sharp that the pressure acting on the area $(A_2 - A_1)$ is the inlet pressure p_1.

For the control volume shown, conservation of mass yields

$$A_1 u_1 = A_2 u_2 \quad . \tag{4.38}$$

Thus,

$$\frac{u_2}{u_1} = \frac{A_1}{A_2} = \frac{\alpha_1}{\alpha_2} \quad . \tag{4.39}$$

Conservation of momentum yields

$$A_2(p_1 - p_2) = \rho A_1 u_1 (u_2 - u_1) \quad . \tag{4.40}$$

Using (4.39) in (4.40) gives for the pressure recovery coefficient

$$C_{p_c} \equiv \frac{p_2 - p_1}{\frac{1}{2}\rho u_1^2} = 2\frac{\alpha_1}{\alpha_2}\left(1 - \frac{\alpha_1}{\alpha_2}\right) \quad . \tag{4.41}$$

The actual recovery can be expected to be greater than this value, which was obtained for very sharp separation.

The pressure recovery given by (4.41) will therefore be referred to as Carnot recovery. The loss in stagnation pressure P_0 is determined by

$$P_{01} - P_{02} = p_1 - p_2 + \tfrac{1}{2}\rho u_1^2 - \tfrac{1}{2}\rho u_2^2 \quad . \tag{4.42}$$

Using Eqs. (4.39) and (4.41) in (4.42) gives

$$\left(\frac{P_{01} - P_{02}}{\frac{1}{2}\rho u_1^2}\right)_c = \left(1 - \frac{\alpha_1}{\alpha_2}\right)^2 > 0 \quad , \tag{4.43}$$

which shows that a severe shock leads to a head loss. Using thermodynamic principles, Oates[27] showed that all shocks (strong or weak) are accompanied by head losses.

If the tube law for the uniform tube is given by

$$(p - p_e) = K_B\, P(\alpha) \quad , \tag{4.44}$$

then

$$C_{P_c} \equiv \frac{p_2 - p_1}{\frac{1}{2}\rho u_1^2} = \frac{2K_B}{\rho u_1^2}\left[P(\alpha_2) - P(\alpha_1)\right] \quad . \tag{4.45}$$

From Eqs. (4.41) and (4.45), α_2 can be found if the inlet conditions (u_1, α_1) are known. For certain simplified forms of the tube law, Shapiro[2] has shown the possibility of critical or supercritical flow at the exit to the shock. However, in the experiments reported here, only subcritical flows at the exit were observed.

B. Model 2

In this approximate analysis, the essential difference from Model 1 is that we do not make the assumption that the wall pressure acting on the area $(A_2 - A_1)$ is equal to the inlet pressure p_1. Instead, we assume that the tube law for uniform collapse is valid throughout the shock region. Hence, this is also a very approximate analysis.

The principle of conservation of momentum applied to the control volume with friction neglected gives

$$p_1A_1 - p_2A_2 + \int_1^2 p\, dA = \rho A_1 u_1 (u_2 - u_1) \quad . \tag{4.46}$$

Using the continuity equation (4.39), this can be written as

$$(p_1 - p_e)\alpha_1 - (p_2 - p_e)\alpha_2 + \int_1^2 (p - p_e)\, d\alpha = \rho\alpha_1 u_1^2\left(\frac{\alpha_1}{\alpha_2} - 1\right) \quad . \tag{4.47}$$

Now,

$$C_p \equiv \frac{p_2 - p_1}{\frac{1}{2}\rho u_1^2} = \frac{(p_2 - p_e) - (p_1 - p_e)}{\frac{1}{2}\rho u_1^2} \quad . \tag{4.48}$$

Using (4.47) and the tube law (4.44) in (4.48) yields, after some manipulation,

$$C_{p_o} = C_{p_c} + \Delta C_p \quad , \tag{4.49}$$

where

$$\Delta C_p \equiv \frac{2K_B}{\rho u_1^2}\left[\frac{1}{\alpha_2}\int_1^2 P(\alpha)\, d\alpha - P(\alpha_1)\left(1 - \frac{\alpha_1}{\alpha_2}\right)\right] \quad , \tag{4.50}$$

where C_{p_c} is the Carnot efficiency given by (4.41). The first term of ΔC_p is negative and $P(\alpha_1) < 0$ for shocks experimentally observed. Thus the possibility exists that

$$\Delta C_p > 0 \quad , \tag{4.51}$$

so that Model 2 predicts a higher pressure recovery than Model 1.

Further,

$$\left(\frac{P_{01} - P_{02}}{\frac{1}{2}\rho u_1^2}\right)_0 = \left(\frac{P_{01} - P_{02}}{\frac{1}{2}\rho u_1^2}\right)_C - \Delta C_p \quad , \tag{4.52}$$

so that the Oates stagnation pressure loss is smaller than Carnot's.

Aside from the simplified analysis such as the preceding ones, it is not possible to theoretically model the detailed structure of a shock wave without resorting to very complex numerical procedures for analyzing the fluid mechanics and the tube mechanics in the shock region. Very few analytical models exist for separated turbulent flows, which

is one of the most difficult and outstanding problems in fluid mechanics. Recently Woolley and Kline[54] have been successful in developing a numerical procedure for predicting the boundary layer development and performance in a fully stalled diffuser flow. Numerical solutions for two-dimensional stall have been reported by Fromm.[55] However, solution of the stalled diffuser problem, in combination with the structural mechanics of the tube, would be a formidable task, well beyond the scope of this work.

4.5 The Structure of Precursor Waves

An important finding in the present experimental work on standing shock waves is that the shock wave is preceded by a train of standing area and pressure waves. These are found to increase in amplitude and wavelength as one proceeds downstream towards the shock as shown in Figs. (30) - (48). No such waves have been observed downstream of the shock.

An analysis of the structure of these precursor waves, unlike that of the shock itself, is possible within the context of the one-dimensional steady flow equations developed in Section 4.2, if the first-order corrections to the uniform collapse tube law is taken into account. Accordingly, in this section, an approximate analysis of the precursor waves, valid for the conditions of the experiments reported here, is presented.

It is assumed in this analysis that the shape of the collapsible tube cross-section in the region sufficiently upstream of the shock, can be approximated by the shape shown in Fig. 8. Thus, the deformation of the wall is represented by the variable η which is related to the area ratio α by Eq. $(2.28)_2$:

$$\frac{\eta}{R_0} = 1 - \sqrt{1 - \alpha} \tag{4.53}$$

If the area gradients are small, then

$$\frac{d^2\eta}{dx^2} \simeq \frac{R_0}{2\sqrt{1-\alpha}} \frac{d^2\alpha}{dx^2} \tag{4.54}$$

It is further assumed that, for small area gradients the steady flow of fluid can still be described by the one-dimensional continuity (4.21) and momentum (4.24) equations. The combined effects of longitudinal wall curvature and wall tension on the tube law is accounted for by means of an effective external pressure $\hat{p}_e$ as defined by (4.19). Thus, Eqs. (4.29) to (4.33) together describe the spatial growth or decay of the flow quantities in the longitudinal direction.

A modified tube law accounting for wall curvature, wall tension, and bending effects was derived in Chapter II and is given by Eq. (2.41). This equation can be considerably simplified by estimating the orders of magnitude of the various terms appearing in it. In particular, it was shown that (Eq. (2.45)) bending effects would be small if

$$\frac{1}{12(1 - \nu^2)\varepsilon_{xx}} \left(\frac{t}{\lambda} \right)^2 \ll 1 \qquad (4.55)$$

In the above inequality, λ is characteristic of the distance over which the area changes significantly; t and ν are the thickness and Poisson ratio of the tube wall respectively.

In the experiments reported here, the smallest wavelengths are of the order of 4.0 cm; $t = 0.083$ cm and $\nu \sim 0.5$. The longitudinal strain ε_{xx} can be taken to be approximately equal to the prestrain (0.06) on the tube wall. Then, the left-hand side of (4.55) is equal to 7.9×10^{-4} and therefore bending effects in the longitudinal direction can be safely neglected.

Replacing the lower limit of the integral in $(2.41)_2$ by $\bar{x}$ and T_1 by $\overline{T}$, where $\bar{x}$ is any arbitrary point along the tube axis, yields

$$(\hat{p} - p_e) = K_B P(\alpha) - \frac{d^2\eta}{dx^2} (\overline{T} - \int_{\bar{x}}^{x} \tau_w dx) \tag{4.56}$$

Definition (4.19) together with (4.18) and (4.56) give the effective external pressure as

$$\hat{p}_e = p_e - \frac{d^2\eta}{dx^2} (\overline{T} - \int_{\bar{x}}^{x} \tau_w dx) \tag{4.57}$$

Using the approximation (4.54) in (4.57) gives

$$\hat{p}_e = p_e - \frac{R_0}{2\sqrt{1-\alpha}} \frac{d^2\alpha}{dx^2} (\overline{T} - \int_{\bar{x}}^{x} \tau_w dx) \tag{4.58}$$

Substituting for $\hat{p}_e$ in (4.29) yields

$$\frac{(1-S^2)}{\alpha} \frac{d\alpha}{dx} = -\frac{S^2}{2} \frac{4f}{D_0} + \frac{1}{\rho c^2} \frac{d}{dx} \left[\frac{R_0}{2\sqrt{1-\alpha}} \frac{d^2\alpha}{dx^2} (\overline{T} - \int_{\bar{x}}^{x} \tau_w dx) \right] \tag{4.59}$$

Also, from (4.29) and (4.30)

$$\frac{dS}{dx} = -\frac{MS}{2\alpha} \frac{d\alpha}{dx} \tag{4.60}$$

Equations (4.59) and (4.60) represent two coupled, nonlinear, ordinary differential equations for the speed index S and the area ratio α. The solution to these equations, subject to appropriate boundary conditions, can be computed using a suitable numerical scheme.

However, the character of the solutions to these equations can be approximately examined by means of a perturbation analysis about an arbitrary location $x = \bar{x}$. The perturbation quantities (α', S', etc.) are taken to be much smaller than the values ($\bar{\alpha}$, $\bar{S}$, etc.) at the point at which the perturbation analysis is performed.

Accordingly,

$$\begin{aligned} x &= \bar{x} + D_0\zeta \\ \alpha &= \bar{\alpha} + \alpha' \\ S &= \bar{S} + S' \\ f &= \bar{f} + f' \\ c &= \bar{c} + c' \\ \tau_w &= \bar{\tau}_w + \tau_w' \end{aligned} \tag{4.61}$$

with

$$\alpha'/\bar{\alpha} << 1; \quad S'/\bar{S} << 1; \quad \text{etc.} \tag{4.62}$$

Further,

$$\frac{d\alpha}{dx} = \frac{1}{D_0}\frac{d\alpha'}{d\zeta} \; ; \quad \frac{d^2\alpha}{dx^2} = \frac{1}{D_0^2}\frac{d^2\alpha'}{d\zeta^2} \tag{4.63}$$

Consistent with the one-dimensional formulation, it is assumed that

$$D_0 \frac{d\alpha}{dx} \sim \left(\frac{\Delta\alpha}{\lambda/D_0}\right) << 1 \tag{4.64}$$

where $\Delta\alpha$ is the change in area occuring over the distance λ which characterizes the longitudinal gradients. This condition is satisfied

by the precursor waves observed. The variation of wall tension due to fluid drag over distances of the order of λ can be neglected if

$$\frac{\int_{\bar{x}}^{x} \tau_w dx}{\bar{T}} \sim \frac{\bar{\tau}_w \lambda}{\bar{T}} << 1 \tag{4.65}$$

For the present experimental conditions, estimation of wall tension by (2.44) and wall friction by (3.21) shows the above quantity to be from one to two orders of magnitude smaller than unity. Consequently, this quantity will be neglected.

With the foregoing approximation, Eq. (4.59) and (4.60) can be linearized about $x = \bar{x}$ as follows.

From Eq. (4.60)

$$S' = \frac{dS}{d\alpha}\Big|_{\bar{\alpha}} \alpha' = -(\bar{M}\,\bar{S}/2\bar{\alpha})\alpha' \tag{4.66}$$

Also,

$$f' = \frac{df}{d\alpha}\Big|_{\bar{\alpha}} \alpha' = -\left(\frac{\bar{\gamma}\,\bar{f}}{\bar{\alpha}}\right)\alpha' \tag{4.67}$$

where

$$\bar{\gamma} \equiv \frac{\bar{\alpha}}{\bar{f}} \frac{d\bar{f}}{d\alpha}$$

Then, from Table I

$$\bar{\gamma} = 0.375 \quad , \quad \bar{\alpha} < 0.36$$

$$\bar{\gamma} = 1.0 \quad , \quad 0.36 \leq \bar{\alpha} \leq 1.0 \tag{4.68}$$

Moreover,

$$\frac{1 - S^2}{\alpha} \frac{d\alpha}{dx} \simeq \frac{1 - \bar{S}^2}{D_0 \bar{\alpha}} \frac{d\alpha'}{d\zeta}$$

$$\frac{S^2}{2} \frac{4f}{D_0} \simeq \frac{\bar{S}^2}{2} \frac{4\bar{f}}{D_0} \left[1 + 2 \frac{S'}{S} + \frac{f'}{\bar{f}}\right] \tag{4.69}$$

Using (4.66) and (4.67)

$$\frac{S^2}{2} \frac{4f}{D_0} \simeq \frac{\bar{S}^2}{2} \frac{4\bar{f}}{D_0} \left[1 - (\bar{M} + \bar{\gamma}) \frac{\alpha'}{\bar{\alpha}}\right] \tag{4.70}$$

$$\frac{1}{\rho c^2} \frac{d}{dx} \left[\frac{R_0}{2\sqrt{1-\alpha}} \frac{d^2\alpha}{dx^2} (\bar{T} - \int_{\bar{x}}^{x} \tau_w dx)\right] \simeq \frac{1}{4\rho \bar{c}^2} \frac{\bar{T}}{D_0^2 \sqrt{1-\alpha}} \frac{d^3\alpha'}{d\zeta^3} \tag{4.71}$$

Thus, Eq. (4.59) for α' becomes

$$\frac{\bar{T} \bar{\alpha}}{4\rho \bar{c}^2 D_0 \sqrt{1-\bar{\alpha}}} \frac{d^3\alpha'}{d\zeta^3} + (\bar{S}^2 - 1) \frac{d\alpha'}{d\zeta} +$$

$$+ 2 \bar{S}^2 \bar{f}(\bar{M} + \bar{\gamma})\alpha' = 2\bar{S}^2 \bar{f} \bar{\alpha} \tag{4.72}$$

The above equation is a third order, linear differential equation to which a solution can be readily found. If longitudinal bending terms

had been retained, a fifth order, linear differential equation would have been obtained. In the above equation, the first term represents the combined effects of wall tension and longitudinal wall curvature. The second term is derived from the inertia of the fluid and the circumferential elastic forces of the tube wall. The third and fourth terms represent the effects of wall friction.

The most important feature of this equation is that due to the presence of the wall curvature term area gradients no longer become singular when the speed index approaches unity. Moreover, there now exists the possibility of oscillatory growth of area with longitudinal distance. To examine this behavior, equation (4.72) is recast as

$$\frac{d^3\alpha'}{d\zeta^3} + 3a\frac{d\alpha'}{d\zeta} + 2b\alpha' = r \tag{4.73}$$

where

$$a \equiv \frac{1}{3}\frac{(\bar{S}^2 - 1)}{\varepsilon}$$

$$b \equiv \frac{\bar{S}^2 \bar{f}(\bar{M} + \bar{\gamma})}{\varepsilon} \tag{4.74}$$

$$r \equiv \frac{2\bar{S}^2 \bar{f}\,\bar{\alpha}}{\varepsilon}$$

$$\varepsilon \equiv \frac{\bar{T}\,\bar{\alpha}}{4\rho\bar{c}^2 D_0\sqrt{1-\bar{\alpha}}}$$

The solution of equation (4.73) has the form

$$\alpha' = C_1 \exp(m_1\zeta) + C_2 \exp(m_2\zeta) + C_3 \exp(m_3\zeta) + \frac{r}{2b} \qquad (4.75)$$

where C_1, C_2, C_3 are arbitrary constants, and m_1, m_2, m_3 are the roots of the cubic equation

$$m^3 + 3am + 2b = 0 \qquad (4.76)$$

If $(a^3 + b^2) > 0$, then (4.76) has one real root and a pair of complex conjugate roots given by

$$m_1 = (s_1 + s_2) \; ; \quad m_2 = \frac{-1}{2}(s_1 + s_2) + i\,\frac{\sqrt{3}}{2}(s_1 - s_2)$$

$$m_3 = -\frac{1}{2}(s_1 + s_2) - i\,\frac{\sqrt{3}}{2}(s_1 - s_2) \qquad (4.77)$$

where s_1, s_2 are real quantities defined by

$$s_1 \equiv [-b + \sqrt{a^3 + b^2}\,]^{1/3} \; ; \quad s_2 = [-b - \sqrt{a^3 + b^2}\,]^{1/3}$$

If $(a^3 + b^2) = 0$, all roots are real and at least two are equal. If $(a^3 + b^2) < 0$, the roots are real and unequal, and they are given by

$$m_1 = 2|a|^{1/2} \cos[\phi/3]$$

$$m_2 = -2|a|^{1/2} \cos[(\phi + \pi)/3] \qquad (4.78)$$

$$m_3 = -2|a|^{1/2} \cos[(\phi - \pi)/3]$$

where

$$\cos \phi = - b|a|^{-3/2}$$

Precursor waves of increasing amplitude can occur only if two roots are complex, and if their real parts are positive. Thus, it is necessary that the following conditions be simultaneously satisfied.

$$\text{Wave existence: } a^3 + b^2 > 0$$

$$\text{Wave growth: } s_1 + s_2 < 0 \quad \text{i.e., } b > 0 \quad . \qquad (4.79)$$

These conditions are equivalent to

$$(\bar{S}^2 - 1)^3 + 27\, \bar{S}^4 \bar{f}^{\,2} (\bar{M} + \bar{\gamma})^2 \; \varepsilon > 0$$

$$\bar{S}^2 \bar{f} (\bar{M} + \bar{\gamma}) / \; \varepsilon > 0 \qquad (4.80)$$

For supercritical flow $a > 0$ and expression (4.80) is satisfied. In Appendix B the values of a, b, γ, and ε are calculated for one location ($\bar{\alpha} = 0.4$) in an experimentally obtained shock-wave area and pressure distribution. These values are typical for the experimental

data reported here. The variation of M with α, as obtained by direct numerical differentiation of tube law data is shown in Fig. (13). It shows M to be a positive function of α except in the range $0.27 < \alpha < 0.33$ when it becomes significantly negative. In this region, however, the tube law shows sharp variations and the numerical differentiation should not be considered too accurate. The quantity $(M + \gamma)$ in $(4.80)_2$ is thus positive over most of the range of α in which precursor waves are observed, in agreement with requirement $(4.80)_2$.

Equation (4.75) for the area perturbation α' can also be written as

$$\alpha' = r/2b + C_1 \exp(-2\beta_1\zeta) + C_2 \exp(\beta_1\zeta) \sin(\beta_2\zeta) + \\ + C_3 \exp(\beta_1\zeta) \cos(\beta_2\zeta) \tag{4.81}$$

where

$$\beta_1 \equiv -(s_1 + s_2)/2 \; ; \; \beta_2 \equiv \frac{\sqrt{3}}{2}(s_1 - s_2) \tag{4.82}$$

In the present experiments, the magnitudes of a and b are such that $b\, a^{-3/2}$ is always a small quantity compared to unity. It is then possible to approximate s_1, s_2 by

$$s_{1,2} = -\frac{1}{3}\frac{b}{a} \pm \sqrt{a} \tag{4.83}$$

provided

$$b\, a^{-3/2} \ll 1 \quad \text{and} \quad a > 0 \quad .$$

Hence,

$$\beta_1 \simeq \frac{1}{3}\frac{b}{a} \quad ; \quad \beta_2 \simeq \sqrt{3\,a} \tag{4.84}$$

Further

$$\frac{r}{2b} = \left(\frac{\bar{\alpha}}{\bar{M} + \bar{\gamma}}\right) \tag{4.85}$$

The area perturbation α' is the total growth in area about the mean area $\bar{\alpha}$. It is useful to consider separately the mean ($\hat{\alpha}$) and oscillatory ($\tilde{\alpha}$) components of this growth as indicated in Fib. (62). Thus,

$$\alpha = \bar{\alpha} + \alpha' = \bar{\alpha} + \hat{\alpha} + \tilde{\alpha} \tag{4.86}$$

where

$$\begin{aligned} \hat{\alpha} &\equiv \left(\frac{\bar{\alpha}}{\bar{M} + \bar{\gamma}}\right) + C_1 \exp(-2\,\beta_1\zeta) \\ \tilde{\alpha} &\equiv C_2 \exp(\beta_1\zeta)\sin(\beta_2\zeta) + C_3 \exp(\beta_1\zeta)\cos(\beta_2\zeta) \end{aligned} \tag{4.87}$$

With the above definitions, $(\bar{\alpha} + \hat{\alpha})$ represents the area in the absence of precursor waves. Also, $\hat{\alpha}$ satisfies equation (4.72) neglecting the effects of longitudinal tension. That is, it satisfies the equation

$$(\bar{S}^2 - 1)\,\frac{d\hat{\alpha}}{d\zeta} + 2\,\bar{S}^2\,\bar{f}\,(\bar{M} + \bar{\gamma})\hat{\alpha} = 2\,\bar{S}^2\,\bar{f}\,\bar{\alpha} \tag{4.88}$$

Setting $\alpha'(0) = \hat{\alpha}(0) = 0$ gives

$$C_1 = -\frac{\bar{\alpha}}{\bar{M} + \bar{\gamma}} \quad ; \qquad C_3 = 0 \ . \tag{4.89}$$

The positions $\bar{x}$ are now chosen to be inflection points in the area curve (see Fig. (62)). This also facilitates the interpretation of the experimental data. Thus,

$$\frac{d^2\alpha}{d\zeta^2}\Big|_{\zeta=0} = \frac{d^2\alpha'}{d\zeta^2}\Big|_{\zeta=0} = 0 \tag{4.90}$$

This is satisfied by the choice

$$C_2 = \frac{\bar{\alpha}}{(\bar{M} + \bar{\gamma})} \frac{2\beta_1}{\beta_2} \tag{4.91}$$

Hence,

$$\begin{aligned} \frac{\hat{\alpha}}{\bar{\alpha}} &= \frac{1}{(\bar{M} + \bar{\gamma})} (1 - \exp(-2\beta_1\zeta)) \\ \frac{\tilde{\alpha}}{\bar{\alpha}} &= \frac{1}{(\bar{M} + \bar{\gamma})} \frac{2\beta_1}{\beta_2} \exp(\beta_1\zeta) \sin(\beta_2\zeta) \end{aligned} \tag{4.92}$$

Using equations (4.84) and (4.74)

$$\frac{\beta_1}{\beta_2} \simeq \frac{b\, a^{-3/2}}{\sqrt{27}} = \frac{\bar{S}^2}{(\bar{S}^2 - 1)^{3/2}} \sqrt{\varepsilon}\ \bar{f}\ (\bar{M} + \bar{\gamma}) << 1 \tag{4.93}$$

and

$$\frac{\tilde{\alpha}}{\bar{\alpha}} = \frac{2\sqrt{\varepsilon}\,\bar{S}^2\,\bar{f}}{(\bar{S}^2 - 1)^{3/2}} \exp(\beta_1\zeta) \sin(\beta_2\zeta) \tag{4.94}$$

The wavelength $\bar{\lambda}$ of the precursor waves is given by

$$\frac{\bar{\lambda}}{D_0} \equiv \frac{2\pi}{\beta_2} \qquad \frac{2\pi}{\sqrt{3a}} \tag{4.95}$$

Over a distance of one wavelength in the neighborhood of $x = \bar{x}$, the amplitude of each term of (4.94) increases by a multiplicative factor equal to

$$\exp(\beta_1 \frac{\bar{\lambda}}{D_0}) \simeq \exp(\frac{2\pi}{3\sqrt{3}} b\, a^{-3/2}) \tag{4.96}$$

Assuming that $\bar{S}^2 >> 1$, it can be shown from (4.95) that

$$\frac{\bar{\lambda}}{D_0} \simeq (\frac{\pi^2 A_0^2}{Q^2} \frac{\bar{T}}{\rho D_0})^{1/2} \frac{\bar{\alpha}^{3/2}}{(1 - \bar{\alpha})^{1/4}} \tag{4.97}$$

Alternatively,

$$\frac{\bar{\lambda}}{D_0} \simeq (\frac{\pi^2 Q}{A_0} \frac{\bar{T}}{\rho D_0})^{1/2} \frac{\bar{u}^{-3/2}}{[1 - \frac{Q}{A_0 \bar{u}}]^{1/4}} \tag{4.98}$$

Similarly, from (4.96)

$$(\frac{2\pi}{3\sqrt{3}} b\, a^{-3/2}) \simeq (\bar{M} + \bar{\gamma}) \frac{\bar{f}}{\bar{u}} (\frac{\bar{T}}{\rho D_0} \frac{\bar{\alpha}}{\sqrt{1 - \bar{\alpha}}})^{1/2} \tag{4.99}$$

The above expression can be expressed entirely in terms of $\bar{\alpha}$ by using the equation of continuity and the appropriate friction factor from Table I. Thus,

$$\left(\frac{2\pi}{3\sqrt{3}} \, b \, a^{-3/2} \right) \simeq \frac{0.0791}{Re_{D_0}^{0.25}} \left(\bar{M} + \bar{\gamma} \right) \frac{\pi A_0}{Q} \left(\frac{\bar{T}}{\rho D_0} \frac{\bar{\alpha}}{\sqrt{1 - \bar{\alpha}}} \right)^{1/2} \tag{4.100}$$

It is useful at this point to estimate the relative contributions of the mean and oscillatory flow components to the total stagnation pressure loss due to fluid friction. The total stagnation pressure drop over one wavelength centered about a mean position $x = \bar{x}$ is given by

$$\Delta p_f = \int_{\bar{x} - \frac{1}{2}\bar{\lambda}}^{\bar{x} + \frac{1}{2}\bar{\lambda}} \frac{4 f}{D_0} \frac{1}{2} \rho u^2 \, dx \tag{4.101}$$

Hence, employing the definitions (4.61)

$$\Delta p_f = 4 \bar{f} \int_{-\frac{1}{2}\bar{\lambda} D_0}^{+\frac{1}{2}\bar{\lambda} D_0} \left(1 + \frac{f'}{\bar{f}}\right)\left(1 + \frac{u'}{\bar{u}}\right)^2 d\zeta \simeq$$

$$\simeq 4 \bar{f} \int_{-\frac{1}{2}\bar{\lambda} D_0}^{+\frac{1}{2}\bar{\lambda} D_0} \left(1 + \frac{f'}{\bar{f}} + 2 \frac{u'}{\bar{u}}\right) d\zeta \tag{4.102}$$

This can be expressed in terms of area ratio components using the following relations

$$\frac{u'}{\bar{u}} = \frac{1}{\bar{\gamma}} \frac{f'}{\bar{f}} = - \frac{\alpha'}{\bar{\alpha}} = - \left(\frac{\hat{\alpha} + \tilde{\alpha}}{\bar{\alpha}} \right) \tag{4.103}$$

As a result, (4.102) can be expressed as follows

$$\Delta p_f = \overline{\Delta p_f} + \hat{\Delta p}_f + \tilde{\Delta p}_f \tag{4.104}$$

where

$$\Delta p_f \equiv \frac{4\bar{f}\,\bar{\lambda}}{D_0}\ \frac{1}{2}\,\rho\,\bar{u}^{\,2} \tag{4.105}$$

$$\frac{\hat{\Delta p}_f}{\overline{\Delta p_f}} = -\,(2 + \bar{\gamma})\,\frac{D_0}{\bar{\lambda}} \int_{-\frac{1}{2}\bar{\lambda} D_0}^{+\frac{1}{2}\bar{\lambda} D_0} \frac{\hat{\alpha}}{\bar{\alpha}}\, d\zeta \tag{4.106}$$

$$\frac{\tilde{\Delta p}_f}{\overline{\Delta p_f}} = -\,(2 + \bar{\gamma})\,\frac{D_0}{\bar{\lambda}} \int_{-\frac{1}{2}\bar{\lambda} D_0}^{+\frac{1}{2}\bar{\lambda} D_0} \frac{\tilde{\alpha}}{\bar{\alpha}}\, d\zeta \tag{4.107}$$

The integrals in (4.106) and (4.107) can be evaluated by using expressions (4.92) for $\hat{\alpha}$ and $\tilde{\alpha}$. This yields

$$\frac{\hat{\Delta p}_f}{\overline{\Delta p_f}} = -\left(\frac{2 + \bar{\gamma}}{\bar{M} + \bar{\gamma}}\right)\left(1 - \frac{\sinh(2\pi\beta_1/\beta_2)}{(2\pi\beta_1/\beta_2)}\right) \tag{4.108}$$

$$\frac{\tilde{\Delta p}_f}{\overline{\Delta p_f}} = -\left(\frac{2 + \bar{\gamma}}{\bar{M} + \bar{\gamma}}\right)\left(\frac{2\beta_1^2}{\beta_1^2 + \beta_2^2}\right)\left(\frac{\sinh(\pi\beta_1/\beta_2)}{(\pi\beta_1/\beta_2)}\right)$$

Since $\beta_1/\beta_2 \ll 1$ relations (4.108) can be approximated by

$$\frac{\hat{\Delta p}_f}{\overline{\Delta p_f}} \simeq -\frac{2\pi}{3}\left(\frac{2+\bar{\gamma}}{\bar{M}+\bar{\gamma}}\right)\left(\frac{\beta_1}{\beta_2}\right)^2$$

$$\frac{\tilde{\Delta p}_f}{\overline{\Delta p_f}} \simeq -2\left(\frac{2+\bar{\gamma}}{\bar{M}+\bar{\gamma}}\right)\left(\frac{\beta_1}{\beta_2}\right)^2 \qquad (4.109)$$

The above relations show that frictional stagnation pressure losses due to mean area growth and oscillatory area growth are very nearly equal. They also show that they are much smaller than the loss $\overline{\Delta p_f}$ which corresponds to the loss at a fixed area ratio $\bar{\alpha}$ over a distance equal to one wavelength.

In an attempt to determine the dispersion relationship that governs the behavior of the waves in the precursor wavetrain we combine Eqs. (4.95), $(4.74)_{1,4}$, and (2.44). The obtained relationship is given as follows.

$$\bar{u}^2 - \bar{c}^2 = \frac{\varepsilon_{xx}\,\bar{\alpha}}{\lambda^2\sqrt{1-\bar{\alpha}}} \quad \frac{\pi E t P}{\rho} \qquad (4.110)$$

where $\bar{c}$ is the speed of propagation of small amplitude waves corresponding to the base area ratio $\bar{\alpha}$, Fig. (2), ε_{xx} is the longitudinal prestrain of the tube, E is the Young's modulus of the tube, t is the thickness of the tube, P is the perimeter of the cross-sectional area of the tube, and ρ is the density of the fluid flowing through the tube. In Eq. (4.110), λ is the wavelength of the precursor wave located at $\bar{x}$, and $\bar{u}$ is equivalent to the speed of propagation of the precursor wave as seen

by one moving with the mean speed of the fluid inside the collapsible tube.

From Eq. (4.110), if $\varepsilon_{xx}\,\bar{\alpha}/\lambda^2\sqrt{1-\bar{\alpha}}$ is plotted against $(\bar{u}^2 - \bar{c}^2)$, it can be seen that the data points should fall on a straight line the slope of which, m_{theo}, is given by the equation

$$m_{theo} = \frac{\rho}{\pi E t P} \qquad (4.110a)$$

Summarizing, it is seen that this approximate one-dimensional model incorporating fluid friction and inertia, and a modified tube law, accounting for longitudinal wall curvature and wall tension, is capable of predicting the formation and behavior of precursor waves. For the uniform tube considered, wall curvature and wall tension are necessary for wave formation and frictional effects are essential for their growth.

The conditions under which precursor waves can exist and grow, within the assumptions of this analysis, are given by $(4.80)_{1,2}$. For the experimental conditions reported here, simplified expressions for the wavelength and rate of growth of the precursor waves are given by (4.87) and (4.89) respectively. In Appendix B, this simplification is justified and the theoretical wavelength is computed from (4.87) for a single location in an experimentally determined area and pressure distribution. The agreement between experimental and theoretical values for the wavelength is found to be satisfactory.

CHAPTER V

EXPERIMENTAL DETERMINATION OF SHOCK STRUCTURE

In the preceding theory, the essential features of a steady shock wave in fluid flow through a collapsible tube were outlined.

The purpose of this experimental investigation is to confirm the basic features predicted by the approximate analyses and to provide a body of experimental data regarding the detailed structure of such shock waves. Specifically, the cross-sectional area and fluid pressure within a steady shock formed in a long, thin-walled rubber latex tube was determined as a function of distance along the tube. This information is expected to provide insight and to form a basis of comparison for detailed theoretical analyses in the future.

In Section 5.1 of this chapter, the design of the experimental apparatus and the criteria established for its overall design are discussed. The instrumentation used in the measurements, the potential sources of error, and the minimization of these errors are presented in Section 5.2. Lastly, the experimental procedure adopted in making the measurements and a listing of the experiments that were performed are given in Section 5.3.

5.1 Design of the Experiment

In order to design the experiment in a physically meaningful way it is first necessary to determine the governing non-dimensional groupings. This can be done either by dimensional arguments or more directly by non-dimensionalizing the governing equations presented in Section 4.2.

Further, the modified tube law of Eq. (2.39) which includes the effect of wall curvature and longitudinal tension is employed in these equations. The dimensionless groupings are obtained by scaling the physical quantities appearing in these equations in the following way:

(1) Transmural pressure $(p - p_e) \sim K_B$, where K_B is the bending stiffness.

(2) Longitudinal distance $x \sim \lambda$, where λ is a distance characterizing the wall curvature.

(3) Changes in cross-sectional area $A \sim \Delta A$ where ΔA is characteristic of the change in cross-sectional area along the tube.

(4) Flow velocity $u \sim u_1$, where u_1 is the flow speed at the inlet to the section upstream of the shock.

(5) Cross-sectional area $A \sim D^2$, where D is the equivalent diameter $\sqrt{4A/\pi}$.

The transmural pressure at any point in the tube must have the functional dependence given by the expression

$$(p - p_e) = fn[u_1, \Delta A, D, \lambda, T_1, K_B, \mu, \rho, p_2 - p_e] \, . \qquad (5.1)$$

As mentioned previously the governing non-dimensional parameters were obtained by non-dimensionalizing the governing equations. This gives

$$\frac{p - p_e}{K_B} = fn\left[\frac{\rho u_1^2}{K_B}, \frac{u_1 D}{\nu}, \frac{D}{\lambda}, \frac{\Delta A}{\lambda D}, \frac{\Delta A}{\lambda D}\frac{T_1}{K_B}, \frac{p_2 - p_e}{K_B} \right] \, . \qquad (5.2)$$

In this expression the first group is proportional to the speed index S which characterizes the relative importance of inertia and elastic forces. The second group is the Reynolds number which characterizes the relative importance of inertia and viscous forces. The third dimensionless parameter is representative of the change in hydraulic diameter with distance. The fourth group represents the effects of wall curvature in general. The sixth group combines the effect of wall curvature with the effect of wall tension and represents the resulting radially directed effective pressure.

It is more convenient if the groups in (5.2) are replaced by the equivalent set given by

$$\frac{p - p_1}{\frac{1}{2} \rho u_1^2} = fn\left[S_1, Re_{D_h}, \frac{D}{\lambda}, \frac{A_2 - A_1}{\lambda D}, \frac{A_2 - A_1}{\lambda D} \frac{T_1}{K_B}, \frac{p_2 - p_e}{K_B}\right] \quad (5.3)$$

This expresses the pressure recovery coefficient as a function of the inlet speed index and the Reynolds number based on the hydraulic diameter at the inlet. The area ΔA has been replaced by the difference between the exit and inlet areas.

In the above expression, S_1, Re_{D_h}, and $(p_2 - p_e)/K_B$ can be continuously controlled by suitable design of the apparatus. The wall tension group can only be controlled in a step-wise manner between experiments by adjusting the pretension on the tube. The range of variation of various parameters in the experiments performed is given in Table 2.

The general criteria that were established for the design of the experiment are listed below:

(1) The collapsible tube should be sufficiently long to avoid edge effects.

(2) The inlet speed index S_1 should be capable of being varied over a wide range. Thus it should be possible to form strong as well as weak shocks.

(3) The upstream and downstream pressures should be independently adjustable.

(4) The wall tension should be adjustable at the beginning of an experiment.

(5) No gradients in density should be present.

(6) The measurement of area and pressure distributions should be possible in a continuous manner in a short time. This is necessary as initial experiments indicated that the shock tends to drift in position.

(7) The measurement system should be sufficiently accurate and should not unduly disturb the fluid flow.

(8) The tube should collapse uniformly along its length.

A. The Apparatus

The apparatus that was designed to satisfy the preceding design criteria is shown in Fig. (17). It consists of a tube of latex rubber (I.D. = 2.54 cm; wall thickness = 0.083 cm; length = 106.5 cm; Young's modulus $E = 1.6 \times 10^7$ dynes/cm^2) mounted on rigid cylindrical end tubes (O.D. = 3.22 cm; I.D. = 2.50 cm) passing through the opposite sides of an open tank. The collapsible tube was immersed in a glycerine-water solution contained in the tank. The density of the glycerine-water solution was matched to better than 1/2% to the density of the salt solution (concentration 20% by weight) within the flow system, thereby eliminating buoyancy effects. The salt solution was supplied to the test section by a recirculating centrifugal pump and was discharged from the

test section into a constant-head sump tank. The recirculating pump was provided with a bypass connection leading to the discharge tank so that its output flow could be more easily controlled. The transmural pressure at the exit of the collapsible tube and the flowrate through it were controlled by adjustment of valves in the rigid supply and discharge lines. The external surface of the rigid support pipe at the downstream end was tapered so that flow disturbances at the exit could be minimized.

Supercritical flow ($S > 1$) was established by an adjustable sphincter formed by a pair of external "fingers" which compressed the tube. Thus, they served the function of a sluice gate in a free-surface flow or a convergent-divergent nozzle in a gas-dynamic flow. This sphincter or constriction shown in Fig. (18) was designed so that it would make the tube collapse symmetrically in its twin-lobed mode. The setting of the constriction also established the area ratio ($\alpha = A/A_0$) of the tube at the beginning of the zone of supercritical flow. By appropriate adjustment of the downstream valve, a shock-like transition of the order of 10 cm in length could be made to stand in the test section. In these experiments, the tube downstream of the transition was always inflated, i.e., $\alpha > 1$.

In arriving at the dimensions and material of the tube to be used, a compromise was made between conflicting requirements of size, availability, and measurement. In selecting the diameter of the tube the major consideration was that its dimensions, even in the collapsed state, with an area ratio of about 0.15, be much larger than that of

the catheters that would have to be inserted inside the tube in order to make the area and pressure measurements. This aspect of the problem is more fully discussed in Section 5.2.

In this particular experiment the edge effects due to differences in cross-sectional area between the test section of the collapsed tube and its supports were not important. The reason was that, at the upstream end, the rigid supply pipe was followed by the constriction which established the proper tube shape downstream of it. At the downstream end of the tube, the tube was always inflated with its area ratio slightly above unity whenever a shock was formed in the test section. Thus, there was a smooth match in area between the tube and the rigid pipe. Since the shock was essentially steady (discounting small amplitude wall flutter that was observed to propagate both upstream and downstream of the shock), no problems were anticipated with reflections at the ends. The tube length was in fact chosen so that it would be possible to locate the shock at several different positions downstream of the constriction and to study the influence of its position with respect to the constriction.

Once the internal diameter of the tube was chosen, the selection of the wall thickness represented a compromise between the required range of speed index and the problem of measurement of small transmural pressures. Since the bending stiffness of the wall is very sensitive to the wall thickness, the wave speed in the collapsed states would be lowered by reduction in wall thickness. Thus, for a given flowrate, a larger inlet speed index and, in general, a stronger shock could be obtained. This is advantageous, as lower flow rates result in a smaller level of turbulence

and wall flutter with the result that cleaner, noise-free measured signals would be obtained. Unfortunately, smaller wall thickness poses problems in the measurement of transmural pressure which would also scale like the bending stiffness and would accordingly be smaller. The negative transmural pressures measured upstream of the shock were no larger than about 4 cm of water. If the tube wall thickness had been halved, the pressures to be measured at the same inlet speed index would be about eight times smaller.

The rigid support pipe at the downstream end of the tube was capable of rotational movement about its axis and of longitudinal movement along its axis. Thus, any twist in the collapsible tube could be corrected by rotating the downstream end. Further, the tube could also be put in tension by moving the downstream end longitudinally. The prestrain was determined by measuring the displacement between two fixed circumferential lines marked on the compliant tube. This prestrain was set at 6% in all the experiments reported here.

5.2 The Instrumentation

The quantities to be measured in this experiment were the cross-sectional area and the fluid pressure at a given location, the position along the tube of these measurements, and the volume flow rate through the tube.

In addition to these measurements, the transmural pressures at two points along the tube, one just downstream of the constriction and one just upstream of the rigid support pipe at the downstream end, were measured by means of manometers. The manometers were connected to the

opposite ends of a teflon catheter tube (O.D. = 0.275 cm, I.D. = 0.180 cm) located longitudinally inside the collapsible tube and held stretched between its ends. This plastic catheter carried a hole exposed to the flow at each end where the pressure measurements were to be made. Also, the inside of the catheter near the center was filled with a short column of epoxy to allow for the individual pressure measurements at the two ends. These measurements were for the purpose of converting the gauge pressure measured by the moving probe to transmural pressures.

Apart from a calibrated rotameter used in the flow measurement, the principal instrumentation was in the form of a translatable catheter (O.D. = 0.275 cm, I.D. = 0.180 cm). A sub-miniature pressure transducer, which communicated with the flow through a hole in the catheter tube wall, was mounted inside this translatable probe (see Fig. (19)). On the two sides of the hole, the catheter also carried two electrodes exposed to the flow and placed approximately 0.4 cm apart. The local cross-sectional area was determined by means of electrical impedance measurements as described in Section 2.3 on the experimental determination of the tube law. The signal leads from the area electrodes and the pressure transducer were led to the outside in opposite directions through the catheter. The volume of fluid inside the catheter was restricted by sealing the probe with epoxy as shown in Fig. (19). This pressure transducer configuration had excellent response. Unfortunately, however, it proved to be extremely delicate and was damaged beyond repair after only a few experiments had been performed.

At this point, the miniature pressure transducer was replaced by an external pressure transducer connected through a rigid stainless steel capillary tube (see Fig. (20)). The steel capillary tube was inserted within the plastic catheter tube up to the point where the hole in the wall of the plastic catheter was located. It was necessary that this capillary tube be rigid as it had to pass through sealing O-rings located at the end of the rigid support pipe and distortion of the pressure signal due to squeezing at the O-ring had to be avoided. No leakage path was established for the current in the flow system due to the presence of the steel tube as the pressure transducer used was a physiological pressure transducer with an insulation resistance between the pressure-sensitive diaphragm and its internal electronics of the order of tens of megaohms. However, in spite of the extremely low compliance of this pressure transducer, the fluid friction in the capillary tube was sufficiently high for its time response to be lowered much below that of the transducer alone.

Step tests were conducted both with and without the capillary tube to determine the time response of the transducer-capillary tube system. Since the pressure transducer by itself was known to have a time response much faster than that of the applied step pressure, the time delay in the step test without the tube was taken to be the time of application of the pressure step. The pressure step was applied by the bursting balloon technique. The result of these tests showed the time constant of the transducer-capillary tube system to be less than 0.05 seconds. Since the pressure transducer signal was sent through a filter with a

cut-off frequency (-3 dB) of 3 Hz to exclude noise due to flow disturbances, and since the range of translation of the probe was only 3 cm/sec, this time response was considered to be satisfactory for our purposes.

The combined area-pressure probe was drawn through the test section at a uniform rate of about 3 cm/sec and provided curves of pressure and area as a function of axial distance. The translation of the probe was accomplished by means of a light chain connected to the catheter at its two ends and driven by a variable speed motor. The distance moved by the probe was measured by means of a potentiometer connected to the spindle of the sprocket driving the chain. The purpose of employing a chain was to ensure that the catheter did not slip relative to the potentiometer. The potentiometer was supplied with a constant D.C. voltage and provided a voltage output directly proportional to the motion of the probe. Its output was calibrated by measuring the probe movement with a meter ruler.

The measurement of area using the electrical impedance method in this experiment was subject to the same kind of errors described in the tube law experiment in Section 2.3. In addition, the shock has regions of rapidly diverging area where the electrical equipotential surfaces are curved. Thus, there exists the possibility that the voltage measured by the area probe would not correspond to the cross-sectional area at that particular location. For area gradients of the kind encountered in shock experiments these errors were studied by other investigators in this laboratory and were found not to be significant.

---

* : page 99* inserted between pages 99 and 100.

The outputs of the probe area, reference area electrodes, and the pressure transducer were fed via high-quality differential amplifiers with high common mode rejection ratio (CMRR) to three channels of a multi-channel visicorder light-beam oscillograph which provides a permanent record on photosensitive paper. The displacement potentiometer signal, being of sufficient signal amplitude, was fed directly to another channel of the visicorder. This provided four traces representing these signals on the visicorder paper. As the probe and reference areas are supplied with a 500 Hz A.C. voltage, these traces appear as broad bands on the paper. In the case of the probe area trace, the envelope of this band is modulated in inverse proportion to the variation in cross-sectional area as the probe moves through the shock. As in the tube law experiment, a correction is made for the cross-sectional area occupied by the two catheters, one fixed and the other moving, that are located longitudinally inside the tube.

The speed of translation of the probe V_p and the frequency f of the A.C. carrier voltage supplied to the area electrodes were also constrained by another requirement. The minimum spatial resolution of the area gradients is determined by the distance d between the area probe electrodes. For a smooth envelope to be obtained, the carrier frequency must be such that, in the time taken by the probe to traverse the distance d, the carrier wave must undergo many oscillations. Thus, it was necessary that

$$\frac{d}{V_p} >> \frac{1}{f} \quad . \tag{5.1}$$

Equivalently,

$$\frac{df}{V_p} >> 1 \quad . \tag{5.2}$$

In the present experimental design (d = 0.4 cm, $V_p \leq 3$ cm/sec, f = 500 Hz), this group was larger than 60 and a smooth envelope was obtained.

The presence of the two catheters inside the collapsible tube could cause deviations from the behavior in their absence in four different ways. They are:

(1) The reduction in flow area by an amount equal to the cross-sectional area of the catheters. The ratio of the area of the two catheters $2a$ to the cross-sectional area at zero transmural pressure A_0 was equal to 0.026. The reduction in flow area would be most severe in the collapsed region upstream of the shock. At the minimum area point within the constriction this ratio was of the order of 10%.

(2) The increased frictional drag on the flow due to increase in wetted perimeter. The ratio of the combined perimeter of the two catheters $2\sqrt{4\pi a}$ to the undistended perimeter of the compliant tube $\sqrt{4\pi A_0}$ was equal to 0.229. The fractional increase in effective wetted perimeter would be more significant in regions where the opposing walls are in contact. At the minimum area location within the constriction this was of the order of 35%.

(3) The motion of the probe may alter the frictional drag. In the turbulent flows that were obtained within the compliant tube, viscous effects are confined to narrow boundary layers and are relatively independent of the shape of the flow channel (Schlichting[51]). Under these conditions, the effect of slow translation of the probe catheter can be estimated by replacing the flow velocity in the frictional drag expressions by the relative velocity between the flow and the surface of the catheter. The ratio of the speed of translation of the probe catheter to the mean flow speed did not exceed 0.05 anywhere within the tube for the flow rates employed. Thus, the effect of catheter motion on the flow was not significant.

(4) The catheters may interfere with the collapse of the tube. For this reason, the two catheters were located opposite to each other, so that they would occupy symmetrical positions in each of the two lobes of the collapsed region of the tube. In the experiments performed, the presence of the catheters did not interfere with the collapse of the tube.

The formulations for the frictional drag coefficient and wave speed of Sections 3.2 and 2.1 can be suitably modified to take into account the effects due to the reduction in flow area and the increase in wetted perimeter.

5.3 Experimental Procedure

In this section, the procedures adopted for setting up the experiment and for checking and calibrating the instrumentation are first described. Next, the conditions under which the experiments were performed and the organization of data acquisition are presented.

A. Setting Up the Experiment

As the first step in setting up the experiment two circumferential lines were drawn on the latex rubber tube (I.D. = 2.54 cm, wall thickness = 0.083 cm, length = 106.5 cm, Young's modulus $E \simeq 1.6 \times 10^7$ dynes/cm^2, Poisson's ratio = 0.5) exactly 15 cm apart at its center. The probe and manometer catheters were then passed through the tube, the end pipes, the sealing O-rings, and the plates which retained the O-rings in place (see Fig. (17)). The constriction at the upstream end was dismantled and the rubber tube was mounted on the rigid end pipes. At each end a rubber strip was wrapped around the latex tube and the rigid mounting. Then, the tube end was securely held in place with a hose clamp. In addition, a piece of stiff large-diameter polyethylene tubing was clamped around the short stretch of latex tubing (approximately 4 cm) between the rigid pipe end and the constriction. This prevented bursting of the latex tube under the high pressures encountered at this point. The distance between the lines marked on the tube was next adjusted for 6% longitudinal strain by adjusting the longitudinal position of the downstream rigid support pipe. The constriction was then re-installed.

The open tank was next filled with glycerine-water solution and the

downstream sump tank was filled with salt solution of 20% by weight NaCℓ concentration. The densities of these two solutions were matched to within 1/2% to prevent buoyancy effects. The recirculating pump was then started and the flow loop was allowed to fill up with salt water. Using the strategically located venting ports, all the trapped air bubbles in the system were eliminated. The constriction was then adjusted for minimum area and a shock was made to stand in the test section by altering the downstream pressure. The collapsed region upstream of the shock was then checked for twist and if any twist was present it was eliminated by suitably rotating the downstream end support pipe. Salt-water was then injected using a syringe at the pressure transducer and into the manometer connectors, and air bubbles were eliminated from the pressure measurement systems.

B. Instrument Checks and Calibrations

At the outset of each experiment, each differential amplifier used for signal amplification was trimmed for maximum common mode noise rejection. The fluid circuit was supplied with a 500 Hz sinusoidal A.C. voltage from a signal generator as shown in Fig. (17). The signals from the probe area and reference area electrodes were routed through the differential amplifiers to the visicorder oscillograph. The pressure transducer was supplied with 10 V D.C. from a well-stabilized, noise-free D.C. power supply. Its output was first amplified by a differential amplifier and then fed to the visicorder via a low-pass filter whose cut-off frequency was set at 3, 10, and 30 Hz. The filter was used to exclude high frequency signal components derived from flow-induced dis-

turbances. The displacement potentiometer was supplied with a stabilized D.C. voltage and its output was directly fed to the visicorder. Shielded cables were used for all connections and their shields were connected at one point to a stable ground to which no other electrical equipment was connected. The downstream supply electrode of the flow loop was connected to a similar but separate ground.

Before running an experiment, the constriction was adjusted for minimum area and the flow rate was adjusted to its maximum value. The gains of the amplifiers, filter, and visicorder were then adjusted so that they would not saturate during all subsequent experiments when signal levels would be generally lower.

Several checks were then made to make sure that the measurement systems were in good order. There was the possibility that the steel capillary tube may be producing noise as a result of shaking when it was in motion. To check this, the flow was stopped and measurements were made when the probe was stationary and when it was moving. Except for a transient at the start of the catheter motion, there was no difference in the signals. With the flow taking place however, there were pressure fluctuations both downstream and upstream of the shock. The same type of fluctuations were recorded previously, using a probe incorporating the sub-miniature pressure transducer. At the end and the beginning of each set of runs, the flow was stopped with upstream and downstream valves fully closed and the pressure transducer was calibrated statically *in situ* against one of the manometers over a range of pressures.

The area probe was checked by withdrawing the probe into the rigid support pipe at the upstream end. The cross-sectional areas of this pipe and the rigid reference section were identical. Thus, with the probe in this position, the calibration constant for the probe area in terms of the ratio of probe area and reference area visicorder traces could be directly obtained. When the signal generator supply voltage was varied while the area probe was in the rigid support pipe, this calibration constant should remain fixed. This served as a spot check on the probe area measurement and was performed after each set of runs.

At the end of each experiment, a tube law experiment was performed *in situ* with the flow stopped and the upstream and downstream valves fully closed. The probe was located at the center of the test section and the area was varied by withdrawing fluid in small amounts from the test section. In doing this, fewer data points were taken in the tube law experiments already described. These measurements served as a check on the tube laws obtained previously. No significant differences were found between these different tube-law measurements.

C. Measurements Performed

The quantities measured during each experimental run were the flow rate, the longitudinal position, the cross-sectional area, and the fluid pressure at each position. The conditions under which these measurements were carried out were the following:

(1) The initial longitudinal wall prestrain was kept at 6%.

(2) The position of the shock was kept approximately constant since there was no way of keeping the shock position exactly fixed. This was done by adjusting the downstream pressure and locating the sharp dip in the shock profile (see Fig. (16)) at approximately the same position marked on a meter ruler fixed to the tank. Once the area, pressure, and distance traces were obtained on the visicorder paper, the position could be accurately determined.

(3) The minimum area at the constriction was varied in steps.

(4) For each constriction area, runs were made for a range of flow rates. At the largest constriction area, it was difficult to keep the shock stable at the same longitudinal position and measurements could be made only for a few flow rates. Tables 4, 5, and 6 summarize the measurements that were made in this experiment.

Measurement of the pressure distribution only and the pressures at the inlet and exit of the apparatus were made for a variety of flow rates, constriction sizes, and shock positions for the purpose of determining the overall flow regulation behavior of the apparatus. This work is discussed in Section 7.2 of this thesis.

CHAPTER VI

INTERPRETATION AND DISCUSSION OF RESULTS

In this chapter, the results of the experiments described in Chapters II and V (and also some supporting results from Chapter VII) will be presented and explained on the basis of the approximate theory developed in this thesis. In Section 6.1 the experimental tube law data will be presented and discussed. In Section 6.2, attention will be focused primarily on the change in flow properties across the shock proper. In Section 6.3, the precursor wave measurements will be presented and discussed in the light of the perturbation theory developed in Section 4.5 and the approximate theory for mean flow properties developed in Part B, Section 7.2.

6.1 Tube Law Measurements

The experimentally determined tube law is shown as a plot of transmural pressure normalized with respect to the bending stiffness K_B as a function of the area ratio. The resting area A_0 was taken to be equal to that for zero transmural pressure. The bending stiffness K_B is the experimentally determined value obtained from the plot of $\log_{10}(p - p_e)$ vs. $\log_{10} \alpha$, in the similarity region. This plot was linear with a gradient very nearly equal to - 3/2 as predicted by the similarity tube law of equation (2.21). In the positive pressure region for $\alpha > 0$, the plot of $(p - p_e)/K_B$ against $(1 - \alpha^{-2})$ was also linear, in accordance with Equation (2.4). The buckling pressure given by (2.7) is in close agreement with the knee of the plot of the tube law (Fig. (1) beyond which

the cross-sectional area decreases rapidly with increasing negative transmural pressure. Thus, the mechanics of the tube law agrees closely with the observed behavior.

The speed of propagation of small amplitude waves in the uniformly collapsed tube is given by Equation (1.1). The wavespeed was obtained by numerical differentiation (Eq. (1.1)) of the tube law data of Fig. (1) and is plotted as a function of the area ratio in Fig. (2). The theoretical predictions of Equation (2.6) for $\alpha \geq 1$ and of Eq. (2.26) for $\alpha \leq 0.21$, are shown for comparison. As expected, the wavespeed is relatively independent of the area ratio in the range $0.3 \leq \alpha \leq 0.9$ within the tube law is very nearly linear. It rises abruptly to a much larger value beyond the buckling point, for increasing area ratio, and subsequently it decreases slowly for increasing area ratio in the positive transmural pressure region.

The property $M(\alpha)$ of the tube defined by Equation (4.33) was obtained by differentiating twice the smoothed data of the experimental tube law. The resulting plot of $M(\alpha)$ vs. α is shown in Fig. (13). Since it is a function of the second derivative of the tube law, it is very sensitive to changes in curvature which occur near the buckling point, just before $\alpha = 1$, and in the region where the opposite sides of the tube wall come into contact. However, within the range $(0.3 < \alpha < 0.8)$, it is also a weak function of α. Except in the narrow range $(0.27 < \alpha < 0.33$; approximately), the value of $M(\alpha)$ is positive. Over the range $(0.37 < \alpha < 0.7$; approximately) it is approximately equal to 3 and for this value the tube law is linear.

6.2 Transshock Measurements

The experimentally obtained plots of area ratio and pressure coefficient as a function of the distance x along the standing shock wave are given in Figs. (30 - 48) for nineteen different runs. Figures (30s - 48s) are smoothed curves obtained from Figs. (30 - 48) with the mean curves having been drawn in. The manner in which the mean curves were drawn, and the meaning of the various quantities measured off these distributions are indicated in Fig. (16). The positions corresponding to those indicated in Fig. (16) are labelled in Fig. (5a) of the flow configuration which shows the constriction, the exit measurement location, the minimum area location etc.

Table 4 gives the flow rate Q, the area ratios at locations such as i) the constriction (α_c), ii) the constriction exit (α_1), iii) the minimum area at the inlet to the shock (α_1'), iv) the hypothetical shock inlet area (α_1'') obtained as in Fig. (16) by projecting the mean area curve beyond the minimum area location, v) the area ratio at the maximum pressure location at the exit of the shock (α_2'), and vi) the area ratio far downstream of the shock (α_2). The position of each of these locations from the inlet position x_1 and the shock length measured as shown in Fig. (16) are also tabulated. In Table 5, the speed indices computed from the measured flow area and from the corresponding wave speed for a uniformly collapsed tube (Fig. (2)), are given for each run. Also tabulated are the pressure recovery coefficients C_p, C_p' (See Table 4), and the Carnot (C_{p_c}') and Oates (C_{p_o}') pressure coefficients which are computed from Equations (4.41) and (4.49). In computing C_{p_o}' the experimental tube law was utilized for given (α_1', α_2').

In obtaining this data, the position of the shock with respect to the constriction ($x_1' - x_1$) was held approximately fixed by adjustment of the downstream pressure. In all these runs, the wall prestrain was also kept fixed at 6% as described in Section 5.3. In Fig. (56), the inlet area ratio α_1 is plotted against the constriction area ratio α_c, and a linear least squares fit to the data has been obtained. It seems reasonable to assume that α_c fixes α_1 and Fig. (56) shows that α_1 increases approximately linearly with α_c though not exactly equal to it. In making the measurements, α_c was kept fixed for a given set of flow rates.

The pressure recovery coefficients C_p and C_p' are shown plotted against α_1 and α_1' respectively in Fig. (49). The area ratio α_2' at the exit was practically unity for all runs as can be seen in Table 4. The plot of C_p' vs. α_1' does not seem to indicate any particular trend either with α_1' or S_1'. The plot of C_p vs. α_1 shows C_p values to be lower than C_p'. This is to be expected as the upstream frictional loss is included in the definition of C_p. The Carnot pressure recovery C_{p_c}' is also plotted in Fig. (49) and seen to be lower than the actual pressure recovery C_p' across the shock. This indicates that the flow separation is not as sharp as assumed in the derivation of Equation (4.41) for the Carnot pressure recovery. To investigate the coefficient further the actual stagnation head loss coefficient across the shock is plotted in Fig. (58) against the Carnot stagnation head loss coefficient given by Eq. (4.43). The linear least squares fit to the data is also shown. The slope of this line corresponds to the loss

coefficient K_L defined for a divergent duct in Equation (7.26) and its value is equal to 0.586. In the limiting case of extremely large area change and infinite Reynolds Number corresponding to Carnot loss conditions, K_L is approximately unity. More generally, in divergent ducts, K_L is found to be a strong function of the inlet momentum boundary layer thickness, the shape of the diffuser, and the area gradient represented by $(\alpha_2' - \alpha_1')D_0/L_s$. It is seen from Table 5 that the Oates pressure recovery C'_{p_o} is always slightly larger than the Carnot recovery C'_{p_c} as predicted by the theory.

The speed index S , calculated from the uniform collapse tube law and the measured area distribution is plotted for Run No. 3 in Fig. (55) as a function of distance along the tube. It shows that the speed index is heavily supercritical in the whole upstream region, and that it oscillates with oscillations in the cross-sectional area. It also shows that it remains supercritical well into the shock region almost until the exit position x_2' . Since S is interpreted as the speed of propagation of small disturbances of large wavelength, it is probably more appropriate to compute it from the mean area rather than from the true area. This would probably reflect the fact that the oscillatory component of area is due to the longitudinal tension and is not derived from the circumferential stresses accounted for in the static tube law.

6.3 Precursor Wave Measurements

A. Mean Flow Quantities

It is appropriate to first discuss the particular form of the mean area and pressure curves in Figs. (30s) - (48s). It is seen from these figures that the mean area curves grow almost linearly with

distance x in every distribution, while the mean pressure increase is extremely small even though the area has significantly increased in value. The reason for the latter is evident from the following expression

$$\frac{\partial p_m}{\partial x} = K_B \frac{\partial P(\alpha_m)}{\partial \alpha_m} \cdot \frac{\partial \alpha_m}{\partial x}$$

In the range of mean area ratios encountered in the upstream region $\partial P(\alpha_m)/\partial \alpha_m$ is a very small quantity as seen from Fig. (1). As a result, $\partial p_m/\partial x$ remains small in spite of the fact that $\partial \alpha_m/\partial x$ is very significant. However, the oscillatory component of pressure is large and is coupled to the oscillatory area terms and the mean area terms.

The relations (7.27) to (7.29) governing the mean area growth are given in Section 7.2 of Part B. Their solution, assuming $M(\alpha)$ = constant $\simeq$ 3 in the upstream region is given by (7.30) to (7.33). From these solutions, it at once becomes evident that (i) The mean speed index decays with increase in area approximately according to a -3/2 power law. This qualitatively agrees with experimental observations (See Fig. (55)). (ii) If $M > 2$ and $S_1^2 >> 1$, then the mean pressure increase is indeed very small. This is also consistent with experimental observations Figs. (30s - 48s). (iii) If $S_1^2 >> 1$, then the mean area ratio α_m grows linearly with distance $(x - x_1)/D_0$ and the gradient is equal to $2f_0$. The quantity f_0 is a friction factor defined by (7.25) and is a weak function of the Nominal Reynolds Number Re_{D_0} only. To verify this finding, the slope of the mean area curves in the upstream region has been measured from Figs. (30s - 48s) and are tabulated in Table 9.

Also tabulated are the theoretical values of $2f_0$. The average error for the runs (1 - 19) is 26%. Further, from the same relation, the shock position was calculated by employing the experimental values of α_1' . The average error is again of the same order.

B. Oscillatory Flow Properties

In Section 4.5, a perturbation analysis of the growth of flow quantities about a base condition chosen to coincide with a point of intersection of the mean and total area distributions (See Fig. (62)) has been performed. This choice of base point is especially convenient in the measurement of oscillatory components and has been employed as shown in Fig. (16). Table 6 gives the wavelengths λ_n , the amplitudes a_n , and the corresponding mean values of position x_{mn} , the pressure recovery coefficient $C_{p_{mn}}$, the area ratio α_{mn} , and the flow velocity u_{mn} for each of the runs (1-19). The total perturbation in area α' about the base value $\bar{\alpha}$ has been further split up into the mean area growth component $\hat{\alpha}$ and the oscillatory component $\tilde{\alpha}$ as shown in Fig. (62).

The solutions to the components $\hat{\alpha}$ and $\tilde{\alpha}$ are given in Section 4.5 by Equation (4.92). The perturbation analysis yields the following implications:

(i) Fluid friction is necessary for growth of mean and oscillatory area components (Eq. $(4.80)_2$), and wall tension and wall curvature lead to oscillatory growth in area, provided the condition $(4.80)_1$ is satisfied. Thus, supercritical flow ($\overline{S} > 1$) is sufficient but not necessary for oscillatory growth of area.

(ii) For a given flowrate the wavelength of the oscillatory components depends on the mean flow velocity approximately according to a - 3/2 power law as given by Eq. (4.98). To verify this finding, the wavelength $\bar{\lambda}$ has been plotted against $\bar{u}$ in Figs. (50 - 54). These plots show the predicted trends. To confirm the power law behavior better, $\text{Log}_{10}\ \bar{\lambda}$ vs. $\text{Log}_{10}\ \bar{u}$ was plotted and straight lines were fitted in a least squares sense. These results are given in Table 7. The correlation coefficient in each case is 80% or better. The average slope of -1.375 is close to the predicted approximate value of -1.5.

(iii) The dispersion relationship that governs the waves in the precursor wavetrain is given by Equation (4.110). To verify this relationship the data in Table 6 have been plotted in Fig. (65). This plot shows the predicted behavior. The theoretical line appears to represent the data adequately.

C. Flow Rate Regulation Behavior

In Section 4.3, it was shown that conditions upstream of a location of supercritical flow in a collapsible tube become independent of downstream conditions. In particular, this led to the flowrate being independent of downstream pressure variations.

In Fig. (27), the flowrate normalized with respect to the constriction area A_c, and the stagnation pressure difference at the inlet is plotted against the normalized downstream pressure difference. This normalization makes the plots approximately the same for a wide range of inlet conditions. It is seen from this figure that there exists a plateau region within which the flowrate is unaffected by downstream pressure

variations. The manner in which the flowrate is dependent on inlet pressure and constriction area is given by Fig. (57) which shows the experimental data and the theoretical prediction of Eq. (7.21). The value of downstream pressure, at which the shock is on the verge of entering the constriction, corresponds to the knee of Fig. (27). The experimental and theoretically computed (Eq. (7.24)) values of this downstream pressure are given in Table 8 and they show satisfactory agreement.

This independence of flowrate of the downstream pressure forms the basis of the design of the flow regulator of Part B in this thesis. The reader is referred to this part for a more detailed analysis of the regulation behavior and comparison with experimental results.

6.4 Conclusions and Recommendations

The objective of this work was the measurement and interpretation of the structure of standing shock waves in collapsible tubes. Among the questions that needed to be answered were the conditions under which such shocks could be created.

Certain features of the shocks, such as supercritical inlet flow, large area changes, large stagnation pressure losses, and independence of inlet conditions of downstream pressure were qualitatively anticipated. However, certain unanticipated and hitherto unobserved new features were encountered during the course of this investigation. These new features include the existence of a train of area and pressure waves preceding the shock, the surprising but now interpretable lack of upstream mean pressure increase, as discussed in Sections 6.3 and 7.2, the sharpness

of the pressure change at the inlet to the shock, and the occurrence of vibrations emanating at the shock and propagating away from it.

The measurements reported in this thesis have established the flow regulation behavior, the magnitude of the trans-shock stagnation pressure losses, the manner of growth of mean upstream area and pressure. Further, the perturbation analysis has extracted the principal features of precursor wave growth and the conditions governing their existence. The experimental results presented in this respect are convincing. However, much less success was had in characterizing the trans-shock pressure recovery. The experimental data did not show any observable trends due to data scatter. It is believed by the author that this was due to severe vibrations experienced by the pressure probe when it was traversing the shock proper. Furthermore, in Fig. (55) the oscillations in the value of the speed index downstream of the shock are believed to be due to experimental error in the measurement of the tube area ratio and in the determination of the corresponding speed of propagation of small amplitude waves.

It is recommended by this author that further experiments be conducted to measure trans-shock losses with thinner tubes, lower flowrates, and smaller constriction area ratios. This would ensure adequately strong shocks with a reduced level of flow induced disturbances. Further, even for the approximate analytical model presented here, numerical computation of the full equations should be performed to determine the effect of reduction in wall tension due to fluid drag.

More importantly, theoretical work should be undertaken to better model the tube mechanics accounting for longitudinal curvature effects. Flow visualization studies by laser-fluorescence or dye-injection methods should be conducted on rigid transparent models of shocks to better characterize the separation phenomena in the shock region. Further, the pressure profiles should be measured. The sharp dip at the shock inlet in the pressure profiles presented in this thesis are quite similar to those predicted by Wooley and Kline[54] in their computational model for stalled diffusers. The latter may be a feasible approach to the analytical solution of the flow problem.

CHAPTER VII

THE COLLAPSIBLE TUBE FLOW REGULATOR

In the preceding chapters of this thesis it was shown that the highly nonlinear pressure-area relationship of a collapsible tube leads to strong coupling between the mechanics of the tube wall and the mechanics of the fluid flow through it. In particular, when the fluid inertia in a uniformly collapsed compliant tube is important, wave-speed-induced flow limitation can occur. Moreover, if a region of supercritical flow is present, then conditions upstream of it, including the flow rate, are independent of the downstream flow conditions. If, however, a shock wave forms downstream of the supercritical region, the position of the shock depends on the downstream pressure, while upstream conditions remain independent of it. At this point, it should be mentioned that when the fluid flow is primarily dominated by viscous forces, the highly nonlinear flow conductivity-transmural pressure relationship of a collapsible tube again results in the flow rate being relatively unaffected by the downstream pressure when the tube is partially collapsed at its downstream end.

The purpose of this chapter is to investigate the possibility of taking advantage of this characteristic of fluid flow through collapsible tubes for the design of an uncomplicated, yet reliable, flow regulator. The specific function of the proposed flow regulator is to maintain the flow rate constant, independent of downstream pressure variations, when it is connected to a fluid supply at fixed pressure. This is indicated in Fig. 22.

In Section 7.1 the behavior of a collapsible tube flow regulator in the inertia-dominated regime is first analyzed. Expressions are developed for predicting its flow rate vs. downstream pressure curve, which will be called the regulation characteristic curve. Subsequently, the behavior of a collapsible tube flow regulator in the viscous-dominated regime is considered.

In Section 7.2 the experimental determination of the regulation characteristic is described, and the results are compared with the theoretical expressions of the previous section.

In Section 7.3, the design criteria for a collapsible tube flow regulator are developed and a design procedure is presented.

7.1 The Principle of Operation

A. Wave Speed Flow Regulator

The flow regulator configuration that is considered here is shown in Fig. 5a. The inlet pressure p_i and the outlet pressure p_o are measured at stations (i) and (o), respectively. The constriction (c) creates a supercritical flow immediately downstream of it at station (1). The shock transition occurs between stations (1)' and (2)', where (1)' corresponds to the minimum point in the pressure and area distributions and (2)' corresponds to the maximum in the pressure downstream of the shock. The constriction exerts a non-uniform external pressure on the outside of the tube so that the tube law is valid only outside the constriction.

The equation of continuity is

$$Q = A_0 \alpha u \quad . \tag{7.1}$$

Neglecting frictional losses over the short distance between (i) and (c) and neglecting losses at the entrance to the constriction gives

$$P_{0_i} = p_c + \frac{1}{2} \rho u_c^2 \quad , \tag{7.2}$$

where P_{0_i} is the stagnation pressure at the inlet. Using (7.1) in (7.2) gives

$$Q = A_0 \alpha_c \quad \frac{2}{\rho} (P_{0_i} - \hat{p}_e) - (p_c - \hat{p}_e) \quad , \tag{7.3}$$

where $\hat{p}_e$ is the effective external pressure on the tube within the constriction. Since the tube law for the tube within the constriction is unknown, it can be approximately represented by

$$(p_c - \hat{p}_e) \simeq F(\alpha_c) \quad . \tag{7.4}$$

We note that $Q \to 0$ as $(p_c - \hat{p}_e) \quad (P_{0_i} - \hat{p}_e)$, and also when $(p_c - \hat{p}_e) \to -\infty$ (i.e., $\alpha_c \to 0$). Thus, the flow rate Q possesses a maximum with respect to α_c and as shown in Section 4.3, this maximum occurs when the mean flow speed is equal to the wave speed computed from the effective tube law (7.4). If the effective tube law is not very different from that of the tube itself, then it follows that whenever the flow is significantly supercritical at the exit of the constriction [i.e., Station (1)] there is some location inside the constriction at which the

flow is critical. Thus, the flow is limited at that point. However, since the effective tube law (7.4) is unknown, the flow rate can be evaluated by considering the flow at the exit of the constriction.

Now, if the losses at the entrance to the constriction are taken into account, (7.2) becomes

$$P_{0_i} = p_1 + \frac{1}{2}\rho u_1^2 + K_c \frac{1}{2}\rho u_c^2 \quad . \tag{7.5}$$

The tube law for station (1) is given by

$$(p_1 - p_e) = K_B P(\alpha_1) \quad . \tag{7.6}$$

Hence, using (7.1) and (7.6) in (7.5) gives

$$\frac{Q}{A_c\sqrt{\frac{2}{\rho}(P_{0_i} - p_e)}} = \left[\frac{1 - \frac{K_B P(\alpha_1)}{P_{0_i} - p_e}}{\left(\frac{\alpha_c}{\alpha_1}\right)^2 + K_c}\right]^{1/2} \tag{7.7}$$

In this expression, the cross-sectional area A_c at the constriction has been introduced as a known parameter depending only on the undeformed dimensions of the tube and the adjustment of the constriction.

It has been experimentally found that α_1 is only slightly larger than the value of α_c. Also, the loss coefficient K_c is small since the entrance region is smooth and has a large radius of curvature. Thus, K_c may be neglected.

If the flow at Station (1) is supercritical (i.e., $S_1 > 1$), then the flow rate given by Eq. (7.7) is unaffected by changes in the downstream pressure p_o. Also, if the flow at Station (1) is supercritical, a shock wave usually forms downstream of it. The position of the shock wave depends on the pressure difference $(p_o - p_e)$. When this is made increasingly positive, the shock moves toward the constriction and at a certain value $(p_o - p_e)^*$, the shock vanishes into the constriction (see Fig. 5b). Then, the flow rate begins to fall. This is due to the fact that the region of supercritical flow no longer exists and the flow inside the constriction becomes subcritical. As a result, downstream pressure variations can now travel upstream and decrease the flow rate. Consequently, the flow regulation curve has the form given in Fig. 24. It has a plateau region when a supercritical flow is present and a fall-off curve when the flow is subcritical everywhere. This situation is analogous to supercritical flow in a convergent-divergent nozzle when the back pressure is gradually increased from below its "design" value (Shapiro[52]). The flow rate corresponding to the plateau region is given by Eq. (7.7). This expression shows how the plateau increases with increasing tube stiffness.

In order to specify the range of downstream pressures over which the flow rate is effectively constant, it is necessary to determine the value $(p_o - p_e)^*$ characterizing the knee of the regulation characteristic. This can be obtained by applying the modified Bernoulli equation to the flow when the shock is at the constriction, as shown in Fig. 5b.

Allowing for contraction and expansion losses at the constriction and for frictional losses downstream of it, the Bernoulli equation yields

$$P_{o_i} = p_o + \frac{1}{2}\rho u_o^2 + (K_e + K_c)\frac{1}{2}\rho u_c^2 + \int_0^L \frac{\tau_w P}{A}\, dx \quad . \tag{7.8}$$

Since conditions downstream are approximately uniform, $(\tau_w P/A)$ can be considered to be constant. It is given by Eq. (3.26) with the friction factor chosen from Table 1. Thus, using the continuity equation gives

$$\left(\frac{p_o - p_e}{P_{o_i} - p_e}\right)^* = 1 - \left[\frac{Q}{A_c\sqrt{\frac{2}{\rho}(P_{o_i} - p_e)}}\right]^{*2} \cdot \left[\left(\frac{\alpha_c}{\alpha_o}\right)^2 + (K_e + K_c) + \frac{4fL}{D_o}\left(\frac{\alpha_c}{\alpha_2}\right)^2\right] \tag{7.9}$$

In the above expression the (*) signifies that the values are those at the knee of the regulation characteristic and α_2 and α_o are the downstream area ratio and the rigid exit pipe area ratio, respectively. The value of the flow rate in (7.9) is equal to that of the plateau region and is thus given by Eq. (7.7).

The expansion loss coefficient K_e can be expressed as

$$K_e = K_L\left(1 - \frac{\alpha_c}{\alpha_2}\right)^2 \quad . \tag{7.10}$$

For a sudden expansion, K_L is only a weak function of the Reynolds number at the constriction. At very high Reynolds numbers, K_L tends to unity. It should be noted, however, that for the diffuser-like geometry of the tube expansion region, K_L would be a function not only of the Reynolds number but also of the shape of the cross-sections and, in particular, of the area gradient in the flow direction. Loss coefficients for conical diffusers as a function of area gradients have been experimentally obtained by Henry.[57] His results indicate that, indeed, K_L is strongly dependent on the area gradient. Another complication is that if the diverging region is followed by a long length of pipe, there is recovery of pressure beyond it as a result of velocity distribution changes due to turbulent mixing.[58] Therefore, any values obtained for K_L from published literature for different geometries must be regarded as very approximate.

In the present investigation, the loss coefficient K_L was experimentally determined from measurement of pressure within the tube with the shock located at the constriction.

When the downstream transmural pressure $(p_o - p_e)$ is decreased from positive values towards zero, the shock moves downstream and remains stable at a new location. When $(p_o - p_e)$ is further decreased to $(p_o - p_e)^{**}$ (a negative value), the tube begins to buckle inwards near the constriction to the downstream rigid pipe and forms a pinch as shown in Fig. 5c. When this occurs, the position of the shock becomes unstable and it begins to oscillate along the tube. During this oscillatory motion, the shock stops short of the constriction, so that there is always a

region of supercritical flow downstream of the constriction. Accordingly, the flow rate at the inlet remains unaffected, but both downstream flow rate and pressure oscillate with a characteristic frequency. The oscillations consist of periods of relatively high outflow, when the region downstream from the shock is approximately uniform, separated by momentary slowing as the downstream end is pinched in and then re-opened.

When the downstream pressure is still further reduced and is equal to $(p_o - p_e)^{***}$, the tube folds in on itself and moves into the downstream rigid pipe as shown in Fig. 5d. Once this happens the flow again becomes stable with a shock standing in the test section. However, contrary to the case when the tube is not sucked into the pipe, initial reduction in downstream pressure moves the shock upstream to a new position and increase in downstream pressure moves the shock downstream. On increasing the downstream pressure further, the shock reverses itself, moves upstream, and suddenly the downstream end of the tube moves out of the rigid end-pipe without any oscillations.

Similar oscillatory behavior in the outflow of collapsible tubes has been observed by Griffiths[34] and has been explained by him on the basis of wave propagation. For the present purpose of designing a flow regulator, however, it is only important to determine the value of $(p_o - p_e)^{**}$ below which the flow rate at the exit would begin to oscillate. This value can be approximately determined from the fact that the downstream end must first buckle before oscillations can begin. The buckling pressure for a collapsible tube is given by Eq. (2.7) and is equal to $(-3K_B)$. Thus,

$$\left(\frac{p_o - p_e}{p_{o_i} - p_e} \right)^{**} \simeq - \frac{3K_B}{p_{o_i} - p_e} \quad . \tag{7.11}$$

The buckling pressure given by (7.11) may also increase or decrease depending on whether the wall tension at the exit Station (2) is positive or negative. Further, oscillations begin at a transmural pressure $(p_o - p_e)$ somewhat lower than that at which the tube first begins to buckle. However, experimental results given in the next section indicate that this is a good approximation.

B. Low Reynolds Number Flow Regulator

When the inertia forces are much smaller than the viscous forces and the Reynolds number based on the hydraulic diameter is much smaller than unity, a collapsible tube can still exhibit insensitivity to downstream pressure variations provided the tube is partially collapsed at its downstream end. This is due to the marked reduction in flow conductivity of the tube at negative transmural pressures.

For small longitudinal gradients, the flow is locally a Poiseuille flow and satisfies Eq. (3.1) derived in Chapter 3. The flow conductivity is given by

$$Q = -\sigma \frac{dp}{dx} \quad . \tag{7.12}$$

For constant external pressure this can be expressed as

$$Q = -\sigma(p - p_e) \frac{d(p - p_e)}{dx} \quad , \tag{7.13}$$

where σ is obtained as a function of $(p - p_e)$ using expressions (3.5),

(3.13), and (3.15). A plot of σ vs. $(p - p_e)$ for a uniformly collapsed tube has been given by Flaherty, Rubinow, and Keller[41]. This is given in Fig. 25, replotted and extended to positive transmural pressures.

Consider now a flow regulator consisting of a collapsible tube of length L mounted between two rigid pipes. If the flow rate is Q and the inlet, exit, and external pressures are p_i, p_o, and p_e, respectively, integration of Eq. (7.13) between the inlet and the exit yields, for constant Q,

$$Q = \frac{R_0^4}{\mu L} \int_{p_o - p_e}^{p_i - p_e} \hat{\sigma}(p - p_e)\, d(p - p_e) \qquad (7.14)$$

where

$$\hat{\sigma} = \frac{\mu\sigma}{R_0^4} \quad .$$

From Fig. 25 it is seen that σ decreases sharply below the buckling pressure $p - p_e = -3K_B$ and that beyond $p - p_e \simeq -5K_B$ it is approximately 1/40 as large as it is when the tube is under zero transmural pressure. In the similarity region of the tube law (i.e., $\alpha \leq 0.21$),

$$\hat{\sigma} = 0.1814\left(\frac{p_e - p}{K_B}\right)^{-4/3} \quad . \qquad (7.15)$$

As a result, below approximately $-5K_B$ (i.e., $\alpha \simeq 0.27$), the downstream pressure difference $(p_o - p_e)$ has very little influence on the flow rate

given by the integral in Eq. (7.14). From (7.14), for $(p_o - p_e) < -5K_B$,

$$\frac{\mu LQ}{K_B R_o^4} = \int_{-5}^{(p_i-p_e)/K_B} \hat{\sigma}(\hat{p})d\hat{p} + \int_{\frac{p_o-p_e}{K_B}}^{-5} \hat{\sigma}(\hat{p})\, d\hat{p} \quad . \tag{7.16}$$

Using (7.15) in (7.16), this is approximately given by

$$\frac{\mu LQ}{K_B R_o^4} = Q_1(p_i - p_e) - 0.5443 \left(\frac{p_e - p_o}{K_B} \right)^{-1/3} , \tag{7.17}$$

where Q_1 is a function of the material parameters and $(p_i - p_e)$ and is independent of $(p_o - p_e)$. From (7.17), for a tube with the exit end in the similarity collapse range, the flow rate is seen to be a weak function of $(p_o - p_e)$.

When $(p_i - p_o)$ is small and $(p_o - p_e) > 0$, then (7.14) can be approximated by

$$\frac{\mu LQ}{R_o^4} \simeq \hat{\sigma}(p_i - p_e)(p_i - p_o) \quad . \tag{7.18}$$

Thus, in this region, the flow rate is directly proportional to the driving pressure difference $(p_i - p_o)$. The value of $\hat{\sigma}(p_i - p_e)$ is obtained from Eqs. (2.4) and (3.15) and is equal to

$$\hat{\sigma} = \frac{\pi}{8} \left(1 - \frac{p - p_e}{K_E}\right)^{-1} , \tag{7.19}$$

where K_E is the extensional stiffness of the tube wall defined by (2.5).

The regulation characteristic of the collapsible tube is conveniently represented by the plot of $\mu LQ/[R_0^4(p_i-p_e)]$ vs. $(p_o-p_e)/(p_i-p_e)$. It has the shape shown in Fig. 26. The knee of the curve corresponds to the knee of the conductivity-transmural pressure relationship, beyond which the conductivity is small. The initial slope of the characteristic when (p_i-p_o) is small and the tube is inflated is given by (7.18). The small negative slope for negative transmural pressures (p_o-p_e) is given by (7.17).

7.2 Experimental Determination of the Flow Regulator Characteristic

In this section, the experimental determination of the regulation characteristic curve of a high Reynolds Number, wave-speed type flow regulator is described. In this experiment, attention is focused on the determination of the overall behavior of the flow regulator as a unit and not on the details of the flow within it. Theoretical expressions are developed from this point of view and are compared, as much as possible, with the measured experimental data.

Experimental Procedure

The apparatus used in this experiment is the same as that employed in the determination of the shock structure in Chapter V. The measurement technique is identical except that, in addition, the pressures p_i and p_o at the inlet and outlet of the apparatus were also measured by means of manometers. For each constriction size, the flow rate was varied in steps. For each flow rate, the position of the shock along the tube was altered in steps by adjustment of the downstream pressure. In particular, measurements were made with the shock at its farthest stable

stable position (FSP) from the constriction, towards the downstream end. It was not always possible to obtain a stable shock. This was especially difficult, as it is to be expected, at low flow rates and large constriction area ratios (α_c). The instability of the shock at positions near the downstream end was preceded by pinching of the tube at this end as shown in Fig. (5c). Subsequently, the shock oscillated along the tube.

Results and Comparison with Theory

A lot of data were obtained during the experiment described above. The most important result that is borne out by this data is that the flow rate is independent of downstream pressure variations, provided upstream conditions ($p_i - p_e$, α_c) are fixed. This result is best presented by a plot of normalized flow rate $Q/A_c \sqrt{2/\rho(P_{0_i} - p_e)}$ against the normalized outlet pressure $(p_o - p_e)/(P_{0_i} - p_e)$ as in Fig. (27). Hence, the data obtained under different inlet and outlet conditions can be presented on a single graph.

The expression for the normalized flow rate when a shock exists downstream of the constriction was earlier derived (Eq. (7.7)) and is restated below.

$$\frac{Q}{A_c\sqrt{2/(P_{0_i} - p_e)}} = \left[\frac{1 - \frac{K_B\, P(\alpha_1)}{P_{0_i} - p_e}}{\left(\frac{\alpha_c}{\alpha_1}\right)^2 + K_c}\right]^{1/2} \qquad (7.7)$$

In the above expression, the cross-sectional area A_c at the constriction has been introduced as a design parameter rather than the

area A_1 immediately downstream of it. The plot of α_1 against α_c obtained from Table 4 is shown in Fig. (56) together with the straight line representing the least squares fit to the experimental data. The correlation coefficient of this least squares fit is 0.94. The straight line is given by

$$\alpha_1 = 1.019\ \alpha_c + 0.049 \tag{7.20}$$

It is thus seen that α_1 is only slightly larger than α_c for α_c values approximately between 0.2 and 0.4. Hence, for design purposes, α_1 may be taken to be approximately equal to α_c. Further, the loss coefficient K_c at the constriction entrance is also small and may be neglected. (The quantity P_{0_i} is the stagnation pressure at the inlet.)

For design purposes, equation (7.7) is more conveniently expressed by

$$\frac{Q}{A_0\sqrt{2K_B/\rho}} = \left[\frac{\frac{p_i - p_e}{K_B} - P(\alpha_1)}{\frac{1}{\alpha_1^2} + \frac{K_c}{\alpha_c^2} - \frac{1}{\alpha_i^2}}\right]^{1/2} \tag{7.21}$$

The areas of the rigid inlet and outlet tubing of the experimental apparatus were equal to the resting area of the latex tube so that $\alpha_i = \alpha_o \simeq 1$. This geometry is convenient and will also be assumed in the subsequent design calculations. Equation (7.21) together with (7.20) yields a relationship between $Q/A_0\sqrt{2K_B/\rho}$ as a function of

$(p_i - p_e)/K_B$ with α_c as an independent parameter. That is

$$\frac{Q}{A_0\sqrt{2K_B/\rho}} = \bar{f}(\alpha_c , \frac{p_i - p_e}{K_B}) \tag{7.22}$$

The theoretical prediction (7.22) and the corresponding experimental data are plotted in Fig. (57) and they show reasonably good agreement.

The above relationship is valid only as long as a stable shock exists downstream of the constriction. Two necessary conditions for shock formation are that the Reynolds number of the flow is large and that the flow downstream of the constriction is supercritical. In addition, the transmural pressure difference $(p_o - p_e)$ must not be so high as to force the shock inside the constriction, nor should it be so low that the tube buckles at its exit end precursory to oscillation of the shock along the tube.

It is therefore necessary to establish the upper and lower limits $(p_o - p_e)^*$ and $(p_o - p_e)^{**}$ between which the downstream pressure difference can be allowed to vary while still maintaining a constant exit flowrate. As discussed in Section 7.1, the lower limit can be approximated by equation (7.11). The validity of this expression is verified by the plot of Fig. (28). For design calculations, (7.11) is better written as

$$(\frac{p_o - p_e}{K_B})^{**} \simeq -3 \tag{7.23}$$

The upper limit can be approximately found as described in Section 7.1 from equations (7.9) and (7.7). For design purposes however, it is more convenient to write (7.9) as

$$\left(\frac{p_o-p_e}{K_B}\right)^* = \left(\frac{p_i-p_e}{K_B}\right) - \left(\frac{Q}{A_0\sqrt{2K_B/\rho}}\right)^2 \left(\frac{1}{\alpha_o^2} - \frac{1}{\alpha_i^2} + \frac{K_c + K_e}{\alpha_c^2} + \right.$$

$$\left. + \frac{4f_0L}{D_0}\frac{1}{\alpha_2^3}\right) \qquad (7.24)$$

where

$$f_{.0} \equiv \frac{0.0791}{Re_{D_0}^{0.25}} \qquad (7.25)$$

The flowrate in (7.24) is taken to be the value on the plateau region of the regulation characteristic as given by (7.21). Thus $\left(\frac{p_o - p_e}{K_B}\right)^*$ corresponds to the knee of the regulation characteristic as indicated in Fig. (24). The loss coefficient K_e can be expressed in the form

$$K_e = K_L\left(1 - \frac{\alpha_c}{\alpha_2}\right)^2 \qquad (7.26)$$

In Fig. (58), the stagnation pressure loss across the shock is plotted against $(1 - \alpha_1'/\alpha_2')^2$ for the shock distributions in Table 4. The slope of the least squares straight line fit to this data may be taken to represent K_L in (7.26) in the absence of better information. Thus, with $K_L = 0.586$ and $\alpha_o = \alpha_i = 1$, $\alpha_2 \simeq 1$, $\left(\frac{p_o - p_e}{K_B}\right)^*$ can be

computed from equation (7.24) for given α_c and $(p_i - p_e)/K_B$. The experimental and theoretical values of $(p_o - p_e/K_B)^*$ for $\alpha_c = 0.213$ and a range of values of $(p_i - p_e/K_B)$ are tabulated in Table 8. The agreement between experiment and theory is good in view of the very approximate nature of the theoretical computation.

Lastly, it is necessary to predict both the stagnation pressure loss upstream of the shock and the position of the shock. These values will be needed in Section 7.3 in order to determine the required length of collapsible tube in the regulator design. This however, is a difficult undertaking as the area increases in an oscillatory fashion between the constriction and the shock. As a result, it is necessary to make some radical assumptions. It is first assumed that the stagnation pressure loss is primarily due to the change in mean area and that the effect of the oscillatory component of area growth on the frictional drop integrated over the entire upstream length is negligible. Secondly, it is assumed that the parameter M is approximately constant. This is approximately valid over most of the range of interest ($0.35 < \alpha < 0.8$). Thus, neglecting the wall tension terms in (4.29), (4.30), and (4.31) the governing equations are

$$\frac{2}{M}\,\frac{1}{S}\,\frac{dS}{dx} = -\,\frac{1}{\alpha}\,\frac{d\alpha}{dx} = \frac{1}{u}\,\frac{du}{dx} \tag{7.27}$$

$$\frac{(1 - S^2)}{S^4} = \frac{M}{2}\,\frac{4f}{D_0} \tag{7.28}$$

$$(1 - S^2) \frac{dp}{dx} = - \frac{4f}{D_0} \frac{1}{2} \rho u^2 \tag{7.29}$$

where $f=f_0/\alpha$ and f_0 is defined by equation (7.25).

Integrating (7.27), (7.28), and (7.29) for specified inlet conditions yields

$$\frac{S}{S_1} = \left(\frac{\alpha}{\alpha_1} \right)^{-M/2} \tag{7.30}$$

$$\frac{2f_0}{\alpha_1} \frac{x - x_1}{D_0} = \left(\frac{\alpha}{\alpha_1} - 1 - \frac{\left(\frac{\alpha}{\alpha_1} \right)^{M+1} - 1}{S_1^2 (M + 1)} \right) \tag{7.31}$$

$$\frac{p - p_1}{\frac{1}{2} \rho u_1} = \frac{2}{S_1^2} \frac{\left(\frac{\alpha}{\alpha_1} \right)^{M-2} - 1}{(M-2)} \tag{7.32}$$

$$\frac{\Delta p_f}{\frac{1}{2} \rho u_1^2} = 1 - \left(\frac{\alpha_1}{\alpha} \right)^2 - \left(\frac{p - p_1}{\frac{1}{2} \rho u_1^2} \right) \tag{7.33}$$

From the above it can be seen that for the computed values of M given in Fig. (13) and for $S_1^2 >> 1$, the mean pressure increase given by (7.32) is very small. This is consistent with the small mean upstream pressure increase measured in the shock experiments. Further, under the same conditions, equation (7.31) predicts that the mean area distribution will be relatively independent of the inlet speed index, and

will be a weak function of the flow rate through the friction factor f_0 . Thus, equation (7.31) reduces to the simple result

$$\alpha = \alpha_1 + 2f_0\left(\frac{x - x_1}{D_0}\right) \tag{7.34}$$

The area distributions in Figs. (30s - 48s) show that the mean area growth is relatively linear as predicted by equation (7.34). The average slope of the mean area curve in these measured distributions and the slope ($2f_0$) predicted by equation (7.34) are tabulated in Table 9. The average error between the experimental and theoretical values is of the order of 30%. Further, it is possible to compute the shock position by substituting (x_1', α_1') in (7.31). The theoretical and experimental values of the shock position are also tabulated in Table 9. The maximum error is again of the order of 30%. This agreement is not unsatisfactory in view of the fact that oscillations have been entirely neglected in the theoretical computation and that the measurements are subject to experimental errors.

It is now possible to develop an approximate expression for the length of tube required for the flow regulator. The shock is at its furthest stable position (FSP) from the constriction, when the outlet end of the tube is about to buckle inwards. The tube length then must exceed this distance by several diameters. Thus, the tube length is arbitrarily taken to be equal to

$$L = (x_1' - x_1)^{**} + 6D_0 \tag{7.35}$$

The furthest stable position $(x_1' - x_1)^{**}$ of the shock is found by writing the modified Bernoulli relation between the inlet and the outlet. Thus,

$$p_i + \frac{1}{2}\rho u_i^2 = p_o^{**} + \frac{1}{2}\rho u_o^2 + \Delta p_c + \Delta p_{f_1} + \Delta p_s + \Delta p_{f_2} \tag{7.36}$$

where Δp_c, Δp_{f_1}, Δp_s, Δp_{f_2}, are the stagnation head losses across the constriction, across the tube section upstream of the shock, across the shock, and across the tube section downstream of the shock respectively. Each of these losses can be expressed approximately by the following relations.

$$\Delta p_c = K_c \frac{1}{2}\rho u_c^2 \tag{7.37}$$

$$\Delta p_{f_1} = \left(1 - \left(\frac{\alpha_1}{\alpha_1'}\right)^2 - \frac{2}{S_1^2}\,\frac{\left(\frac{\alpha_1'}{\alpha_1}\right)^{M-2} - 1}{M-2}\right)\frac{1}{2}\rho u_1^2 \tag{7.38}$$

$$\Delta p_s = K_L\left(1 - \frac{\alpha_1'}{\alpha_2'}\right)^2 \frac{1}{2}\rho u_1'^2 \tag{7.39}$$

$$\Delta p_{f_2} \simeq \frac{4f_o}{D_o}\left(\frac{L - (x_1' - x_1)^{**}}{\alpha_2'}\right)\frac{1}{2}\rho u_2^2 \tag{7.40}$$

Equation (7.38) has been obtained from equations (7.31) and (7.33). As before, it will be assumed that $\alpha_i = \alpha_o = 1$, $\alpha_2' \simeq 1$, $K_C \simeq 0$. Further, it can be estimated that the last term of (7.38) is negligible and that

$\Delta p_{f_2} << \Delta p_{f_1}$. Hence, equation (7.36) can be written as

$$\left(\frac{p_i - p_e}{K_B} \right) \simeq \left(\frac{p_o - p_e}{K_B} \right)^{**} + \left(\frac{Q}{A_0 \sqrt{2K_B/\rho}} \right)^2 \left(\frac{1}{\alpha_1^2} - \frac{1}{\alpha_1'^2} + \right.$$

$$\left. + K_L \left(\frac{1}{\alpha_1'} - 1 \right)^2 \right) \tag{7.41}$$

Using equations (7.23) and (7.21) in (7.41) gives

$$\left(\frac{p_i - p_e}{K_B} \right) \simeq -3 + \left(\frac{p_i - p_e}{K_B} - P(\alpha_1) \right) \left(1 - \left(\frac{\alpha_1}{\alpha_1'} \right)^2 + \right.$$

$$\left. + K_L \, \alpha_1^2 \left(\frac{1}{\alpha_1'} - 1 \right)^2 \right) \tag{7.42}$$

For given $\left(\alpha_c , \frac{p_i - p_e}{K_B} \right)$, α_1' can be found by using (7.20) and the above equation. Having found α_1' , the distance $(x_1' - x_1)^{**}$ can be found from the approximate relation

$$(x_1' - x_1)^{**} = \frac{D_0}{2f_0} (\alpha_1' - \alpha_1) \tag{7.43}$$

and the tube length can be computed from the ad hoc relation (7.35).

In summary, in this section, the flow regulator experimental data and some features of the distributions obtained in the shock experiments were explained with reasonable agreement by means of an

approximate analysis. Next, on the basis of this analysis, approximate expressions have been developed for the selection of design parameters in the subsequent flow regulator design. In particular, for large Reynolds Number and large inlet speed index, the required length of collapsible tube for the minimum possible downstream pressure and specified inlet conditions is given by (7.20), (7.42), (7.43), and (7.35). Further, equations (7.24) and (7.26) lead to the determination of the maximum possible downstream pressure for continuous flow regulation.

7.3 Design Criteria for a Collapsible Tube Flow Regulator

In the first part of this section, an approximate procedure for the design of a collapsible tube flow regulator will be developed on the basis of the approximate relations derived in Section 7.2. In the second part, the design procedure will be illustrated by means of a design example. In the third and last part, this design will be compared with a flow regulator of a type that is usually employed for such flow regulation in industry.

A. Design Procedure

The function of the proposed flow regulator is indicated in Fig. (22). The objective is to maintain the flow rate at the outlet fixed within a narrow specified range independent of downstream pressure which varies by a predetermined finite amount. The upstream pressure is held fixed at a specified value. The basic configuration of the flow regulator is shown in Fig. (5a) while two possible design realizations are shown in Figs. (23a) and (23b). Two external control variables

are allowed, namely, the constriction area ratio α_c and the external pressure p_e. For instance, the area ratio α_c may be varied by means of a mechanical constriction as in Fig. (23b). The external pressure p_e may be kept fixed either by connection to the atmosphere or may be made adjustable by connection to a regulated, external air supply.

The variables that need to be considered in the design of the flow regulator fall into two separate categories, namely, specified variables, and design variables. The latter group can be divided into primary design variables and secondary design variables depending on the degree of their importance in the design. This categorization of variables is given in Table 10. Neglecting for the moment the secondary design variables, the flow rate Q can be expressed as a function of all the remaining specified and design variables. Thus,

$$Q = f(A_0, L, K_B, \mu, \rho, A_c, p_i - p_e, p_o - p_e, T_0) \tag{7.44}$$

In the above expression, on the basis of prior knowledge, only the inlet and outlet transmural pressure differences have been included. By dimensional analysis, this can be alternatively compressed as a relation between non-dimensional groups as given below.

$$\frac{Q}{A_0\sqrt{2K_B/\rho}} = f(Re_{D_0}, L/D_0, \alpha_c, (p_i - p_e)/K_B, (p_o - p_e)/K_B, T_0/D_0K_B) \tag{7.45}$$

The functional relationship indicated above reduces to a simpler form when the specified variables and the design variables fall within the design range of the flow regulator. As shown in Section 7.2, it then assumes the form

$$\frac{Q}{A_0\sqrt{2K_B/\rho}} = \bar{f}_R(\alpha_c \ , \ \frac{p_i - p_e}{K_B}) \tag{7.46}$$

provided the following conditions, which specify its range of validity, are satisfied.

1) The flow is inertia dominated

$$Re_{D_0} >> 1 \tag{7.47}$$

2) The flow immediately downstream of the constriction is supercritical

$$S_1^2 > 1 \tag{7.48}$$

3) The range of variation of the pressure difference at the outlet is such that

$$\left(\frac{p_{o\ max} - p_e}{K_B}\right) < \left(\frac{p_o - p_e}{K_B}\right)^* \tag{7.49}$$

$$\left(\frac{p_{o\ min} - p_e}{K_B}\right) > \left(\frac{p_o - p_e}{K_B}\right)^{**} \simeq -3 \tag{7.50}$$

At the first limit given above, the shock vanishes into the constriction and the flow is no longer regulated. Beyond the second limit, the shock

begins to oscillate along the tube and the outlet flow also oscillates in time.

4) The length of the collapsible tube must be greater than the maximum distance from the constriction at which a stable shock can be formed. That is,

$$L > (x_1' - x_1)^{**} \tag{7.51}$$

A performance index (P.I.) for the flow regulator can be defined as

$$P.I. = \frac{\Delta Q}{Q} \times 100\% \tag{7.52}$$

where Q is the specified flow rate and ΔQ is the maximum deviation of flow rate from its specified value when the downstream pressure p_o varies over its full specified range of variation. Unfortunately, the value of ΔQ cannot be predicted with reasonable accuracy by means of the present approximate analysis and must be experimentally measured. However, by making the specified range lie well within the limits $(p_o - p_e)^*$ and $(p_o - p_e)^{**}$, the performance index can be made to satisfy the specifications.

The procedure for the design of the flow regulator for a given set of specified variables (Q, p_i, $p_{o\ max}$, $p_{o\ min}$, ρ, μ) is shown in Fig. (60) and is described below.

1) Selection of A_0, K_B, p_e:

The resting area A_0 (or equivalently D_0), the bending stiffness K_B, and the external pressure p_e are selected to satisfy conditions (7.47), (7.48), and (7.50).

In making this selection, the designer should also be guided by other practical considerations in the choice of materials and dimensions. For example, the structural strength, resistance to corrosion and wear, fabrication constraints, cost etc. should be considered. If the critical Reynolds Number for turbulence is not exceeded, then the appropriate friction factors should be employed in the subsequent calculations. In employing (7.48), the area ratio α_1 can be approximated by the constriction area ratio α_c, and its useful practical range of variation should be taken as $0.15 < \alpha_c < 0.45$. The wavespeed for a given α_c in computing (7.48) can be obtained from the non-dimensional plot in Fig. (2). A convenient estimate of the flow rate Q^* at which $S_1 = 1$ for the selected parameters can be obtained from Fig. (59). It is also suggested that $(p_{o\ min} - p_e)$ be selected to be a positive quantity and that S_1 be chosen to be greater than about 3.

2) Selection of α_c:

Once (A_0, K_B, p_e) have been chosen, the values of the normalized flow rate $(Q/A_0\sqrt{2K_B/\rho}$ and the normalized inlet pressure difference $\left(\frac{p_i - p_e}{K_B}\right)$ are computed next. The corresponding value of the constriction area ratio α_c is then calculated from equation (7.21) or is obtained from the plot of Fig. (57).

If the same flow regulator is required to function over a range of flow rates $(Q_{min} < Q < Q_{max})$ and a range of inlet pressures $(p_{i\ min} < p_i < p_{i\ max})$, the corresponding values of the constriction area ratio α_c can be located in the plot of Fig. (57) within a design region as shown in Fig. (61). Once again the practical lower and upper limits of α_c have been taken as 0.15 and 0.45 respectively.

3) Selection of L:

The length of the collapsible tube is found from relation (7.35) which expresses the fact that the tube length must be several diameters greater than the distance $(x_1' - x_1)^{**}$ of the shock from the constriction when it is at its furthest stable position (FSP). The value of the area ratio α_1' at the entry to the shock in this position is first calculated from (7.20) and (7.42). Then relation (7.43) is used to compute the distance $(x_1' - x_1)^{**}$.

4) Check on $p_{o\ max}$:

Finally, one must make sure that the maximum downstream pressure is not so high as to force the shock inside the constriction since this would cause the flow rate to fall below its specified value for fixed inlet pressure. Thus, it must be checked that (7.49) is satisfied by computing $(p_o - p_e)^*/K_B$ from (7.24) and (7.25).

If step (4) is satisfied, allowing for a suitable margin of error, then the basic design is complete. If it is not satisfied, then the design values of (A_0, K_B, p_e, L) have to be suitably altered until all the conditions are satisfied. For this purpose, it is useful to know how

sensitive the design is to changes in the values of variables. A sensitivity analysis of this type is given next. The actual performance index (P.I.) defined by (7.52) can be estimated approximately using the experimental correlation of Fig.(27). For more accurate values of the performance index measurements must be made on the prototype design.

The sensitivity of the regulated flowrate to changes in design variables can be found from equation (7.21) with $\alpha_i = 1$ and $K_c \simeq 0$. The fractional change in flow rate Q due to fractional changes in the design variables is obtained by differentiating (7.21).

$$\frac{dQ}{Q} = Q_{A_0} \frac{dA_0}{A_0} + Q_{K_B} \frac{dK_B}{K_B} + Q_{(p_i - p_e)} \frac{d(p_i - p_e)}{(p_i - p_e)} + Q_{\alpha_c} \frac{d\alpha_c}{\alpha_c} \tag{7.53}$$

where

$$\begin{aligned} Q_{A_0} &= 1 \\ Q_{K_B} &= -\frac{1}{2(\beta - 1)} \\ Q_{(p_i - p_e)} &= \frac{\beta}{2(\beta - 1)} \\ Q_{\alpha_c} &= \left(\frac{1}{1 - \alpha_c^2} - \frac{1}{2(\beta - 1)} \frac{\alpha_c}{P(\alpha_c)} \frac{dP}{d\alpha}\bigg|_{\alpha_c} \right) \\ \beta &\equiv \frac{p_i - p_e}{K_B P(\alpha_c)} \end{aligned} \tag{7.54}$$

The sensitivity coefficients are calculated for a typical design example in the following section.

B. A Typical Flow Regulator Design

The design example that will be presented here applies to

a situation in which a relatively large flow rate of water is to be delivered from a constant low pressure source to a vessel in which the pressure varies by as much as 100% of its average value.

The specified variables are:

Flow rate $Q = 17.5$ ℓ/min (to be maintained fixed)

Source pressure $p_i = 35$ cm H_2O (fixed)

Vessel pressure $p_{o\ min} = 5$ cm H_2O ; $p_{o\ max} = 15$ cm H_2O

$\mu = 0.01$ gm/cm sec; $\rho = 1.0$ gm/cm^3

The design procedure developed in part A gives the following results.

1) Selection of A_0, K_B, p_e:

$D_0 = 2.54$ cm ; $A_0 = 5.067$ cm^2

$K_B = 400$ dynes/cm^2 ; $p_e = 5$ cm H_2O

The value K_B selected corresponds to a latex rubber tube of approximately 1 mm wall thickness. This is satisfactory from the point of view of strength and durability. These values yield

$$Re_{D_0} = 14{,}620 \gg 1$$

$$S_1^2 \simeq 13.4 > 1 \qquad (\text{taking } \alpha_1 \simeq 0.2)$$

$$\left(\frac{p_{o\ min} - p_e}{K_B}\right) \simeq 0.$$

2) Selection of α_c:

Assuming $\alpha_c \simeq \alpha_1$, $K_c \simeq 0$, the values obtained are:

$$Q/A_0\sqrt{2K_B/\rho} = 2.035 \ ; \ (p_i - p_e)/K_B = 73.58$$

Hence, $\alpha_c \simeq 0.217$.

3) Selection of L:

This step yields:

$\alpha_1' = 0.722$, $(x_1' - x_1)^{**} = 89.2$ cm.

Hence, $L = 104.4$ cm.

4) Check on $p_{o\ max}$:

This calculation gives $(p_o - p_e)^*/ K_B = 37.1$, and $p_o^* = 20.1$ cm H_2O, whereas $p_{o\ max} = 15$ cm H_2O so that the shock will not be driven to the constriction at the highest vessel pressure. Hence, this design meets all the requirements.

The sensitivity analysis yields

$$\frac{dQ}{Q} = \frac{dA_o}{A_o} + 0.061\,\frac{dK_B}{K_B} + 0.439\,\frac{d(p_i - p_e)}{(p_i - p_e)} + 0.958\,\frac{d\alpha_c}{\alpha_c} \qquad (7.55)$$

As a result of (7.55), in the neighborhood of the design values employed, an increase in each of the variables (A_o, K_B, $p_i - p_e$, α_c) leads to an increase in flow rate. If A_o and K_B are considered to be fixed for this design, then the flow rate is more sensitive to changes in constriction area ratio than to changes in inlet pressure difference.

C. Comparison Between a Collapsible Tube Flow Regulator and a Standard Diaphragm Type Flow Regulator.

It is the purpose of this part to compare the collapsible tube flow regulator designed in part A of this section with a typical flow regulator design of a type used in industry for the same function. Such a comparison serves to identify and establish the performance and cost standards the proposed flow regulator must meet in order to be feasible.

A flow rate control system usually consists of three key components.

1. A flow measuring device which is sometimes made up of two units, a primary element such as an orifice plate, venturi tube, or pilot float, and a differential pressure transmitter.
2. A controller which amplifies and/or transmits, in suitable form, the differential pressure signal to the final control element.
3. A control valve which is the final control element that directly influences the flow.

Generally, such control systems require an external source of power such as electricity or a pressurized air line. The term regulator is reserved for a self-contained control system with a built in controller and which does not require an external source of power for its operation. It usually derives the power from the flow itself.

Regulators usually cost less than the combination controller, transmitting device, and control valve. They are generally smaller, cheaper to buy, to install, and to maintain in service. However, they have relatively narrow ranges of operation, lack the flexibility of a control system and have poorer performance " droop " inherent in proportional controllers. When the size gets bigger, and performance demands are also stringent, the economics begin to shift in favor of control systems. In general, if either a control system or a regulator is suitable, a lower cost regulator is preferred.

A type of flow regulator usually employed in industry for flow rate regulation, and the one considered here as typical of its class, is shown in Fig.(63). The final control element is a valve which may be one

of several different types. Here, it is considered to be a globe valve. The flow rate is measured by means of an orifice plate included in the exit pipe. It is proportional to the differential pressure developed across the orifice plate. The controller is the diaphragm arrangement which transmitts the differential pressure signal to the control valve. If the size of the diaphragm required to directly operate the valve at the differential pressure developed across the orifice plate is excessive, then a pilot valve may be employed as in Fig.(63). It derives its source power from the pressure at the inlet and provides an amplified differential pressure to activate the diaphragm. The system is arranged in such a way that an increase in flow rate causes the control valve to close thus tending to nullify the initial flow rate increase. The base or set point flow rate is set by means of the initial spring compression.

The design of a flow regulator of the type described above, and meeting the specifications used for the collapsible tube flow regulator design in section (7.3) is given in Appendix C. Table 11 summarizes the performance predictions and cost estimates for the regulators.

The design of Appendix C was used to determine the rough sizes of the various components of the standard flow regulator. The costs for this regulator were in part established by consulting with a representative of the Foxboro Company, Foxboro, Massachusetts which manufactures a wide variety of flow control equipment.

The cost of the collapsible tube flow regulator is based on the dimensions established in Section (7.3) and is for the configuration of Fig.(23a). It employs a collapsible tube immersed in a tank of water,

the surface of the water being exposed to the atmosphere. Thus, it does not require an external, regulated air supply. The cost is based on current material, labor, and overhead costs for a typical large manufacturing outfit. The cost thus estimated is very approximate since no previously established cost figures exist, as this is a radically new design for a flow rate regulator.

The performance figures for the two regulators are listed in Table 11. The first quantity listed is the performance index (P.I) (also called regulator droop) which is the percentage change in flow rate as the outlet pressure varies beyond its full specified range, while the inlet pressure is held constant. The calculation of this index for the standard regulator was given in Appendix C. As the specified maximum outlet pressure is only 75% of the value at the knee of the regulation curve, the droop over this pressure range is expected to be very small. This is substantiated by the experimental plot of Fig.(27).

The next quantity of importance in characterizing the regulator performance is termed rangeability. Rangeability is defined as the ratio of the maximum to the minimum regulated flow rate of the regulator while inlet and outlet pressures are kept fixed. In the standard flow regulator, this is achieved by changing the initial spring compression Δ . Assuming that Δ can be varied by as much as $\pm$ 50%, the maximum and minimum flow rates can be obtained from Fig.(64), for a specified regulator droop. In the collapsible tube regulator, the rangeability was obtained by the following way. Q_{max} was computed as the value for which $\alpha_c = \alpha_{c\ max} = 0.45$ and $\left(\frac{p_o - p_e}{K_B} \right)^* = \left(\frac{p_{o\ max} - p_e}{K_B} \right)$. Q_{min} was computed by setting $\alpha_c = \alpha_{c\ min}$

and $\left(\frac{p_o - p_e}{K_B}\right)^{**} = -3$. This is indicated in Fig.(57) which defines the design range subject to the additional requirements that $S_1^2 >> 1$, and $Re_{D_o} >> 1$.

In conclusion, it is seen from Table 11 that the performance of the collapsible tube flow regulator is superior to that of the standard regulator. The cost of the former is only about a third of the latter. The collapsible tube regulator has the advantage of not having any movable parts but suffers from the relatively long length of tube required. The standard regulator would require regular maintenance to eliminate friction at the valve stem, valve seat wear, and blockage of the differential pressure tubing. If the inlet pressure exceeds the bursting pressure of the tube, then additional devices such as relief valves have to be installed to ensure safety. Thus, the collapsible tube flow regulator should be considered useful primarily at inlet pressures lower than the tube bursting pressure. However, the use of a pressurized external chamber or a protective cuff around the collapsible tube just before the constriction could eliminate this requirement.

REFERENCES

1. Shapiro, A.H., "Physiologic and medical aspects of flow in collapsible tubes," Proc. 6th Canadian Congr. of Appl. Mech., Vancouver, 1977.

2. Shapiro, A.H., "Steadyflow in collapsible tubes," J. Biomed. Engrg., Trans. ASME, 99, 126-147 (1977).

3. Conrad, W.A., "Pressure-flow relationships in collapsible tubes," IEEE Trans. Bio-Med. Engrg., BME-16(4), 284-295 (1969).

4. Kirshner, J.M., Fluid Amplifiers, New York: McGraw-Hill, 1966.

5. Knowlton, F.P. and Starling, E.H., "The influence of variations in temperature and blood pressure on the performance of the isolated mammalian heart," J. Physiol., 44, 206-219 (1912).

6. Holt, J.P., "The collapse factor in the measurement of venous pressure; the flow of fluid through collapsible tubes," Am. J. Physiol., 134, 292-299 (1944).

7. Holt, J.P., "Flow of liquids through collapsible tubes," Am. Heart J., 46, 715-725 (1953).

8. Holt, J.P., "Flow of liquids through collapsible tubes," Am. Heart J., 7, 342-353 (1959).

9. Rodbard, S. and Saiki, H., "Flow through collapsible tubes," Am. Heart J., 46, 715-725 (1953)

10. Rodbard, S., "Hydrodynamics illustrated in an artificial circulation model," J. Appl. Physiol., 5, 191-194 (1952).

11. Rodbard, S., "Flow through collapsible tubes; augmented flow product by resistance at the outlet," Circulation, 11, 280-287 (1955).

12. Rodbard, S., "A hydrodynamic mechanism for autoregulation of flow," Cardiologia, 48, 532-535 (1966).

13. Rodbard, S. and Takacs, L., "Hydrodynamics of autoregulation," Cardiologia, 48, 433-440 (1966).

14. Bradley, S.E., "The hepatic circulation," in Handbook of Physiology (W.F. Hamilton and D. Dow, eds.), Section 2: Circulation; American Physiology Society, Washington, D.C., 1963, pp. 1387-1438.

15. Katz, A.I., Chen, Y., and Moreno, A.H., "Flow through a collapsible tube; experimental analysis and mathematical model," Biophys. J., 9, 1261-1279 (1969).

16. Brower, R.W., and Noordergraaf, A., "Pressure flow characteristics of collapsible tubes: a reconciliation of seemingly contradictory results," Ann. Biomed. Engrg., 1, 333-335 (1973).

17. Lambert, R.K., and Wilson, T.A., "Flow limitation in a collapsible tube," J. Appl. Physiol., 33(1), 150-153 (1972).

18. Brecher, G.A., Am. J. Physiol., 169, 423 (1952).

19. Wild, R., Pedley, T.J., and Riley, D.S., "Viscous flow in collapsible tubes of slowly varying elliptical cross-section," J. Fluid Mech., 81, 273-294 (1977).

20. Olsen, J.H., and Shapiro, A.H., "Large amplitude unsteady flow in liquid filled elastic tubes," J. Fluid Mech., 29, 513-538 (1967).

21. Lambert, H., "On the nonlinearities of fluid flow in non-rigid tubes," J. Franklin Institute, 266(2), 83-102 (August 1958).

22. Streeter, V.L., Keitzer, W.F., and Bohr, D.F., "Energy dissipation in pulsatile flow through distensible tapered vessels," J. Pulsatile Blood Flow (E.O. Attinger, ed.), New York: McGraw-Hill, pp. 149-177.

23. Anliker, M., Rockwell, R.L., and Ogden, E., "Nonlinear analysis of flow pulses and shock waves in arteries," Z. Agnew. Math. Phys., 22, 217-246 and 563-581 (1971).

24. Maxwell, J. and Anliker, M., "The dissipation and dispersion of small waves in arteries and veins with viscoelastic wall properties," Biophys. J., 8, 920-950 (1968).

25. Rudinger, G., "Shock waves in mathematical models of the aorta," J. Appl. Mech., ASME Series E, 37, 34 (1970).

26. Kivity, Y. and Collins, R., "Steady state fluid flow in viscoelastic tubes: Application to blood flow in human arteries," J. Mech., 26(5), 921-931, Warszawa (1974).

27. Kivity, Y. and Collins, R., "Nonlinear wave propagation in viscoelastic tubes: application to aortic rupture," J. Biomech., 7, 1 (1974).

28. King, A.L., "Waves in elastic tubes: velocity of pulse wave in large arteries," J. Appl. Phys., 18, 255 (1947).

29. Beam, R.M., "Finite amplitude waves in fluid-filled elastic tubes, wave distortion, shock waves, and Korotkoff sounds," NASA Rpt. No. TN D-4803, 1968.

30. Griffiths, D.J., "Urethral elasticity and micturition hydrodynamics in females," Med. & Biol. Engrg., 7, 201-215 (1969).

31. Griffiths, D.J., "Hydrodynamics of male micturition: I & II. Theory of steady flow through elastic-walled tubes," Med. & Biol. Engrg., 9, 581-596 (1971).

32. Griffiths, D.J., "Steady flow through veins and collapsible tubes," Med. & Biol. Engrg., 9, 597-602 (1971).

33. Griffiths, D.J., "The mechanics of the urethra and of micturition," Brit. J. Urol., 45, 497-507 (1973).

34. Griffiths, D.J., "Oscillations in the outflow from a collapsible tube," Med. & Biol. Engrg., 15, 357-362 (1977).

35. Danahy, D.T., and Ronan, J.A. Jr., "Cervical venous hums in patients on chronic hemodialysis," N.E. J. Med., 291, 237 (1974).

36. Groom, D., Boone, J.A., and Jenkins, M., "Venous hum in cardiac auscultation," J.A.M.A., 159, 639 (1955).

37. Oates, G.C., "Fluid flow in soft-walled tubes, Part I: Steady flow; Pa-t II: Behavior of finite waves," Med. & Biol. Engrg., 13, 773-784 (1975).

38. Rubinow, S.I., and Keller, J.B., "Flow of a viscous fluid through an elastic tube with applications to blood flow," J. Theor. Biol., 35, 299-313 (1972).

39. Griffiths, D.J., "Oscillations in the outflow from a collapsible tube," Med. & Biol. Engrg., 15, 357-362 (1977).

40. Tadbakhsh, I. and Odeh, F., "Equilibrium states of elastic rings," J. Math. Anal. & Appl., 18, 59-74 (1967).

41. Flaherty, J.E., Keller, J.B., and Rubinow, S.I., "Post-buckling behaviour of elastic tubes and rings with opposite sides in contact," SIAM. J. Appl. Math., 24(4), 446-455 (1972).

42. Kresh, E., and Noordergraaf, A., "Cross-sectional shape of collapsible tubes," Biophys. J., 12, 274-294 (1972).

43. Heywood, J.H., "Post-buckling analysis of a circular elastic ring on a long cylindrical shell," Proc. Symp. on Theory of Thin Elastic Shells (W.T. Koiter, ed.), North Holland Publ. Co., 1960, pp. 122-133.

44. Love, A.E.H., The Mathematical Theory of Elasticity, 4th Ed., Dover, 1944, p. 574.

45. Taylor, L.A., and Gerrard, H.J., "Pressure-radius relationships for elastic tubes and their application to arteries; Part I: Theoretical relationships; Part II: A comparison of theory and experiment for a rubber tube," Med. & Biol. Engrg. & Comput., 15, 11-18 and 18-21 (1977).

46. Treloar, L.R.G., The Physics of Rubber Elasticity, Clarendon Press, 1958.

47. Shapiro, A.H., "A proposal for a broad program of experimental and theoretical research on flow in collapsible tubes," unpublished report, Fluid Mechanics Laboratory, MIT, October 1975.

48. Brower, R.W. and Scholten, C., "Experimental evidence on the mechanism for the instability of flow in collapsible vessels," Med. & Biol. Engrg., Nov. 1975.

49. Kamm, R.D., "A study of external pneumatic compression for the prevention of deep vein thrombosis," Ph.D. Thesis, MIT, May 1977.

50. White, F.M., Viscous Fluid Flow, New York: McGraw-Hill, 1974, p. 123.

51. Schlichting, H., Boundary Layer Theory, New York: McGraw-Hill, 1968, pp. 561 and 575.

52. Shapiro, A.H., The Dynamics and Thermodynamics of Compressible Fluid Flow, Vol. II, New York: The Ronald Press Co., 1953.

53. Nicholson, H., Heiser, W.H., and Olsen, J.H., "Wave propagation in liquid-filled elastic tubes," Bul. Mech. Engrg. Educ., Vol. 6, 1967, pp. 371-376.

54. Woolley, R.L., and Kline, S.J., "A method for calculation of a fully stalled flow," Report MD-33, Dept. Mechanical Engineering, Stanford University, Nov. 1973.

55. Fromm, J.F., "Numerical solution of two-dimensional stall in fluid diffusers," Phys. of Fluids Suppl., Vol. 12(12), Part II, II.113-II.119 (1969).

56. Rohsenow, W.M. and Choi, H.Y., Heat, Mass, and Momentum Transfer, Prentice Hall, Inc., 1961.

57. Henry, J.R., National Advisory Comm. Aeronatucis, ARR No. 14F26, June 1944.

58. Patterson, G.N., "Modern diffuser design," Aircraft Engrg., 10, 267-273 (1938).

APPENDIX A:

EXPERIMENTAL DETERMINATION OF ERRORS DUE TO LEAKAGE CURRENTS IN PROBE AREA MEASUREMENT

In this experiment, a latex tube of the same dimensions and properties as the ones used in the tube law and shock experiments was inflated against the walls of a rigid plexiglas cylinder of known cross-sectional area. The inside of the cylinder was lined with aluminum foil and wetted with salt-water. The intention was to perform the area measurement under the most adverse conditions of external chamber conductivity and contact resistance. The internal area of the tube could be calculated knowing the wall thickness of the tube and the internal diameter of the rigid tube. A rigid reference section was also arranged in series with this tube section as shown in Fig.12 . Since all areas and lengths of the probe and reference section are known, the value that the ratio of the probe voltage to the reference voltage should take was also known.

During the experiment, the ratio of these voltages was measured for different frequencies, varying from D.C. to 800 kHz. It was observed that the deviation of this ratio from that calculated increased with increasing frequency. The cumulative error was of the order of 6% at approximately 500 Hz. When the same experiment was performed without the metal foil or salt-water on the outside, the deviation was negligible. Thus, it was concluded that under the conditions prevailing in the actual tube law and shock experiments, when the external conductivity is much smaller, the error in area measurement due to leakage currents would be well within the self-imposed 4% limit.

APPENDIX B:

ESTIMATION OF CONSTANTS APPEARING IN THE PERTURBATION ANALYSIS OF PRECURSOR WAVES

In this appendix, constants a and b appearing in the perturbation analysis of section (4.5) and defined by expressions (4.74) are estimated. These values are calculated for the location x = 31.6 cm in the experimentally obtained area and pressure distribution given in Figs. (31) and (31s). At this point, the mean curves intersect the distributions and the wavelength is measured as indicated in Fig.(16). The measured values of area ratio, flow rate, and wavelength are 0.40, 21.0 ℓ/min, and 43.0 cm respectively. Once a and b are calculated and approximation (4.81) is justified, expression (4.86) can be used to compute the approximate theoretical value of the wavelength in the neighborhood of this location.

Constants a and b can be defined by

$$a \equiv \frac{(\bar{S}^2 - 1)}{3\,\varepsilon} \tag{B.1}$$

$$b \equiv \frac{\bar{S}^2\,\bar{f}\,(\bar{M} + \bar{\gamma})}{\varepsilon} \tag{B.2}$$

where

$$\varepsilon \equiv \frac{\bar{T}\,\bar{\alpha}}{4\rho\bar{c}^2 D_0\,\sqrt{1 - \alpha}} \tag{B.3}$$

$$\bar{f} \equiv \frac{0.0791}{Re_{D_0}^{0.25}}\,\frac{1}{\bar{\alpha}} \tag{B.4}$$

$$Re_{D_0} \equiv \frac{Q}{\nu}\sqrt{\frac{4}{\pi A_0}} \tag{B.5}$$

The data obtained from the distributions are

$\bar{\alpha} = 0.40$; $\bar{\lambda} = 4.30$ cm

$Q = 21.0$ ℓ/min ; $A_0 = 4.53$ cm^2

The value of wave speed $\bar{c}$ and parameter $\bar{M}$ corresponding to $\bar{\alpha} = 0.40$ are obtained from Figs.(2) and (13) respectively.

$$\bar{c} = 31.54 \text{ cm/sec} \quad ; \quad \bar{M} = 2.91.$$

Also, $\bar{\gamma} = 1.0$

$$\bar{u} = \frac{Q}{A_0 \alpha} = 193.16 \text{ cm/sec}$$

$$\bar{S} = \frac{\bar{u}}{\bar{c}} = 6.125.$$

Hence,

$$\bar{S}^2 = 37.52 \gg 1.$$

Taking $\nu = 0.01$ cm^2/sec, from (B.5) and (B.4)

$$Re_{D_0} = 18{,}560 \quad ; \quad \bar{f} = 0.0169$$

The wall tension $\bar{T}$ is approximated as before from the initial strain,

$$\bar{T} \simeq Et\varepsilon_{xx} = (1.6 \times 10^7 \text{ dynes/cm}^2)(0.083 \text{ cm})(0.06) = 7.97 \times 10^4 \text{ dynes/cm}$$

Therefore, from (B.3)

$$\varepsilon = 4.072$$

From (B.1) and (B.2)

$$a = 2.989$$

$$b = 0.609$$

Hence,

$$ba^{-3/2} = 0.11 \ll 1$$

Thus, approximation (4.81) would be valid and the wavelength $\bar{\lambda}$ is given by (4.86)

$$\frac{\bar{\lambda}}{D_0} \simeq \frac{2\pi}{\sqrt{3a}} = 2.098$$

Hence, $\bar{\lambda}$ = 5.33 cm while the experimentally obtained value for $\bar{\lambda}$ is 4.30 cm.

APPENDIX C

DESIGN OF A STANDARD TYPE DIAPHRAGM ACTUATED FLOW RATE REGULATOR

In this appendix, the equations governing the steady state operation of a diaphragm operated flow rate regulator will be derived. Subsequently, they will be used to design a flow regulator satisfying the operating conditions specified for the collapsible tube flow regulator in Section 7.3.

The basic configuration of this flow rate regulator is shown in Fig. (63). The control element is a valve which may be one of many different types. Here, it will be considered to be a globe valve. The valve is opened or closed by the diaphragm driven valve stem. The pressure applied across the diaphragm is the differential pressure developed across the orifice plate placed at the exit of the valve. This differential pressure is proportional to the kinetic energy of the fluid at the exit. The system is arranged in such a way that an increase in differential pressure leads to the closing of the valve which in turn decreases the flow rate. Thus, it acts as a feedback mechanism tending to maintain a steady flow rate preset by means of the initial compression of the spring. The size of the diaphragm required to operate the valve, especially for low flow rates, can be reduced by using a pilot valve connected as shown. It employs the inlet line pressure as a power source and acts as a fluid amplifier producing an output pressure difference

equal to a multiple of the value of the input pressure difference. In the following analysis, nonlinearities such as those due to friction experienced by the valve stem, change in effective area of the diaphragm, and spring nonlinearities will be neglected. Further, only incompressible fluids will be considered.

The flow rate at any location is given by,

$$Q = Au = (\alpha A_0)u \tag{C.1}$$

where A_0 is the pipe area at the exit and the area ratio is defined as $\alpha \equiv A/A_0$. The position of the diaphragm at which the valve is fully closed is designated $x = 0$. In this position the spring has an initial compression equal to Δ. The variation of flow area A_v at the valve throat is assumed to be linear with x so that

$$\alpha_v = \bar{\alpha}\, x/\ell \tag{C.2}$$

where $\bar{A} = A_0\bar{\alpha}$ is the throat area when the valve is fully open and ℓ is the travel of the valve.

Balance of forces on the valve stem gives:

$$(p_i - p_1)\bar{A} - (p_2' - p_r')\, A_D + k(\Delta - x) = 0 \quad . \tag{C.3}$$

where A_D is the effective diaphragm area, k is the spring constant, $(p_2' - p_r')$ is the differential pressure delivered by the pilot valve in response to the orifice pressure differential $(p_2 - p_r)$. If the pilot valve gain is $G(= 1$ if directly connected in the absence of the pilot valve), then

$$(p_2' - p_r') = G(p_2 - p_r) \tag{C.4}$$

Thus, (C.3) can be recast as

$$\left(\frac{p_i - p_1}{K_B} \right) \frac{\bar{\alpha}}{\alpha_D} - \left(\frac{p_2 - p_r}{K_B} \right) G + \left(1 - \frac{x}{\Delta}\right) = 0 \tag{C.5}$$

where the equivalent diaphragm stiffness K_B is defined by

$$K_B = \frac{k\Delta}{A_D} \tag{C.6}$$

The variation of pressure at selected locations along the flow path are obtained by the modified Bernoulli relation accounting for the flow losses. Thus,

$$p_i + \frac{1}{2} \rho u_i^2 = p_1 + (1 + K_v) \frac{1}{2} \rho u_v^2 \tag{C.7}$$

$$p_2 = p_1 + \frac{1}{2} \rho u_1^2 = p_r + (1 + K_c) \frac{1}{2} \rho u_r^2 \tag{C.8}$$

$$p_2 = p_o + \frac{1}{2} \rho u_o^2 + (K_c + K_e) \frac{1}{2} \rho u_r^2 \tag{C.9}$$

In writing (C.8), the pressure p_2 measured at the upstream orifice tap is taken to be equal to the stagnation pressure and the pressure p_r is taken to be equal to the pressure within the orifice jet flow. The coefficients K_v, K_c, K_e are the loss coefficients at the valve throat, at the orifice entry, and at the orifice exit respectively. An

assumption implied in (C.7) - (C.9) is that

$$Re_{D_0} \equiv Q/\nu\sqrt{4/\pi A_0} \gg 1 \tag{C.10}$$

From (C.1) and (C.7) - (C.9) one obtains

$$\left(\frac{p_2 - p_r}{K_B}\right) = \frac{(1 + K_c)}{\alpha_r^2}\hat{Q}^2 \quad ; \quad \hat{Q} \equiv \frac{Q}{A_0\sqrt{2K_B/\rho}} \tag{C.11}$$

$$\left(\frac{p_i - p_1}{K_B}\right) = \left(\frac{1}{\alpha_1^2} - \frac{1}{\alpha_i^2} + \frac{K_v}{\alpha_v^2}\right)\hat{Q}^2 \tag{C.12}$$

$$\left(\frac{p_i - p_o}{K_B}\right) = \hat{Q}^2\left(1 - \frac{1}{\alpha_i^2} + \frac{K_c + K_e}{\alpha_r^2} + \frac{K_v}{\alpha_v^2}\right) \tag{C.13}$$

Substituting from (C.2), (C.11) and (C.12) in (C.5) we obtain

$$\hat{Q}^2 = \left(\frac{1 - \frac{\ell}{\Delta}\frac{\alpha_v}{\bar{\alpha}}}{G\frac{(1+K_c)}{\alpha_r^2} - \frac{\bar{\alpha}}{\alpha_D}\left(\frac{1}{\alpha_1^2} - \frac{1}{\alpha_i^2} + \frac{K_v}{\alpha_v^2}\right)}\right) \tag{C.14}$$

By elimination of α_v between equations (C.13) and (C.14) it is possible to obtain the flow regulation characteristic for the regulator as

$$\frac{p_i - p_o}{K_B} = f(\hat{Q}^2) \tag{C.15}$$

In this design it will be assumed that $\alpha_i = \alpha_1 = 1$. Then (C.13) and (C.15) become

$$\left(\frac{p_i - p_o}{K_B} \right) = \hat{Q}^2 \left(\frac{K_c + K_e}{\alpha_r^2} + \frac{K_v}{\alpha_v^2} \right) \tag{C.16}$$

$$\hat{Q}^2 = \left(\frac{1 - \frac{\ell}{\Delta} \frac{\alpha_v}{\bar{\alpha}}}{G \frac{1 + K_c}{\alpha_r^2} - \frac{\bar{\alpha}}{\alpha_D} \frac{K_v}{\alpha_v^2}} \right) \tag{C.17}$$

The design specifications employed here are the same as those specified for the collapsible tube flow regulator. They are

$$Q = 17.5 \ \ell/\text{min}$$

$$p_i = 35 \text{ cm } H_2O$$

$$p_{o\ min} = 5 \text{ cm } H_2O$$

$$p_{o\ max} = 15 \text{ cm } H_2O$$

$$\mu = 0.01 \text{ gm/cm-sec}$$

$$\rho = 1.0 \text{ gm/cm}^3$$

The regulator can be designed without the assistance of a pilot valve so that $G = 1$. The other chosen variables are

$\alpha_r = 0.25$, $\ell/\Delta = 0.25$, $K_c = 0.5$, $K_v = 0.8$, $K_e = 0.28$.

Equations (C.16) and (C.17) yield the plot of Fig. (64) for the variation of $\hat{Q}$ vs. $(p_i - p_o)/K_B$. As yet, however, A_0 and K_B have not been specified. An operating point is selected on the relatively flat and linear portion of the curve as

$$\hat{Q} \equiv Q/A_0\sqrt{2K_B/\rho} = 0.125$$

$$(p_i - p_o)/K_B = 0.9$$

Selecting p_o equal to the mean exit pressure for the operating point gives

$$K_B = 21{,}800 \text{ dynes/cm}^2$$

$$A_0 = 11.2 \text{ cm}^2$$

Thus,

$$D_0 \simeq 1.5 \text{ inches} .$$

Hence,

$$A_D = \alpha_D A_0 = 44.8 \text{ cm}^2$$

$$D_D \simeq 3 \text{ inches} .$$

The values of k , ℓ, Δ can be chosen to give the value of K_B calculated above and the relation $\ell = 0.25\ \Delta$ used in the design.

From the plot of Fig. (64), in the linear region of regulation, the "droop" inherent in this design is given by

$$P.I. = \frac{\Delta Q}{\hat{Q}_0} \times 100 = \left(\frac{0.129 - 0.121}{0.125} \right) \times 100 = 6.4\% \quad .$$

APPENDIX D:

TECHNICAL SPECIFICATIONS OF INSTRUMENTS USED

The relevant specifications are given below:

(1) Bell and Howell Physiological Pressure Transducer 4-327-I.

Specifications: Range -50 to 300 mm Hg; sensitivity 50 $\mu V/V/cm$ Hg; compliance 0.04 $mm^3/100$ mm Hg; input and output impedance 600 and 300 Ω respectively; frequency response 10 kHz; nonlinearity and hysteresis $\pm 0.5\%$ of F.S.; zero temperature shift $\leq$ 0.14 mm Hg/^{o}F.

(2) Teledyne Philbrick FET Instrumentation Amplifiers Model 4253.

Specifications: Gain 1-6000; input impedance 10^3 Ω; output impedance 1Ω ; CMRR 110 dB min up to 100 Hz; 1 $\mu V/^{o}C$ maximum drift; 2 μV p-p noise; differential configuration.

(3) Honeywell Test Div. Visicorder Oscillograph 1508A.

Specifications: M1650 galvanometers; frequency response $\pm 5\%$ flat up to 1000 Hz; time markers 0.01 to 100 sec in factors of 10; wide range of paper speeds.

(4) Hewlett-Packard Function Generator 3311A.

Specifications: Frequency range 0.1-100 kHz; maximum output 10 VDC; D.C. output offset capability.

(5) Fluke Digital Voltmeter Model 8600 A.

(6) Twin Channel Stabilized DC Power Supply.

Specifications: 2-30 VDC output volts; 1 A output current; can be operated in constant voltage or constant current modes; 0.1% line and output voltage regulation; 0.1 mV output ripple.

TABLE 1.

Flow Regime	Area Ratio and Shape	Friction Factor f $Re_{D_0} \equiv \frac{Q}{\nu}\sqrt{\frac{4}{\pi A_0}}$
TURBULENT	$\alpha \leq 0.36$	$f = \frac{0.0791}{Re_{D_h}^{0.25}}\sqrt{\frac{2}{\alpha}}$ $Re_{D_h} = \frac{Re_{D_0}}{\sqrt{2\alpha}}$
	$0.36 \leq \alpha \leq 1.0$	$f = \frac{0.0791}{Re_{D_h}^{0.25}} \cdot \frac{1}{\alpha}$ $Re_{D_h} = Re_{D_0}$
LAMINAR	$\alpha \leq 0.36$	$f = \frac{16}{Re_{D_h}} \times 1.969$ $Re_{D_h} = \frac{Re_{D_0}}{\sqrt{2\alpha}}$
	$0.36 \leq \alpha \leq 1.0$	$f = \frac{16}{Re_{D_h}}\frac{1}{\alpha}$ $Re_{D_h} = Re_{D_0}$
	$\alpha \geq 1.0$	$f = \frac{16}{Re_{D_h}}$ $Re_{D_h} = Re_{D_0}$

Table 2

Quantity	Symbol	Range
Reynolds Number based on resting diameter	Re_{D_0} $\frac{Q}{\nu}\sqrt{\frac{4}{\pi A_0}}$	12,000 - 20,000
Inlet Reynolds Number based on hydraulic diameter	$Re_{D_h} \equiv \frac{Re_{D_0}}{\sqrt{2\alpha_1}}$	18,000 - 33,000
Inlet Speed Index	$S_1 = \frac{u_1}{c_1}$	2.7 - 11
Constriction Area Ratio	$\alpha_c \equiv \frac{A_c}{A_0}$	0.17 - 0.38
Flow Rate	Q	13.5 - 23 /min
Longitudinal Prestrain	ε_{xx}	0.06 (fixed)
Shock position from Constriction	$\frac{x_1' - x_1}{D_0}$	10 - 15

TABLE 3.

ANALOGOUS PHYSICAL QUANTITY	COLLAPSIBLE TUBE FLOW	GAS DYNAMIC FLOW	OPEN CHANNEL FLOW
FLOW SPEED	u	u	u
FLUID PRESSURE	p	p	p
MASS STORAGE VARIABLE	A	ρ	h
EQUATION OF STATE	$A = A(p - p_e)$	$\rho = \rho(p)$	$h = \dfrac{p - p_a}{\rho g}$
WAVE SPEED	$c^2 = \dfrac{A}{\rho}\dfrac{d(p-p_e)}{dA}$	$c^2 = \dfrac{\rho}{\rho}\dfrac{dp}{d\rho} = \left(\dfrac{dp}{d\rho}\right)_s$	$c^2 = \dfrac{h}{\rho}\dfrac{dp}{d\rho} = gh$
SPEED INDEX	$S = u/c$ SPEED INDEX	$M = u/c$ MACH NUMBER	$F = u/c$ FROUDE NUMBER

TABLE 4.

RUN NO.	FIG NO.	Q LIT/MIN	α_c	α_1	α_1'	α_1''	α_2'	α_2	$x_1' - x_1$ CM	$x_1'' - x_1$ CM	L_s/D_o
1	30	23.0	0.195	0.227	0.421	0.542	0.960	1.024	28.1	30.0	1.949
2	31	21.0	0.195	0.223	0.421	0.538	0.980	1.018	30.6	31.5	2.047
3	32	18.8	0.195	0.217	0.400	0.542	0.985	1.008	34.1	35.4	2.047
4	33	17.5	0.195	0.218	0.422	0.501	0.995	1.008	35.1	37.0	1.969
5	34	22.7	0.213	0.244	0.420	0.530	0.965	1.018	32.0	32.7	0.984
6	35	21.5	0.213	0.289	0.423	0.521	0.983	1.019	27.6	28.5	1.161
7	36	20.0	0.213	0.317	0.480	0.570	0.987	1.009	28.5	29.7	1.772
8	39	17.9	0.213	0.276	0.452	0.581	0.960	1.004	36.1	37.5	2.520
9	40	15.0	0.213	0.294	0.457	0.579	0.972	1.001	34.4	37.1	3.050
10	41	13.5	0.213	0.284	0.382	0.600	0.965	0.996	37.1	39.7	3.110
11	42	22.1	0.279	0.318	0.500	0.657	0.982	1.007	34.3	36.5	1.575
12	43	19.9	0.279	0.343	0.470	0.607	0.980	1.003	34.7	36.2	1.673
13	44	17.0	0.279	0.320	0.487	0.559	0.947	1.000	33.2	35.6	2.224
14	45	15.0	0.279	0.364	0.520	0.640	0.960	0.991	34.3	36.8	2.264
15	37	20.0	0.332	0.397	0.587	0.650	1.001	1.001	31.1	33.7	2.559
16	38	17.2	0.332	0.377	0.597	0.678	0.995	1.000	32.7	35.3	3.150
17	46	22.8	0.332	0.375	0.520	0.678	0.980	1.002	37.1	38.0	2.283
18	47	22.0	0.378	0.427	0.587	0.710	0.930	1.000	36.2	42.6	3.346
19	48	20.0	0.378	0.432	0.597	0.728	0.998	0.996	39.2	41.3	3.622

FLOW RATE = Q , AREA RATIO = $A/A_0 = \alpha$, D_o = 2.54 CM.

REFER TO FIGURES (5) & (16) FOR EXPLANATION OF NOTATION.

TABLE 5.

RUN NO.	FIG NO.	S_1	S_1'	S_1''	S_2	C_p	C_p'	C_{pc}'	C_{po}'
1	30	5.978	8.739	6.491	0.113	0.140	0.830	0.488	0.498
2	31	5.957	7.979	5.829	0.099	0.130	0.905	0.485	0.497
3	32	5.209	7.685	5.306	0.096	0.155	0.702	0.476	0.491
4	33	4.820	7.661	5.445	0.089	0.145	0.670	0.465	0.483
5	34	5.239	9.721	6.572	0.107	0.110	0.639	0.473	0.483
6	35	6.732	8.789	6.350	0.102	0.210	0.779	0.476	0.488
7	36	10.028	7.581	5.344	0.100	0.220	0.674	0.485	0.498
8	39	3.340	6.817	4.686	0.115	0.150	0.601	0.488	0.504
9	40	2.873	5.673	3.941	0.128	0.180	0.772	0.487	0.510
10	41	2.743	4.224	3.412	0.186	0.160	0.737	0.500	0.529
11	42	11.001	7.527	4.983	0.116	0.155	0.622	0.494	0.506
12	43	10.837	6.675	4.969	0.139	0.190	0.521	0.495	0.509
13	44	8.734	7.442	4.638	0.161	0.160	0.450	0.474	0.490
14	45	7.524	4.415	3.505	0.331	0.190	0.600	0.500	0.523
15	37	8.834	6.432	4.578	0.171	0.270	0.630	0.496	0.512
16	38	8.183	5.261	3.699	0.163	0.240	0.587	0.499	0.521
17	46	10.924	6.409	4.904	0.175	0.190	0.591	0.499	0.510
18	47	8.472	5.450	4.388	0.208	0.230	0.689	0.471	0.479
19	48	7.840	4.860	3.819	0.276	0.167	0.580	0.485	0.500

SPEED INDEX = $S \equiv u/c$, PRESSURE RECOVERY COEFFICIENT = C_p (INLET AT x_1, EXIT AT x_2')

= C_p' (INLET AT x_1', EXIT AT x_2')

REFER TO FIGURES (5) & (16) FOR EXPLANATION OF NOTATION.

TABLE 6.

RUN NO.	n	λ_n CM	$2a_n$	$x_{mn_{CM}}$	C_{pmn}	α_{mn}	$u_{mn}\frac{CM}{S}$	λ'_n CM	$2a'_n$	$x'_{mn_{CM}}$	C'_{pmn}	α'_{mn}	$u'_{mn}\frac{CM}{S}$
1	1	5.75	0.129	39.50	0.022	0.512	174.1	5.15	0.097	36.40	0.008	0.460	195.0
	2	5.15	0.066	34.10	0.021	0.428	210.5	4.50	0.060	31.80	0.018	0.390	232.5
	3	4.50	0.061	29.20	0.016	0.377	241.1	5.15	0.048	27.20	0.013	0.348	262.8
	4	3.75	0.067	25.20	0.007	0.341	268.6	3.25	0.050	22.80	0.002	0.310	298.0
	5	3.25	0.032	21.50	0.005	0.301	307.7	2.95	0.033	19.80	0.005	0.292	318.1
	6	4.00	0.036	18.20	0.004	0.275	339.8						
2	1	6.85	0.116	40.20	0.028	0.509	160.0	5.50	0.096	36.60	0.028	0.435	188.9
	2	5.25	0.081	34.20	0.033	0.425	193.6	4.30	0.062	31.60	0.025	0.401	206.0
	3	4.00	0.066	29.50	0.023	0.382	217.0	5.00	0.050	27.10	0.016	0.359	232.0
	4	4.70	0.046	25.10	0.017	0.341	245.3	3.50	0.017	22.80	0.003	0.326	257.5
	5	3.30	0.025	21.20	0.001	0.312	270.1	3.00	0.033	19.50	0.003	0.299	283.0
	6	3.00	0.040	18.00	0.000	0.285	298.3						
3	1	6.50	0.114	40.70	0.039	0.530	137.2	5.50	0.095	37.20	0.034	0.455	161.2
	2	5.40	0.090	34.80	0.035	0.430	171.2	5.00	0.070	32.00	0.025	0.399	185.4
	3	5.15	0.066	29.50	0,028	0.391	189.5	5.10	0.045	27.00	0.018	0.379	196.0
	4	5.50	0.050	24.40	0.015	0.362	205.9	5.20	0.025	21.80	0.005	0.335	223.8
	5	4.00	0.030	19.45	0.003	0.320	235.3	3.00	0.026	17.70	-0.001	0.299	253.4
	6	3.00	0.023	16.00	-0.002	0.283	269.1	3.70	0.020	14.35	-0.003	0.263	291.8

REFER TO FIGURE (16) FOR EXPLANATION OF NOTATION.

SUBSCRIPT 'm' DENOTES MEAN QUANTITIES MEASURED FROM MEAN CURVE.

TABLE 6. (Continued)

RUN NO.	n	λ_n CM	$2a_n$	x_{mn} CM	C_{pmn}	α_{mn}	u_{mn} $\frac{CM}{S}$	λ'_n CM	$2a'_n$	x'_{mn} CM	C'_{pmn}	α'_{mn}	u_{mn} $\frac{CM}{S}$
4	1	6.15	0.120	38.00	0.038	0.483	140.9	5.50	0.104	34.60	0.034	0.433	158.2
	2	5.85	0.090	32.15	0.039	0.428	160.2	5.25	0.061	29.20	0.026	0.383	180.4
	3	4.10	0.061	27.15	0.026	0.372	186.1	3.45	0.048	25.00	0.017	0.360	192.8
	4	4.20	0.060	23.00	0.011	0.348	200.0	4.20	0.032	21.00	0.002	0.330	211.8
	5	4.00	0.030	18.85	0.002	0.319	219.7	3.15	0.018	17.20	-0.005	0.301	234.1
	6	2.55	0.024	15.80	-0.009	0.292	242.1	3.60	0.035	13.80	-0.003	0.274	259.6
	7	4.60	0.026	12.00	0.001	0.255	281.2	4.80	0.025	9.60	0.000	0.233	311.0
5	1	9.00	0.151	37.40	0.000	0.503	175.1	6.00	0.129	33.10	-0.004	0.449	197.4
	2	5.40	0.105	30.10	0.007	0.440	201.7	4.45	0.095	27.80	0.002	0.403	221.5
	3	3.65	0.067	25.60	0.006	0.392	228.2	3.60	0.065	23.80	-0.004	0.378	237.3
	4	3.35	0.065	22.20	-0.005	0.360	250.1	3.50	0.057	20.20	-0.008	0.348	259.4
	5	3.50	0.036	18.80	0.000	0.338	267.7	3.00	0.045	16.90	0.006	0.321	283.1
	6	3.65	0.025	15.20	0.014	0.307	297.2	4.80	0.031	13.20	0.014	0.280	328.8
6	1	6.90	0.200	38.20	0.044	0.495	168.7	5.75	0.176	34.90	0.039	0.450	186.6
	2	5.50	0.156	31.90	0.050	0.428	196.8	5.50	0.135	29.30	0.041	0.407	207.6
	3	4.80	0.117	26.60	0.045	0.407	207.6	5.00	0.075	24.00	0.023	0.379	224.1
	4	5.20	0.007	21.80	0.025	0.343	249.5	5.40	0.061	18.80	0.019	0.325	264.6
7	1	7.25	0.233	39.20	0.060	0.522	148.4	7.40	0.200	34.60	0.053	0.501	154.9
	2	6.90	0.184	32.20	0.058	0.502	154.6	4.70	0.157	28.50	0.044	0.432	181.2
	3	5.60	0.146	25.80	0.046	0.413	190.1	5.30	0.093	23.50	0.030	0.381	207.3
	4	4.40	0.098	20.75	0.023	0.362	219.0	5.20	0.092	18.20	0.016	0.352	225.7

TABLE 6. (Continued)

RUN NO.	n	λ_n CM	$2a_n$	x_{mn} CM	C_{pmn}	α_{mn}	u_{mn} $\frac{CM}{S}$	λ'_n CM	$2a'_n$	x'_{mn} CM	C'_{pmn}	α'_{mn}	u'_{mn} $\frac{CM}{S}$
8	1	8.05	0.157	39.60	0.028	0.540	128.1	7.25	0.156	34.80	0.034	0.470	148.3
	2	8.05	0.125	31.60	0.044	0.453	154.2	6.50	0.102	28.00	0.037	0.401	175.6
	3	5.55	0.116	24.70	0.027	0.400	176.1	5.25	0.077	22.15	0.009	0.380	186.0
	4	4.85	0.080	19.50	0.006	0.360	197.2	5.35	0.063	16.90	-0.002	0.342	208.4
	5	5.25	0.054	14.50	0.002	0.322	222.5	5.05	0.070	11.80	0.010	0.308	233.5
9	1	9.75	0.172	37.50	0.038	0.530	109.5	8.00	0.162	32.20	0.041	0.482	121.0
	2	7.60	0.145	28.80	0.048	0.440	133.3	6.50	0.107	25.00	0.030	0.385	153.7
	3	6.60	0.120	21.75	0.025	0.372	159.5	6.75	0.095	18.40	0.012	0.353	168.8
	4	6.00	0.090	15.50	0.014	0.340	175.8	5.50	0.123	10.25	0.029	0.310	194.3
10	1	11.25	0.160	39.00	0.065	0.540	96.6	8.50	0.132	34.30	0.052	0.483	108.7
	2	6.55	0.125	30.00	0.052	0.440	120.0	8.10	0.080	25.90	0.029	0.400	132.8
	3	7.80	0.083	22.80	0.028	0.394	135.0	6.25	0.080	18.75	0.027	0.375	142.3
	4	6.20	0.100	15.80	0.019	0.350	153.3	6.30	0.080	12.50	0.010	0.315	171.9
11	1	7.90	0.208	37.80	0.012	0.590	144.2	7.30	0.169	33.70	-0.004	0.520	164.6
	2	6.60	0.147	30.60	0.006	0.500	171.5	6.00	0.146	27.00	0.007	0.441	195.9
	3	5.35	0.133	24.50	0.013	0.433	199.8	4.60	0.109	21.70	0.002	0.422	205.3
	4	5.00	0.118	19.40	-0.001	0.422	205.3	4.30	0.106	17.30	-0.005	0.379	230.3
	5	4.05	0.092	14.80	0.000	0.352	249.4	4.70	0.090	12.80	0.000	0.340	258.9
12	1	8.20	0.205	37.60	0.015	0.572	134.1	7.60	0.192	33.00	0.018	0.530	145.3
	2	7.65	0.182	29.70	0.020	0.512	150.7	6.50	0.160	25.80	0.011	0.468	165.6
	3	5.45	0.165	23.20	0.007	0.461	168.3	5.70	0.126	19.70	-0.012	0.422	184.9
	4	5.05	0.126	17.80	-0.013	0.419	186.3	3.80	0.110	14.80	-0.015	0.392	200.0
	5	4.05	0.065	13.40	-0.003	0.385	203.9	4.60	0.096	10.70	0.012	0.372	211.6

TABLE 6. (Continued)

RUN NO.	n	λ_n CM	$2a_n$	x_{mn} CM	C_{pmn}	α_{mn}	u_{mn} $\frac{CM}{S}$	λ'_n CM	$2a'_n$	x'_{mn} CM	C'_{pmn}	α'_{mn}	u'_{mn} $\frac{CM}{S}$
13	1	8.00	0.234	33.70	0.017	0.560	117.1	7.70	0.207	29.20	0.008	0.480	137.8
	2	8.00	0.202	25.80	0.010	0.474	139.6	6.50	0.157	22.20	-0.012	0.438	151.8
	3	5.75	0.146	18.80	-0.007	0.432	154.1	5.10	0.130	16.30	-0.015	0.400	167.2
	4	5.25	0.098	13.50	0.002	0.382	175.7	6.20	0.115	10.50	0.012	0.358	188.4
14	1	12.25	0.287	37.20	0.031	0.572	101.1	9.40	0.260	30.30	0.017	0.482	121.0
	2	8.65	0.228	26.60	0.029	0.481	121.3	7.35	0.175	21.90	0.005	0.421	139.7
	3	6.80	0.162	18.80	0.011	0.400	147.6	6.10	0.122	15.30	-0.011	0.381	155.5
15	1	8.35	0.372	34.60	0.025	0.621	123.7	5.45	0.334	30.25	0.006	0.600	128.2
	2	6.40	0.258	27.30	0.042	0.580	132.8	6.70	0.226	24.30	0.029	0.542	142.6
	3	6.00	0.233	21.10	0.026	0.505	153.6	5.00	0.209	18.40	0.013	0.472	165.0
	4	4.50	0.180	15.75	0.023	0.461	169.2	6.30	0.156	12.80	0.009	0.439	178.2
16	1	10.80	0.240	36.20	0.059	0.640	103.1	9.70	0.208	30.70	0.044	0.550	120.8
	2	7.45	0.200	27.00	0.047	0.535	124.3	7.15	0.170	22.20	0.031	0.510	130.7
	3	9.00	0.212	18.70	0.015	0.481	139.1	8.10	0.212	14.60	0.014	0.431	156.3

TABLE 6. (Continued)

RUN NO.	n	λ_n CM	$2a_n$	x_{mn} CM	C_{pmn}	α_{mn}	u_{mn} $\frac{CM}{S}$	λ'_n CM	$2a'_n$	x'_{mn} CM	C'_{pmn}	α'_{mn}	u'_{mn} $\frac{CM}{S}$
17	1	7.00	0.220	40.65	0.036	0.635	137.7	7.65	0.187	35.75	0.022	0.580	151.4
	2	7.80	0.192	33.35	0.020	0.572	153.6	6.50	0.164	28.65	0.010	0.530	166.4
	3	6.33	0.140	26.20	0.018	0.520	169.8	5.55	0.120	22.60	0.010	0.491	180.4
	4	5.45	0.120	20.00	0.011	0.480	184.8	5.30	0.113	17.20	0.005	0.452	196.9
	5	4.88	0.113	14.90	0.005	0.442	201.6	5.60	0.130	11.70	0.013	0.413	216.8
18	1	10.75	0.290	36.90	0.040	0.650	129.7	7.90	0.235	31.70	0.019	0.588	144.0
	2	7.00	0.225	28.00	0.025	0.575	147.4	5.50	0.185	24.90	0.008	0.548	155.1
	3	6.70	0.168	21.20	0.010	0.534	159.3	7.50	0.132	18.40	-0.003	0.498	171.5
	4	6.10	0.110	15.20	0.004	0.475	180.3	5.80	0.142	11.80	0.015	0.458	187.4
19	1	12.40	0.215	41.70	0.014	0.680	112.5	10.05	0.205	37.00	0.012	0.620	123.9
	2	7.60	0.206	31.60	0.010	0.591	130.2	7.90	0.184	28.00	0.000	0.572	134.8
	3	7.10	0.154	24.50	0.012	0.549	140.7	5.70	0.145	21.20	0.008	0.514	150.8
	4	6.40	0.145	17.70	0.007	0.489	158.9	8.00	0.143	14.40	0.006	0.465	167.6

TABLE 7.

RUN NO.	FIG NO.	C_1	C_2	CORR. COEFF.
1	30	3.153	-1.056	0.903
2	31	3.658	-1.284	0.920
3	32	3.155	-1.079	0.866
4	33	3.461	-1.238	0.870
5	34	5.959	-2.253	0.916
6	35	3.437	-1.174	0.909
7	36	3.086	-1.029	0.856
8	39	2.863	-0.924	0.890
9	40	2.776	-0.888	0.970
10	41	3.200	-1.100	0.835
11	42	3.839	-1.354	0.969
12	43	4.775	-1.800	0.952
13	44	3.658	-1.311	0.898
14	45	4.241	-1.575	0.994
15	37	3.523	-1.273	0.770
16	38	4.611	-1.769	0.890
17	46	3.466	-1.199	0.911
18	47	4.518	-1.669	0.917
19	48	5.462	-2.142	0.943

LINEAR LEAST SQUARES FIT TO $\text{Log}_{10}\ \lambda$ Vs $\text{Log}_{10}\ u_m$

$$\text{Log}_{10}\ \lambda = C_1 + C_2\ \text{Log}_{10}\ u_m$$

Table 8

FLOW REGULATOR DATA FOR $(x_1' - x_1) = 0$, $\alpha_c = 0.213$

Q ℓ/MIN	p_i cm H_2O	p_2 cm H_2O	p_e cm H_2O	$\frac{p_i - p_e}{K_B}$	$(\frac{p_o - p_e}{K_B})^*_{EXP}$	$(\frac{p_o - p_e}{K_B})^*_{TH}$
11.0	36.08	26.30	14.41	54.46	29.88	27.17
13.0	39.87	26.83	14.41	63.98	31.21	32.83
15.0	39.77	20.72	14.41	63.73	15.86	32.78
17.7	47.87	34.93	14.41	84.01	51.57	44.70
20.0	59.23	38.40	14.41	112.63	60.29	61.52

Note: $K_B = 406$ dynes/cm^2

Table 9.

RUN No.	SLOPE	Re_{D_0}	$2f_0$	% ERROR	$\frac{x_1' - x_1}{D_0}$ EXP	$\frac{x_1' - x_1}{D_0}$ TH	% ERROR
1	0.0226	20323	0.0133	41.2	11.06	14.64	-32.4
2	0.0222	18556	0.0136	38.7	12.05	14.61	-21.2
3	0.0203	16662	0.0139	31.5	13.43	13.14	2.2
4	0.0203	15463	0.0142	30.1	13.82	14.38	- 4.1
5	0.0205	20058	0.0133	35.1	12.68	13.24	- 5.1
6	0.0141	18997	0.0135	4.3	10.87	9.94	8.6
7	0.0222	17672	0.0137	38.3	11.22	11.88	- 5.9
8	0.0179	15816	0.0141	21.2	14.21	12.48	12.2
9	0.0203	13254	0.0147	27.6	13.54	11.06	18.3
10	0.0179	11929	0.0151	15.6	14.61	10.47	28.4
11	0.0230	19528	0.0134	41.7	13.50	13.60	- 0.7
12	0.0188	17584	0.0137	27.1	13.66	9.24	32.4
13	0.0189	15021	0.0143	24.3	13.07	11.69	10.6
14	0.0190	13254	0.0147	22.6	13.50	10.58	21.6
15	0.0222	17672	0.0137	38.3	12.24	13.85	-13.2
16	0.0216	15198	0.0143	33.4	12.87	15.44	-20.0
17	0.0180	20146	0.0133	26.1	14.61	10.92	25.3
18	0.0180	19439	0.0134	25.6	14.25	11.94	16.2
19	0.0178	17672	0.0137	23.0	15.43	12.03	22.0

$$\% \text{ ERROR} = \frac{\text{EXP} - \text{THEO}}{\text{EXP}} \times 100$$

Table 10

LIST OF FLOW REGULATOR VARIABLES

SPECIFIED VARIABLES

Flow Rate Q ($Q_{max} > Q > Q_{min}$)

Inlet Pressure p_i ($p_{i\,max} > p_i > p_{i\,min}$)

Outlet Pressure p_o ($p_{o\,max} > p_o > p_{o\,min}$)

Fluid Viscosity μ

Fluid Density ρ

DESIGN VARIABLES

Primary Design Variables:

Resting Area $A_0 = \frac{1}{4}\pi D_0^2$ ┐

Tube Bending Stiffness K_B ├ Tube Parameters

Tube Length L ┘

External Pressure p_e ┐

Constriction Area Ratio $\alpha_c = A_c/A_0$ ┘ Control Variables

Wall Pretension T_0

Secondary Design Variables:

Rigid Inlet Area A_i

Rigid Outlet Area A_e

Loss Coefficients K_c, K_e

TABLE 11.

	Collapsible Tube Flow Regulator	Standard Flow Regulator
Specifications	Fluid: Water; Flow Rate: 17.5 ℓ/min Inlet Pressure: 35 cm H_2O Outlet Pressure: (5 - 15) cm H_2O	
Materials	Tube: Latex Rubber Tank body, End pipes, Constriction, and Hand-wheel: Hard Aluminum Alloy	Globe Valve, Diaphragm Actuator, Orifice Plate, and Flanges: Bronze
Nominal Dimensions	Tube Diameter: 1 in. Tube Thickness: 1 mm Tube Length: 41 in. Tank Body: 4 in. I.D. End Pipes: 1 in. I.D.	Inlet and Outlet Pipes : 1.5 in. I.D. Globe Valve: 1.5 in. Diaphragm: 3 in. I.D. (Orifice Area/ Outlet Area): 0.25
Performance	Regulator Droop : Negligible over specified outlet pressure range. Max. Exit Pressure: 20 cm H_2O Min. Exit Pressure: 3.75cm H_2O Rangeability: 10 (Approximately) Also see Figs.27,57,61	Regulator Droop: 6.4% over specified inlet pressure range. Rangeability: 2 (Approximately) Also see Fig.64
Cost (Production, Sales, Overhead)	$300.0	Globe Valve & Diaphragm Actuator: $1000.0 Orifice Plate: $50.0 Orifice Plate Flanges: $100.0 TOTAL COST: $ 1150.0

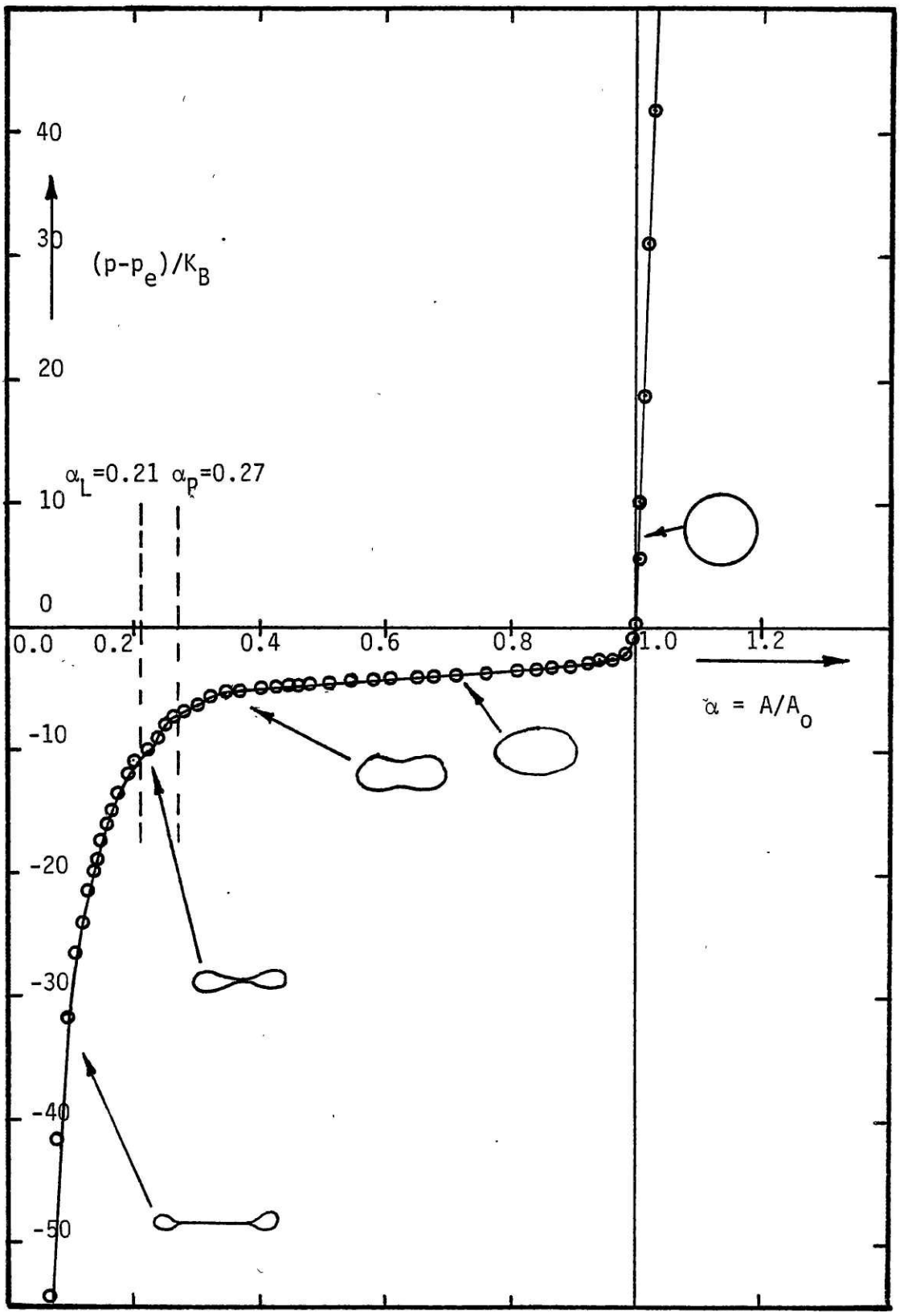

FIG (1): Experimentally Determined Tube Law for a Uniformly Collapsed Thin Walled Rubber Latex Tube. (K_B obtained from logarithmic plot in the Similarity Region = 406 dynes/cm^2).

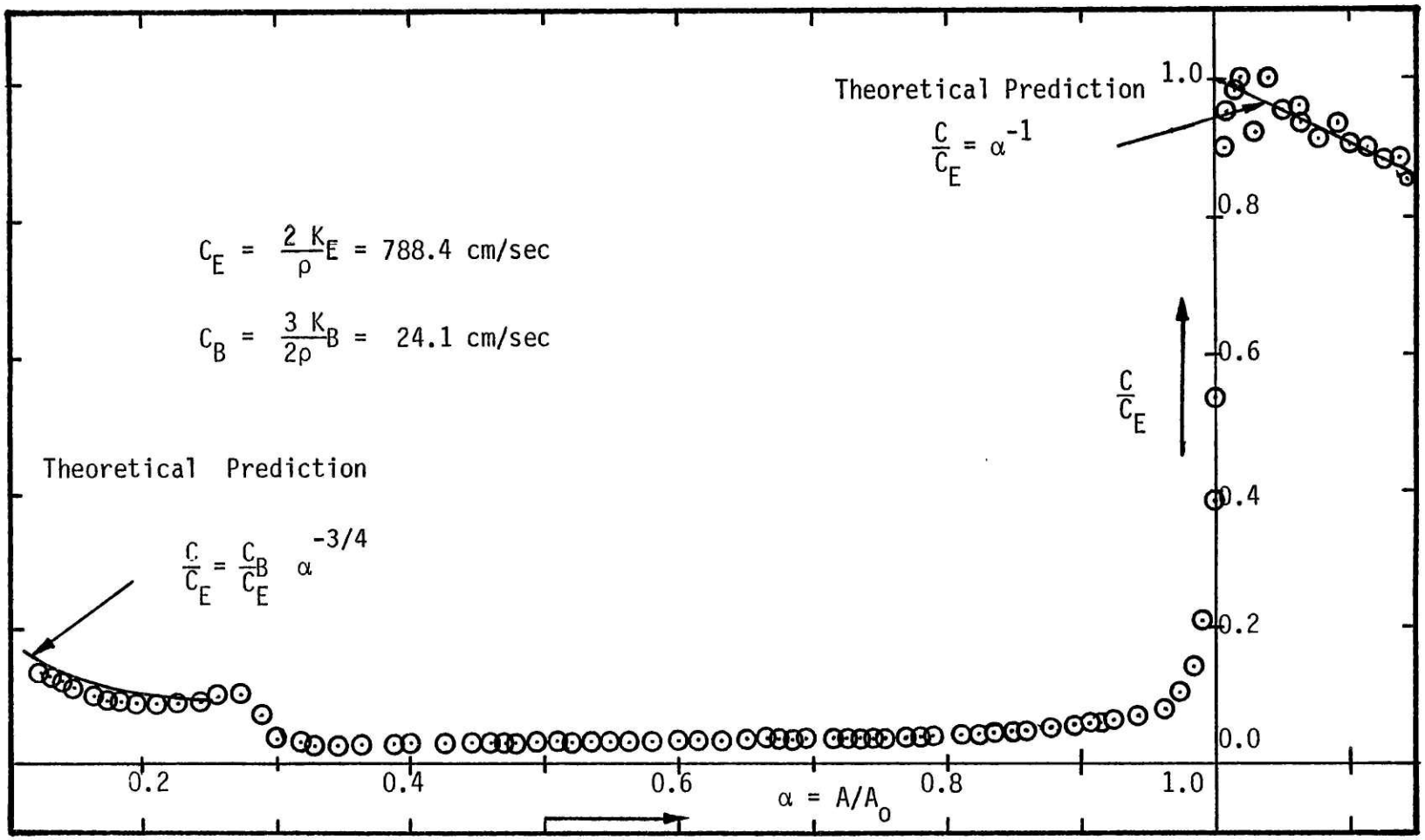

FIG (2): SPEED OF PROPAGATION OF SMALL AMPLITUDE WAVES OBTAINED BY DIFFERENTIATION OF SMOOTHED TUBE LAW DATA OF FIG (1).

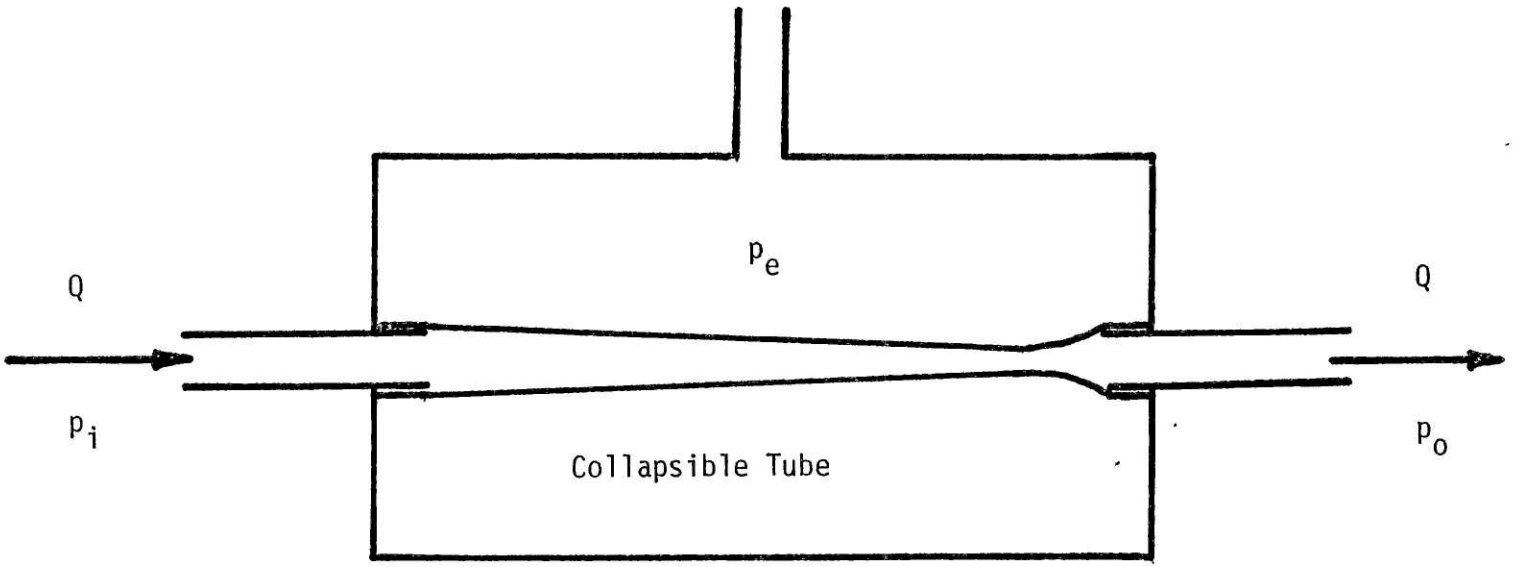

FIG (3): THE STARLING RESISTOR

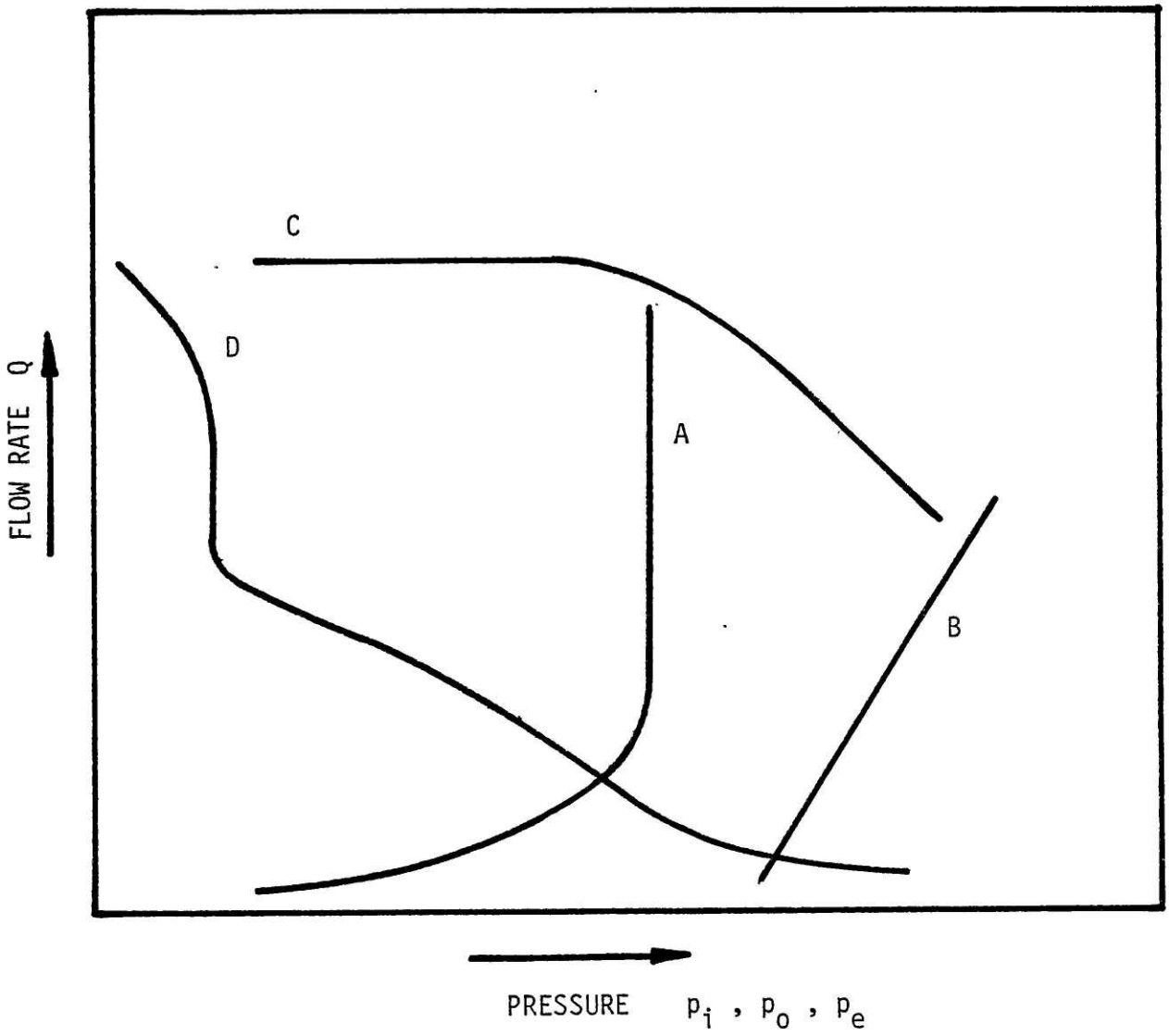

FIG (4): TYPICAL STEADY FLOW RESULTS OF STARLING RESISTOR EXPERIMENTS IN WHICH ONLY ONE OF PRESSURES p_i, p_o, p_e WERE VARIED.

CURVE A: p_i varied from less than p_e to greater than p_e, p_o held less than or equal to p_e.

CURVE B: p_i varied greater than or equal to p_e, p_o constant at greater than or equal to p_e.

CURVE C: p_o varied from greater than to less than p_e, p_i constant at greater than or equal to p_e.

CURVE D: p_i and p_o are constant, p_e varied from less than p_o to greater than p_i.

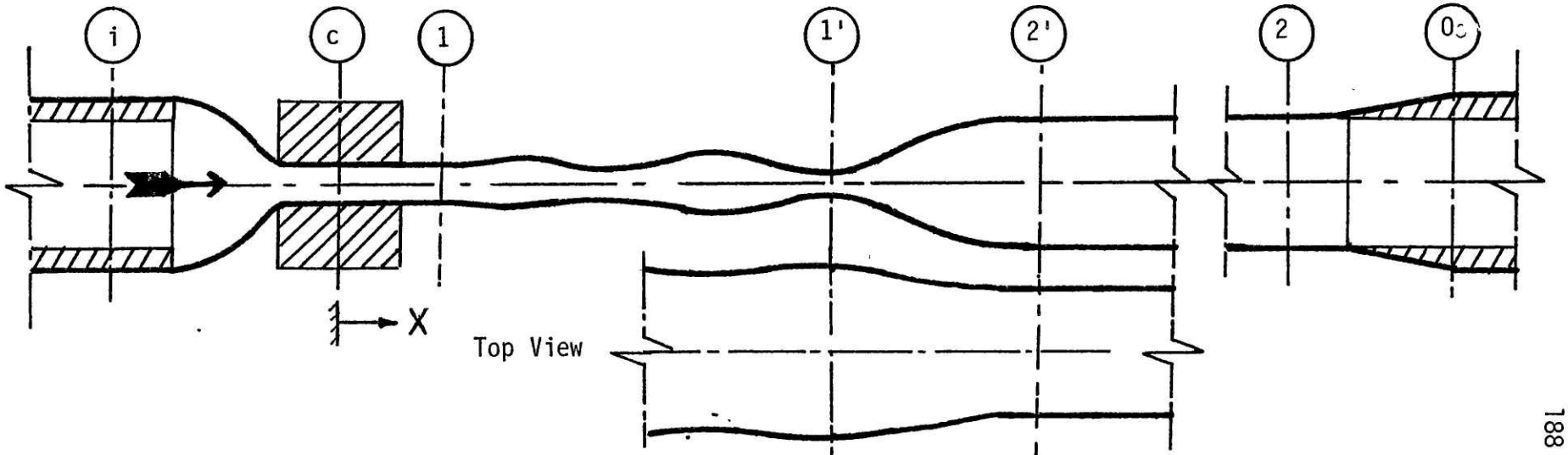

FIG (5 a): Top and Side Views of Precursor Waves and Shock Transition in a Collapsible Tube.

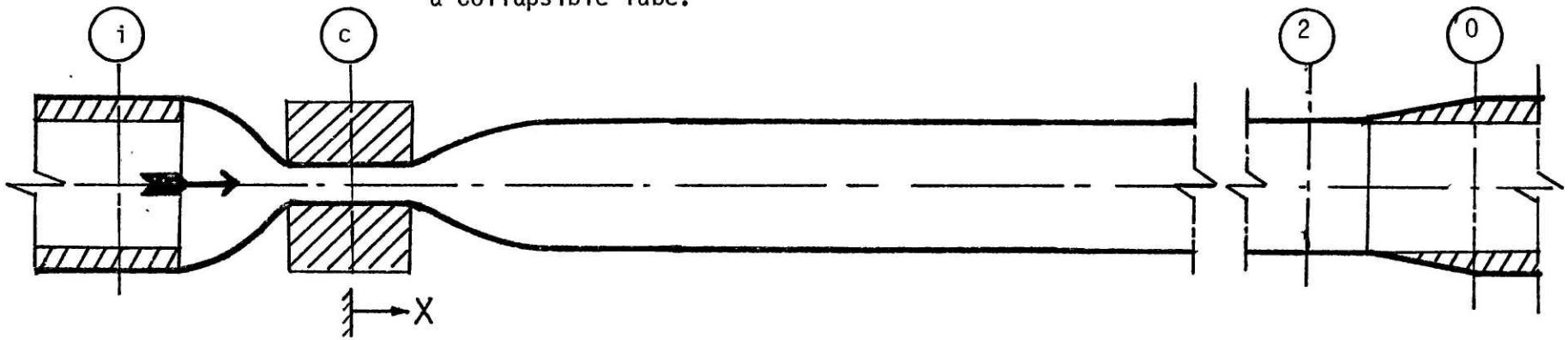

FIG (5 b): Shock located at the Exit of the Constriction at positive Downstream Transmural Pressure.

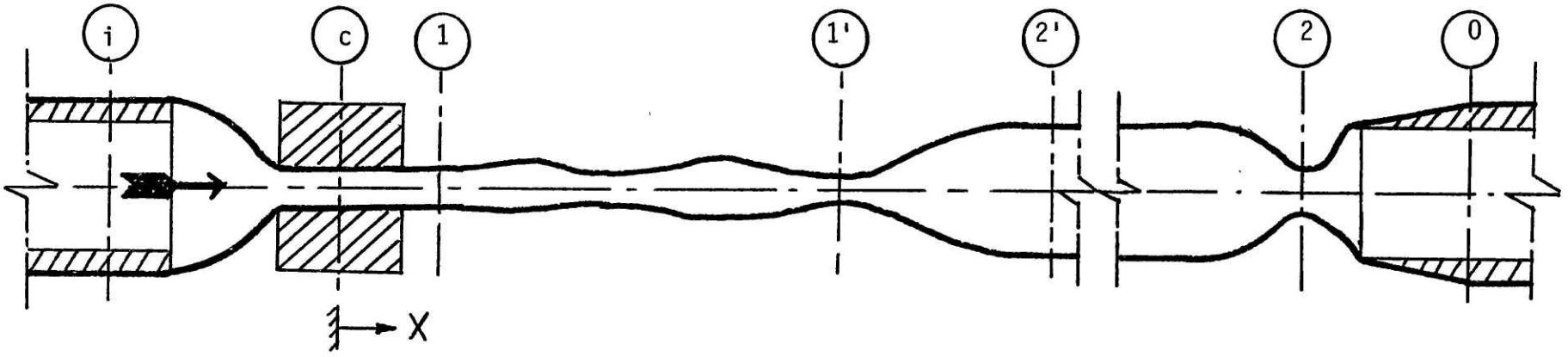

FIG (5 c): Pinching of the Downstream End of the Collapsible Tube just before and during the occurrence of oscillations.

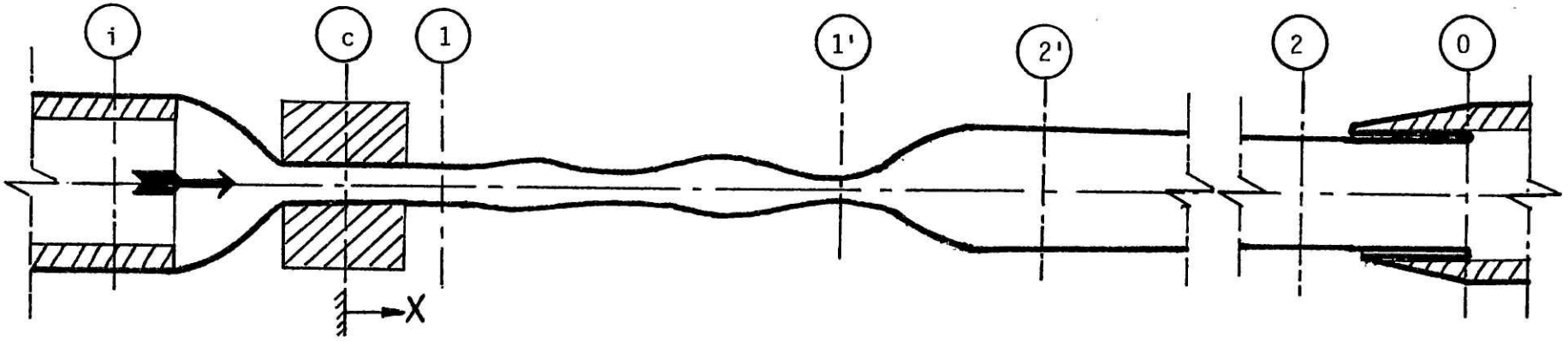

FIG (5 d): Folding in of the Downstream End of the Collapsible Tube at large negative downstream transmural pressures.

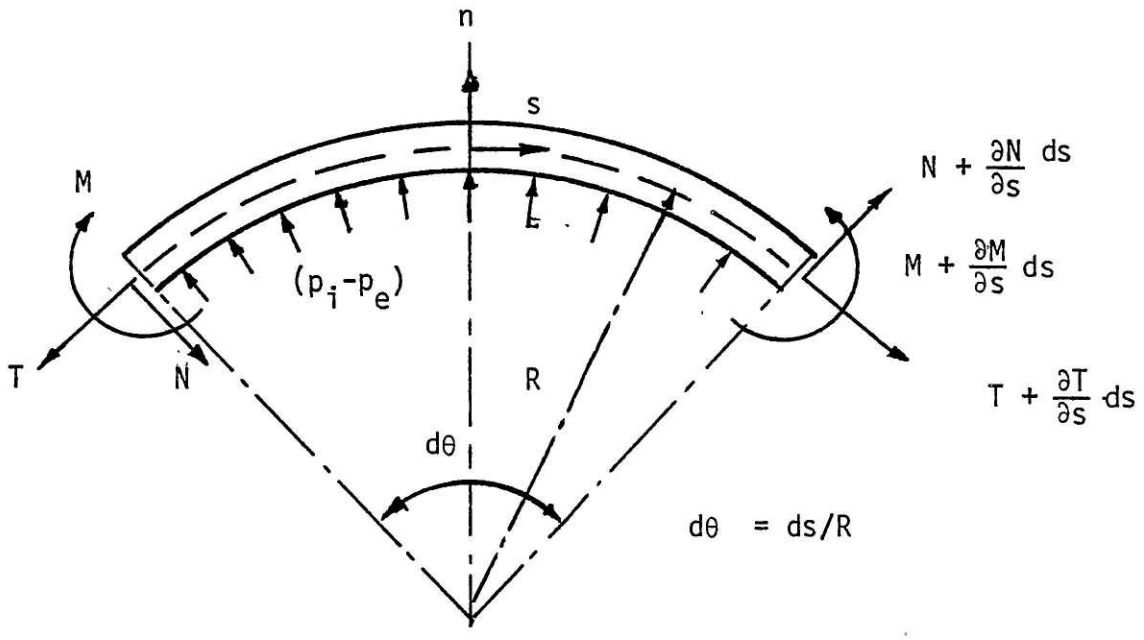

FIG (6): Forces and Moments acting on a Tube Wall Element.

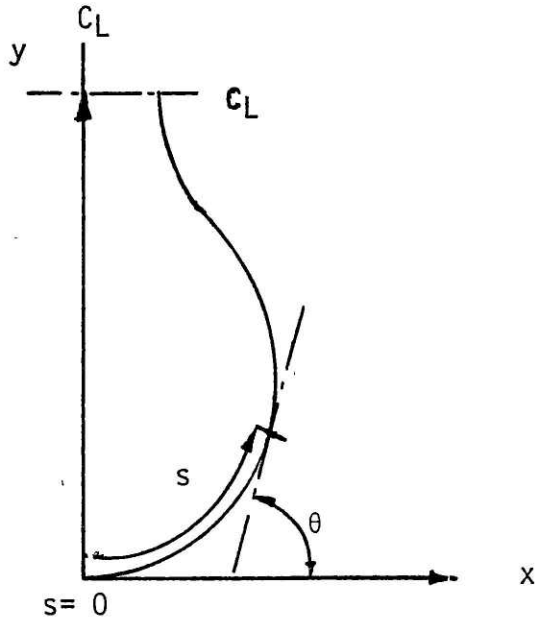

FIG (7): Tube Wall Coordinates.

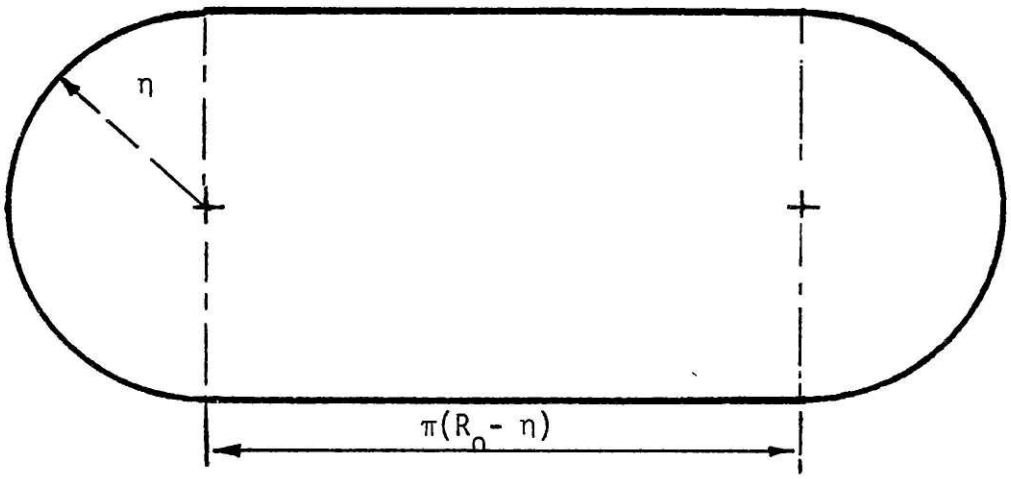

FIG. (8): Idealized Cross-sectional Shape for Collapsed Tube.

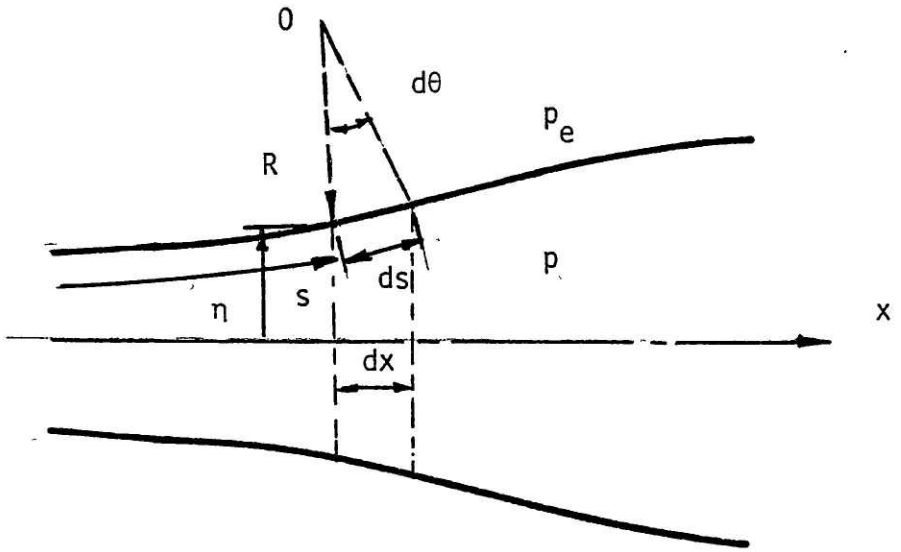

(a): Idealized Two-Dimensional Wall Deformation.

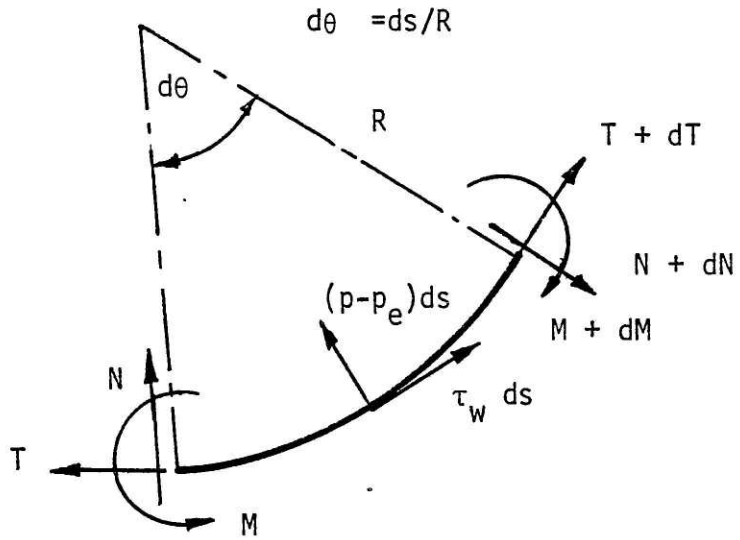

(b): Forces and Moments acting on the Tube Wall Element.

FIG (9): Idealized Two-Dimensional Deformation of the Collapsible Tube possessing the cross-sectional shape of FIG (8).

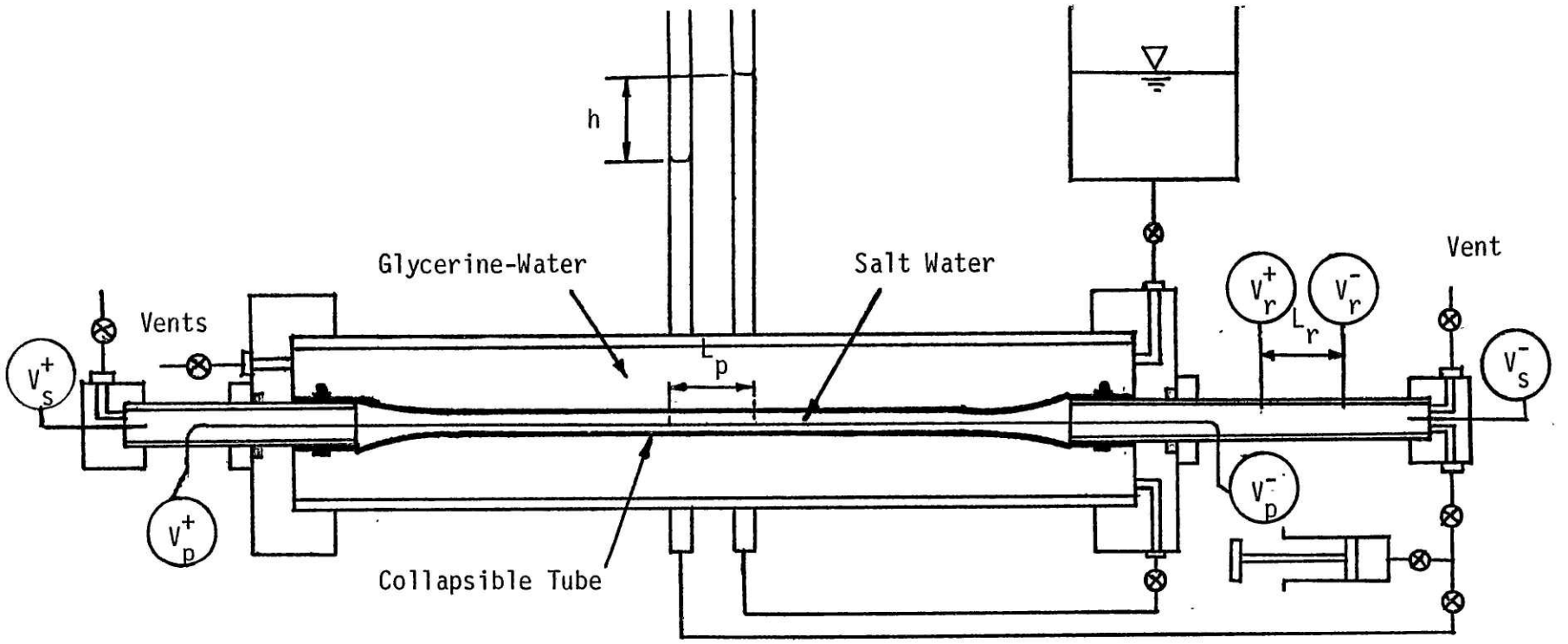

FIG (10): THE APPARATUS FOR THE DETERMINATION OF THE UNIFORM COLLAPSE TUBE LAW.

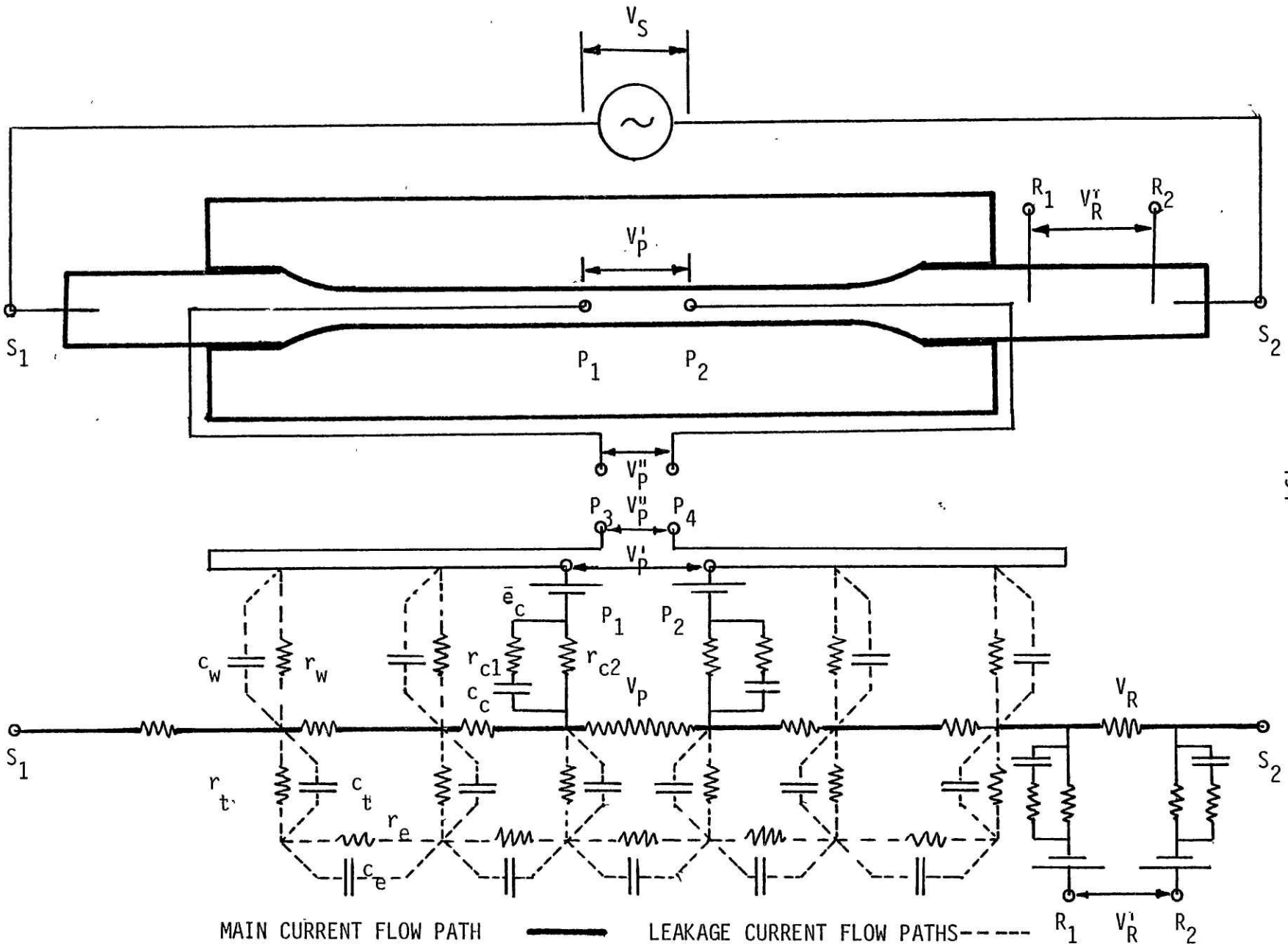

FIG (11): LUMPED PARAMETER MODEL OF THE AREA MEASUREMENT ELECTRICAL CIRCUIT. Resistance and Capacitance elements: Tube Wall (r_t,c_t);External liquid (r_e,c_e); Probe wire insulation (r_w,c_w);Electrodes (r_c,c_c,e_c)

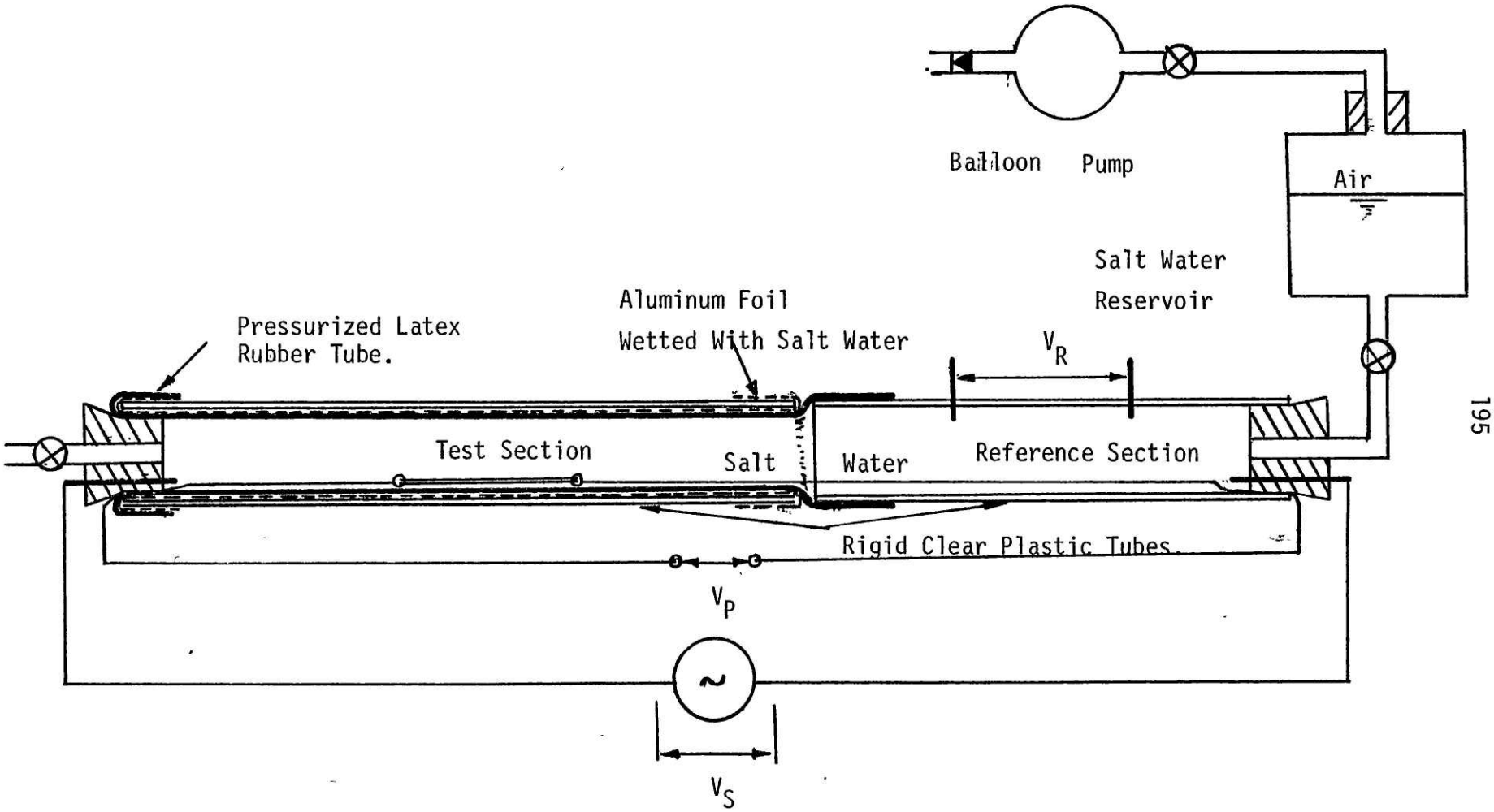

FIG (12): APPARATUS FOR THE DETERMINATION OF FREQUENCY DEPENDENCE OF THE AREA MEASUREMENT.

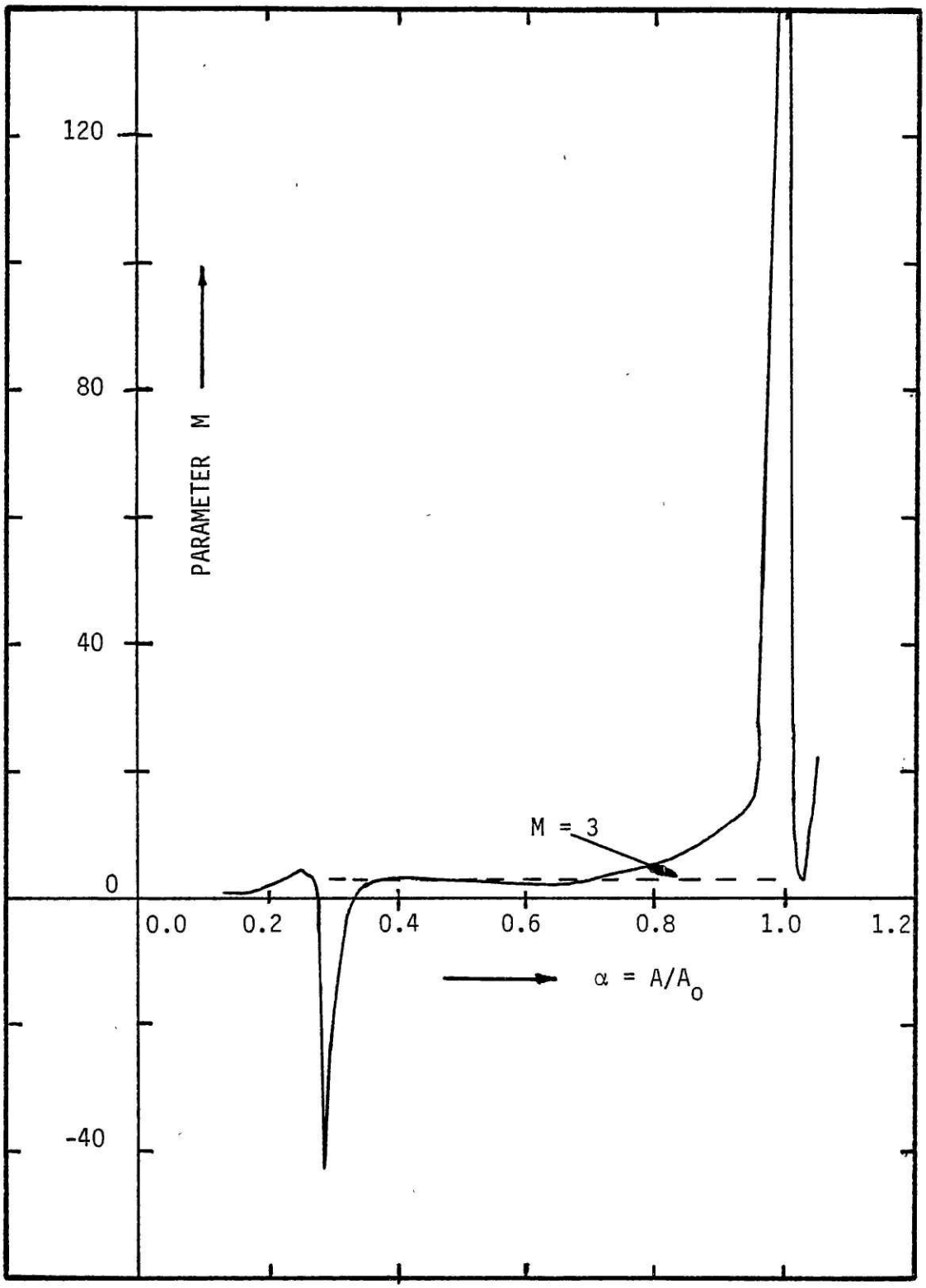

FIG (13): PARAMETER M VS. AREA RATIO; OBTAINED BY DIFFERENTIATION OF SMOOTHED DATA OF FIG(1)

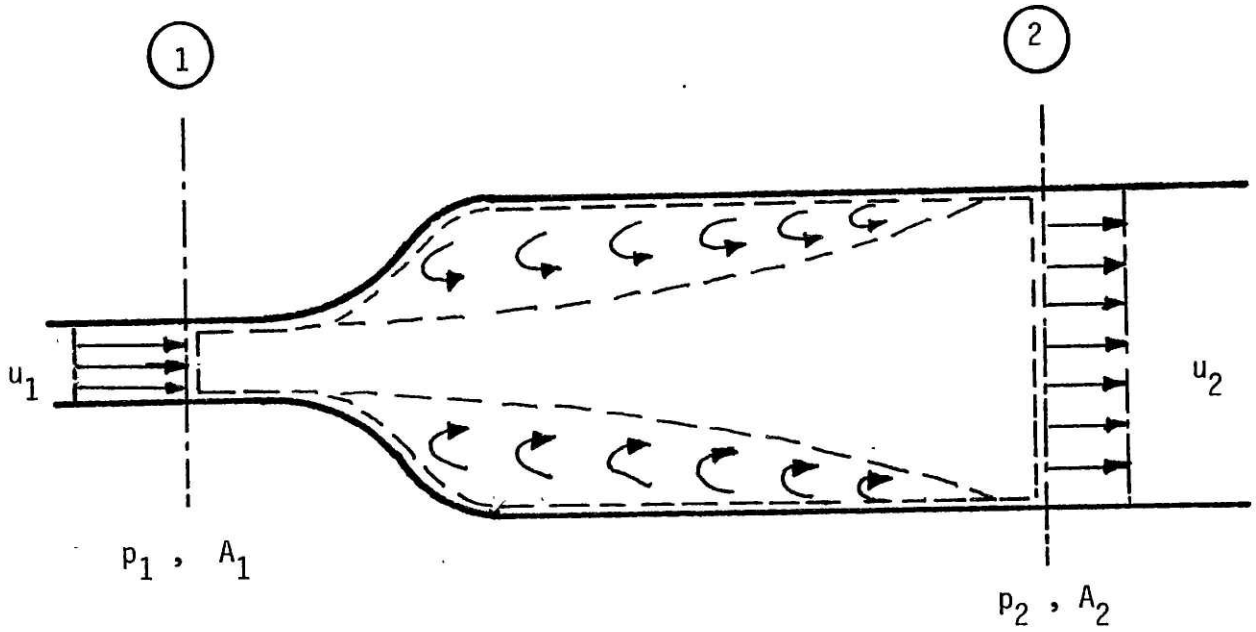

FIG (14): MODEL (1); Simplified Model of Shock Transition

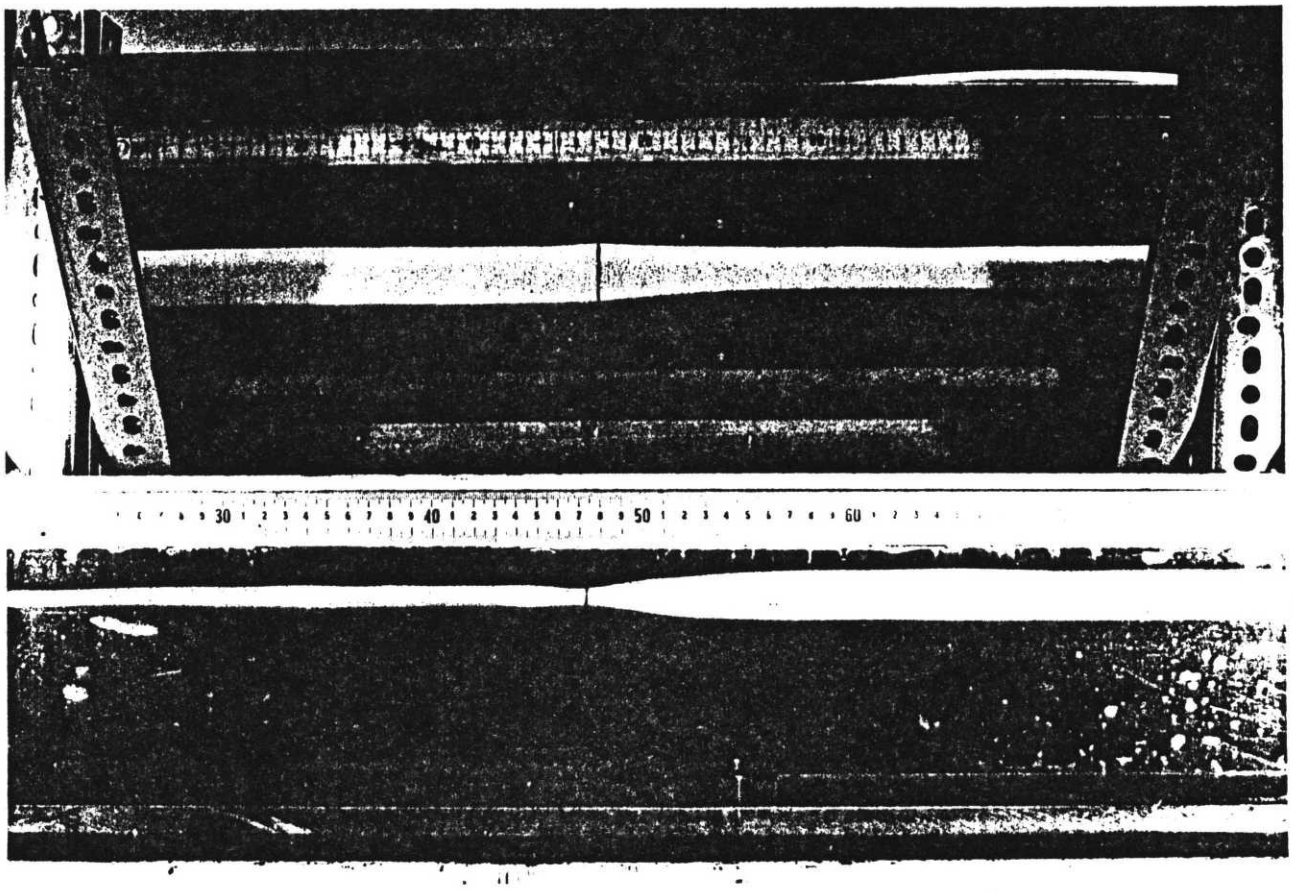

FIG (15): The Top and Side Views of a Shock Wave formed in a Collapsible Tube showing the Precursor Area Waves.

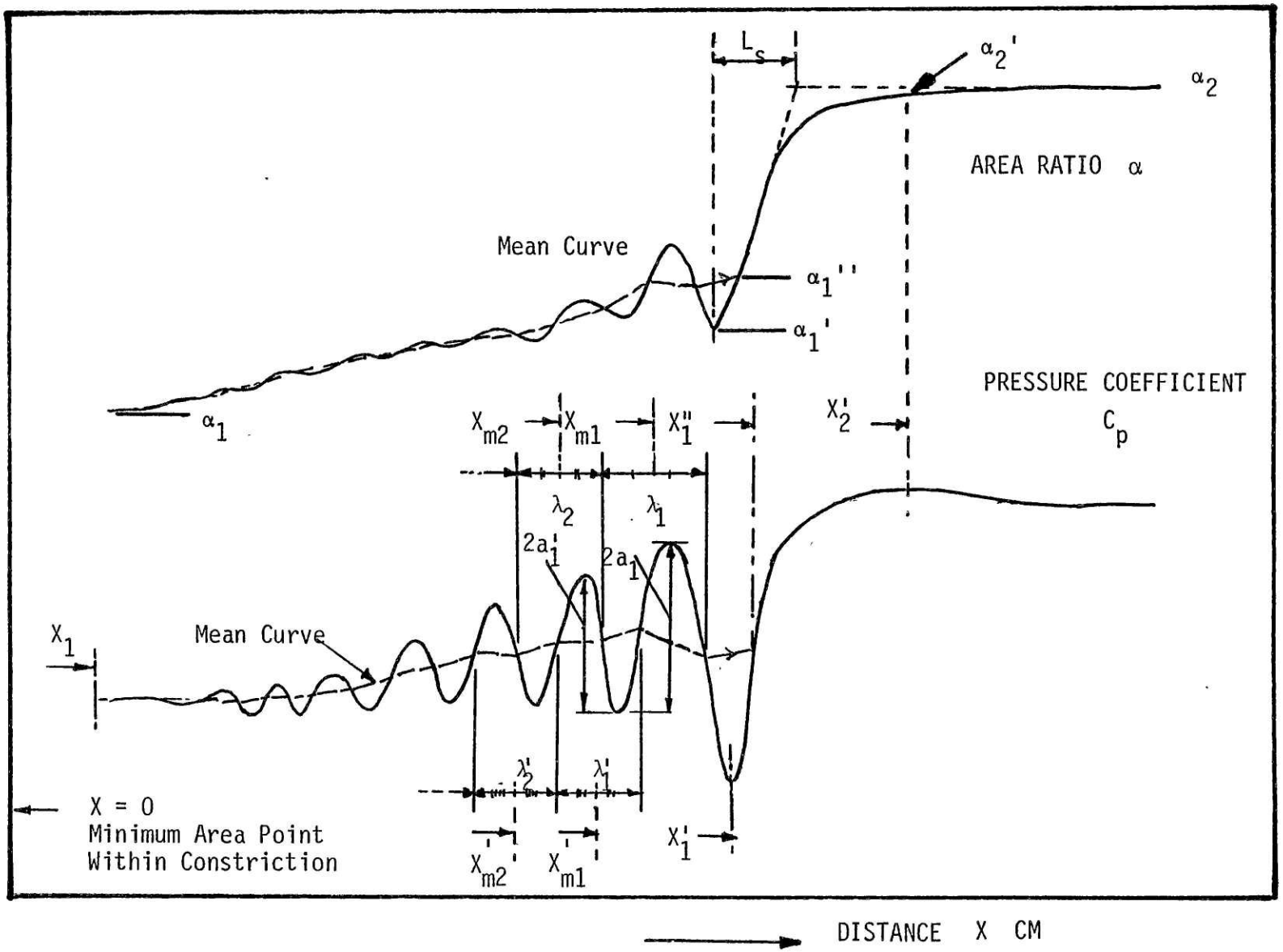

FIG (16): MEASUREMENTS FROM EXPERIMENTALLY OBTAINED AREA AND PRESSURE DATA.

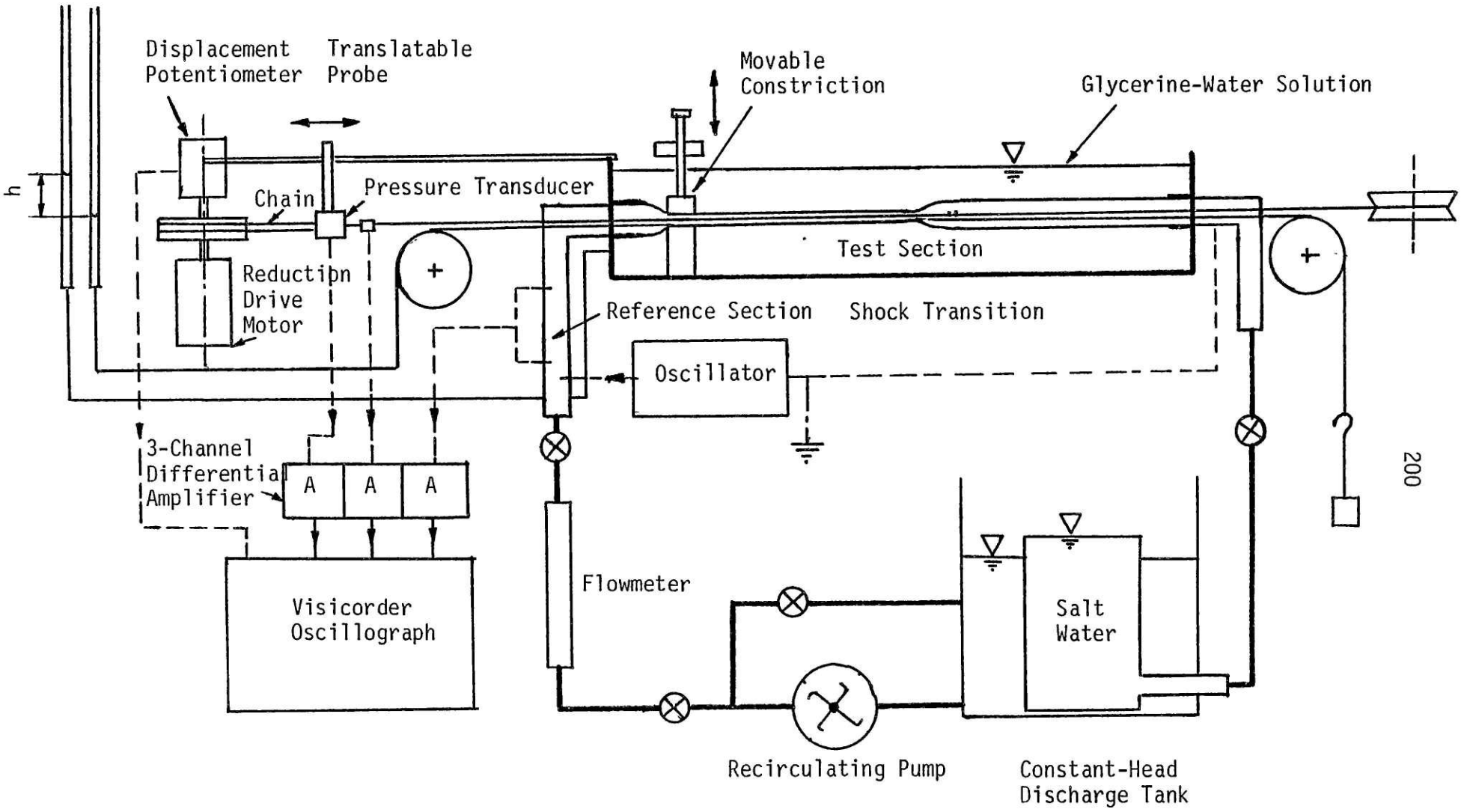

FIG (17): APPARATUS FOR THE MEASUREMENT OF AREA AND PRESSURE DISTRIBUTIONS WITHIN A STANDING SHOCK WAVE IN A COLLAPSIBLE TUBE.

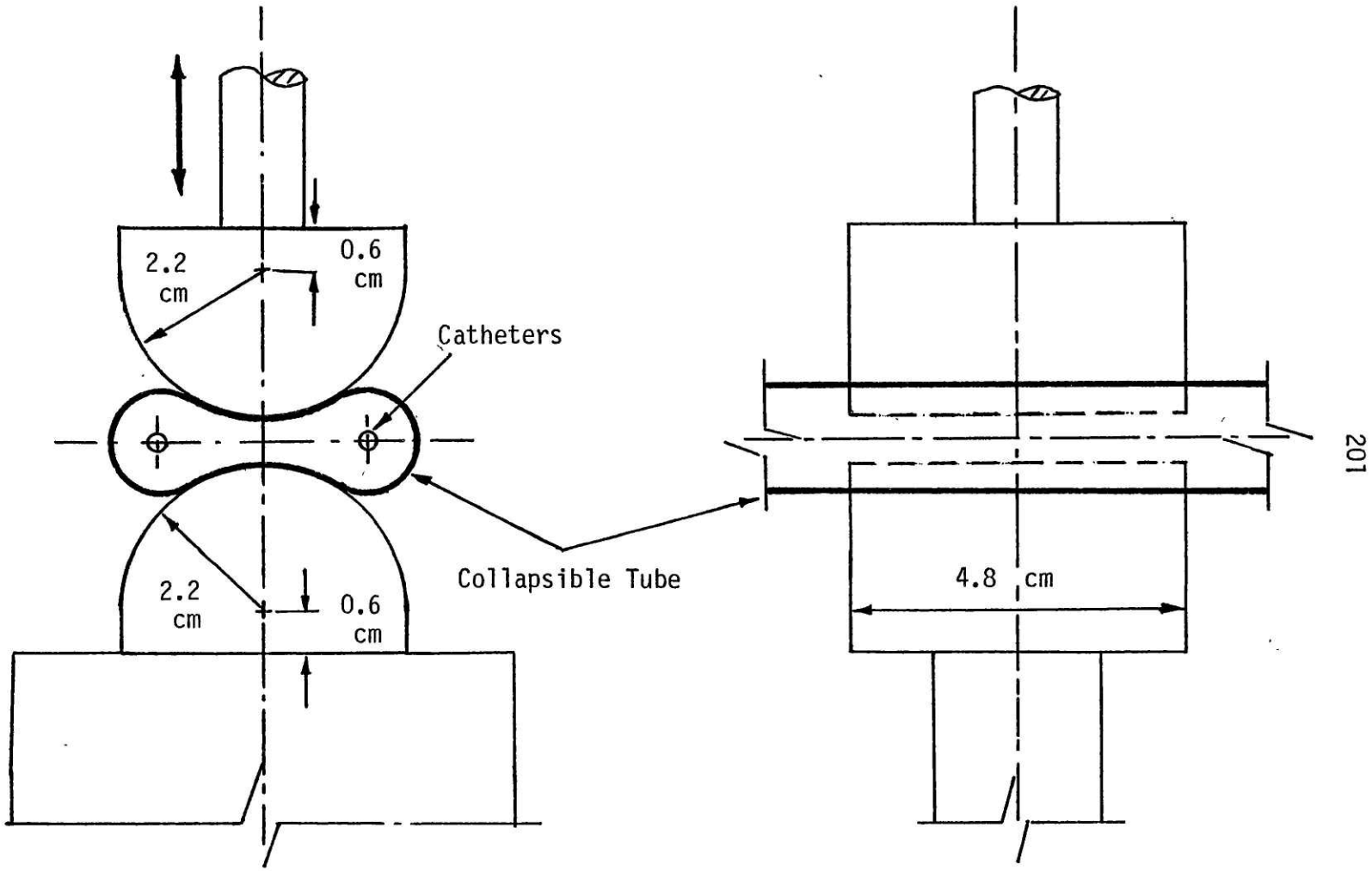

FIG (18): SHOCK WAVE APPARATUS CONSTRICTION DETAILS

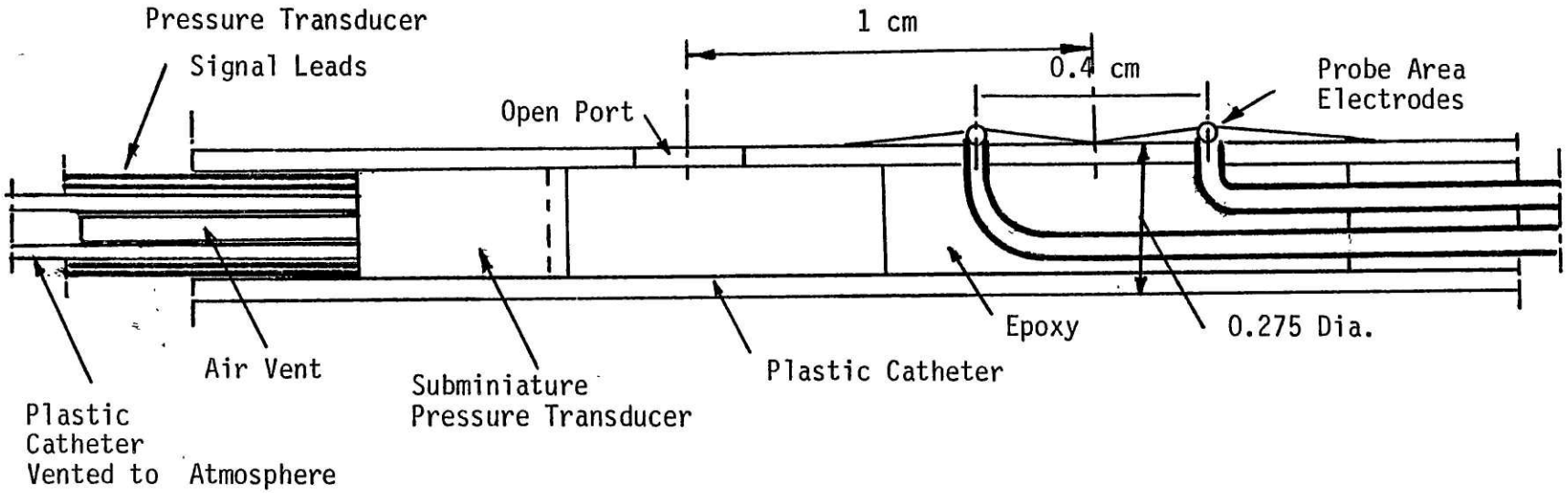

FIG (19): Details of Area and Pressure Probe; Model (1)

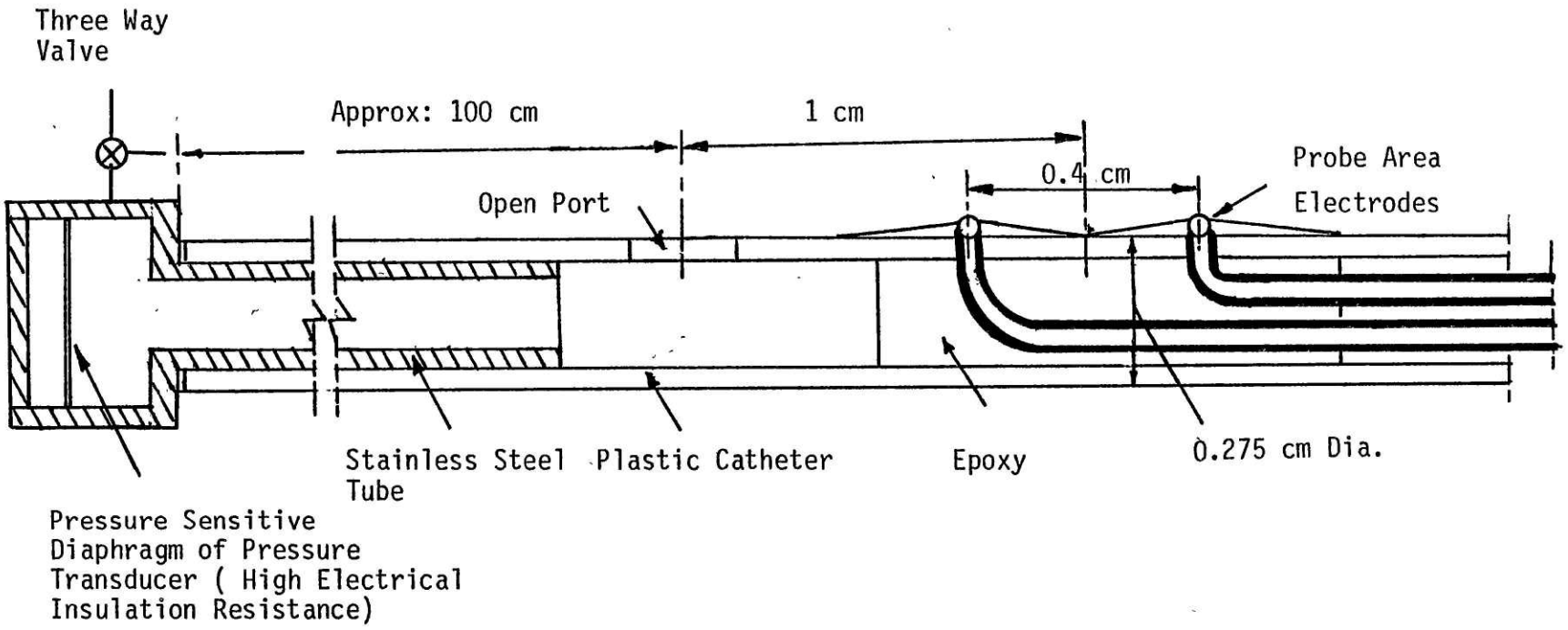

FIG (20): Details of Area and Pressure Probe; Model (2).

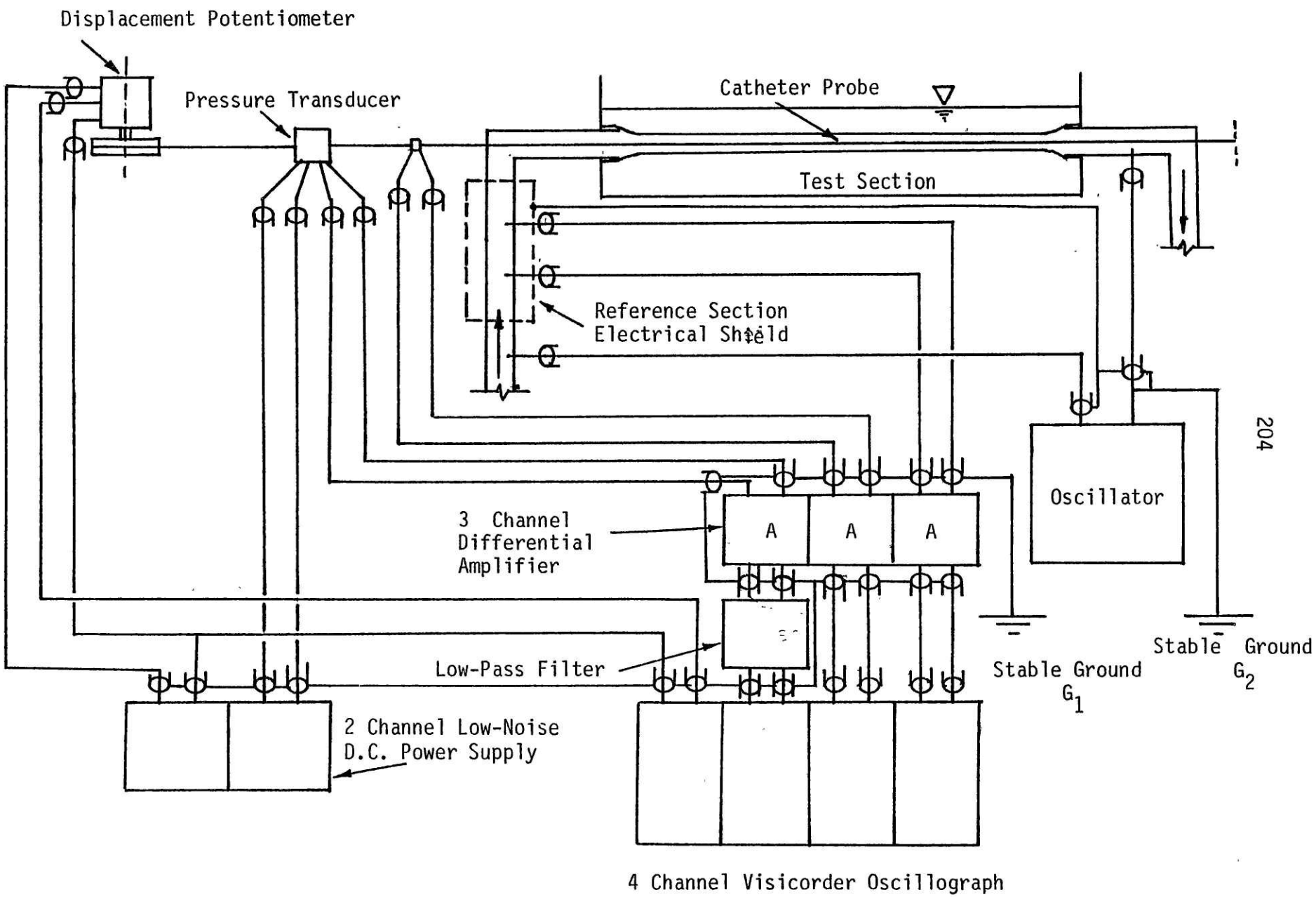

FIG (21): MEASUREMENT SYSTEM ELECTRICAL CONNECTIONS.

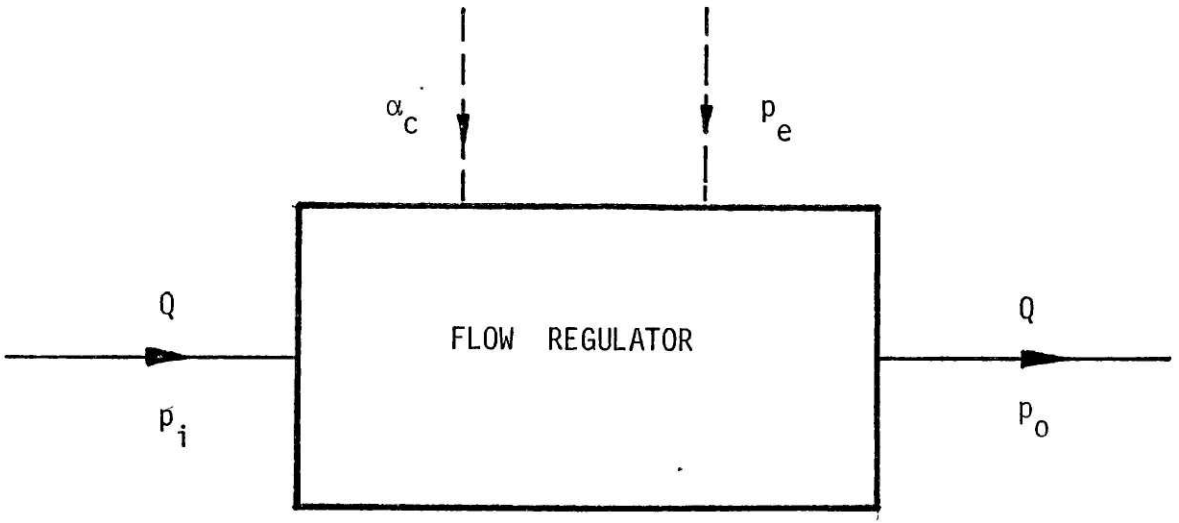

CONTROL VARIABLES: External Pressure p_e ; Constriction Size α_c

FLOW VARIABLES: Flow Rate Q ; Inlet Pressure p_i ; Outlet Pressure p_o

FLOW REGULATOR FUNCTION: Maintain Q Constant For Fixed p_i and Variable p_e

FIG(22): THE COLLAPSIBLE TUBE FLOW REGULATOR.

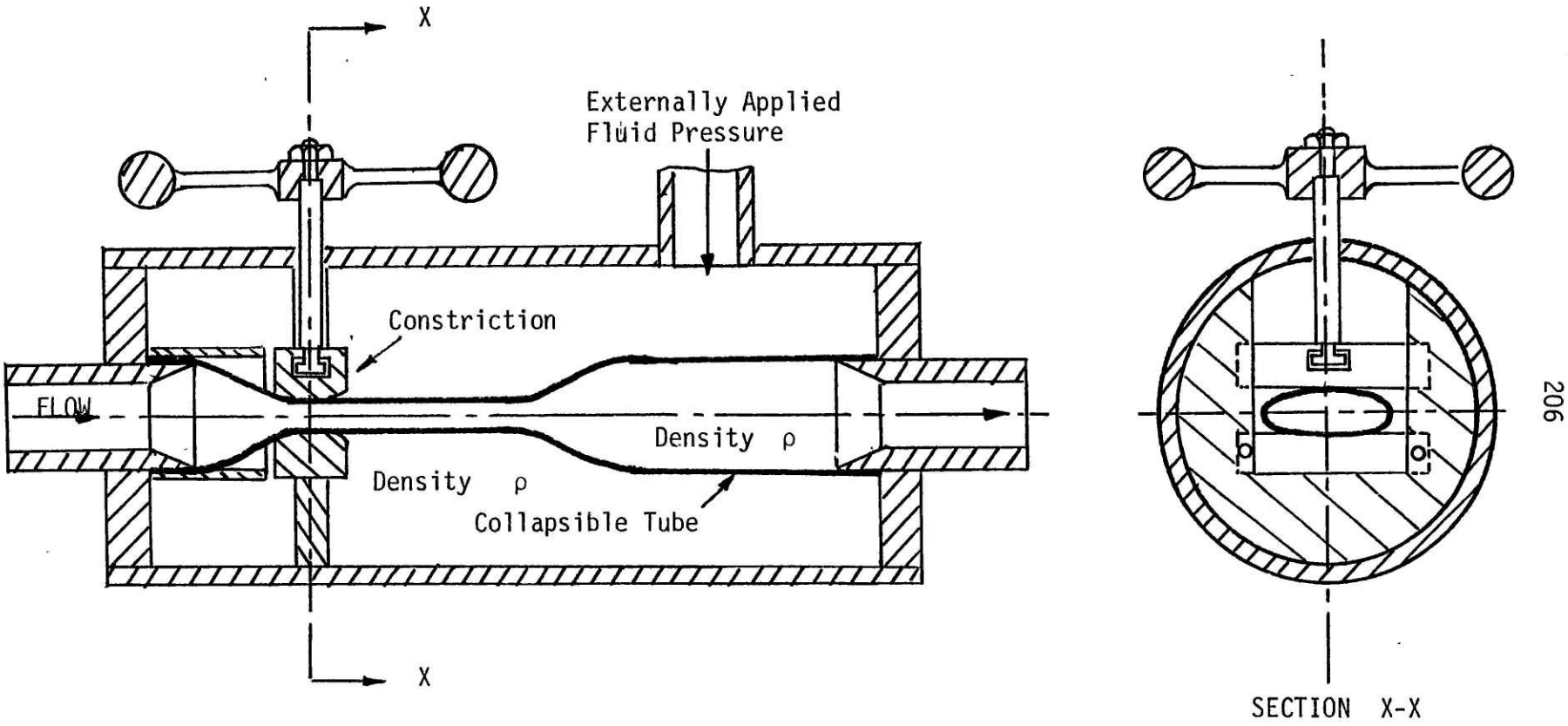

FIG (23a): PROPOSED FLOW REGULATOR CONFIGURATION

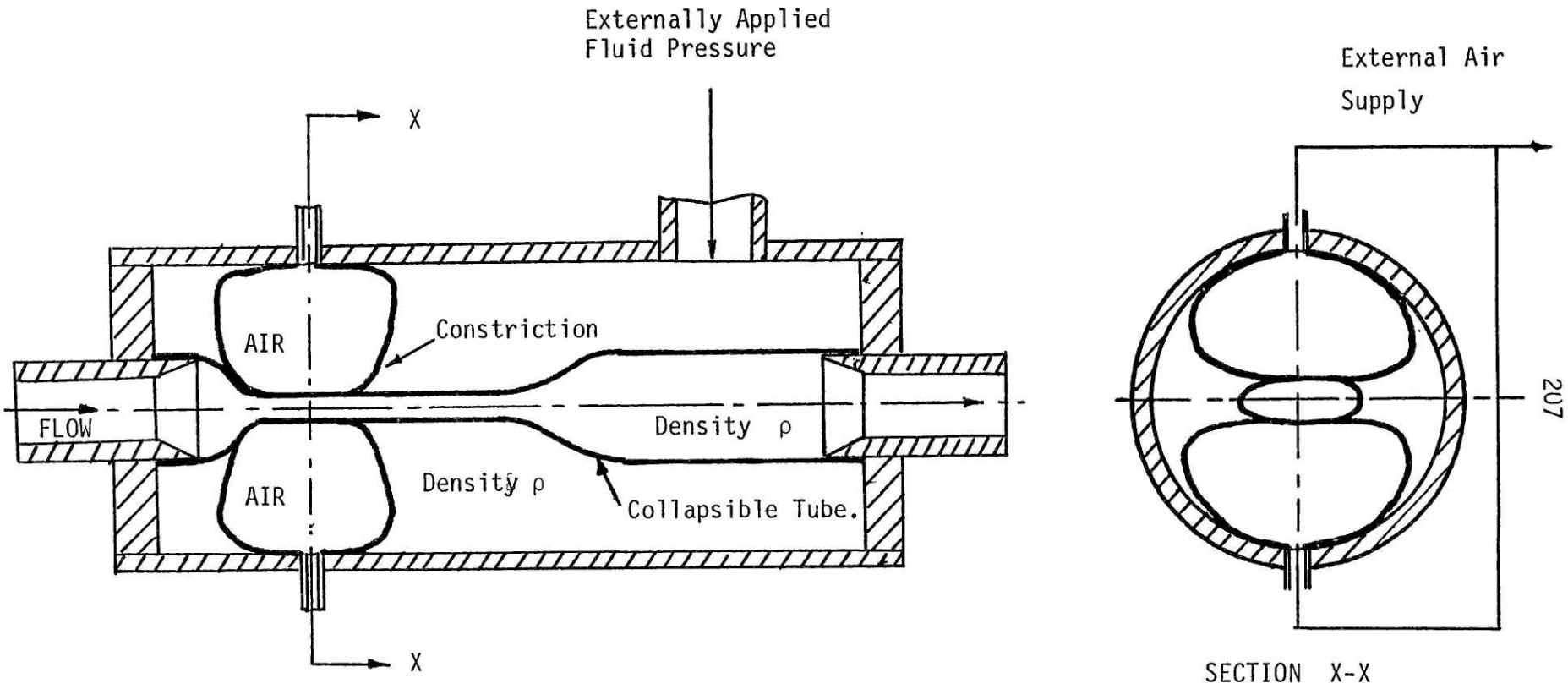

FIG (23b): ALTERNATIVE FLOW REGULATOR CONFIGURATION.

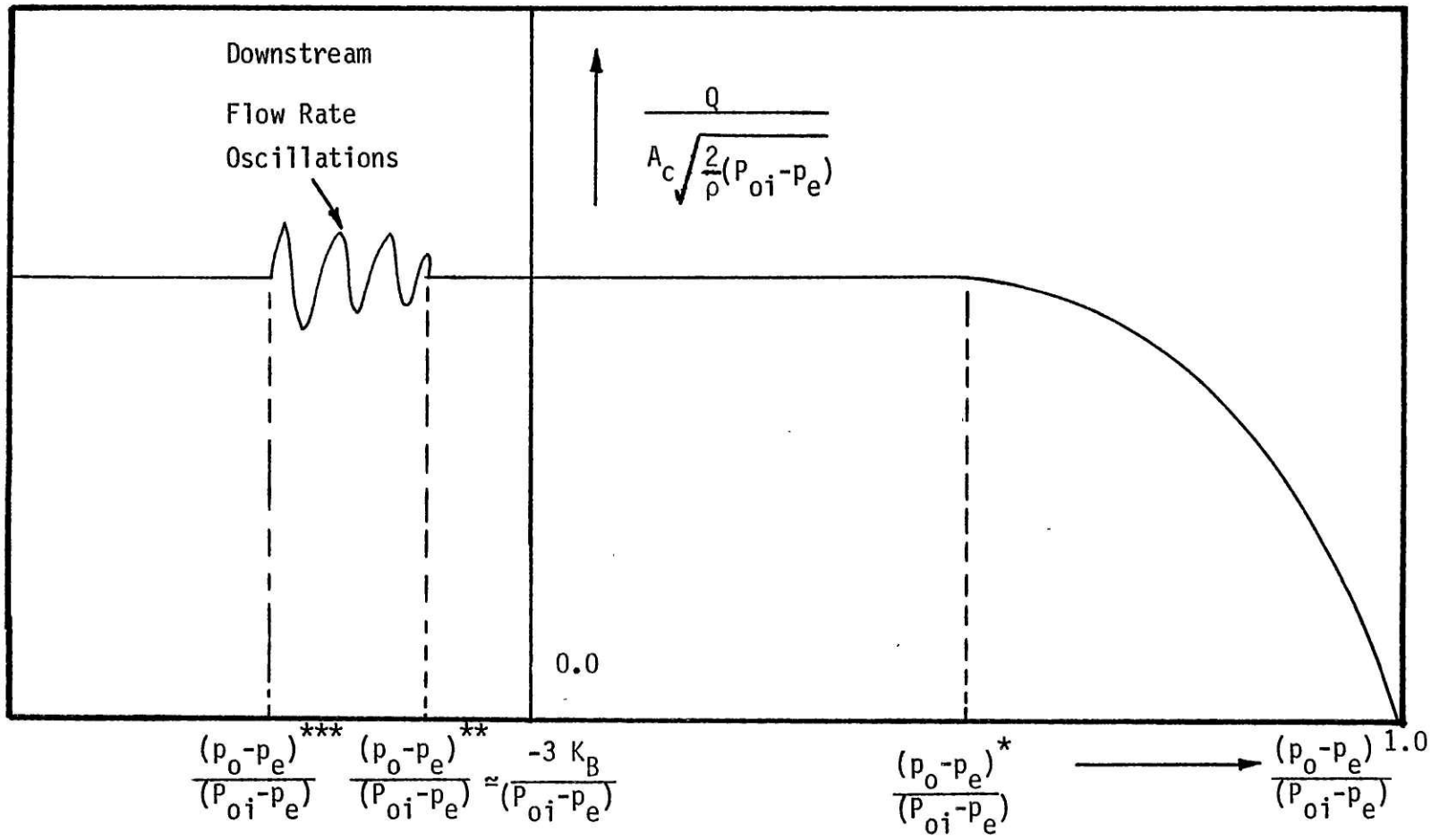

FIG (24): Flow Regulator Characteristic for a Wave Speed Type Collapsible Tube Flow Regulator. (Normalized Flow Rate Vs Normalized Downstream Pressure)

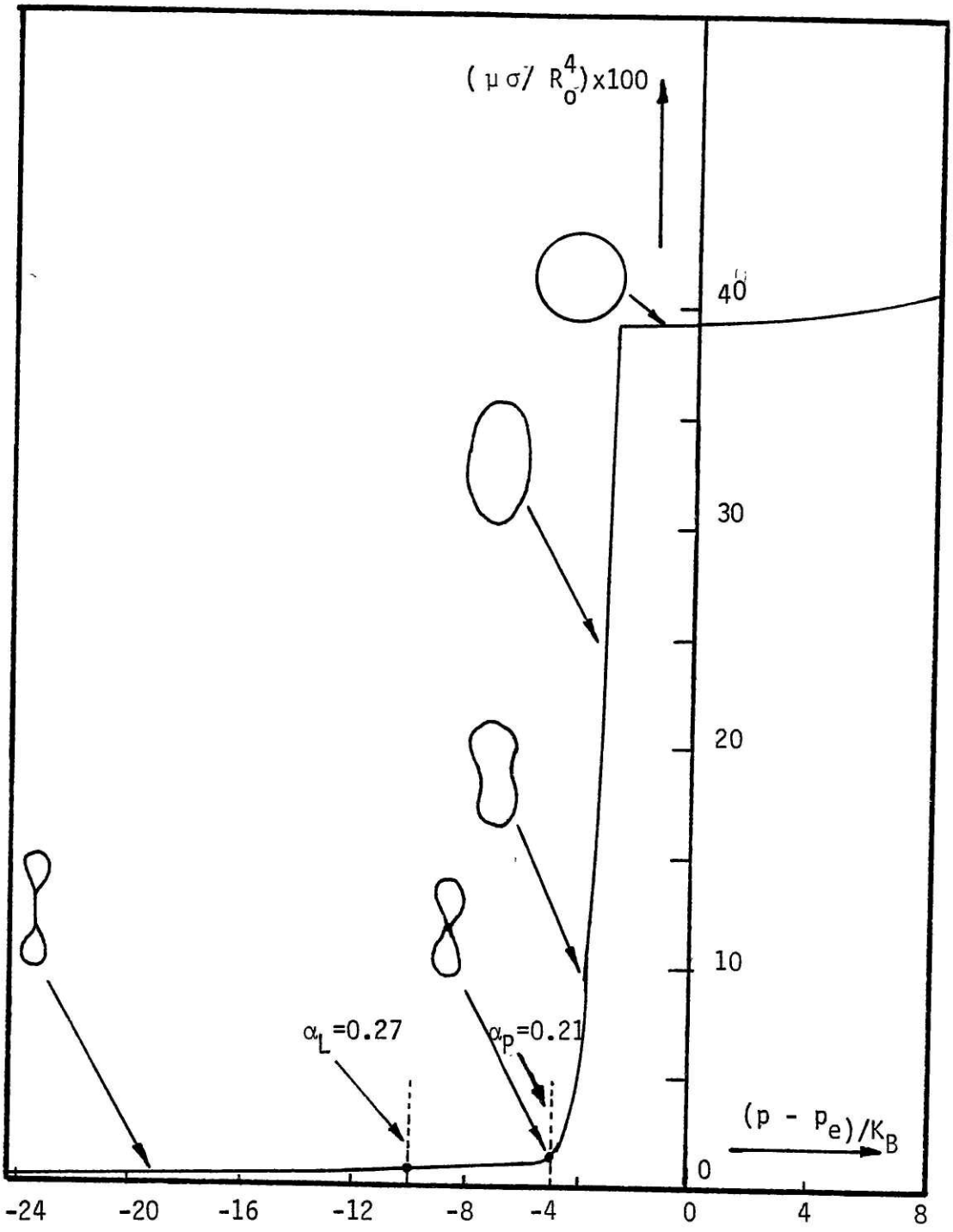

FIG (25): Flow Conductivity σ Vs. Transmural Pressure $(p-p_e)/K_B$ for a Uniformly Collapsed Tube in the Viscous Flow Regime.

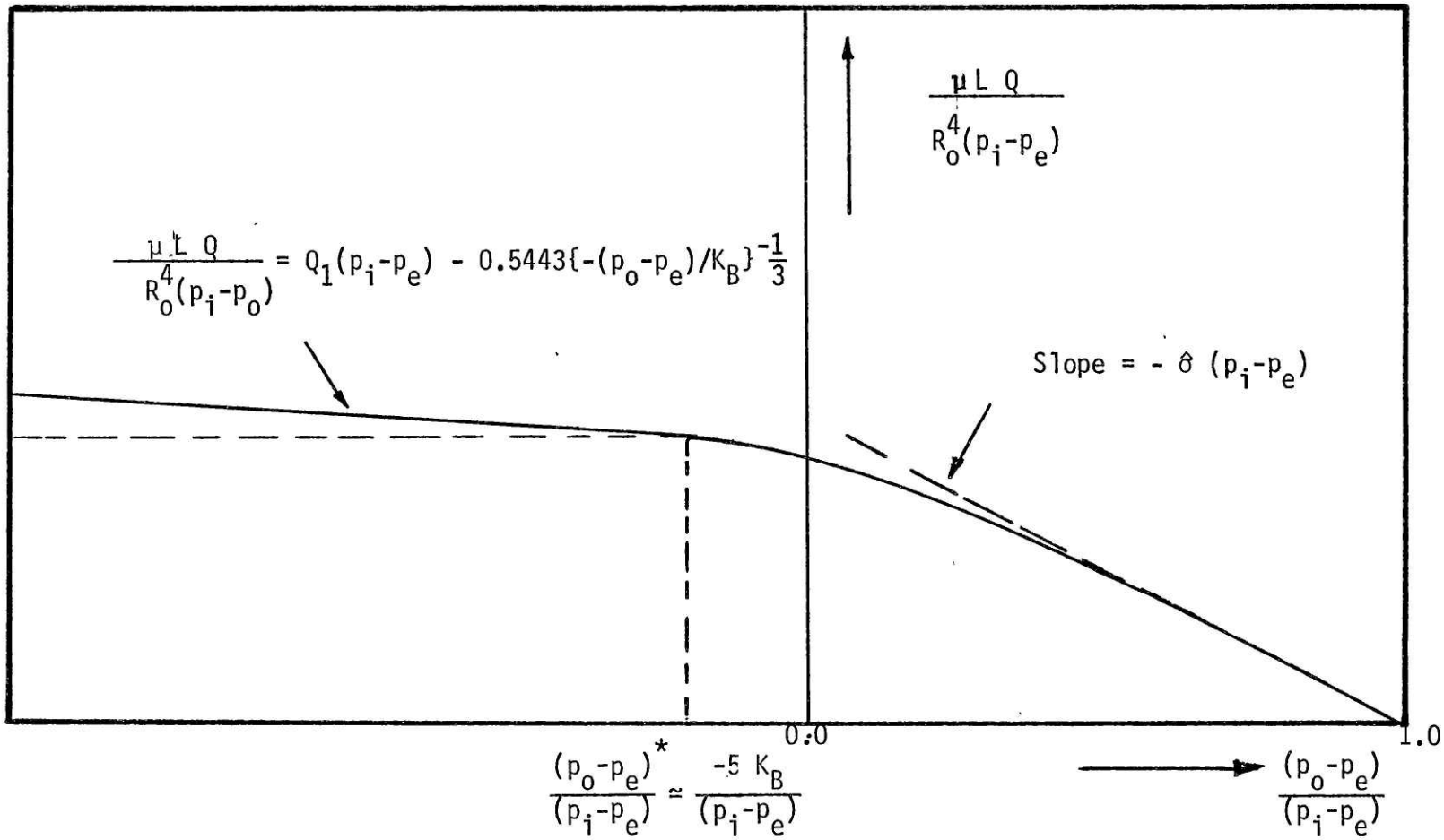

FIG (26): Flow Regulation Characteristic for a Low Reynolds Number Type Collapsible Tube Flow Regulator.(Normalized Flow Rate Vs. Normalized Downstream Pressure).

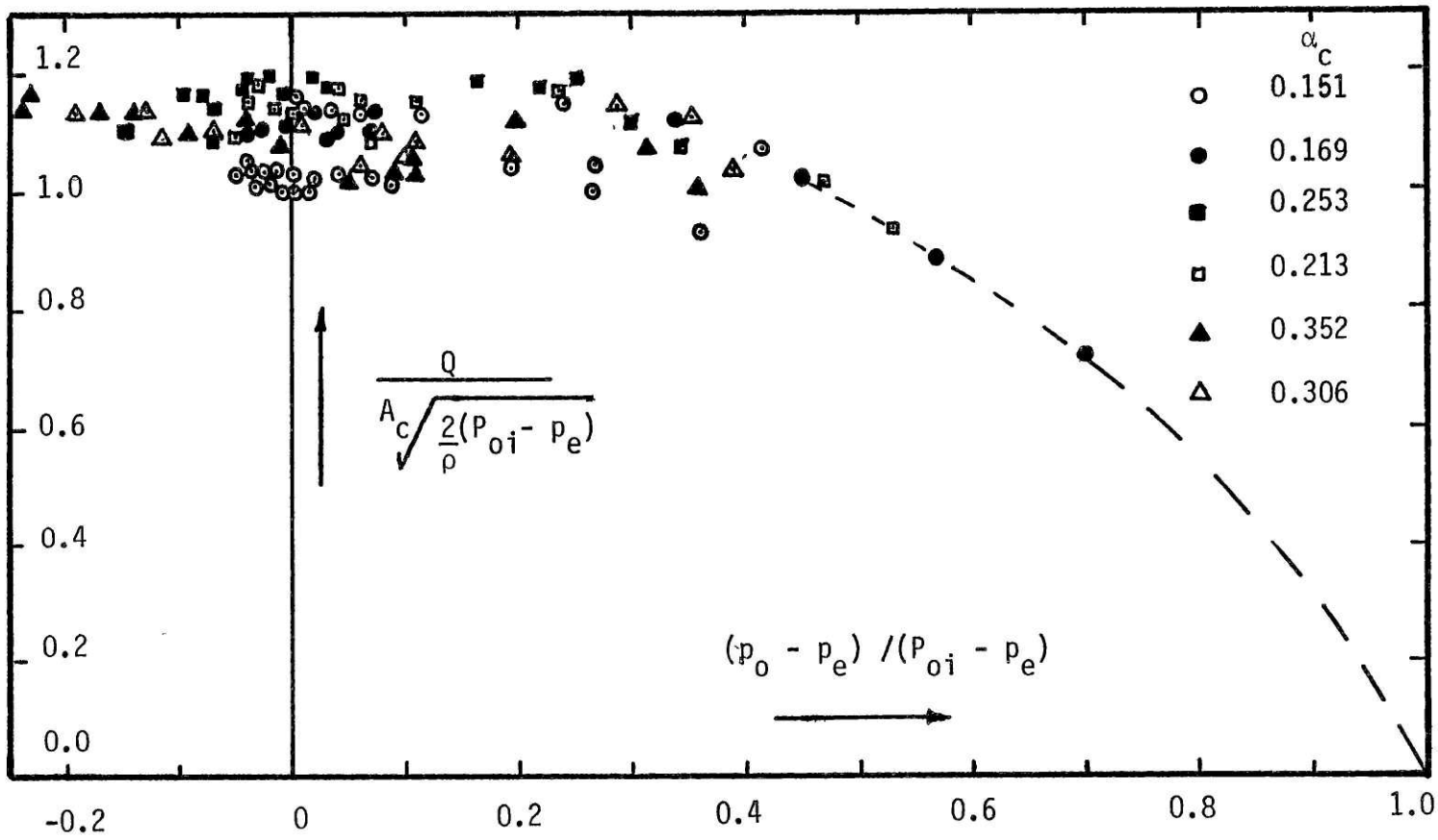

FIG (27): Flow Regulator Characteristic : Normalized Flowrate Vs. Normalized Downstream Transmural Pressure; Parameter : Constriction Area Ratio α_c.

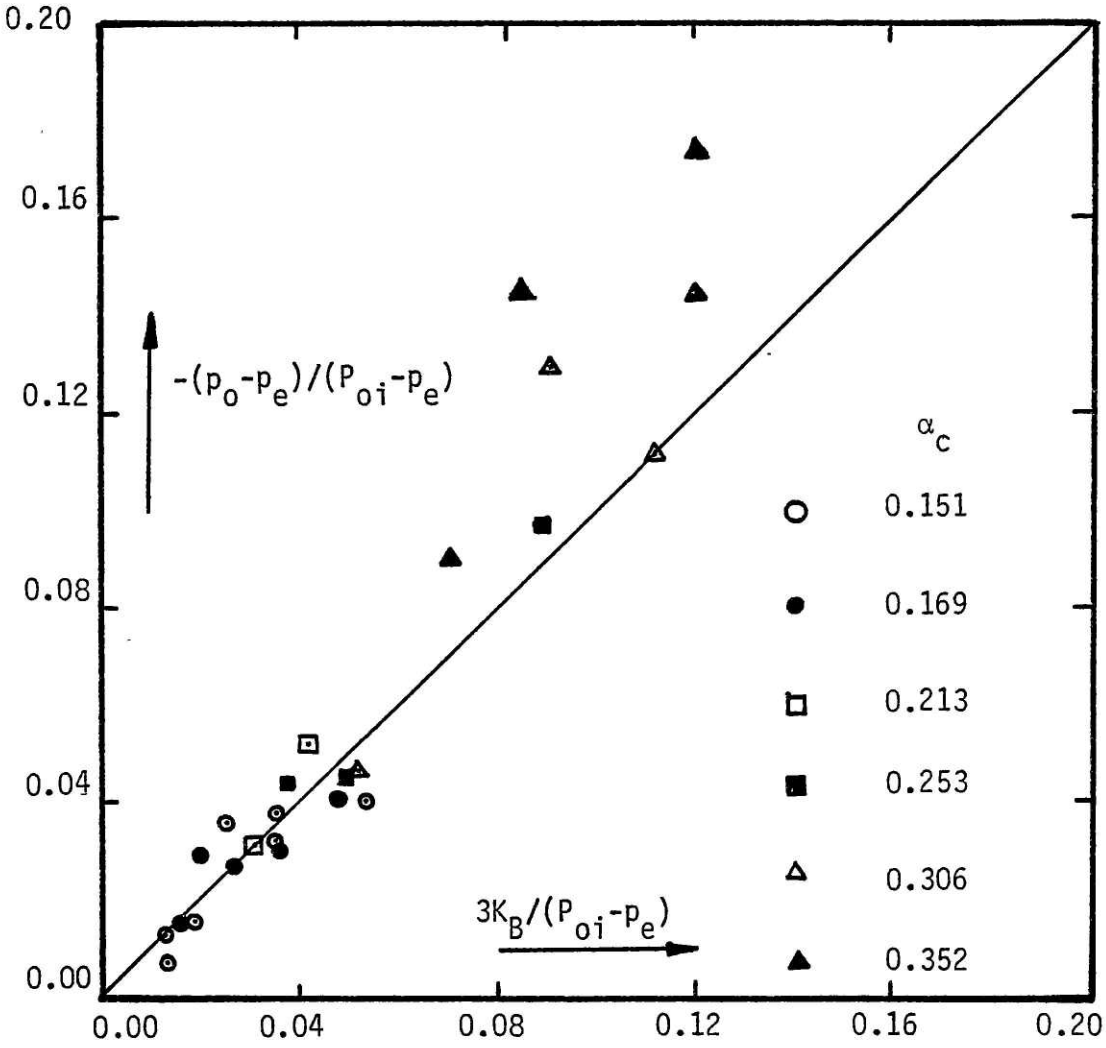

FIG (28): Normalized Downstream Pressure at Furthest Downstream Stable Position Vs. Normalized Buckling Pressure. (Parameter: Constriction Area Ratio α_c)

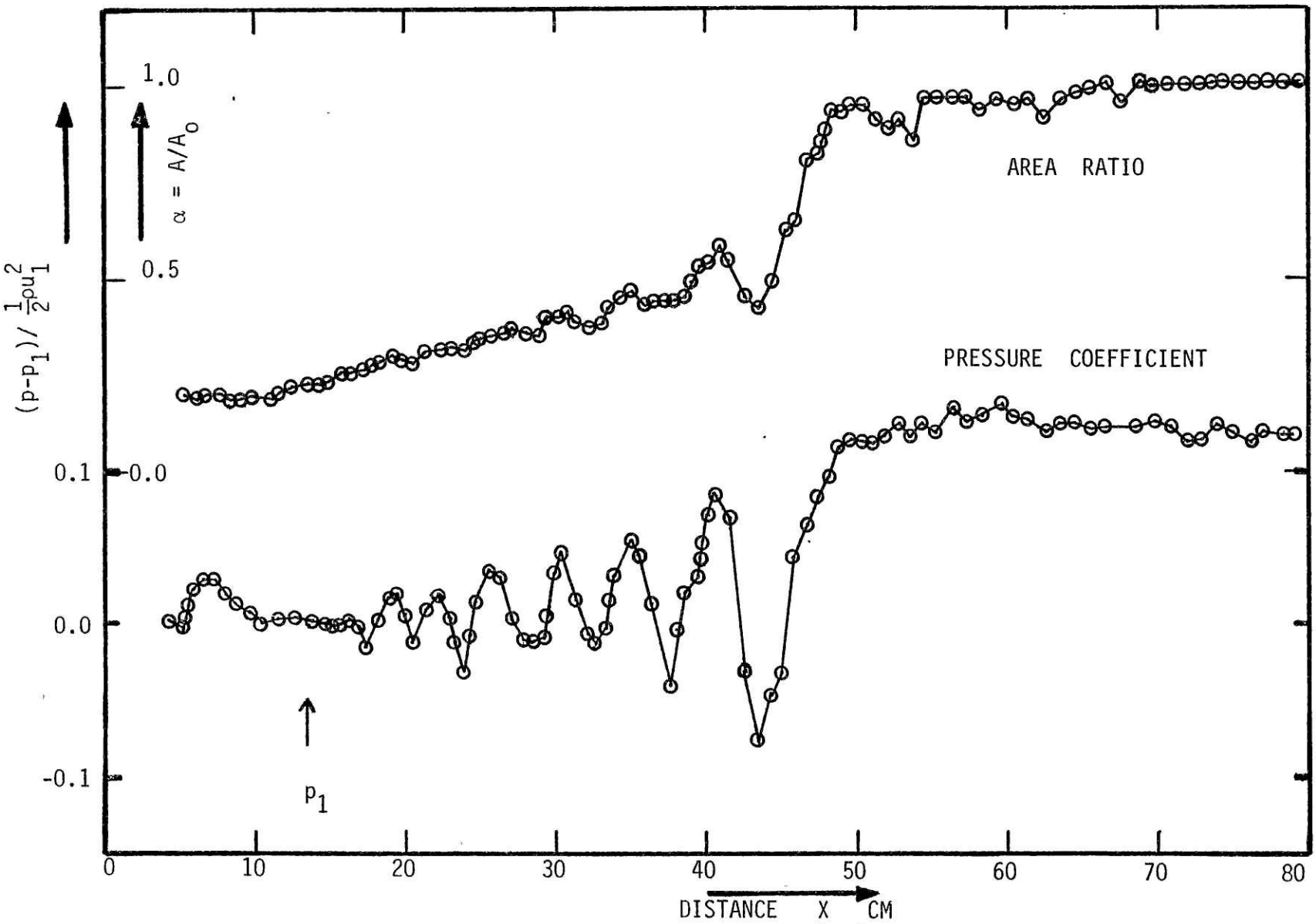

FIG (30): AREA RATIO α AND PRESSURE COEFFICIENT $(p-p_1)/\frac{1}{2}\rho u_1^2$ VS DISTANCE X ALONG THE SHOCK WAVE
Flow Rate = 23.0 Lit/Min; Constriction Area Ratio = 0.195; Inlet Speed Index = 5.98;
Outlet Speed Index = 0.113; Resting Area A_o = 4.530 cm^2.

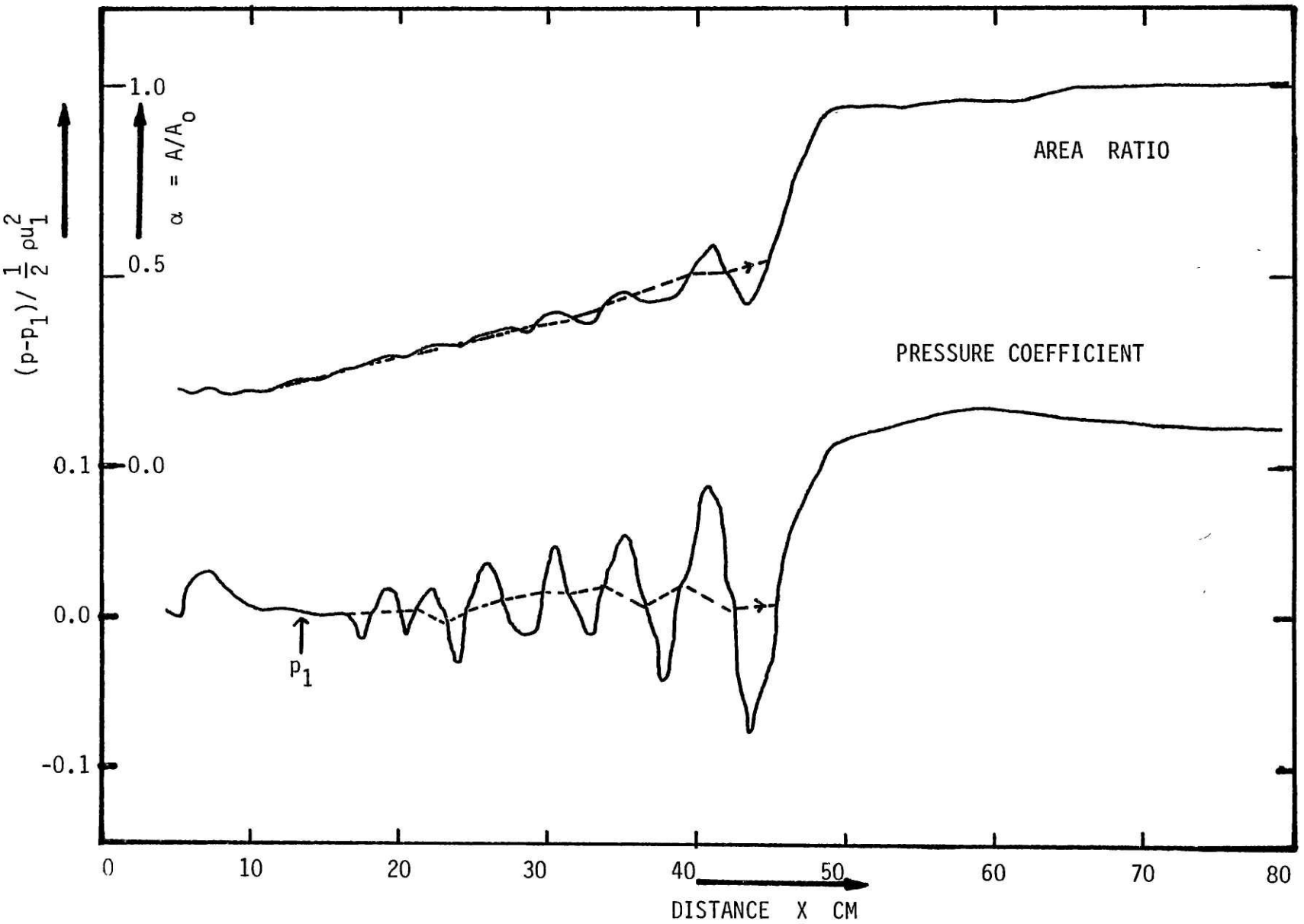

FIG (30s): AREA RATIO α AND PRESSURE COEFFICIENT $(p-p_1)/\frac{1}{2}\rho u_1^2$ VS DISTANCE X ALONG THE SHOCK WAVE
Flow Rate = 23.0 Lit/Min; Constriction Area Ratio = 0.195; Inlet Speed Index = 5.98;
Outlet Speed Index = 0.113; Resting Area $A_o = 4.530\ cm^2$.

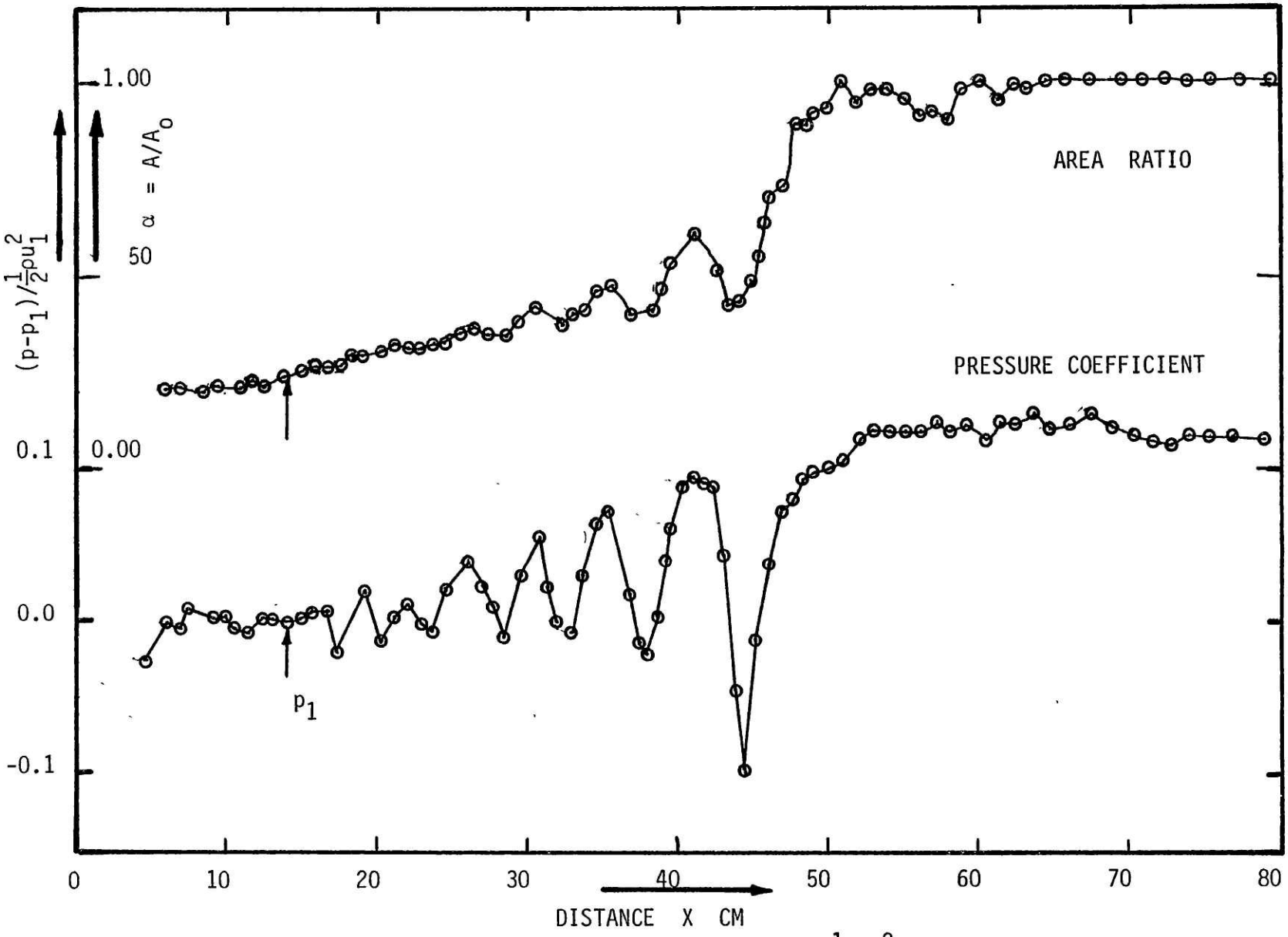

FIG (31): AREA RATIO α AND PRESSURE COEFFICIENT $(p-p_1)/\frac{1}{2}\rho u_1^2$ VS DISTANCE X ALONG THE SHOCK WAVE.
Flow Rate = 21.0 Lit/Min; Constriction Area Ratio = 0.195; Inlet Speed Index = 5.96; Outlet Speed Index = 0.099; Resting Area = 4.530 cm^2.

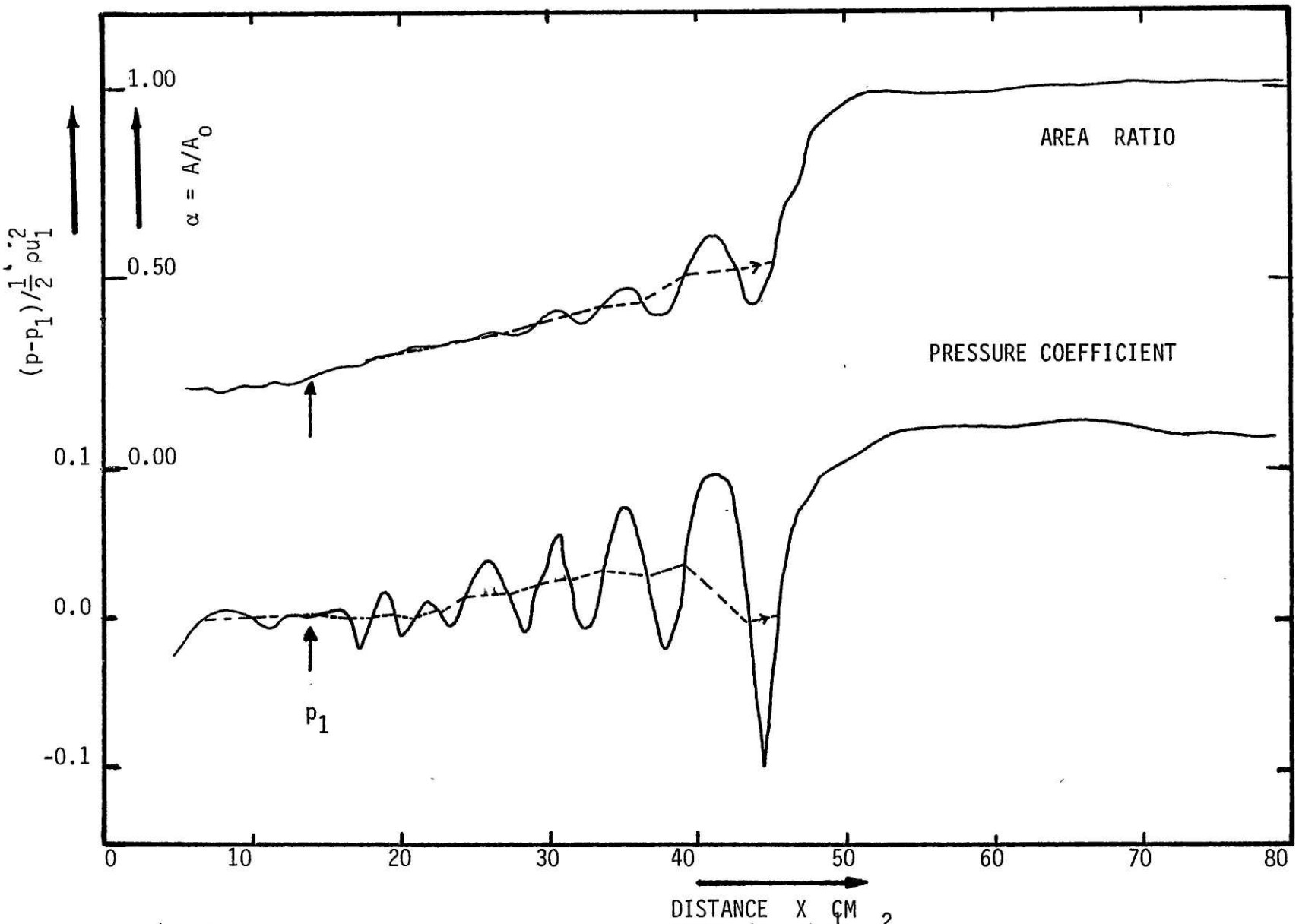

FIG (31s): AREA RATIO α AND PRESSURE COEFFICIENT $(p-p_1)/\frac{1}{2}\rho u_1^2$ VS DISTAMCE ALONG THE SHOCK WAVE
Flow Rate = 21.0 Lit/Min; Constriction Area Ratio = 0.195; Inlet Speed Index = 5.96;
Outlet Speed Index = 0.099; Resting Area = 4.53 cm^2.

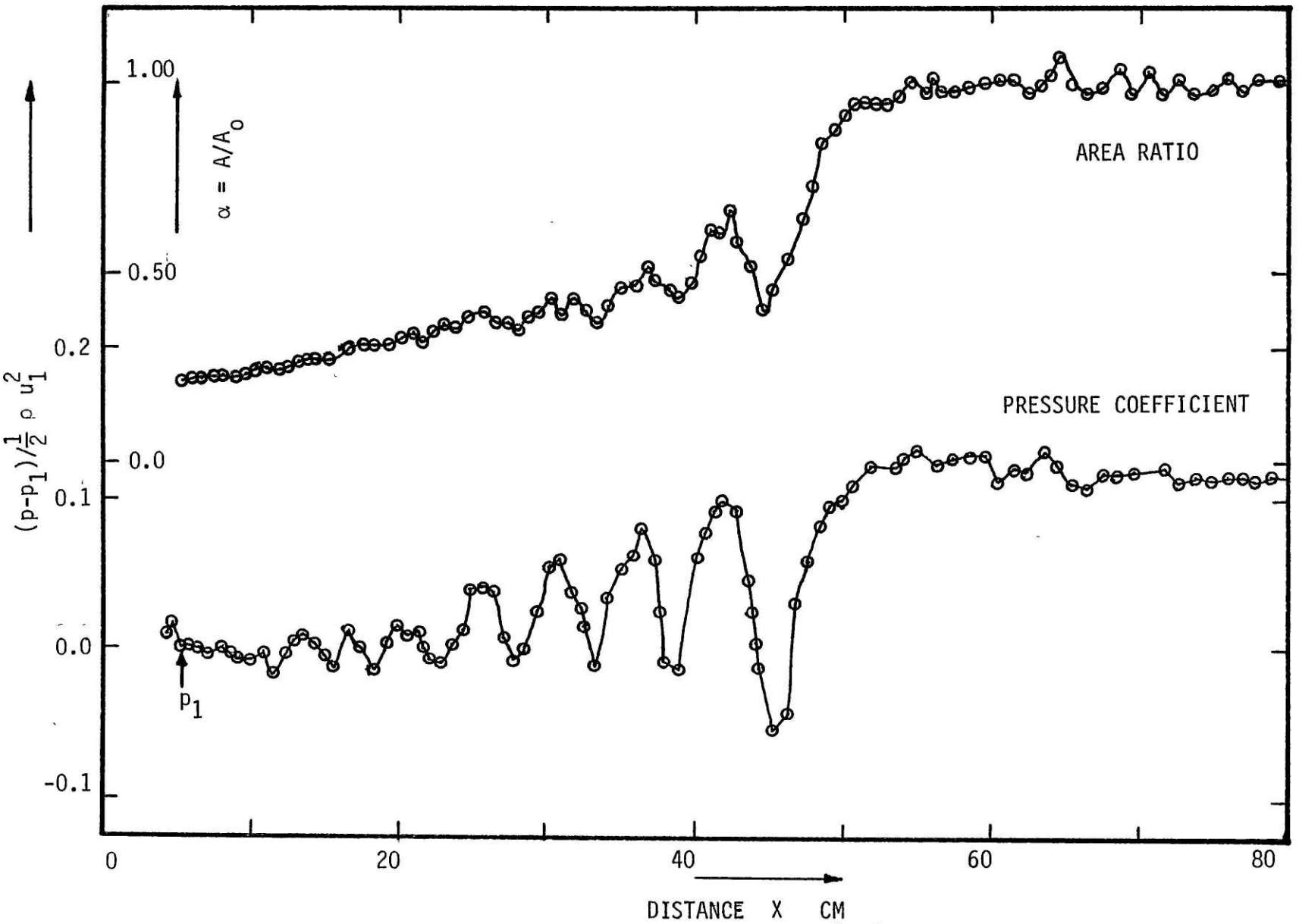

FIG (32): AREA RATIO α AND PRESSURE COEFFICIENT $(p-p_1)/\frac{1}{2}\rho u_1^2$ VS DISTANCE X ALONG THE SHOCK WAVE.
Flow Rate = 18.8 Lit/Min;Constriction Area Ratio = 0.195; Inlet Speed Index = 5.21; Outlet Speed Index = 0.096; Resting Area A_o = 4.530 cm^2.

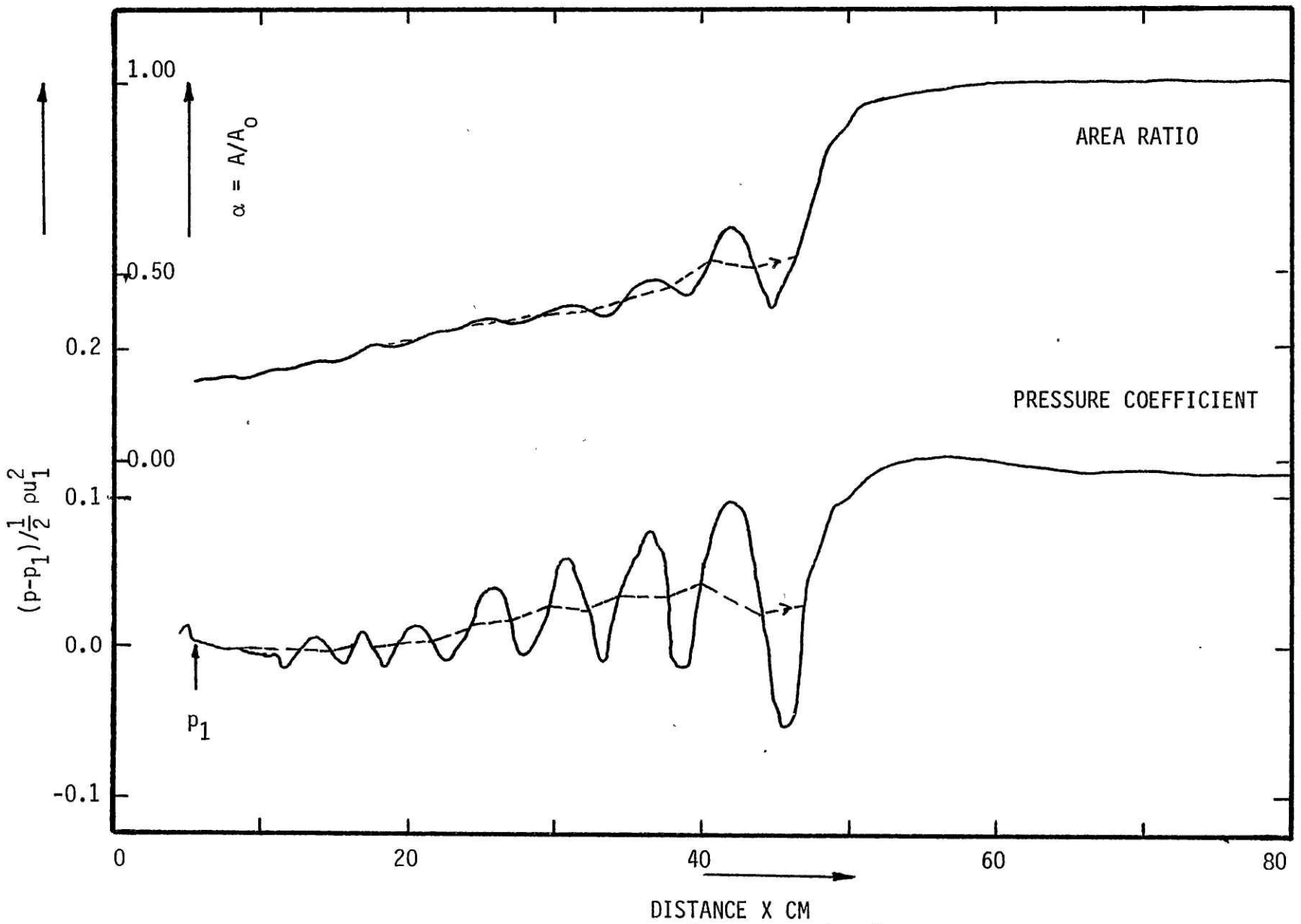

FIG (32s): AREA RATIO α AND PRESSURE COEFFICIENT $(p-p_1)/\frac{1}{2}\rho u_1^2$ VS DISTANCE ALONG THE SHOCK WAVE. Flow Rate = 18.8 Lit/Min; Constriction Area Ratio = 0.195; Inlet Speed Index = 5.21; Outlet Speed Index =).096; Resting Area A_o = 4.530 cm^2.

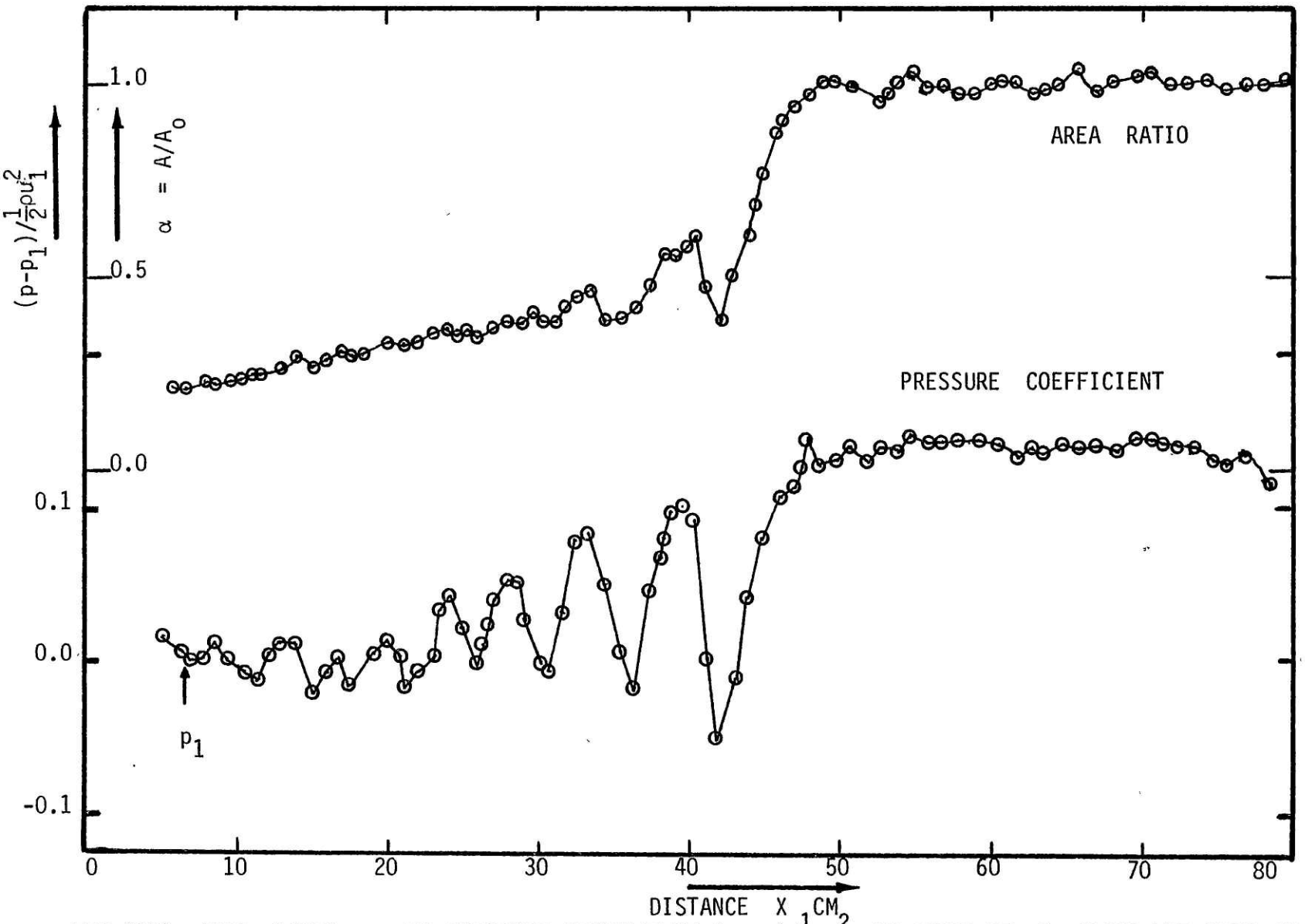

FIG (33): AREA RATIO α AND PRESSURE COEFFICIENT $(p-p_1)/\frac{1}{2}\rho u_1^2$ VS DISTANCE X ALONG THE SHOCK WAVE

Flow Rate = 17.5 Lit/Min; Constriction Area Ratio = 0.195; Inlet Speed Index = 4.82; Outlet Speed Index = 0.089; Resting Area A_o = 4.53 cm^2.

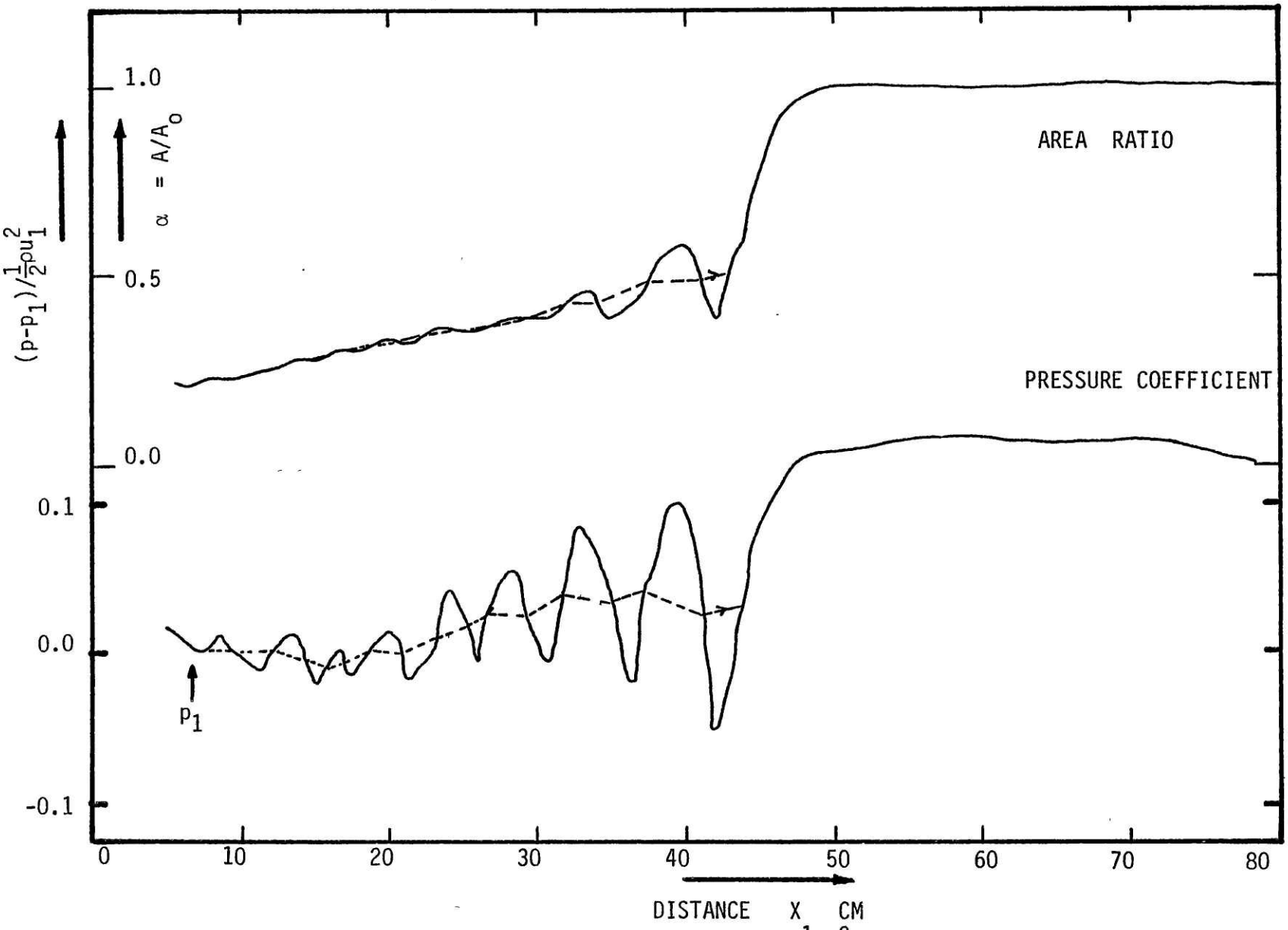

FIG (33s): AREA RATIO α AND PRESSURE COEFFICIENT $(p-p_1)/\frac{1}{2}\rho u_1^2$ VS DISTANCE ALONG THE SHOCK WAVE
Flow Rate = 17.5 Lit/Min; Constriction Area Ratio = 0.195; Inlet Speed Index = 4.82;
Outlet Speed Index = 0.089; Resting Area = 4.530 cm^2.

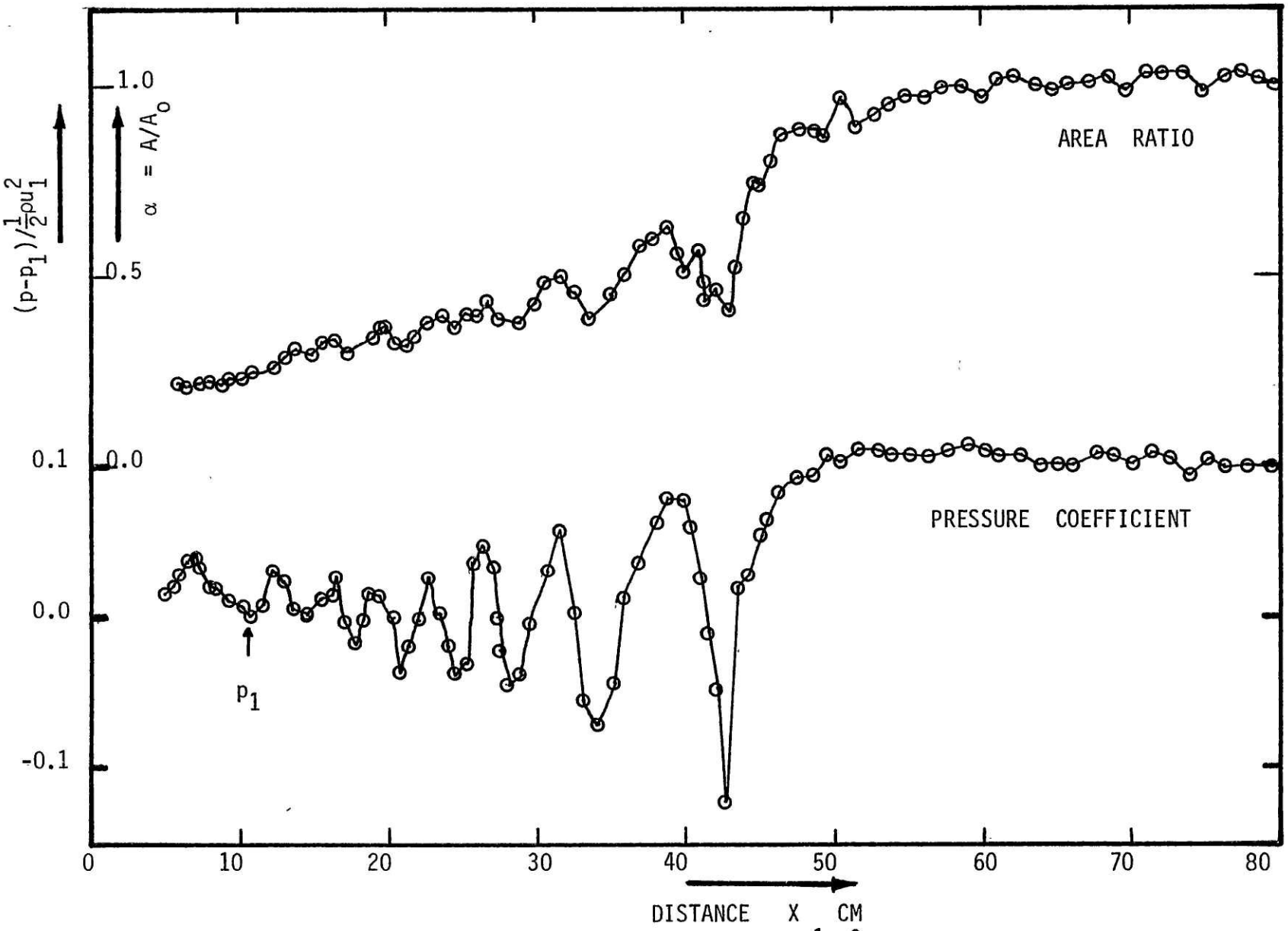

FIG (34): AREA RATIO α AND PRESSURE COEFFICIENT $(p-p_1)/\frac{1}{2}\rho u_1^2$ VS DISTANCE X ALONG THE SHOCK WAVE
Flow Rate = 22.7 Lit/Min; Constriction Area Ratio = 0.213; Inlet Speed Index = 5.24;
Outlet Speed Index = 0.107; Resting Area A_o = 4.530 cm^2.

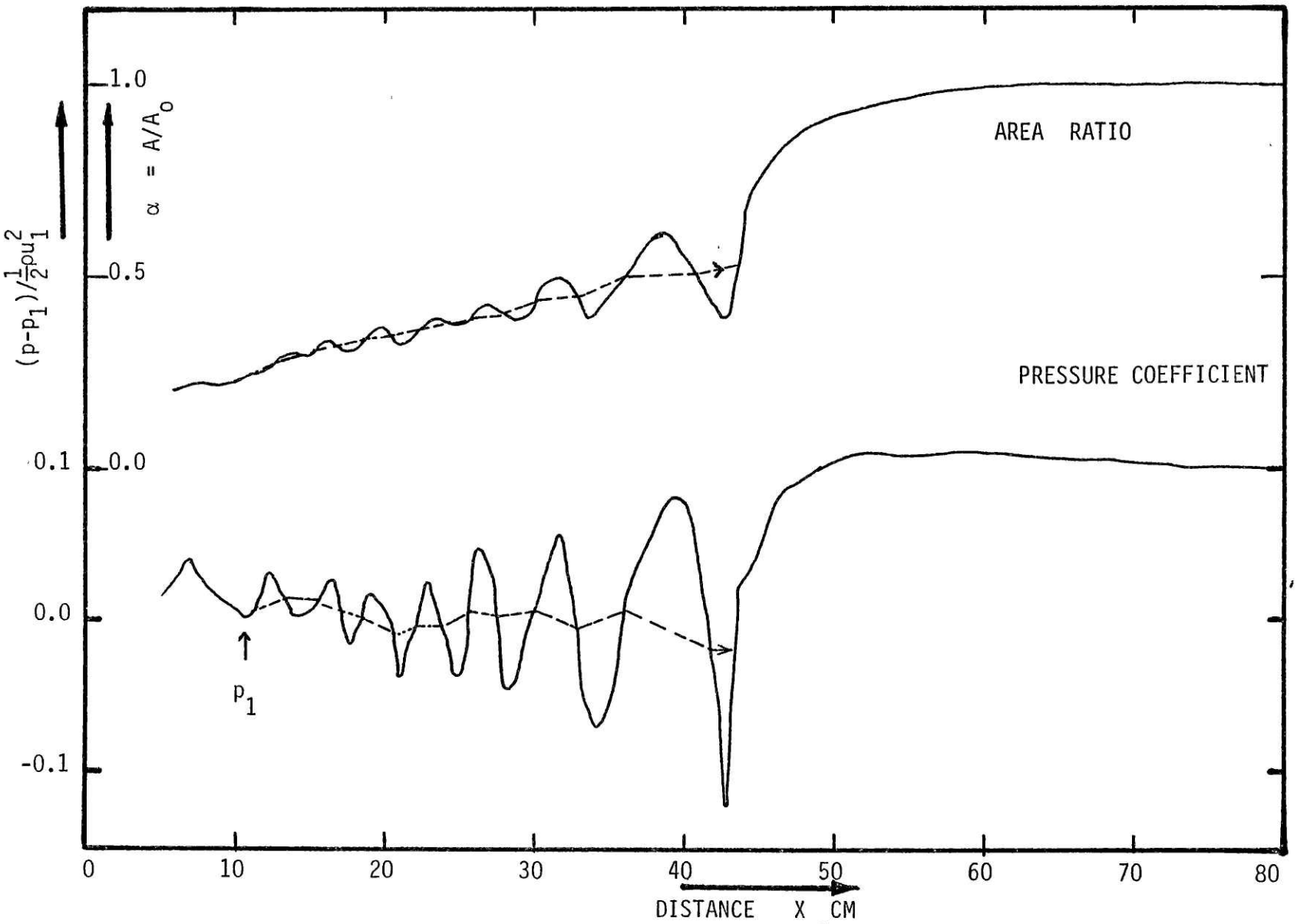

FIG (34s): AREA RATIO α AND PRESSURE COEFFICIENT $(p-p_1)/\frac{1}{2}\rho u_1^2$ VS DISTANCE X ALONG THE SHOCK WAVE
Flow Rate = 22.7 Lit/Min; Constriction Area Ratio = 0.213; Inlet Speed Index = 5.24;
Outlet Speed Index = 0.107; Resting Area $A_o = 4.530\ cm^2$.

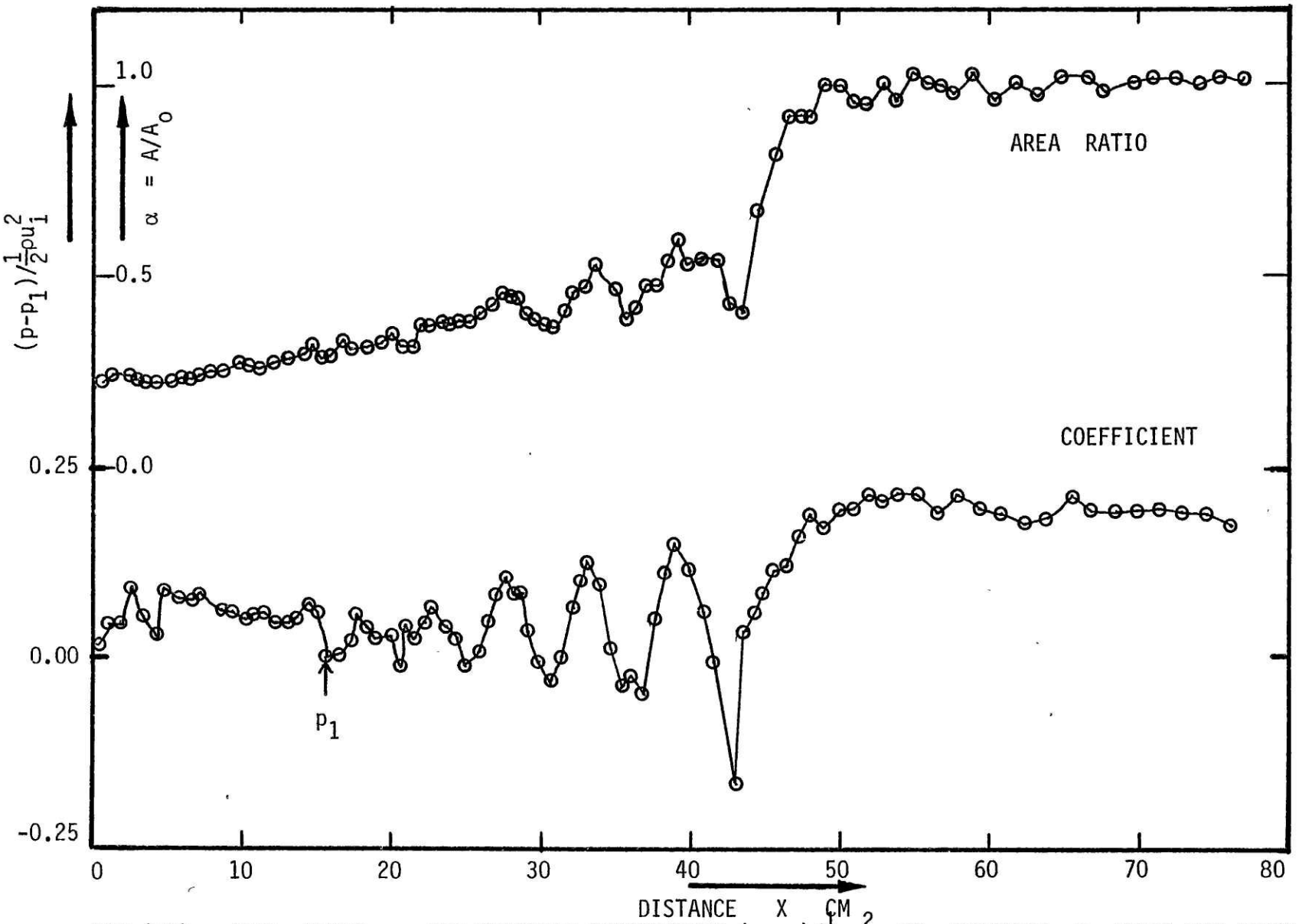

FIG (35): AREA RATIO α AND PRESSURE COEFFICIENT $(p-p_1)/\frac{1}{2}\rho u_1^2$ VS DISTANCE X ALONG THE SHOCK WAVE

Flow Rate = 21.5 Lit/Min; Constriction Area Ratio = 0.213; Inlet Speed Index = 6.73; Outlet Speed Index = 0.102; Resting Area = 4.530 cm^2.

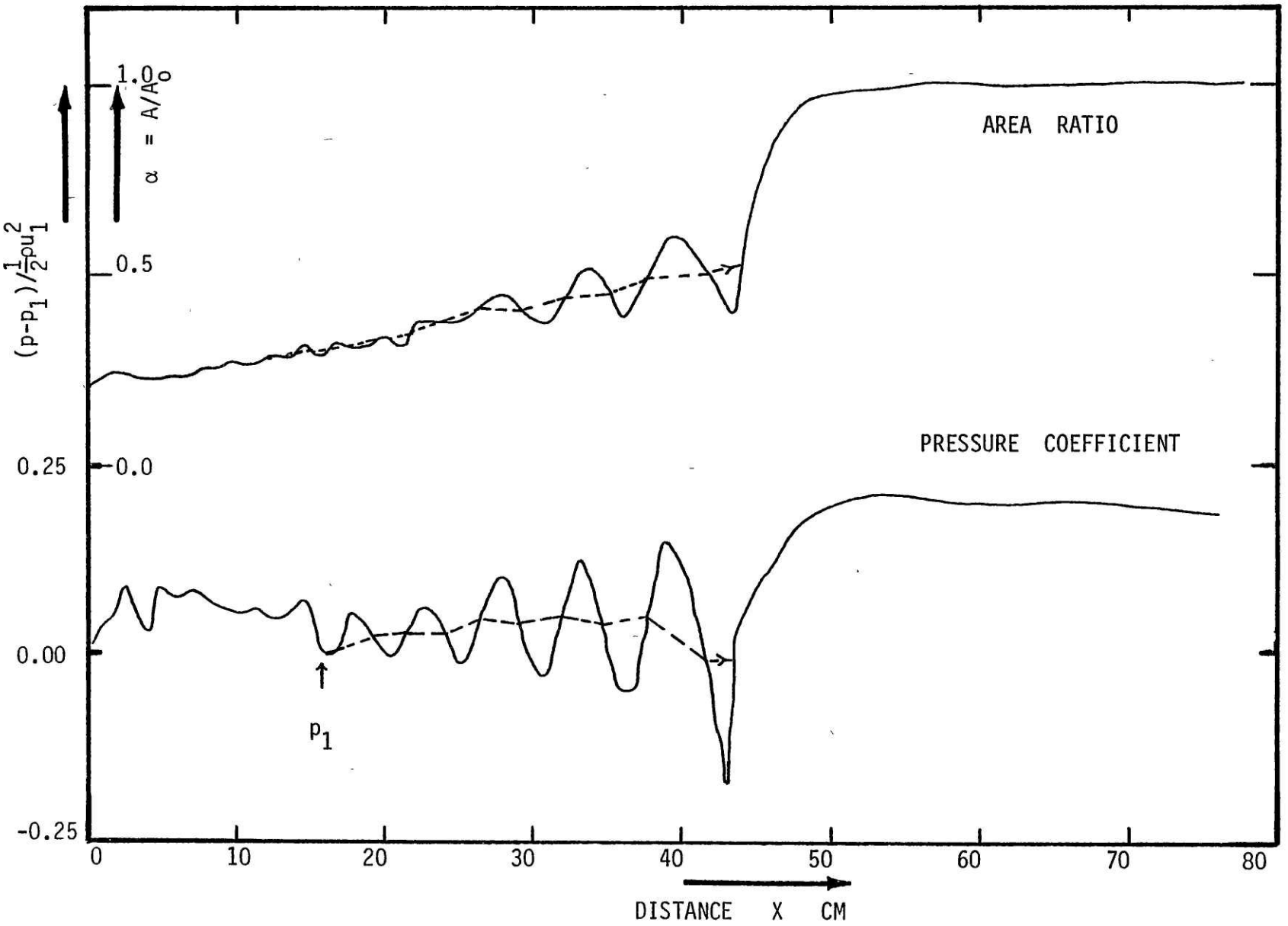

FIG (35s): AREA RATIO α AND PRESSURE COEFFICIENT $(p-p_1)/\frac{1}{2}\rho u_1^2$ VS DISTANCE X ALONG THE SHOCK WAVE
Flow Rate = 21.5 Lit/Min;Constriction Area Ratio =0 .213; Inlet Speed Index = 6.73;
Outlet Speed Index = 0.102; Resting Area A_o = 4.530 cm^2.

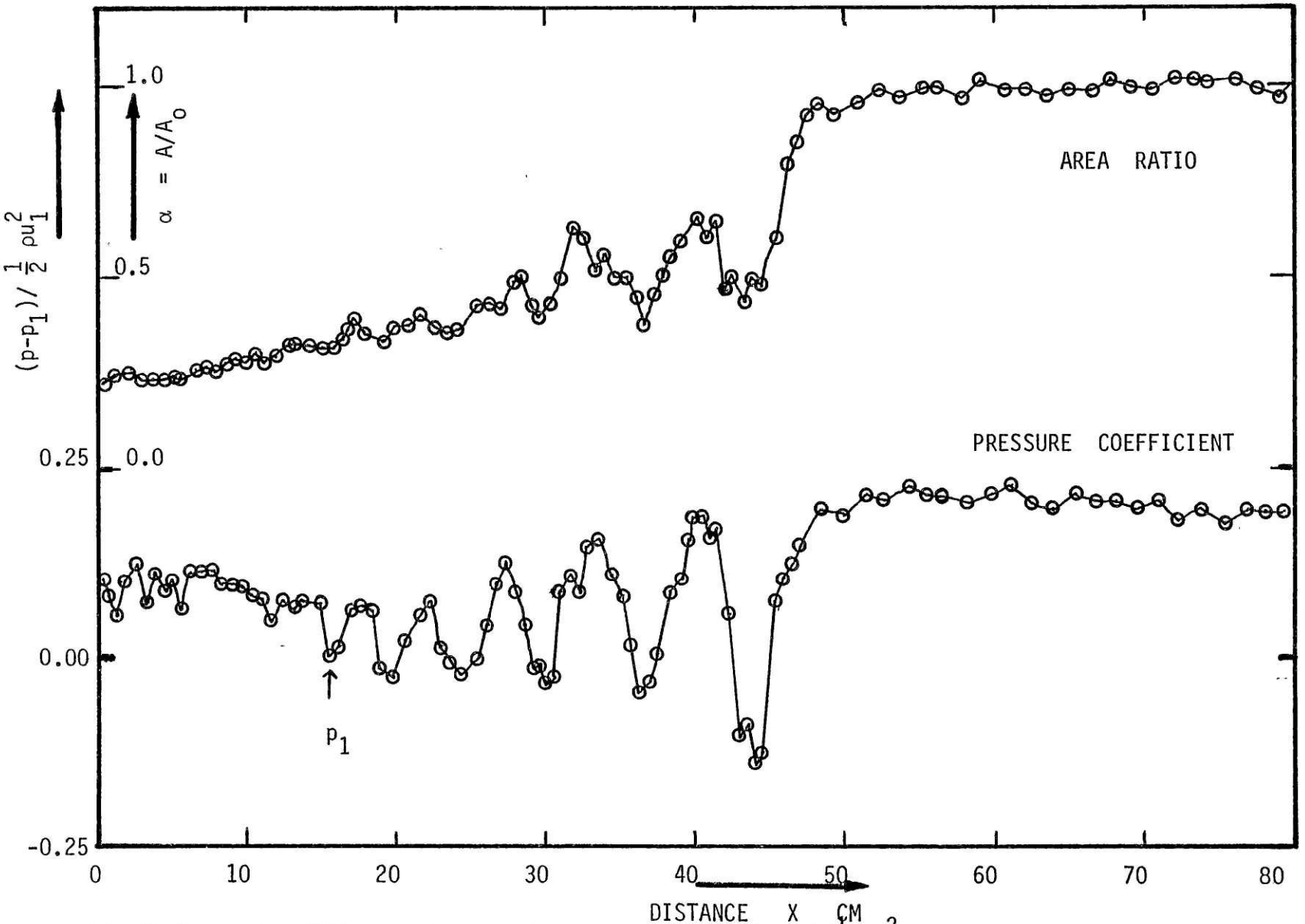

FIG (36): AREA RATIO α AND PRESSURE COEFFICIENT $(p-p_1)/\frac{1}{2}\rho u_1^2$ VS DISTANCE X ALONG THE SHOCK WAVE

Flow Rate = 20.0 Lit/Min; Constriction Area Ratio = 0.213; Inlet Speed Index = 10.03; Outlet Speed Index = 0.100; Resting Area A_o = 4.530 cm^2.

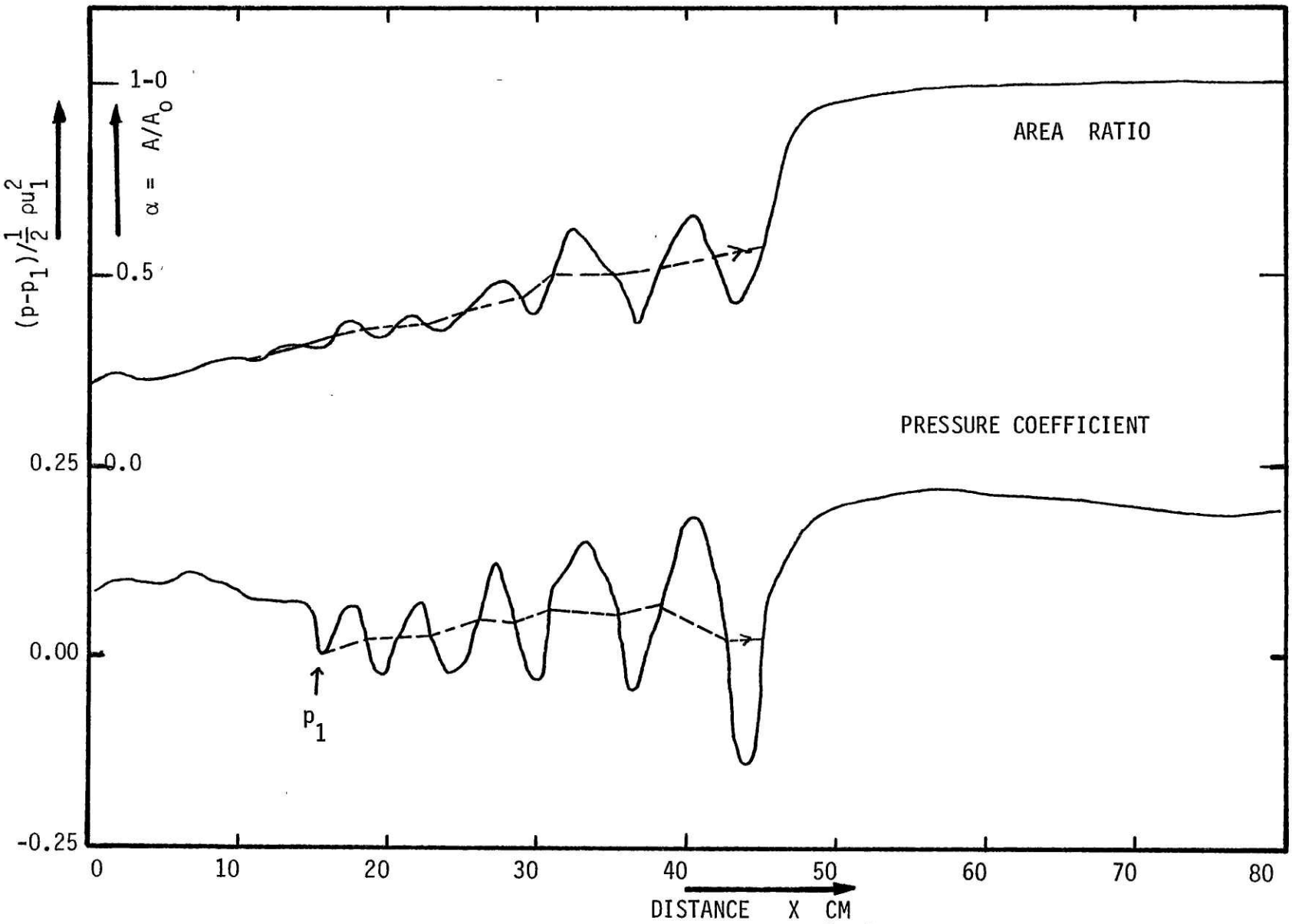

FIG (36s): AREA RATIO α AND PRESSURE COEFFICIENT $(p-p_1)/\frac{1}{2}\rho u_1^2$ VS DISTANCE X ALONG THE SHOCK WAVE

Flow Rate = 20.0 Lit/Min; Constriction Area Ratio = 0.213; Inlet Speed Index = 10.03; Outlet Speed Index = 0.100; Resting Area A_o = 4.530 cm^2.

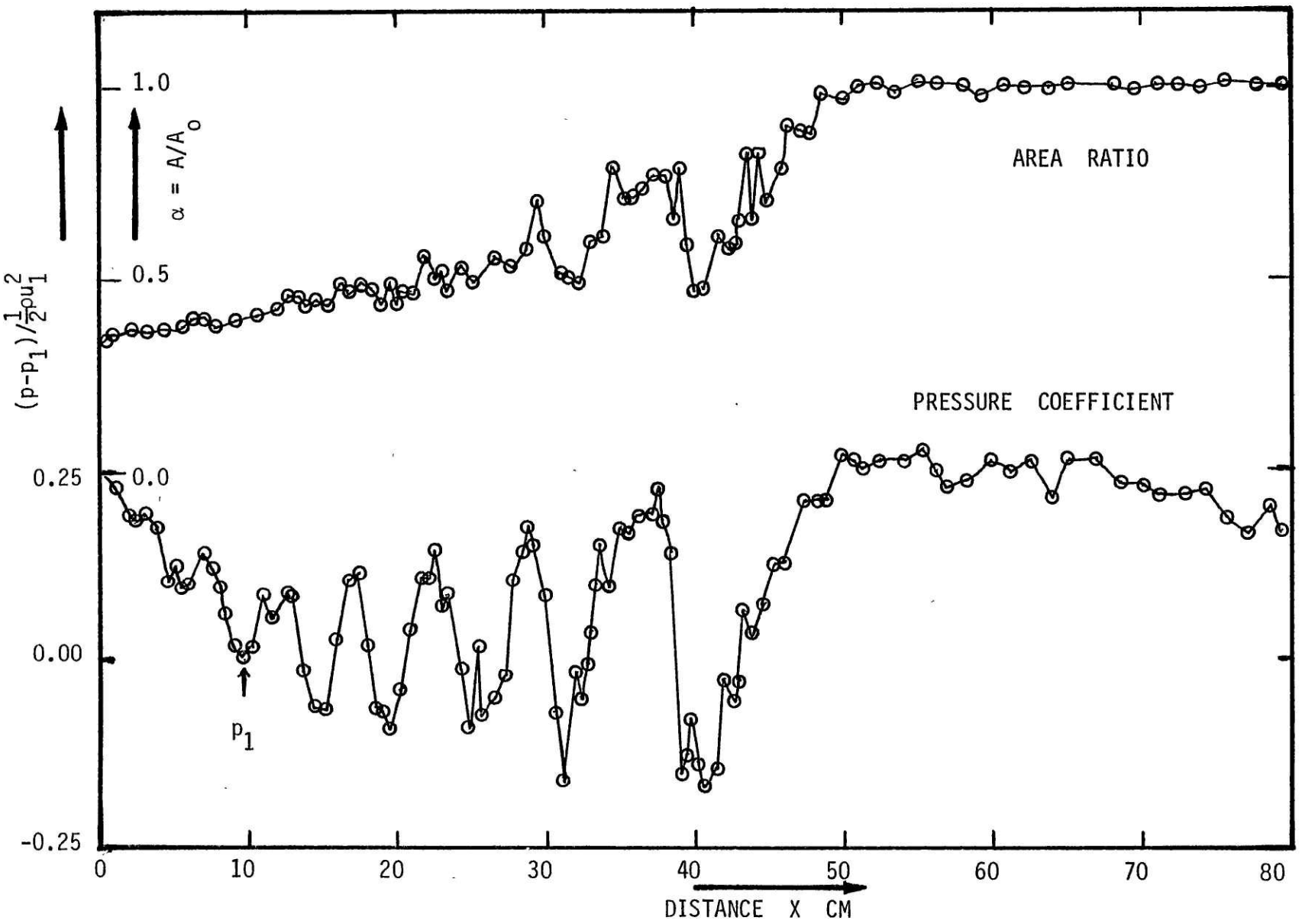

FIG (37): AREA RATIO α AND PRESSURE COEFFICIENT $(p-p_1)/\frac{1}{2}\rho u_1^2$ VS DISTANCE X ALONG THE SHOCK WAVE
Flow Rate = 20.0 Lit/Min;Constriction Area Ratio = 0.332; Inlet Speed Index = 8.83;
Outlet Speed Index = 0.171; Resting Area = 4.530 cm^2.

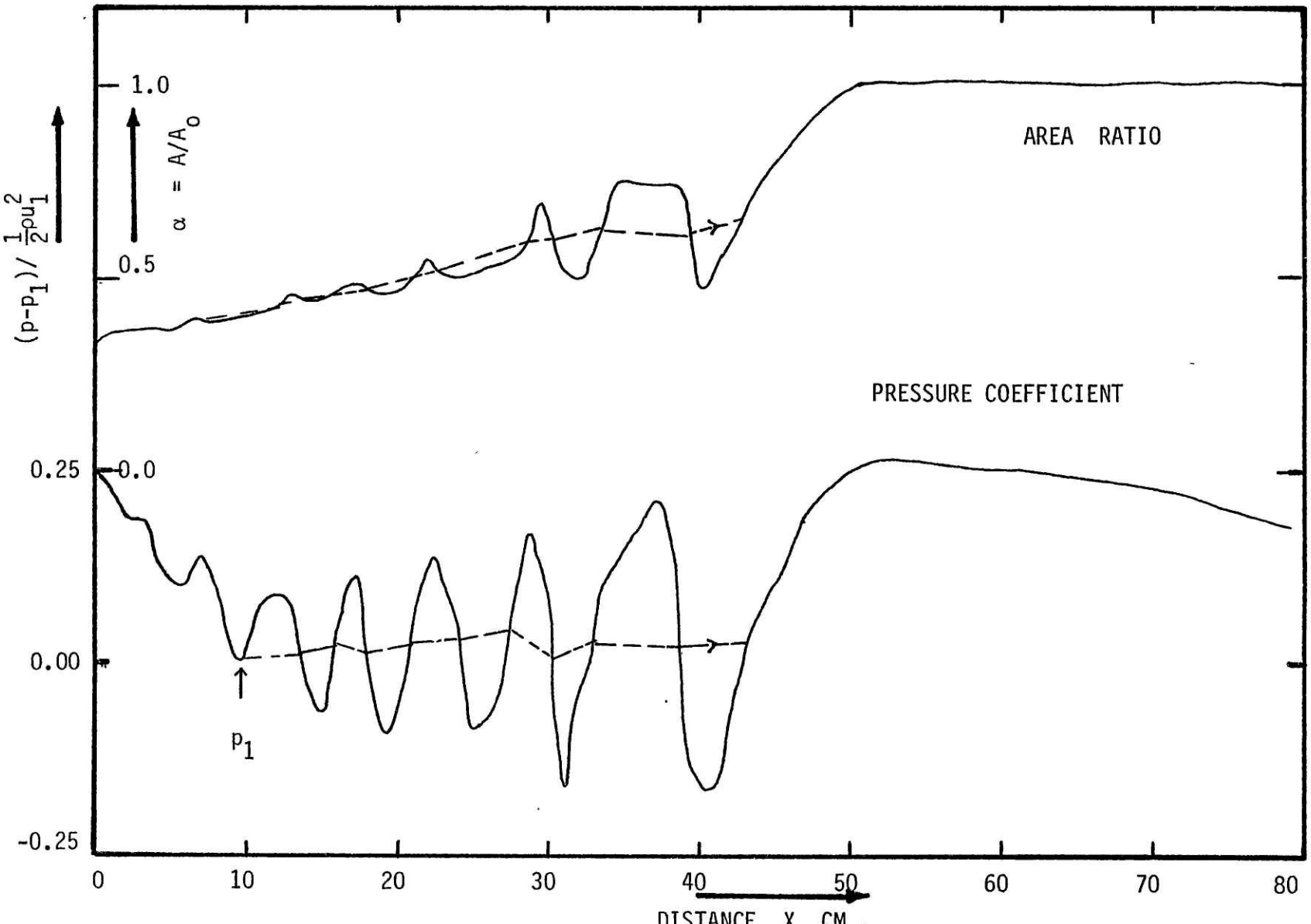

FIG (37s): AREA RATIO α AND PRESSURE COEFFICIENT $(p-p_1)/\frac{1}{2}\rho u_1^2$ VS DISTANCE X ALONG THE SHOCK WAVE
Flow Rate = 20.0 Lit/Min;Constriction Area Ratio = 0.332; Inlet Speed Index = 8.83;
Outlet Speed Index = 0.171; Resting Area A_o = 4.530 cm^2.

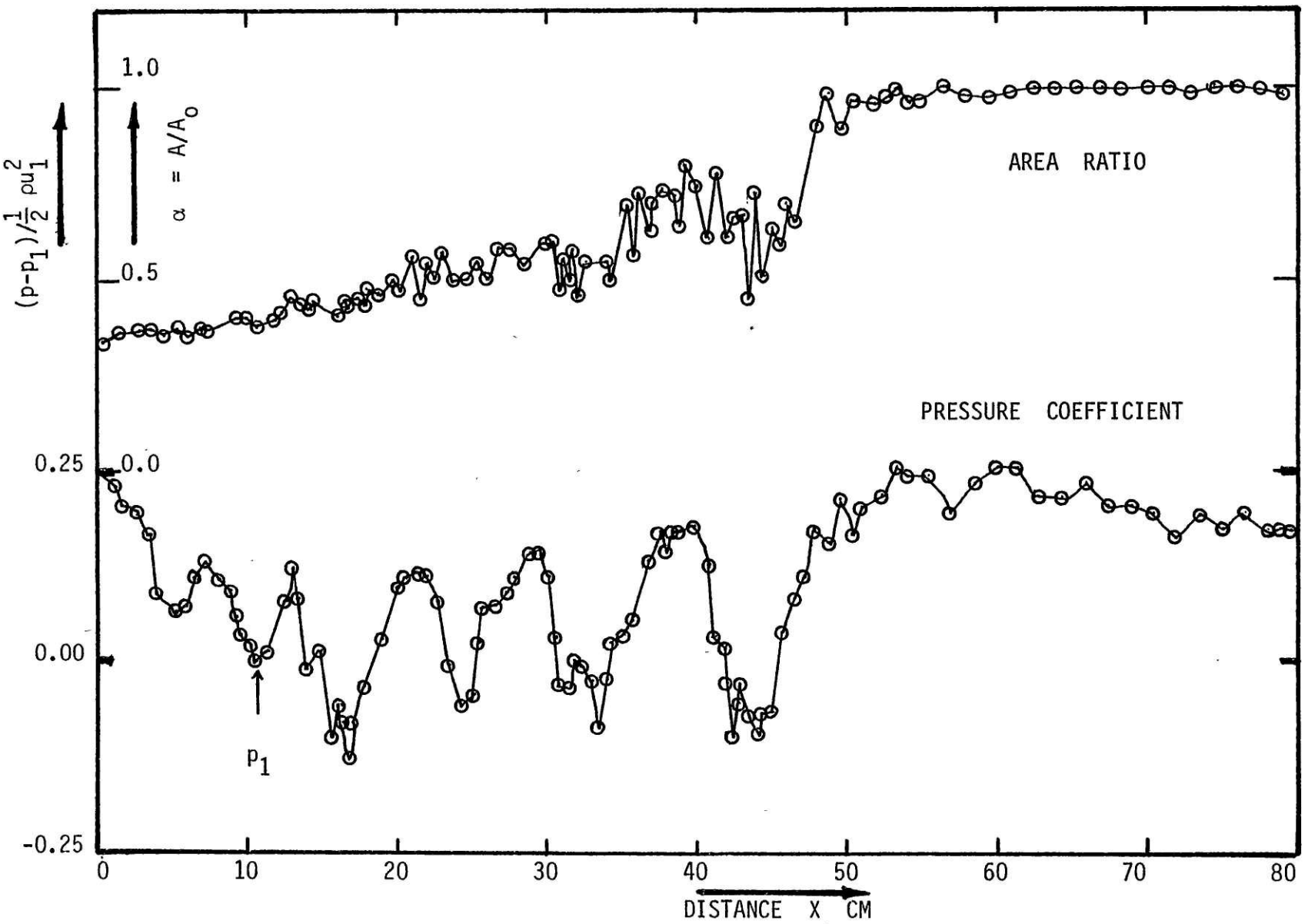

FIG (38): AREA RATIO α AND PRESSURE COEFFICIENT $(p-p_1)/\frac{1}{2}\rho u_1^2$ VS DISTANCE X ALONG THE SHOCK WAVE

Flow Rate = 17.2 Lit/Min; Constriction Area Ratio = 0.332; Inlet Speed Index = 8.18; Outlet Speed Index = 0.163; Resting Area A_o = 4.530 cm^2.

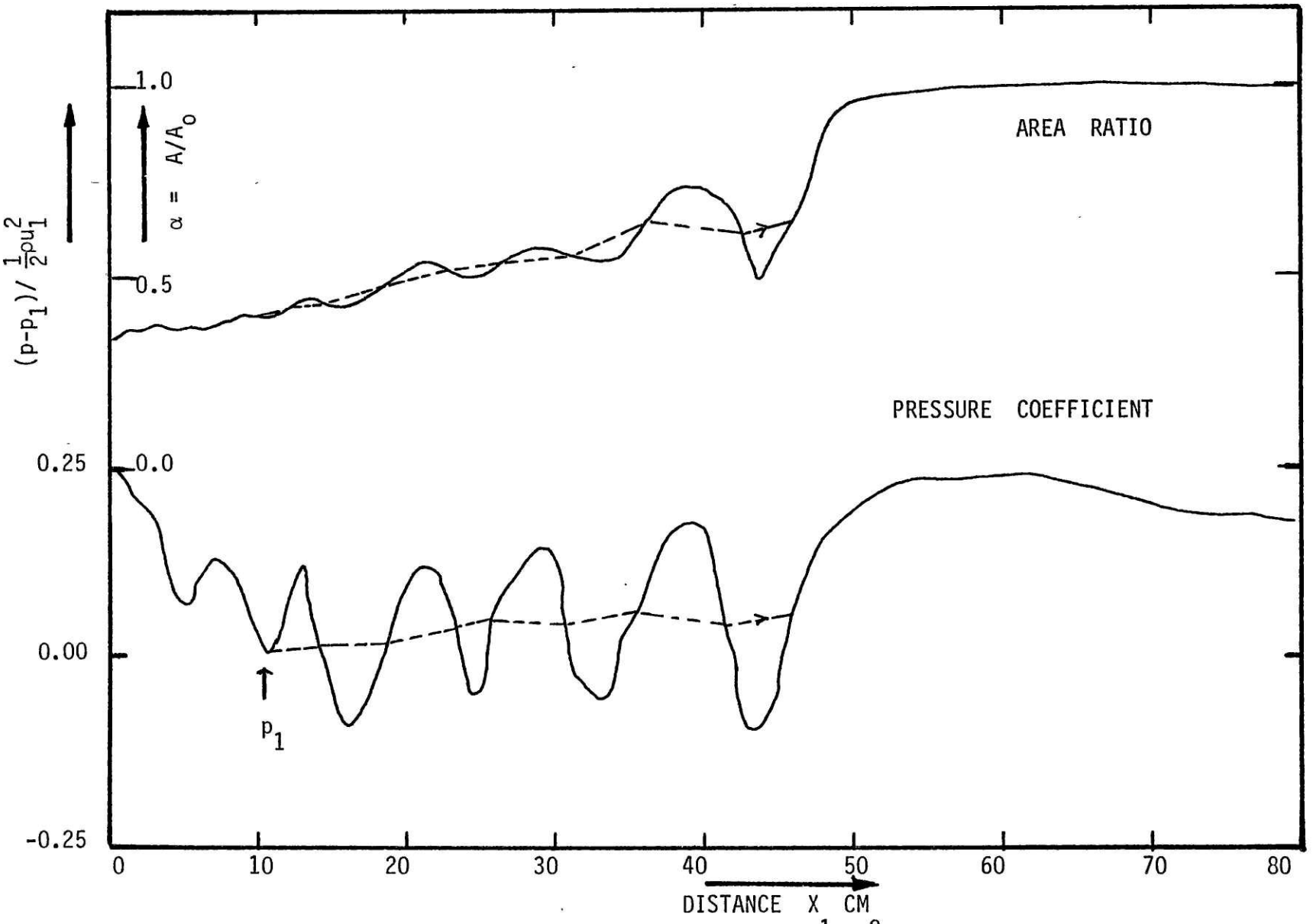

FIG (38s): AREA RATIO α AND PRESSURE COEFFICIENT $(p-p_1)/\frac{1}{2}\rho u_1^2$ VS DISTANCE X ALONG THE SHOCK WAVE
Flow Rate = 17.2 Lit/Min;Constriction Area Ratio = 0.332; Inlet Speed Index = 8.18;
Outlet Speed Index = 0.163; Resting Area = 4.530 cm^2.

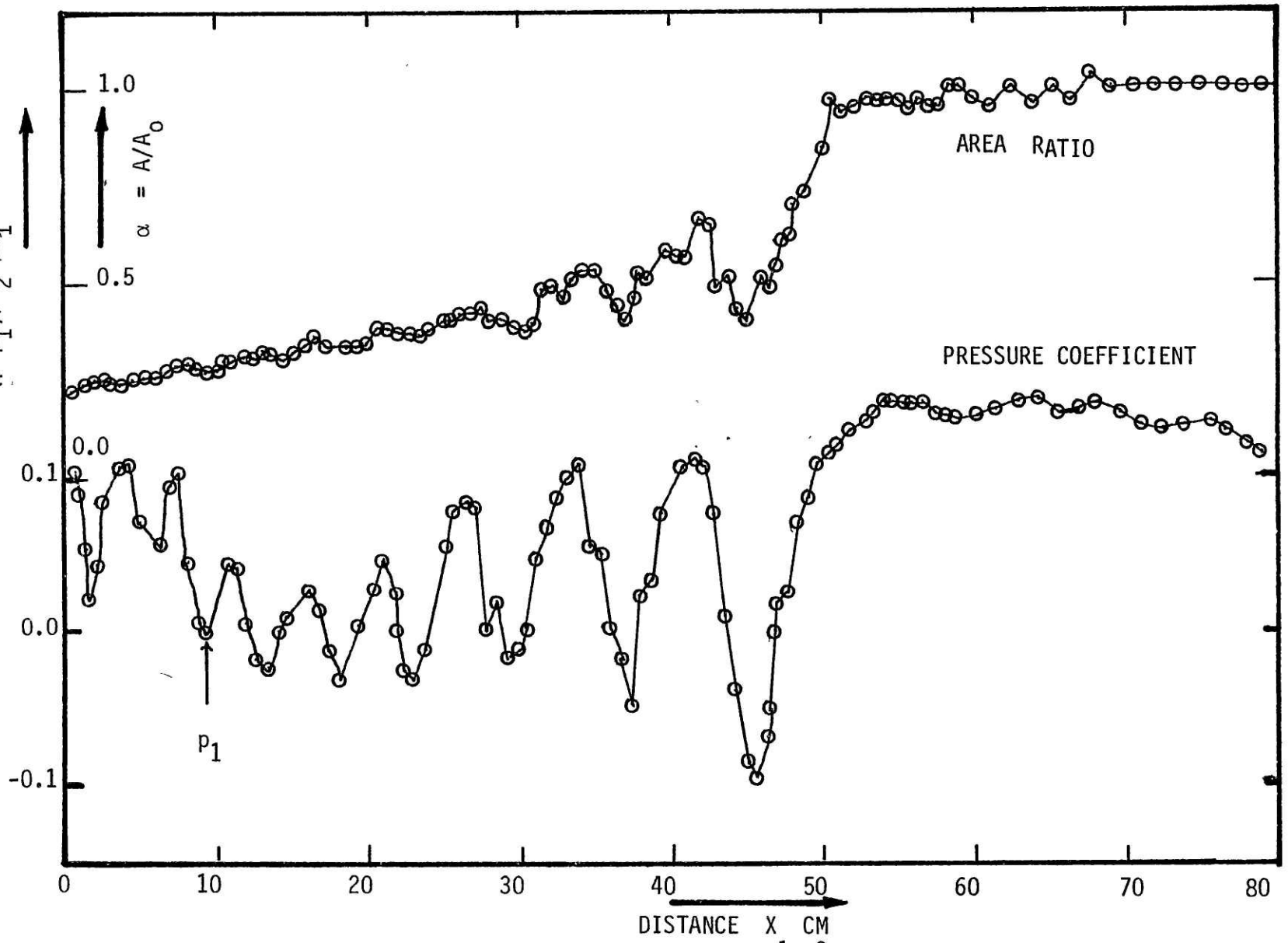

FIG (39): AREA RATIO α AND PRESSURE COEFFICIENT $(p-p_1)/\frac{1}{2}\rho u_1^2$ VS DISTANCE X ALONG THE SHOCK WAVE

Flow Rate = 17.9 Lit/Min; Constriction Area Ratio = 0.213; Inlet Speed Index = 3.34; Outlet Speed Index = 0.115; Resting Area A_o = 4.530 cm^2.

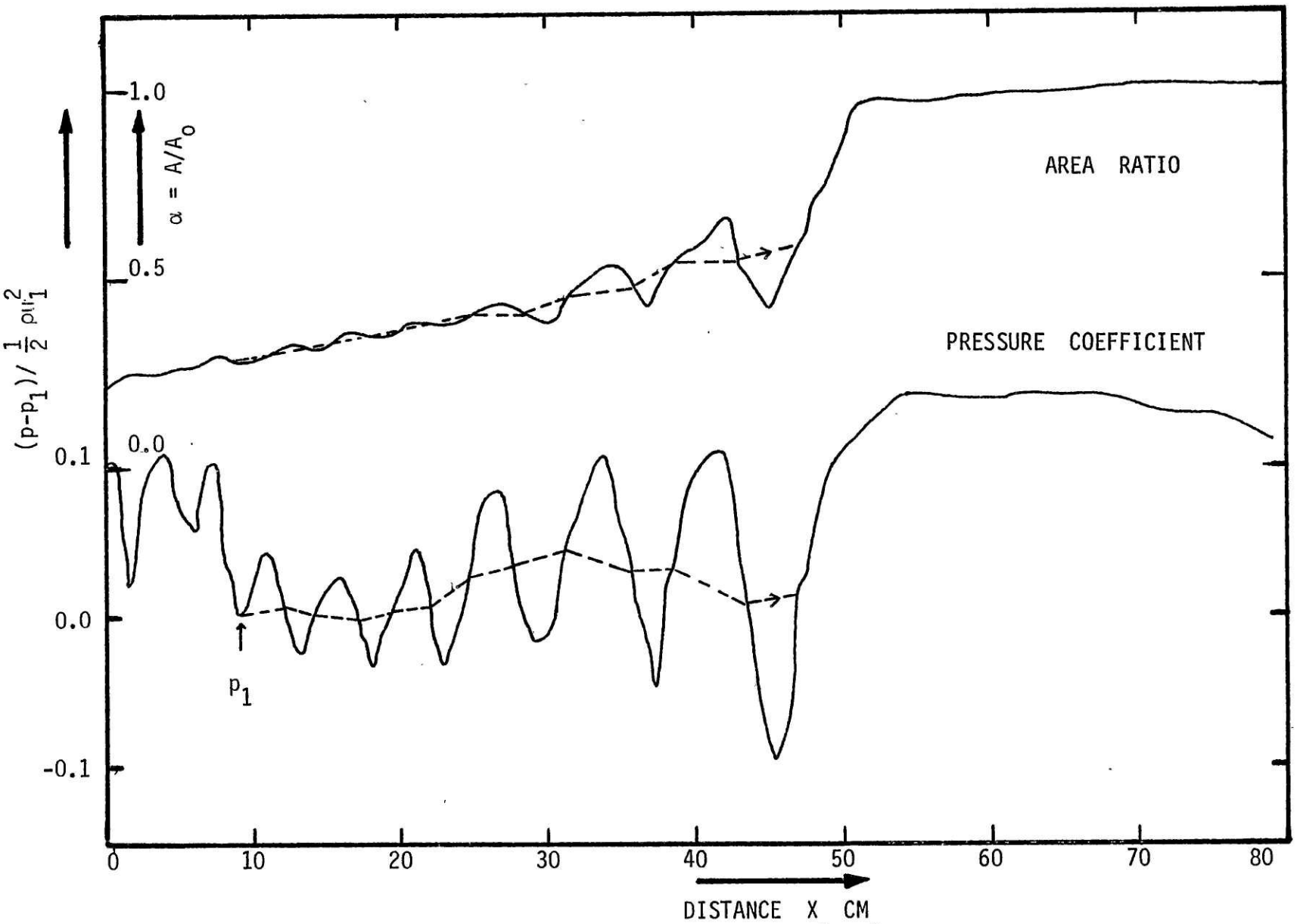

FIG (39s): AREA RATIO α AND PRESSURE COEFFICIENT $(p-p_1)/\frac{1}{2}\rho u_1^2$ VS DISTANCE X ALONG THE SHOCK WAVE
Flow Rate = 17.9 Lit/Min; Constriction Area Ratio = 0.213; Inlet Speed Index = 3.34;
Outlet Speed Index = 0.115; Resting Area A_o = 4.530 cm^2.

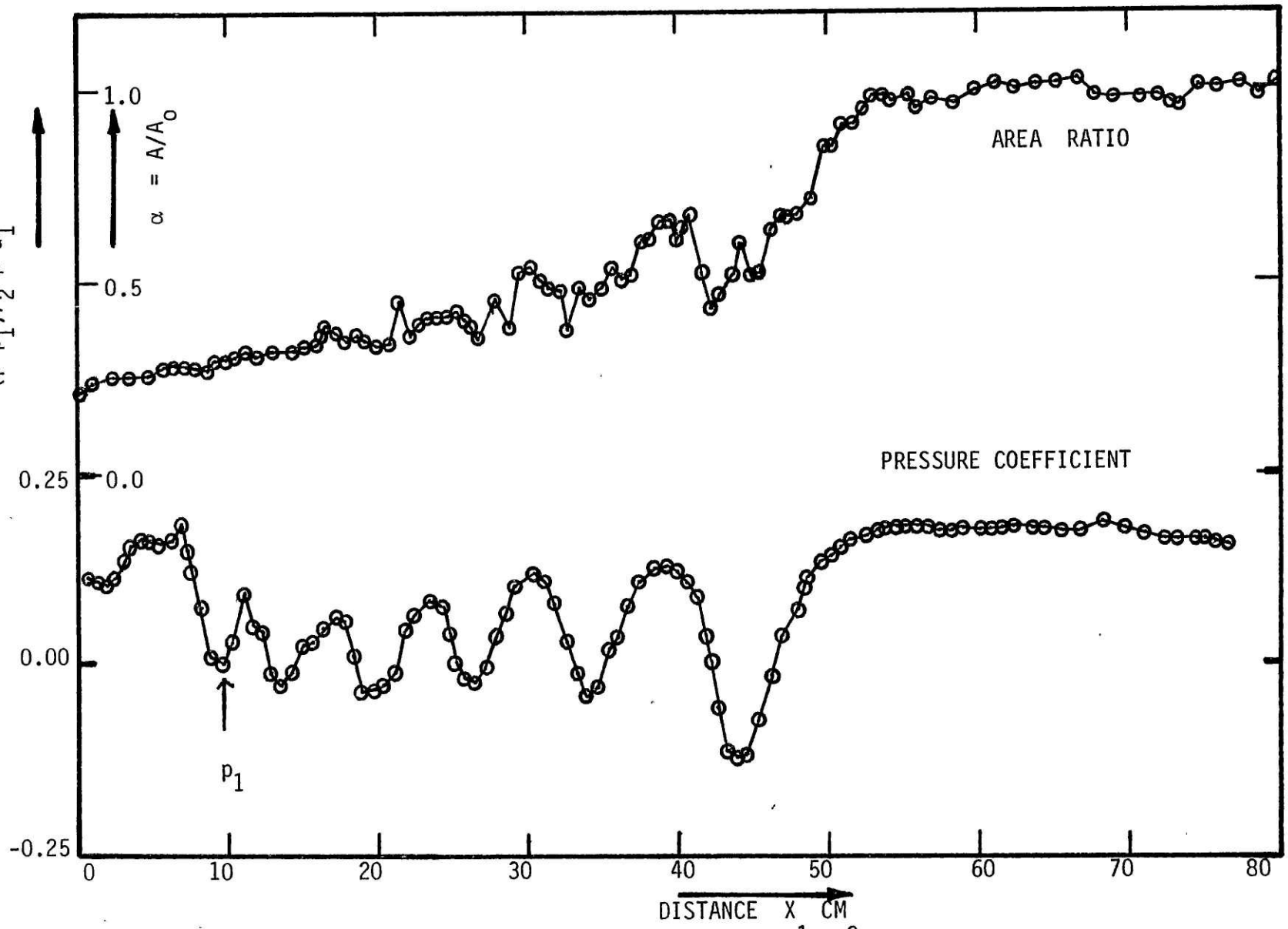

FIG (40): AREA RATIO α AND PRESSURE COEFFICIENT $(p-p_1)/\frac{1}{2}\rho u_1^2$ VS DISTANCE X ALONG THE SHOCK WAVE
Flow Rate = 15.0 Lit/Min; Constriction Area Ratio = 0.213; Inlet Speed Index = 2.87;
Outlet Speed Index = 0.128; Resting Area A_o = 4.530 cm^2 .

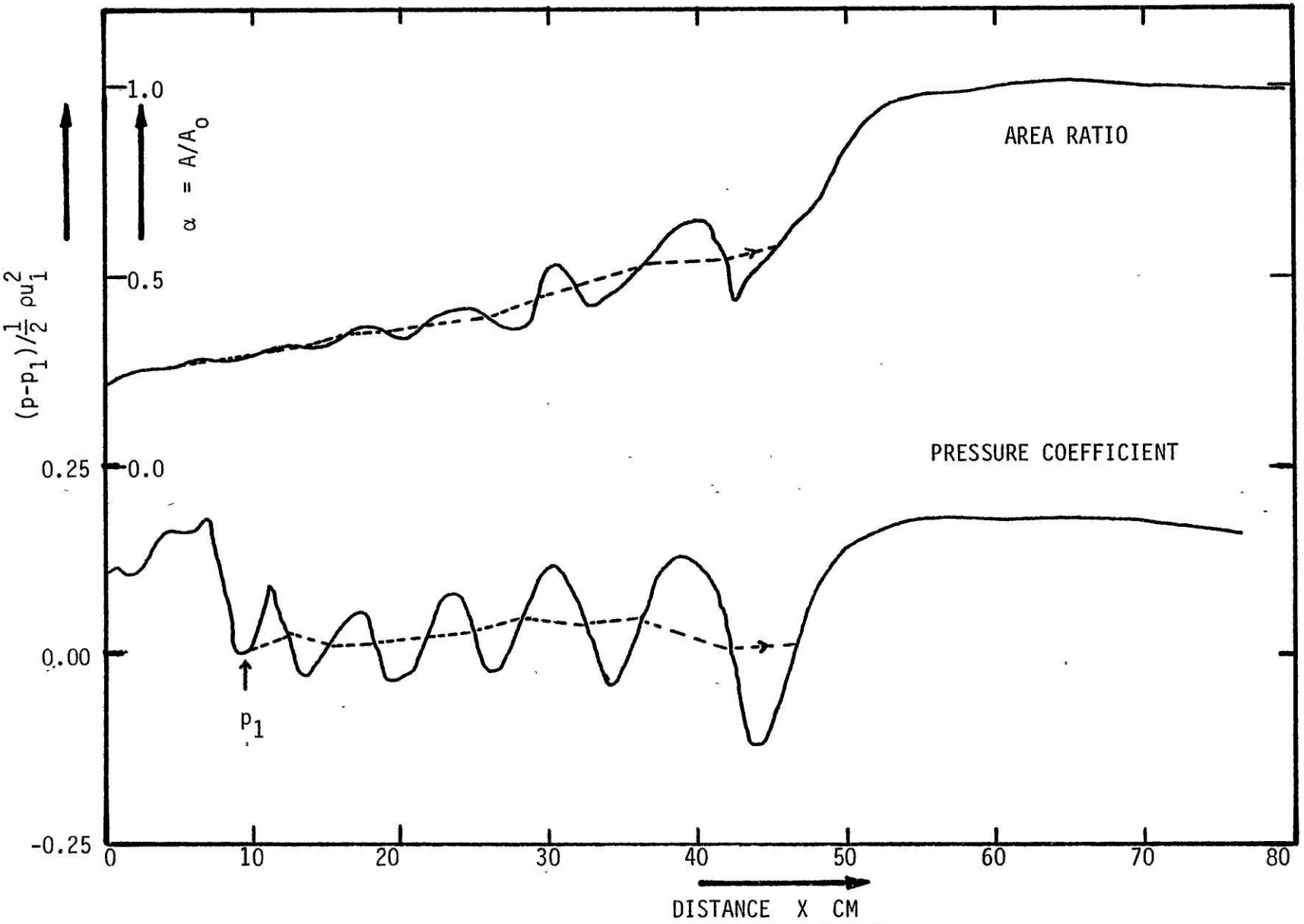

FIG (40s): AREA RATIO α AND PRESSURE COEFFICIENT $(p-p_1)/\frac{1}{2}\rho u_1^2$ VS DISTANCE X ALONG THE SHOCK WAVE
Flow Rate = 15.0 Lit/Min; Constriction Area Ratio = 0.213; Inlet Speed Index = 2.87;
Outlet Speed Index = 0.128; Resting Area A_o = 4.530 cm^2.

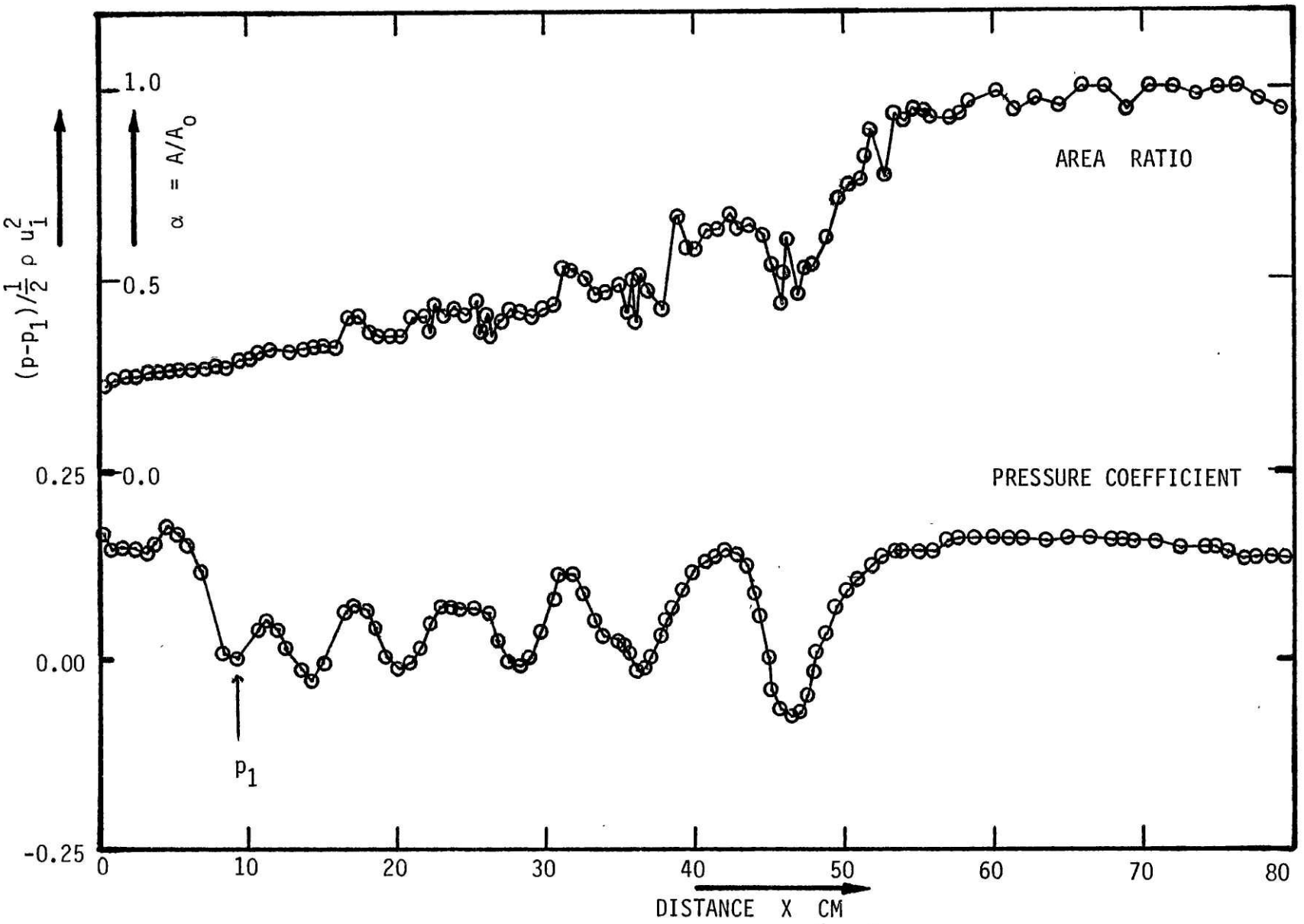

FIG (41): AREA RATIO α AND PRESSURE COEFFICIENT $(p-p_1)/\frac{1}{2}\rho u_1^2$ VS DISTANCE X ALONG THE SHOCK WAVE
Flow Rate = 13.5 Lit/Min;Constriction Area Ratio = 0.213; Inlet Speed Index = 2.74;
Outlet Speed Index = 0.186; Resting Area A_o = 4.530 cm^2.

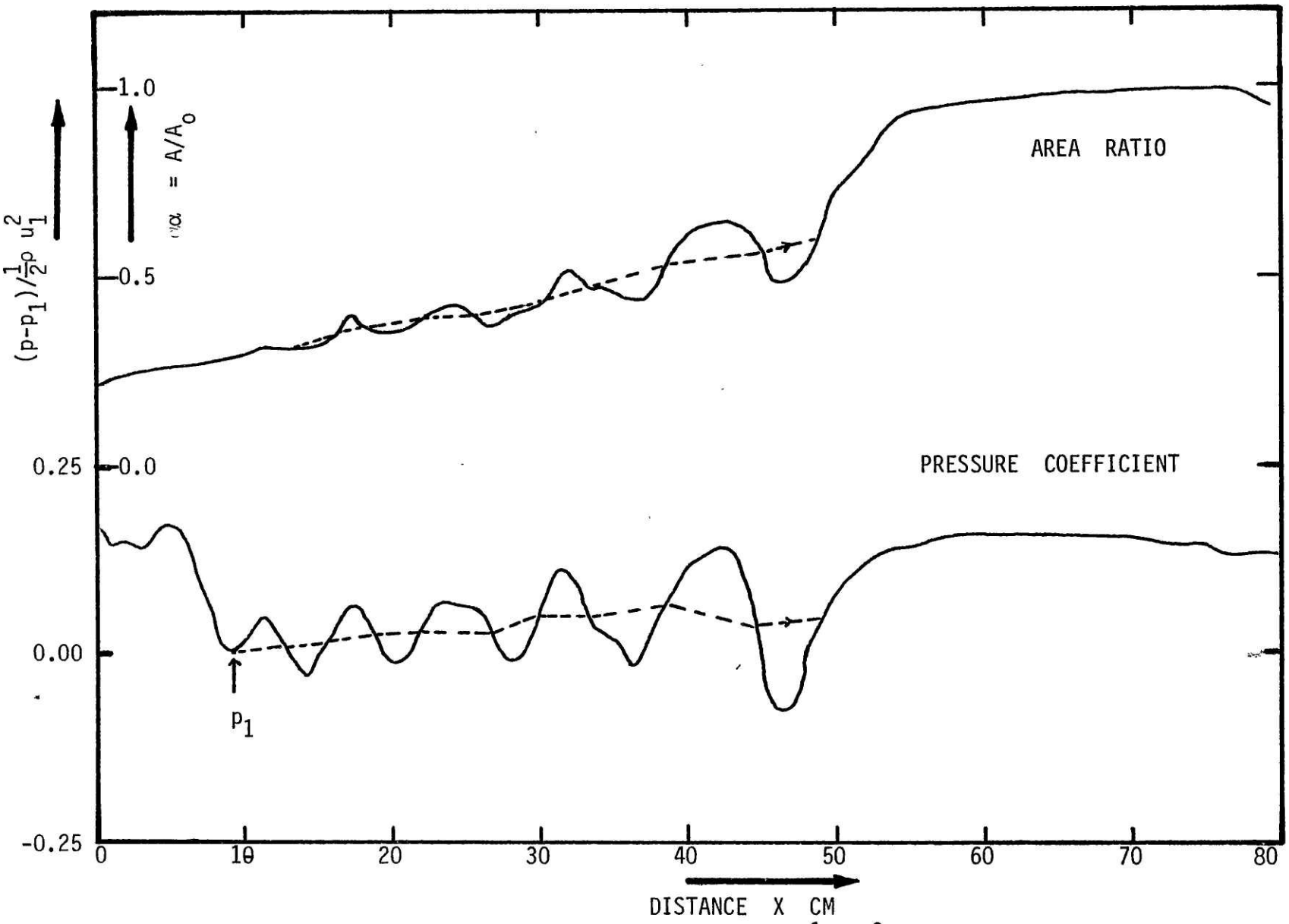

FIG (41s): AREA RATIO α AND PRESSURE COEFFICIENT $(p-p_1)/\frac{1}{2}\rho u_1^2$ VS DISTANCE X ALONG THE SHOCK WAVE
Flow Rate = 13.5 Lit/Min;Constriction Area Ratio = 0.213; Inlet Speed Index = 2.74;
Outlet Speed Index = 0.186; Resting Area A_o = 4.530 cm^2.

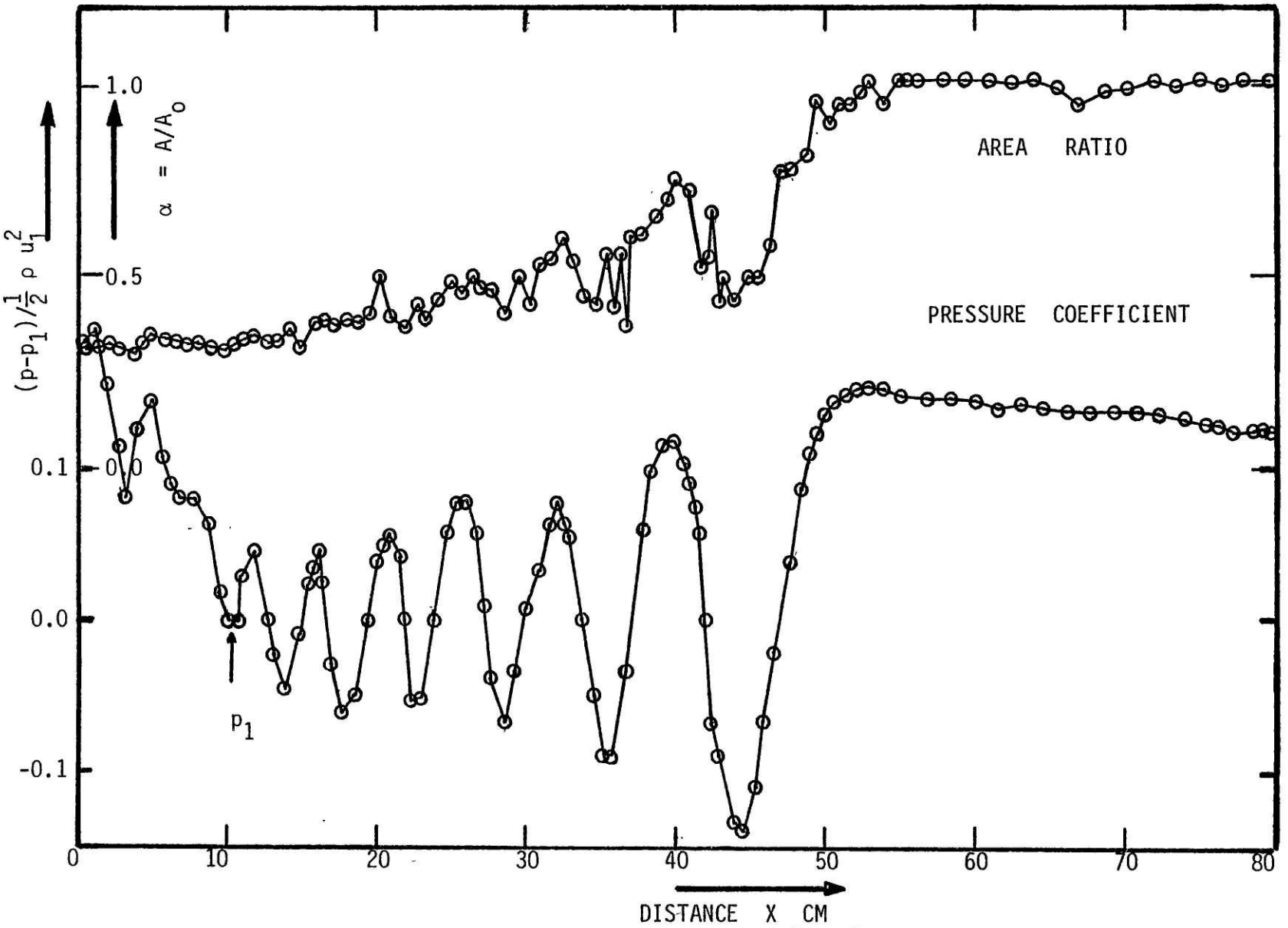

FIG (42): AREA RATIO α AND PRESSURE COEFFICIENT $(p-p_1)/\frac{1}{2}\rho u_1^2$ VS DISTANCE X ALONG THE SHOCK WAVE
Flow Rate = 22.1 Lit/Min; Constriction Area Ratio = 0.279; Inlet Speed Index = 11.00;
Outlet Speed Index = 0.116; Resting Area A_0 = 4.530 cm^2.

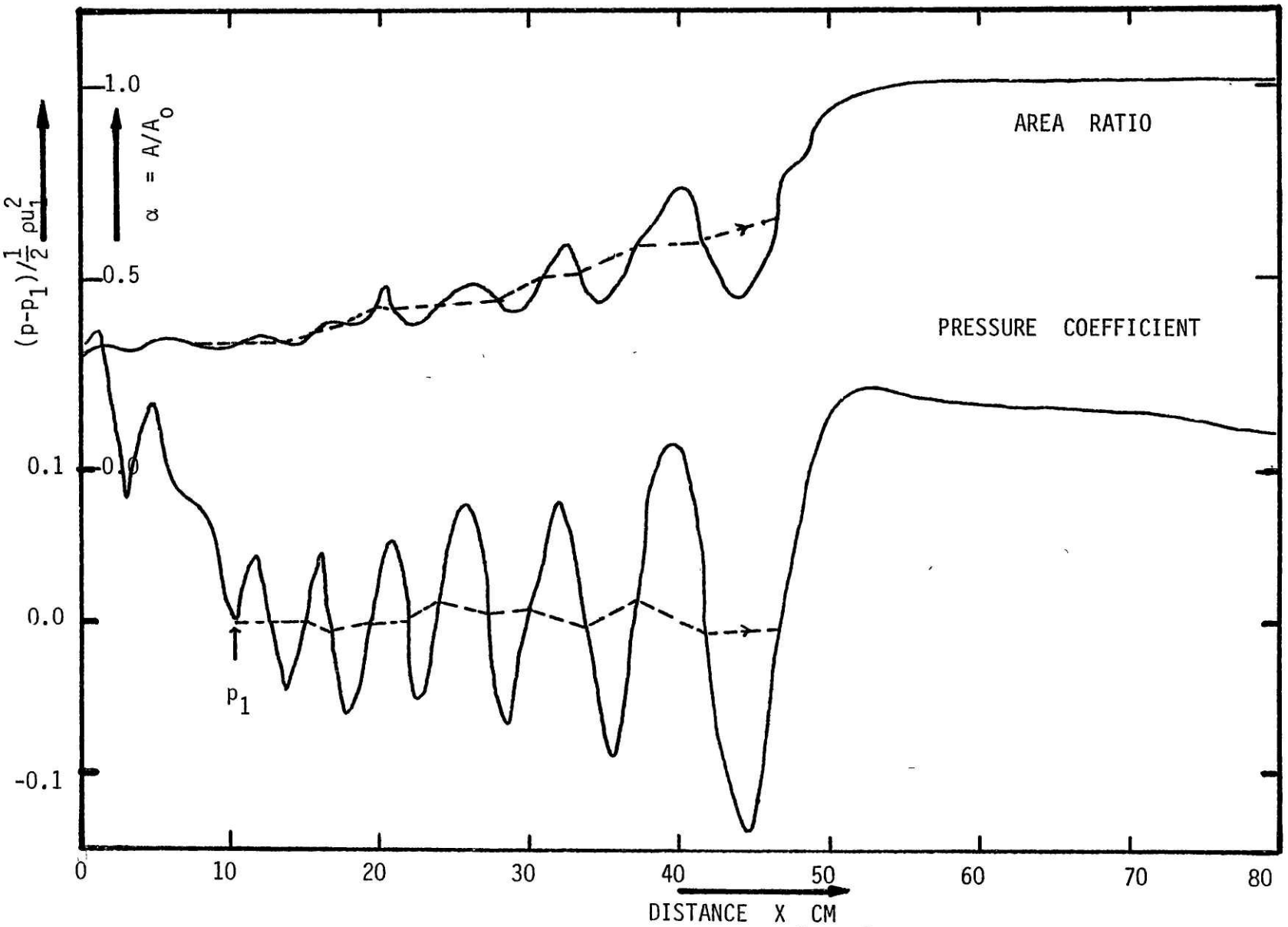

FIG (42s): AREA RATIO α AND PRESSURE COEFFICIENT $(p-p_1)/\frac{1}{2}\rho u_1^2$ VS DISTANCE X ALONG THE SHOCK WAVE
Flow Rate = 22.1 Lit/Min;Constriction Area Ratio = 0.279; Inlet Speed Index = 11.00;
Outlet Speed Index = 0.116; Resting Area A_o = 4.530 cm^2.

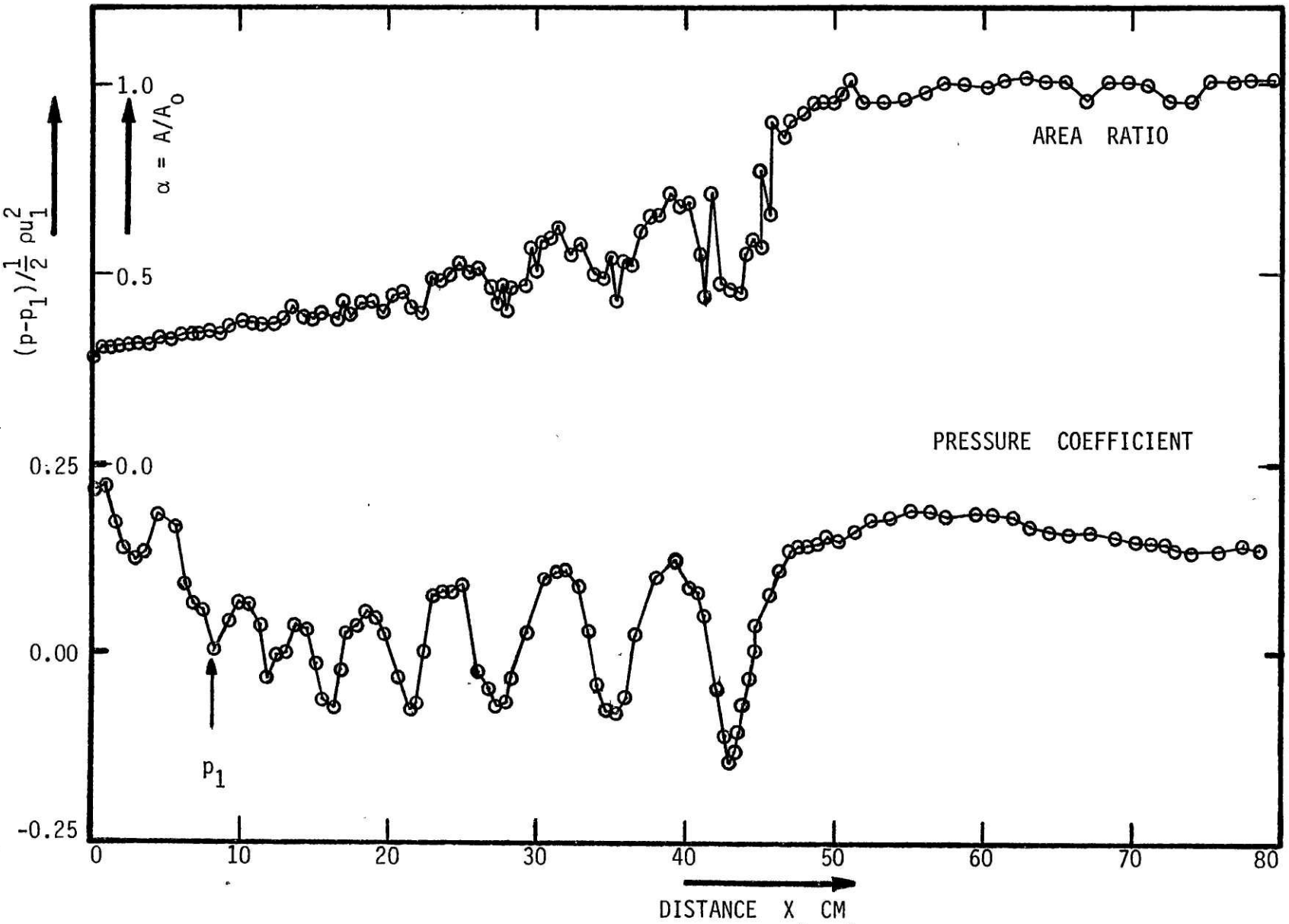

FIG (43): AREA RATIO α AND PRESSURE COEFFICIENT $(p-p_1)/\frac{1}{2}\rho u_1^2$ VS DISTANCE X ALONG THE SHOCK WAVE
Flow Rate = 19.9 Lit/Min; Constriction Area Ratio = 0.279; Inlet Speed Index = 10.84;
Outlet Speed Index = 0.139; Resting Area $A_o = 4.530\ cm^2$.

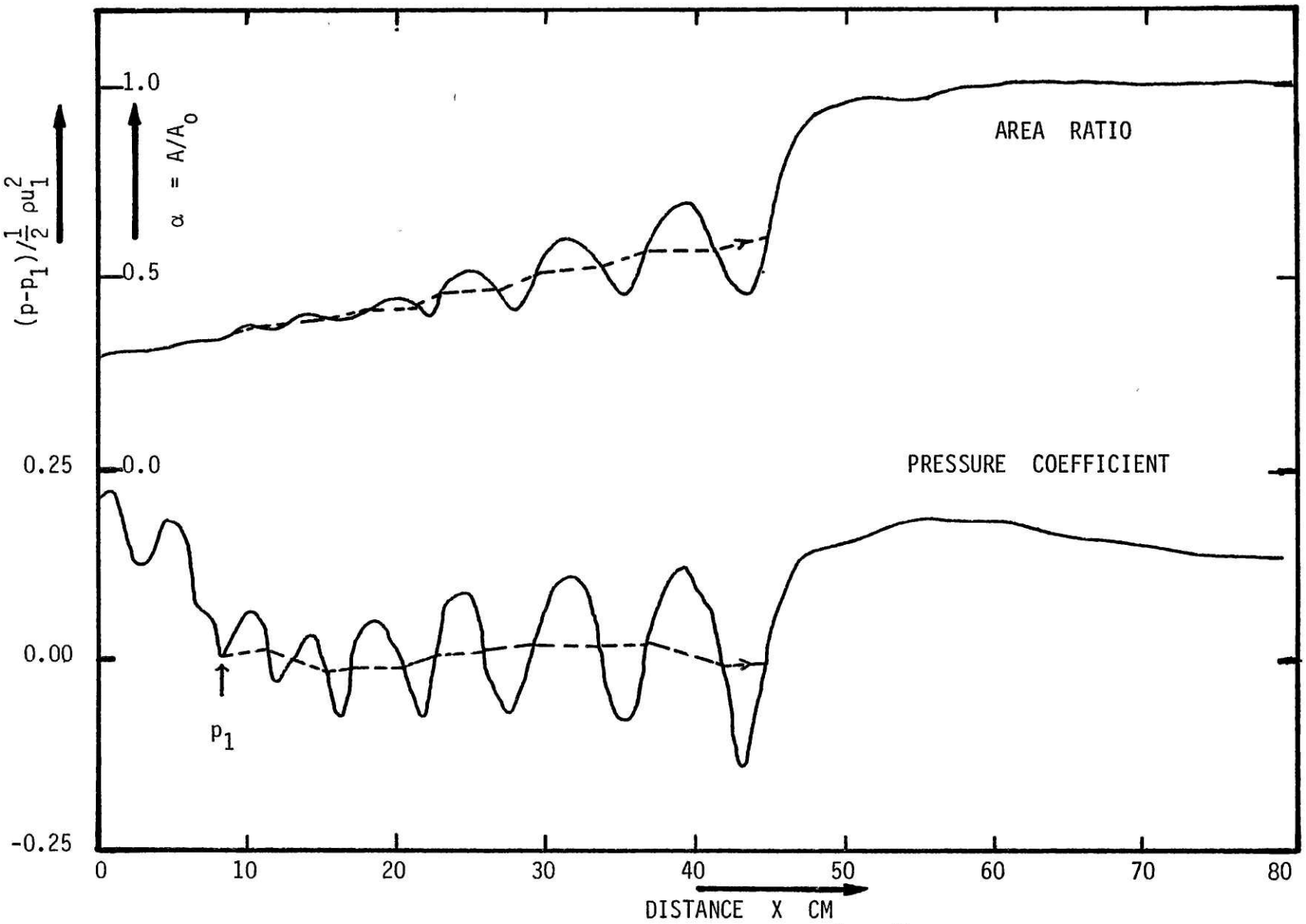

FIG (43s): AREA RATIO α AND PRESSURE COEFFICIENT $(p-p_1)/\frac{1}{2}\rho u_1^2$ VS DISTANCE X ALONG THE SHOCK WAVE
Flow Rate = 19.9 Lit/Min;Constriction Area Ratio = 0.279; Inlet Speed Index = 10.84;
Outlet Speed Index = 0.139; Resting Area A_o = 4.530 cm^2.

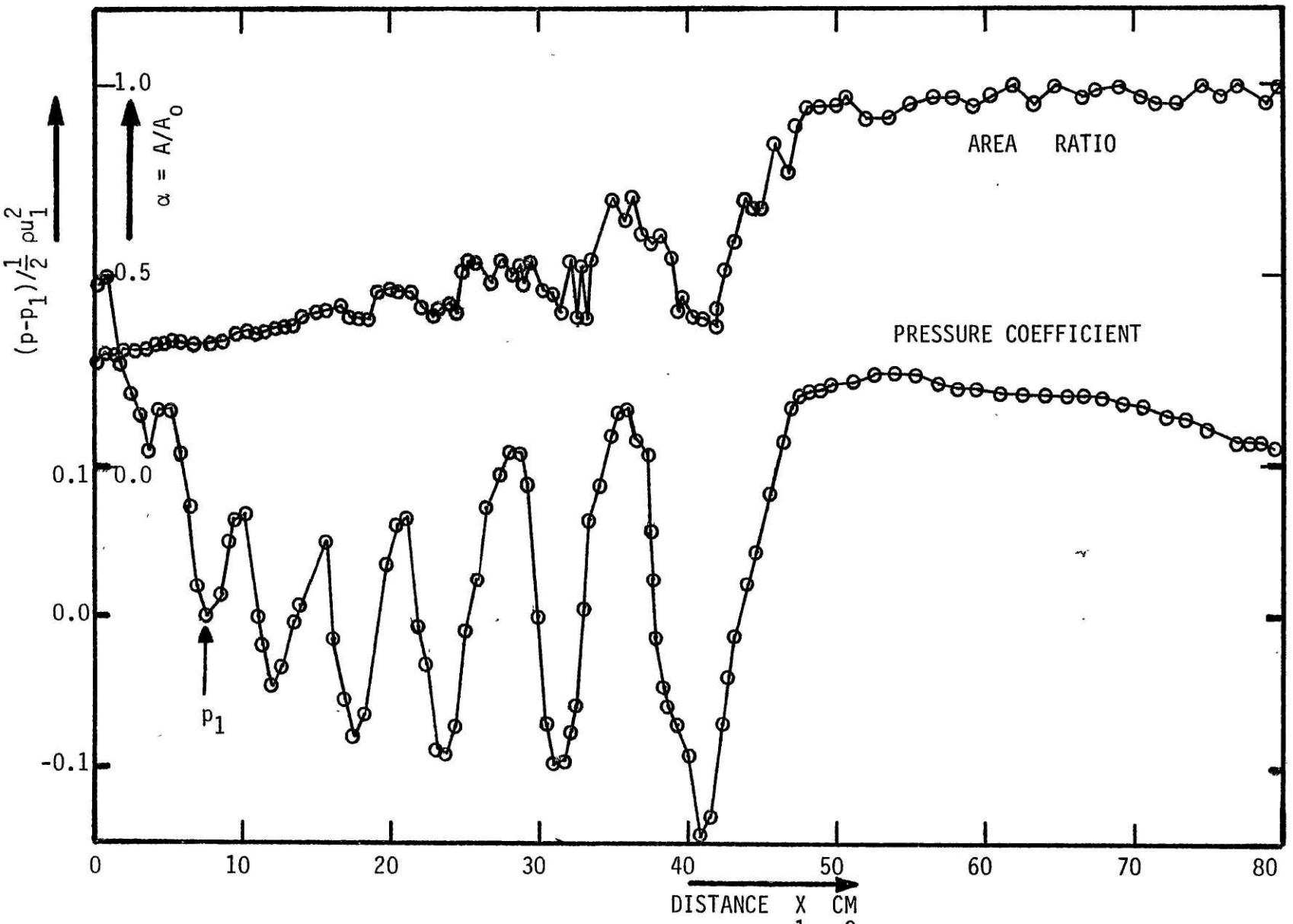

FIG (44): AREA RATIO α AND PRESSURE COEFFICIENT $(p-p_1)/\frac{1}{2}\rho u_1^2$ VS DISTANCE X ALONG THE SHOCK WAVE
Flow Rate = 17.0 Lit/Min;Constriction Area Ratio = 0.279; Inlet Speed Index = 8.73;
Outlet Speed Index = 0.161; Resting Area A_o = 4.530 cm^2.

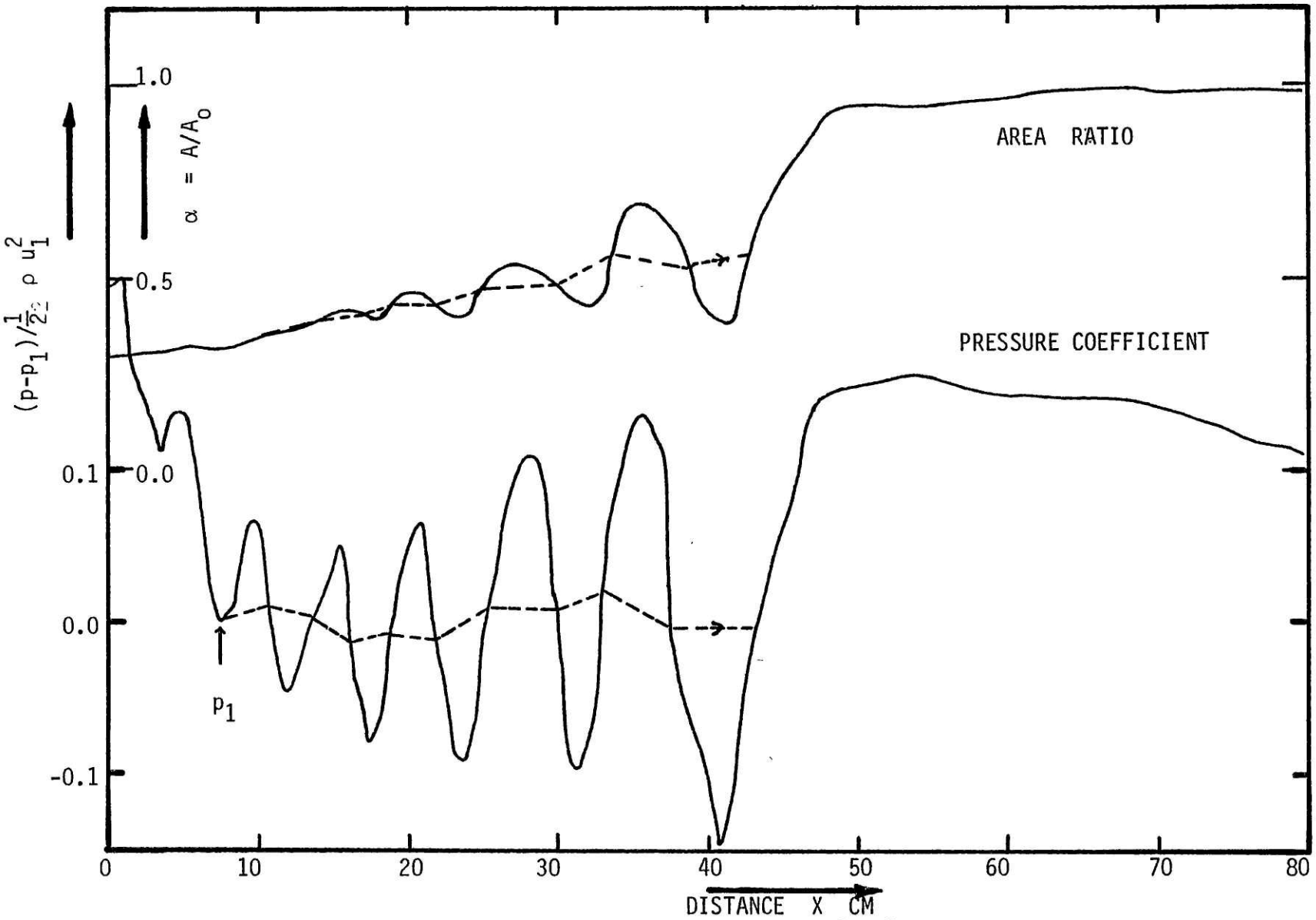

FIG (44s): AREA RATIO α AND PRESSURE COEFFICIENT $(p-p_1)/\frac{1}{2}\rho u_1^2$ VS DISTANCE X ALONG THE SHOCK WAVE
Flow Rate = 17.0 Lit/Min; Constriction Area Ratio = 0.279; Inlet Speed Index = 8.73;
Outlet Speed Index = 0.161; Resting Area $A_o = 4.530\ cm^2$.

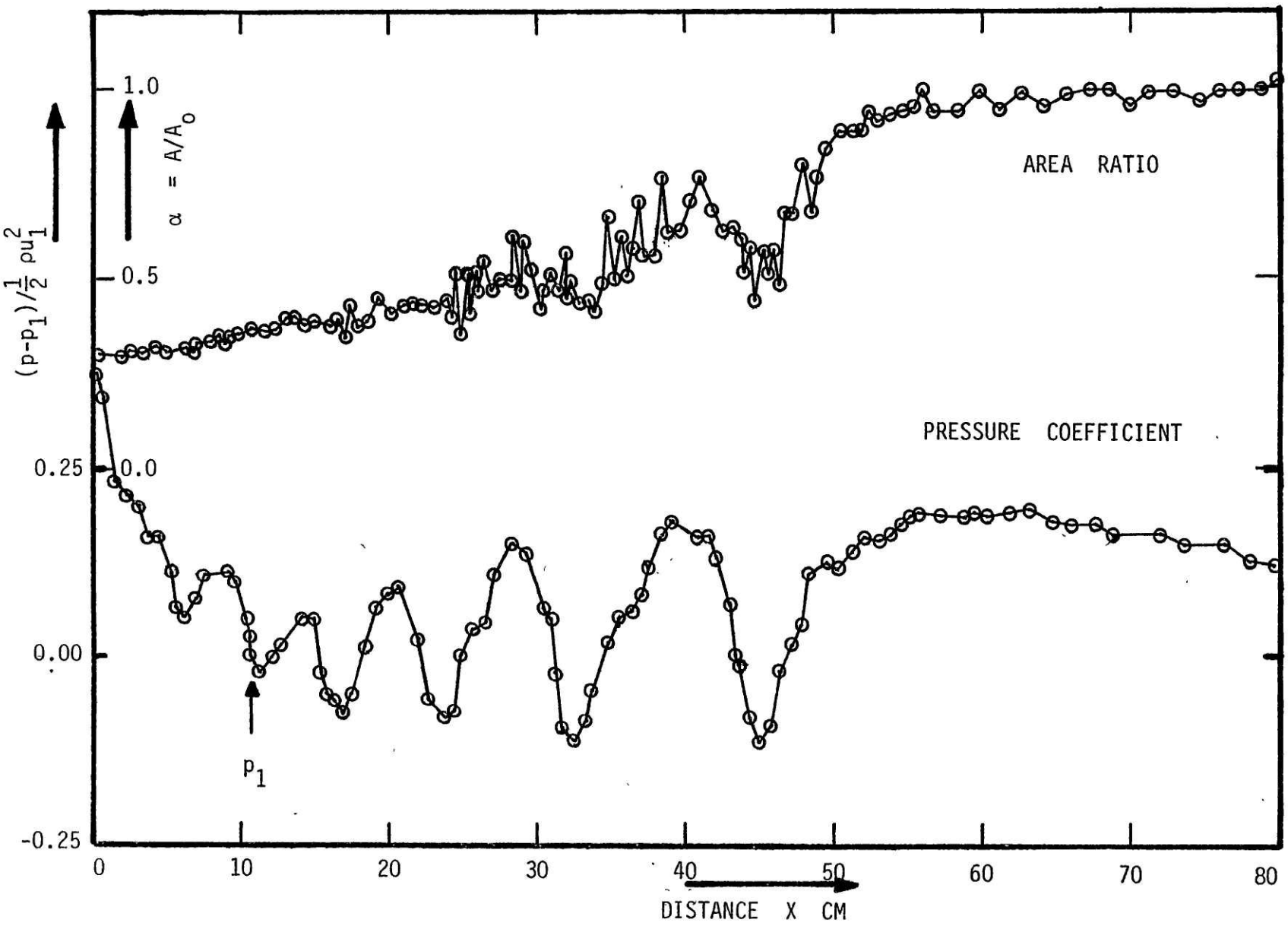

FIG (45): AREA RATIO α AND PRESSURE COEFFICIENT $(p-p_1)/\frac{1}{2}\rho u_1^2$ VS DISTANCE X ALONG THE SHOCK WAVE
Flow Rate = 15.0 Lit/Min; Constriction Area Ratio = 0.279; Inlet Speed Index = 7.52;
Outlet Speed Index = 0.331; Resting Area $A_o = 4.530\ cm^2$.

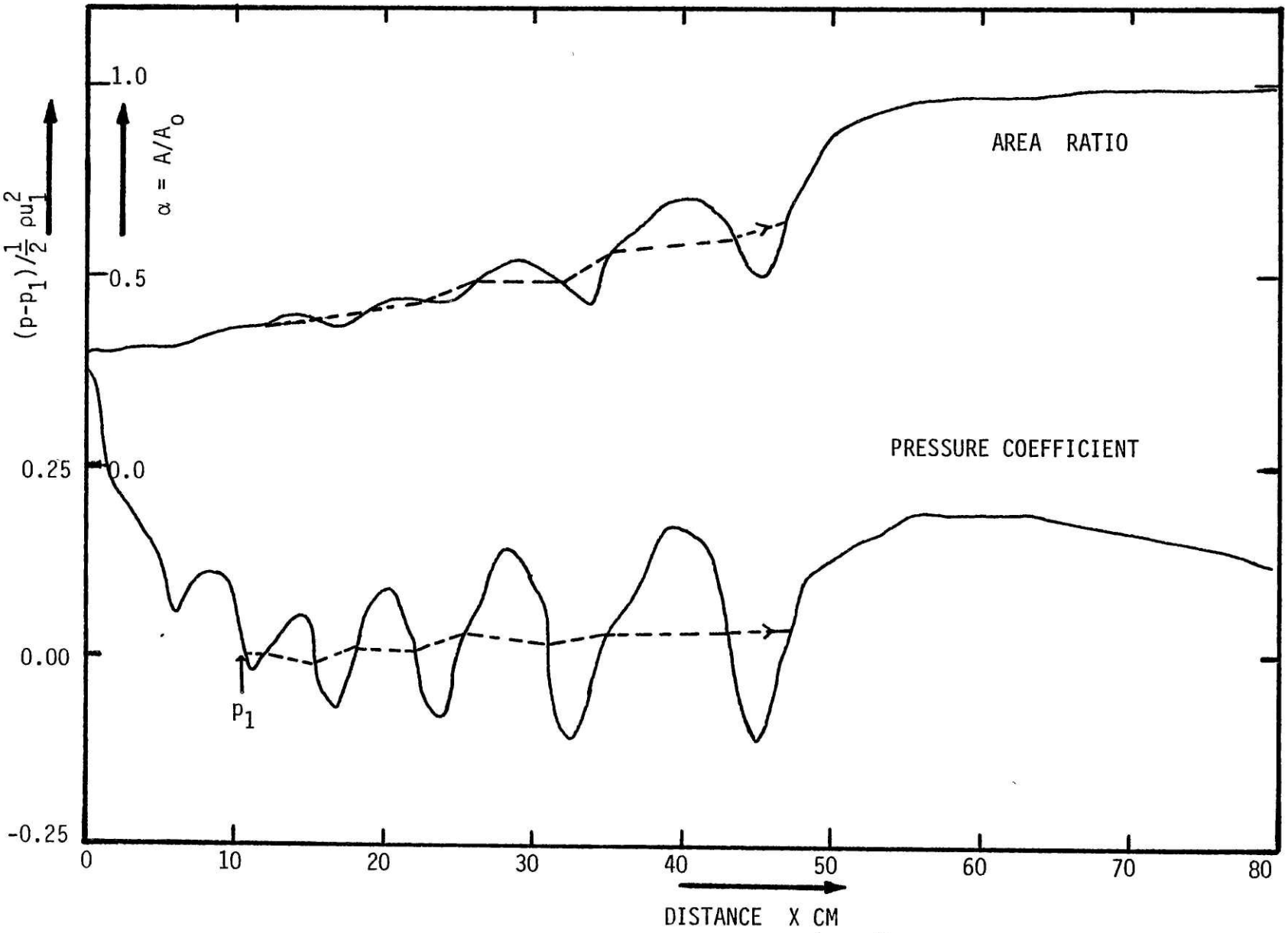

FIG (45s): AREA RATIO α AND PRESSURE COEFFICIENT $(p-p_1)/\frac{1}{2}\rho u_1^2$ VS DISTANCE X ALONG THE SHOCK WAVE
Flow Rate = 15.0 Lit/Min; Constriction Area Ratio = 0.279; Inlet Speed Index = 7.52;
Outlet Speed Index = 0.331; Resting Area $A_o = 4.530\ cm^2$.

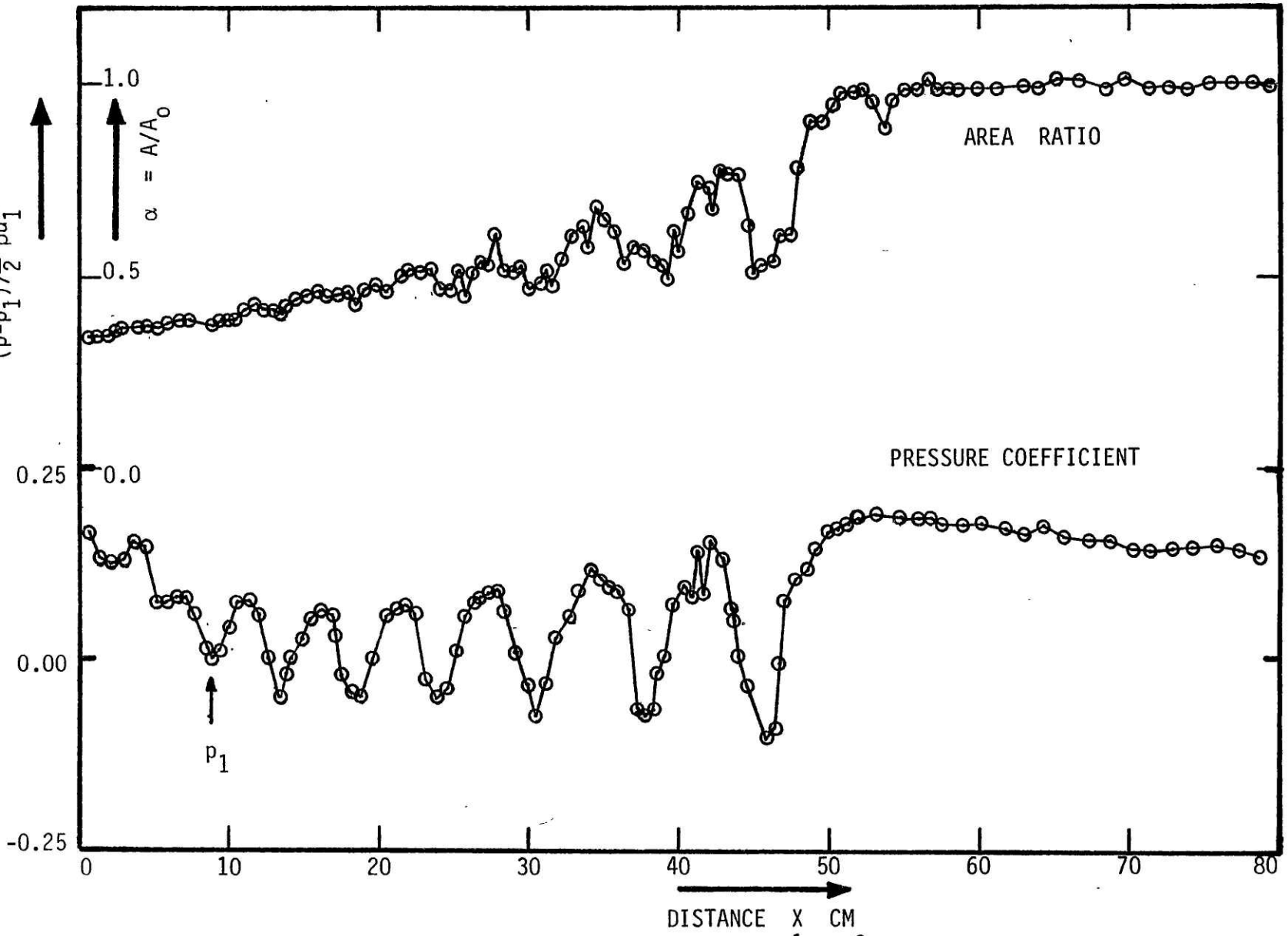

FIG (46): AREA RATIO α AND PRESSURE COEFFICIENT $(p-p_1)/\frac{1}{2}\rho u_1^2$ VS DISTANCE X ALONG THE SHOCK WAVE
Flow Rate = 22.8 Lit/Min;Constriction Area Ratio = 0.332; Inlet Speed Index = 10.92;
Outlet Speed Index = 0.175; Resting Area A_o = 4.530 cm^2.

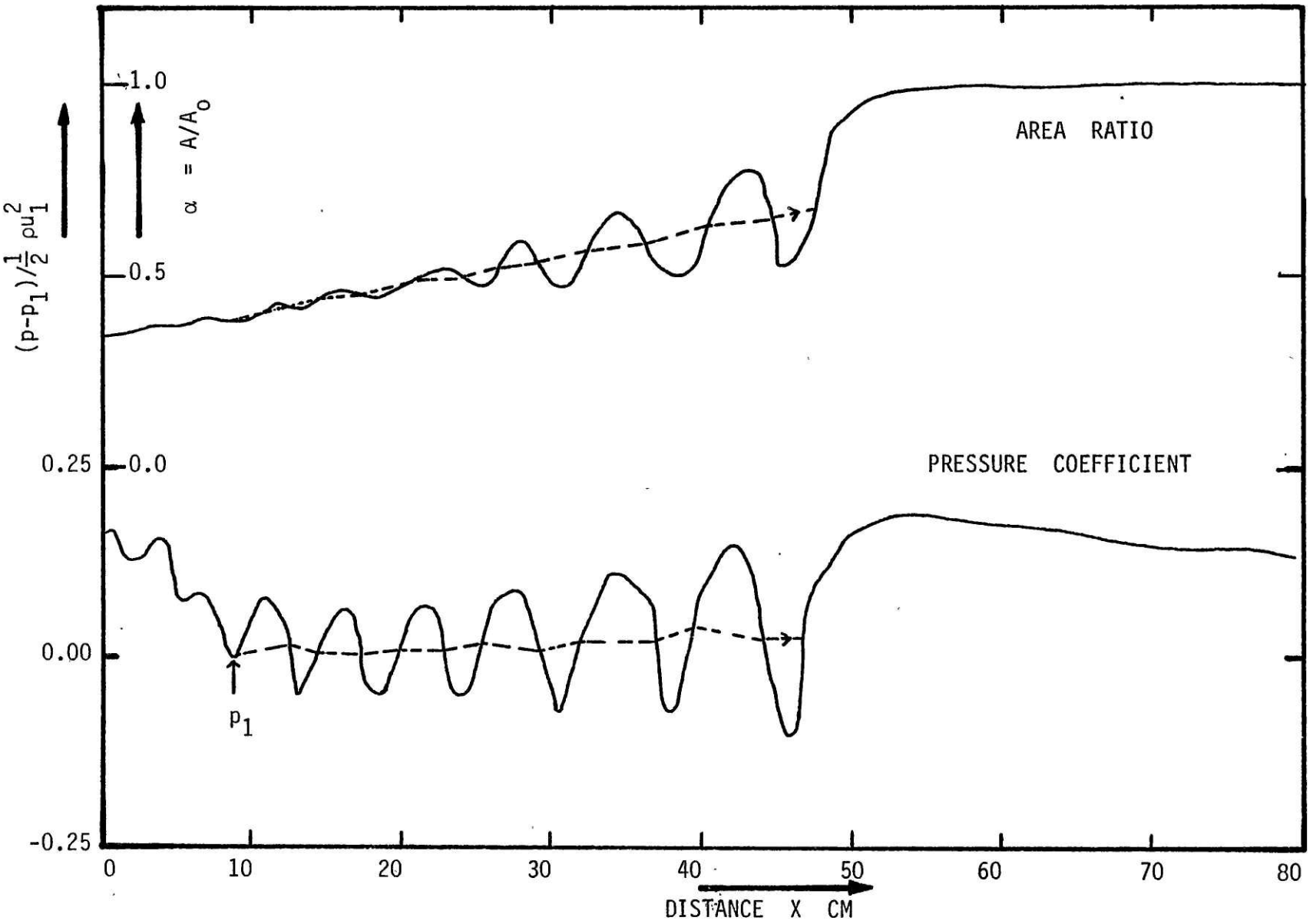

FIG (46s): AREA RATIO α AND PRESSURE COEFFICIENT $(p-p_1)/\frac{1}{2}\rho u_1^2$ VS DISTANCE X ALONG THE SHOCK WAVE
Flow Rate = 22.8 Lit/Min;Constriction Area Ratio = 0.332; Inlet Speed Index = 10,92;
Outlet Speed Index = 0.175; Resting Area A_o = 4.530 cm^2.

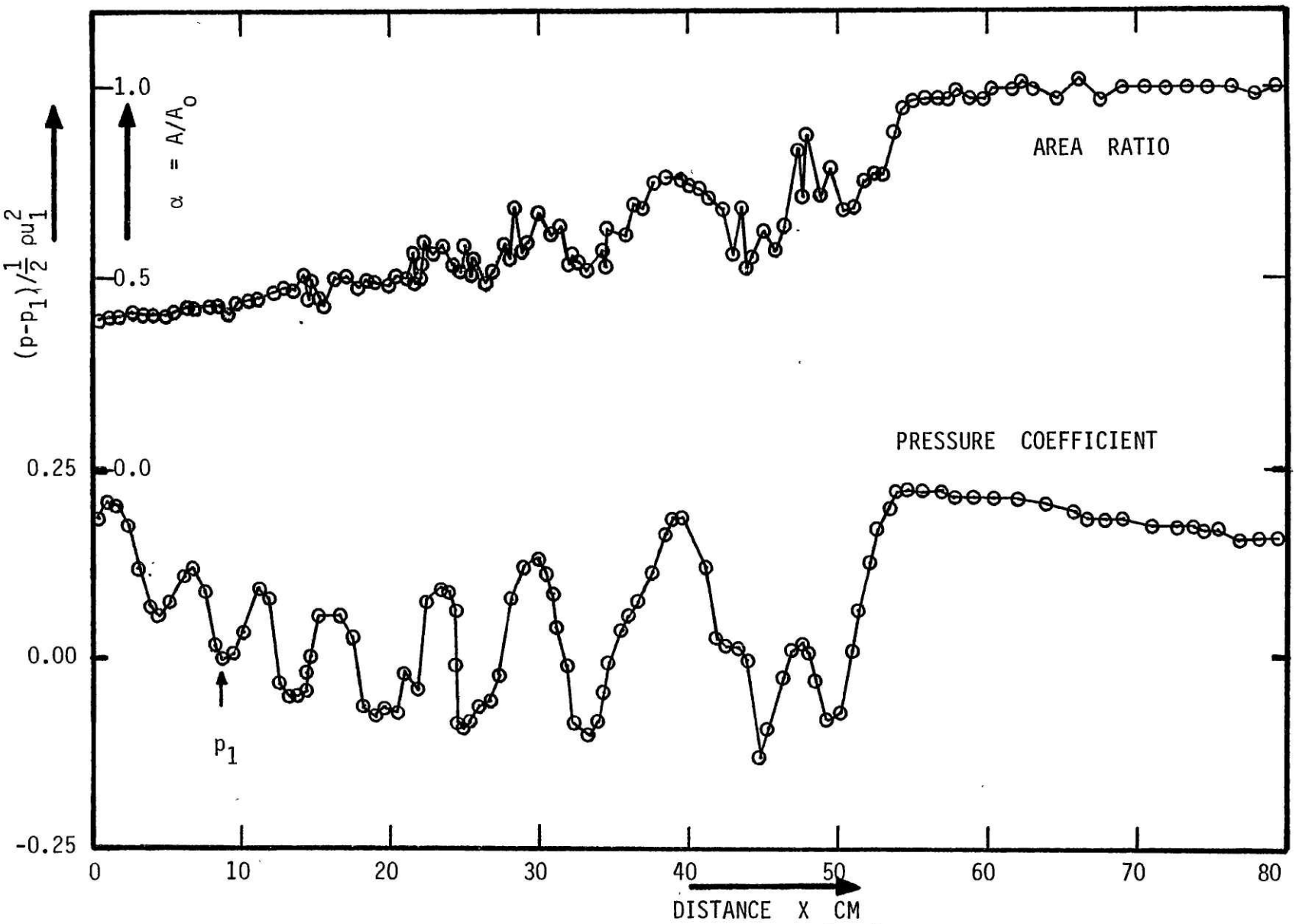

FIG (47): AREA RATIO α AND PRESSURE COEFFICIENT $(p-p_1)/\frac{1}{2}\rho u_1^2$ VS DISTANCE X ALONG THE SHOCK WAVE
Flow Rate = 22.0 Lit/Min; Constriction Area Ratio = 0.378; Inlet Speed Index = 8.47;
Outlet Speed Index = 0.208; Resting Area $A_o = 4.530\ cm^2$.

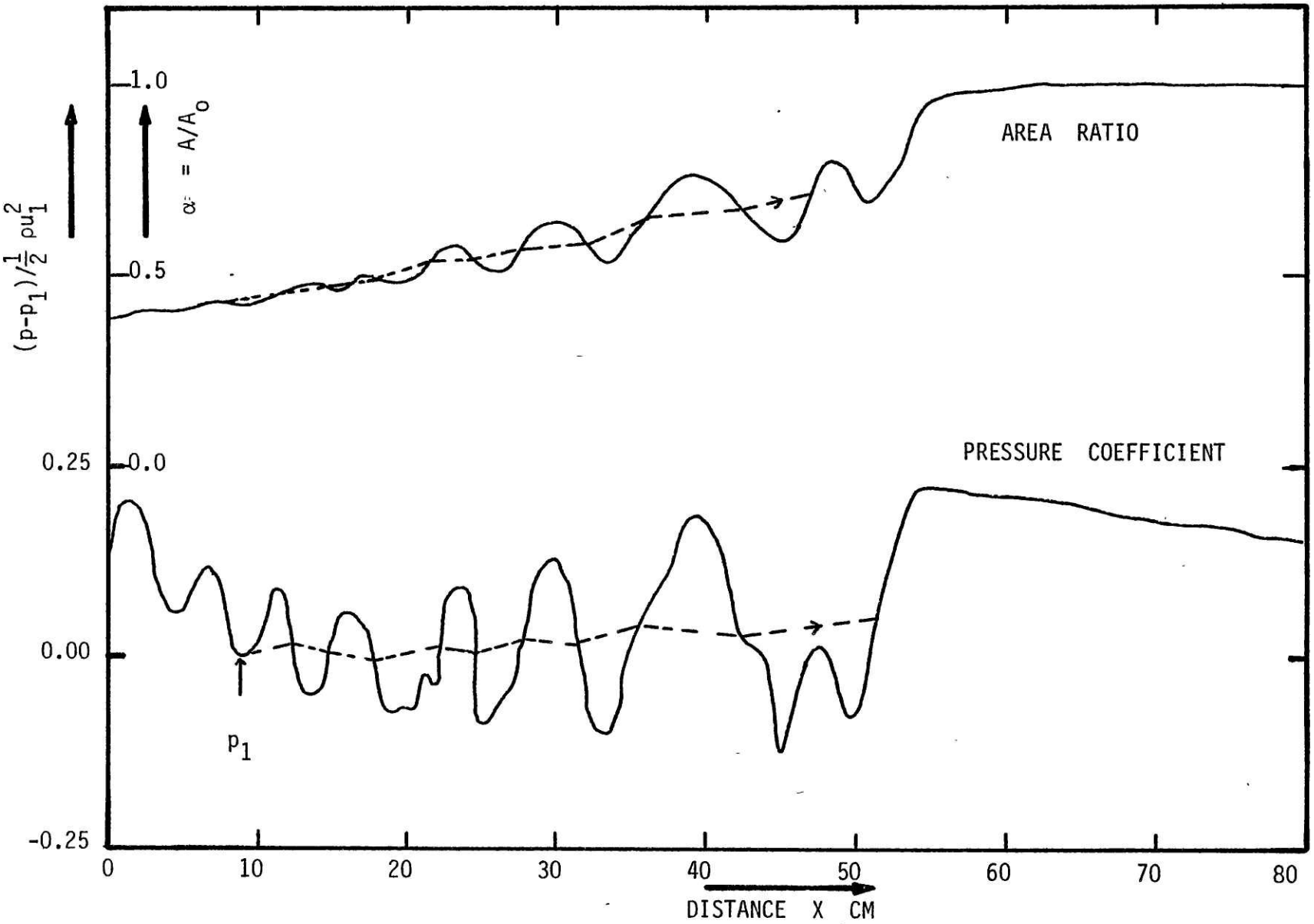

FIG (47s): AREA RATIO α AND PRESSURE COEFFICIENT $(p-p_1)/\frac{1}{2}\rho u_1^2$ VS DISTANCE X ALONG THE SHOCK WAVE
Flow Rate = 22.0 Lit/Min; Constriction Area Ratio = 0.378; Inlet Speed Index = 8.47;
Outlet Speed Index = 0.208; Resting Area A_o = 4.530 cm^2.

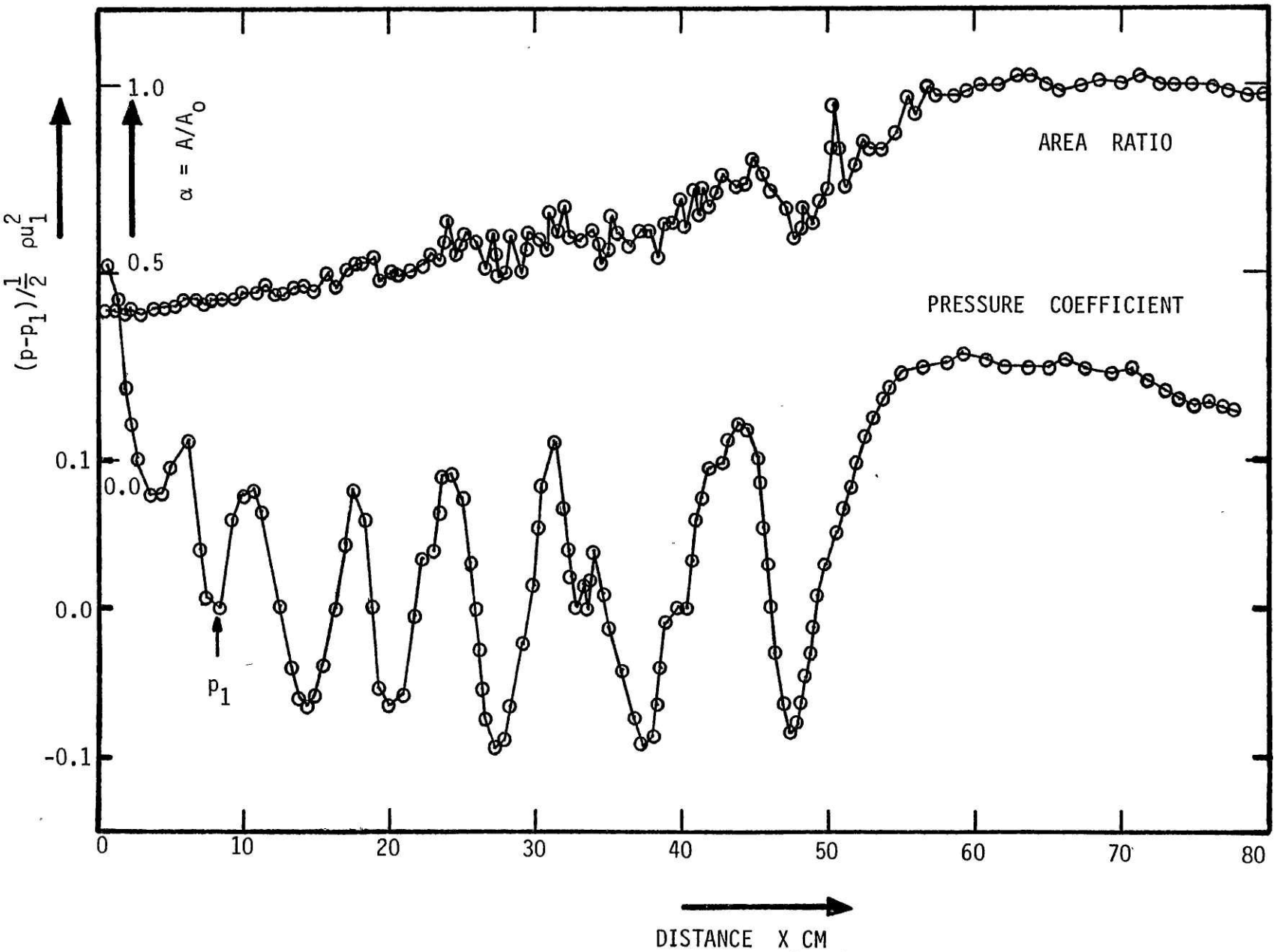

FIG (48): AREA RATIO α AND PRESSURE COEFFICIENT $(p-p_1)/\frac{1}{2}\rho u_1^2$ VS DISTANCE X ALONG THE SHOCK WAVE.
Flow Rate = 20.0 Lit/Min; Constriction Area Ratio = 0.378; Inlet Speed Index = 7.84;
Outlet Speed Index = 0.276; Resting Area $A_o = 4.530\ cm^2$.

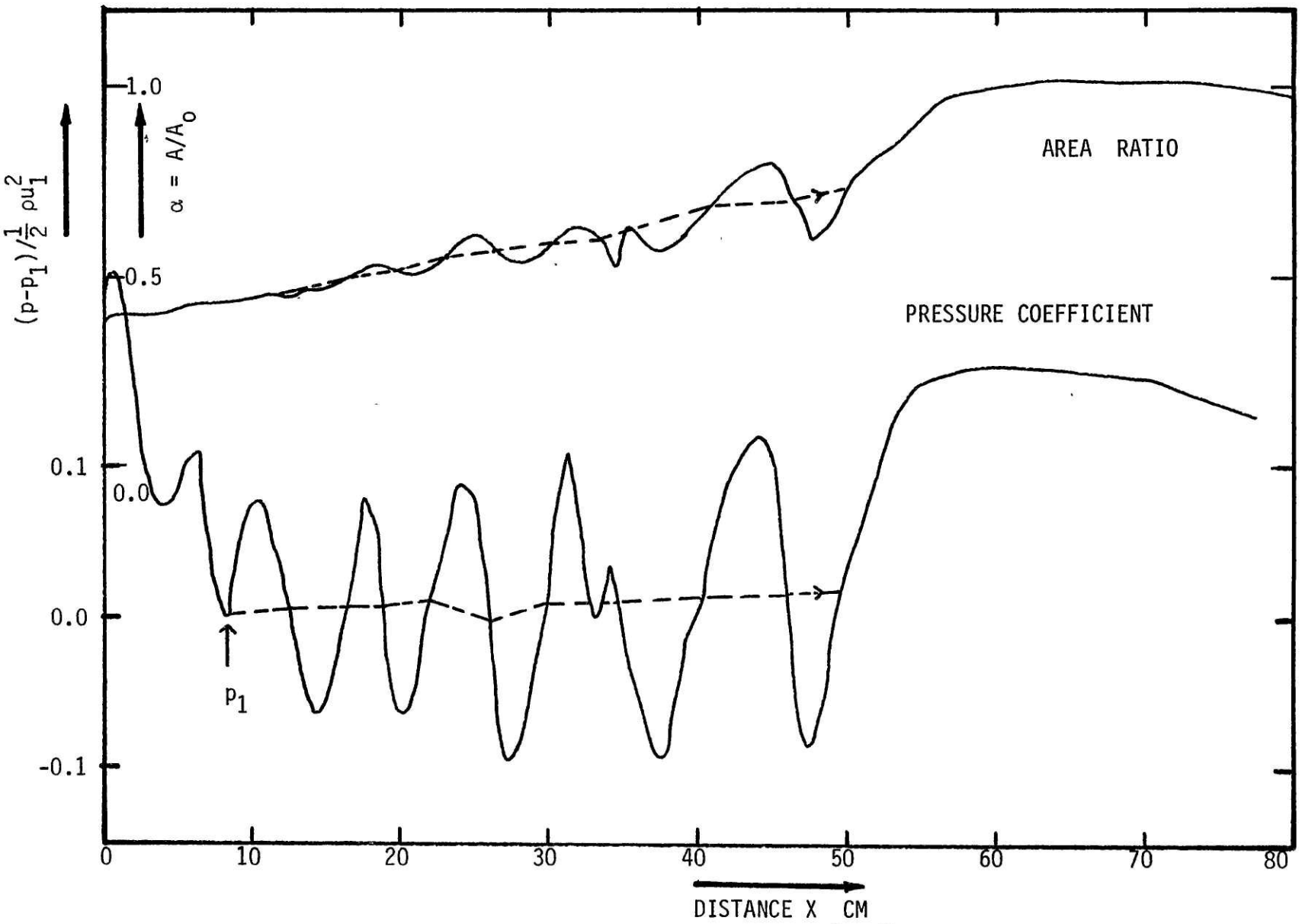

FIG (48s): AREA RATIO α AND PRESSURE COEFFICIENT $(p-p_1)/\frac{1}{2}\rho u_1^2$ VS DISTANCE X ALONG THE SHOCK WAVE
Flow Rate = 20.0 Lit/Min; ConstrictionArea Ratio = 0.378; Inlet Speed Index = 7.84;
Outlet Speed Index = 0.276; Resting Area A_o =m4.530 cm^2.

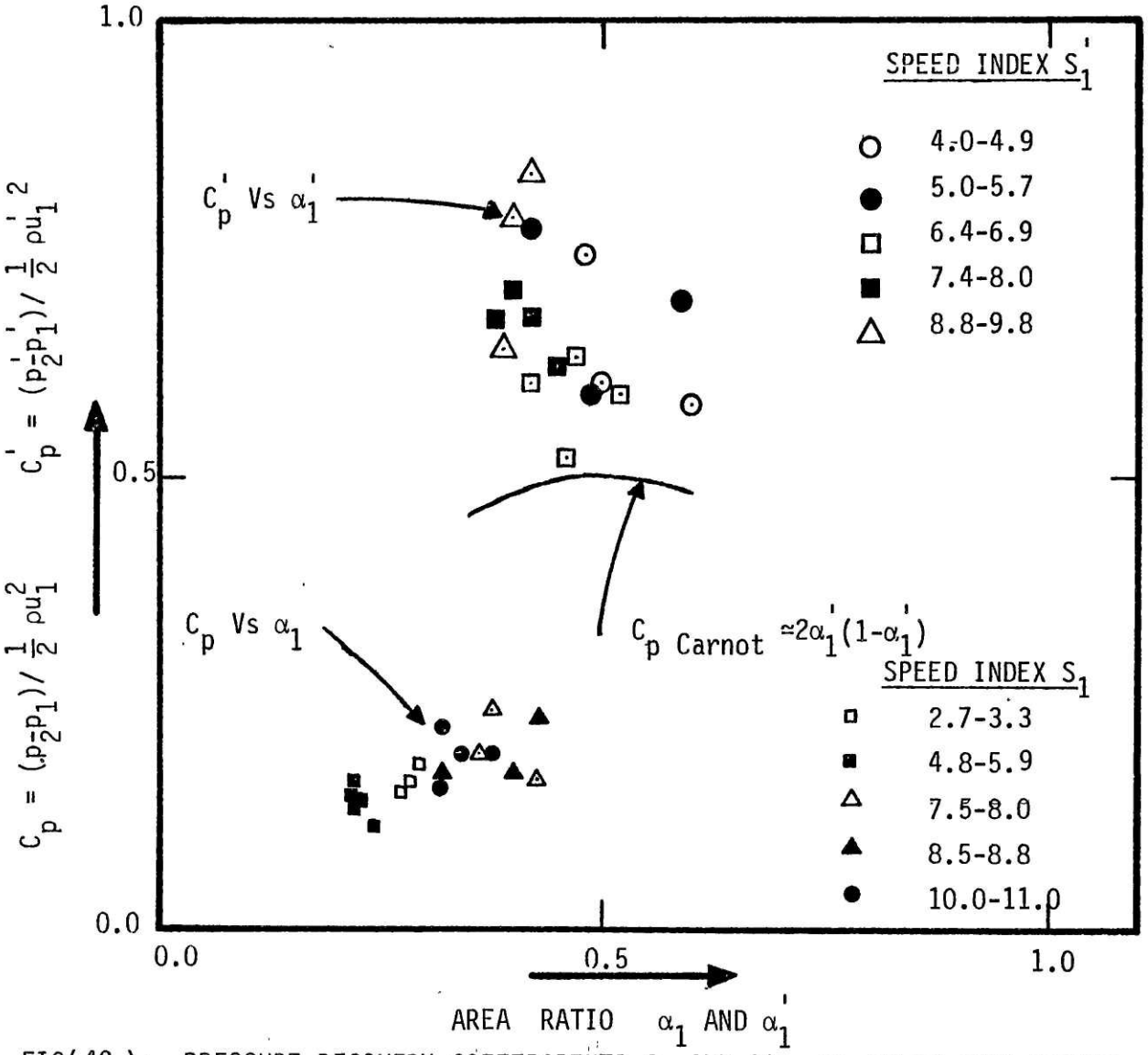

FIG(49): PRESSURE RECOVERY COEFFICIENTS C_p AND C_p' Vs INLET AREA RATIOS α_1 AND α_1'

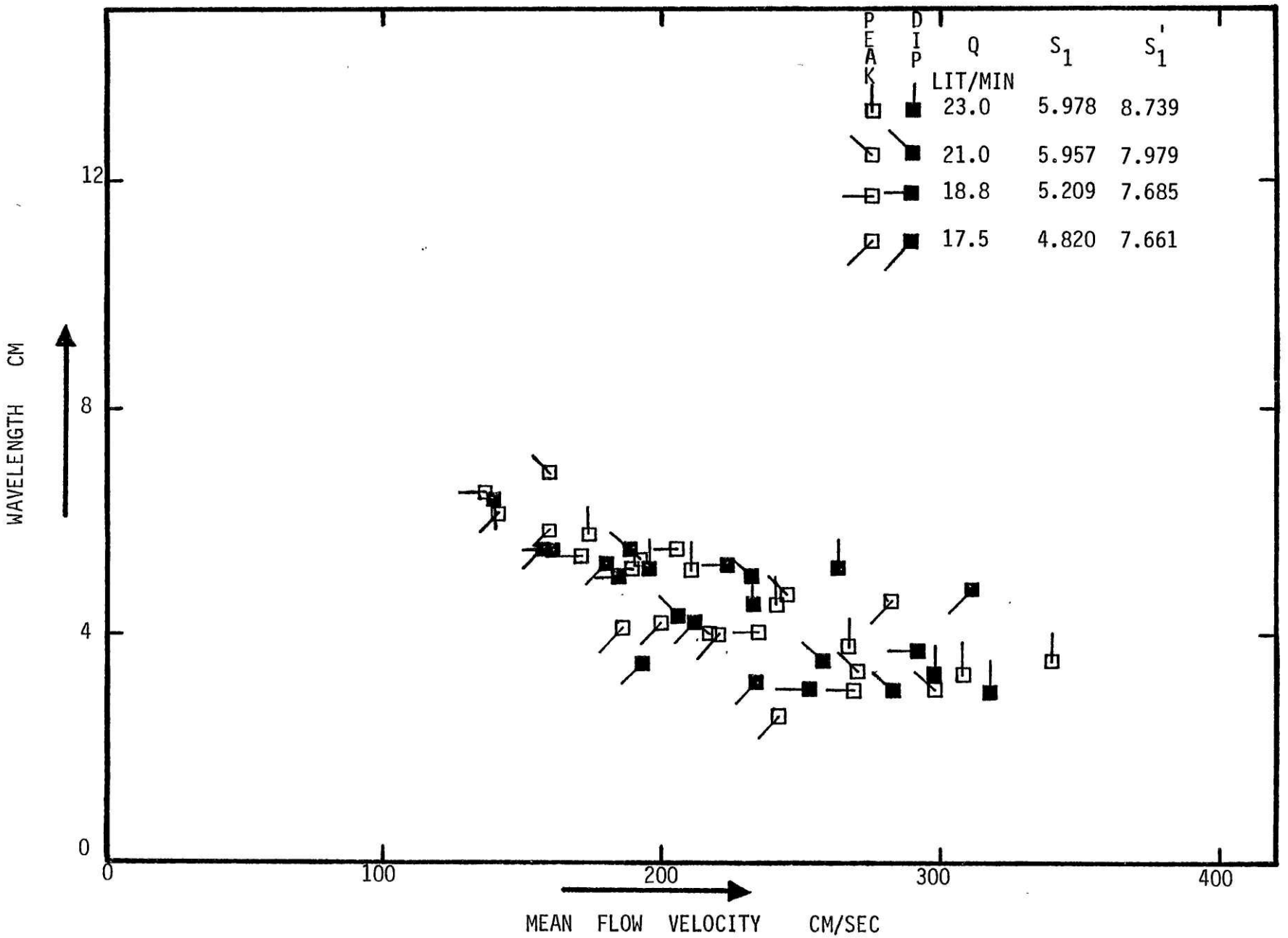

FIG(50): WAVELENGTH OF PRECURSOR WAVES VS MEAN FLOW VELOCITY AT FIXED CONSTRICTION AREA RATIO $\alpha_c = 0.195$

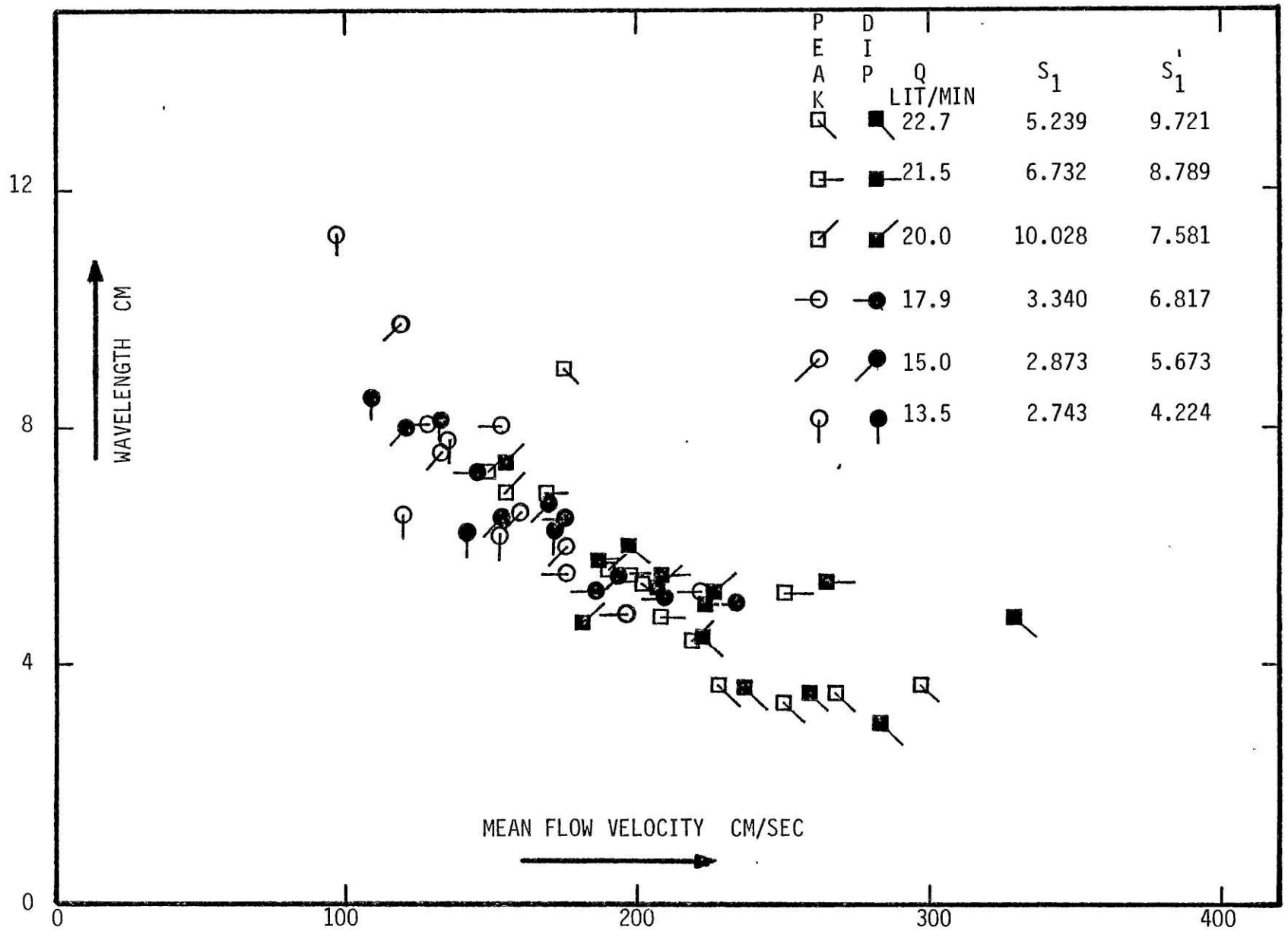

FIG(51): WAVELENGTH OF PRECURSOR WAVES VS MEAN FLOW VELOCITY AT FIXED CONSTRICTION AREA RATIO $\alpha_c \simeq 0.213$

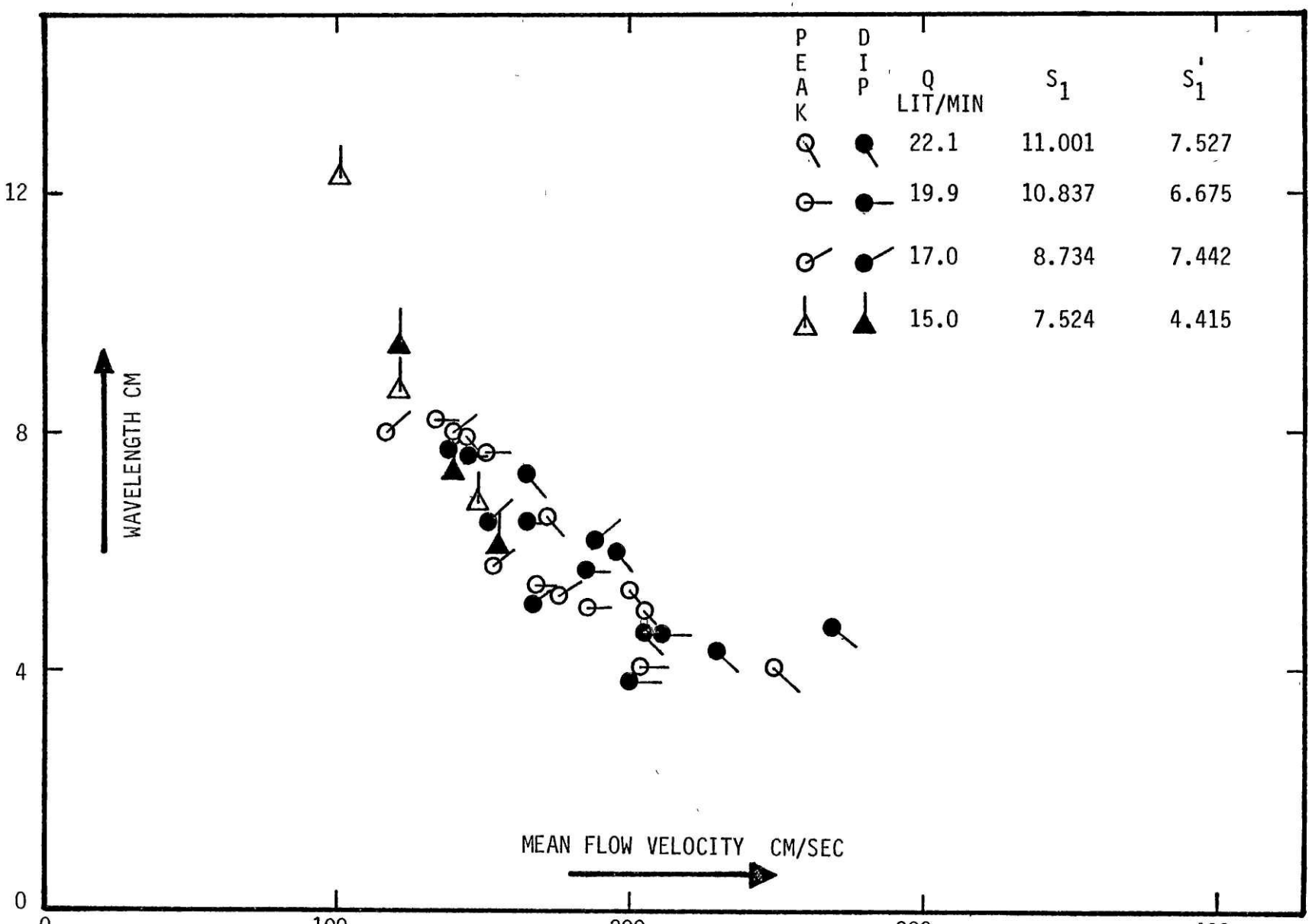

FIG(52): WAVELENGTH OF PRECURSOR WAVES VS MEAN FLOW VELOCITY AT FIXED CONSTRICTION AREA RATIO $\alpha_c \simeq 0.279$

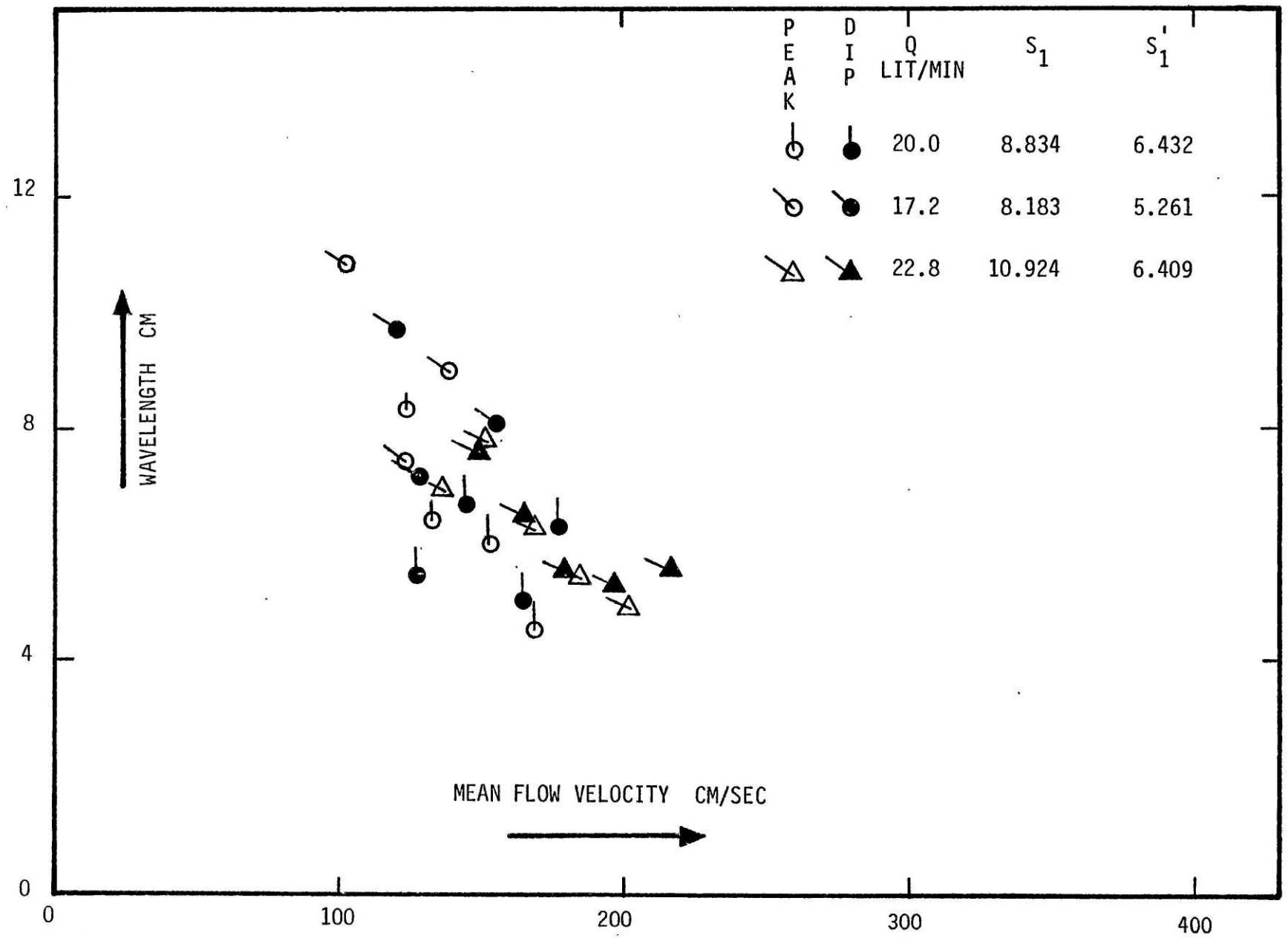

FIG(53): WAVELENGTH OF PRECURSOR WAVES VS MEAN FLOW VELOCITY AT FIXED CONSTRICTION AREA RATIO $\alpha_c \simeq 0.332$

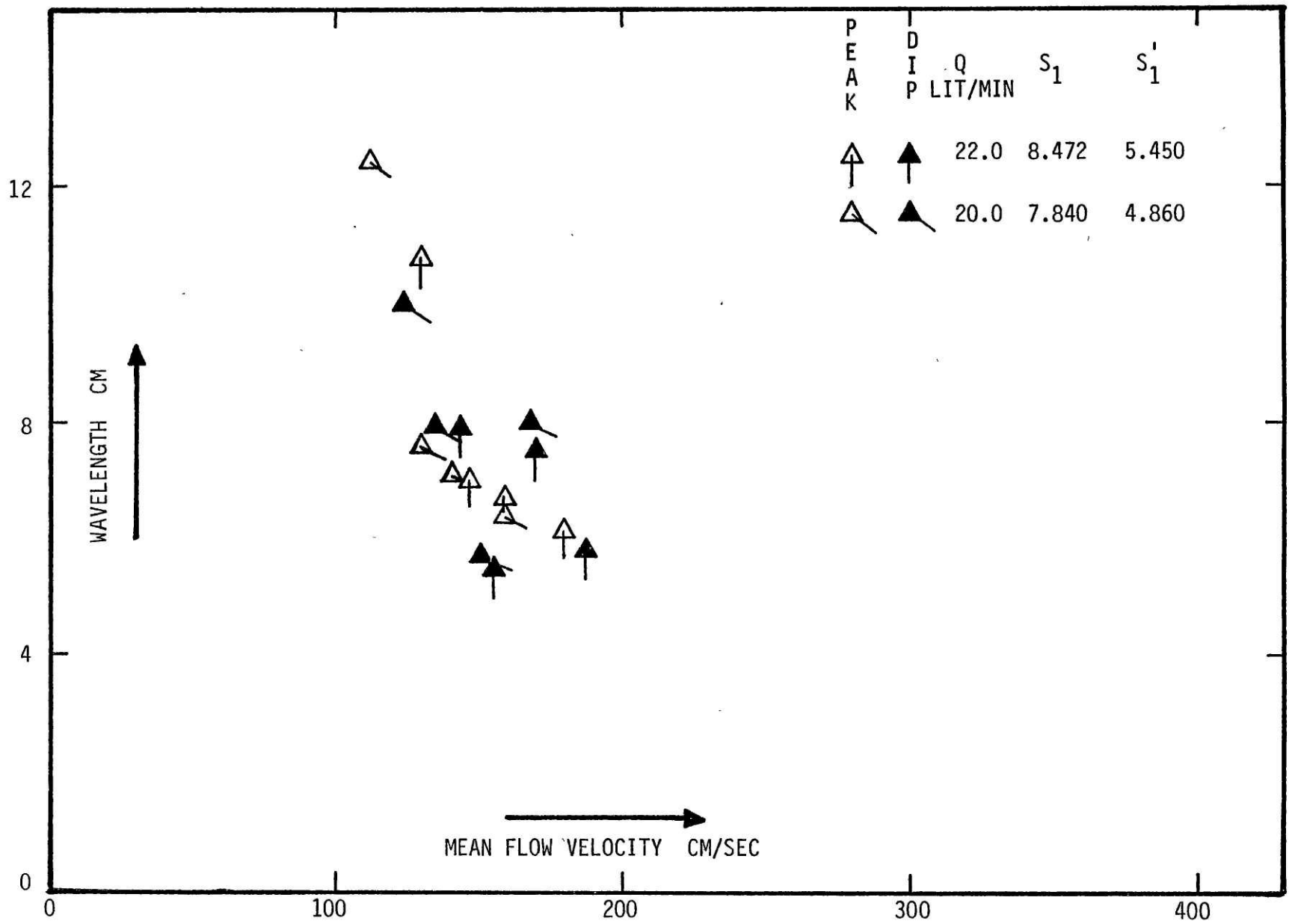

FIG(54): WAVELENGTH OF PRECURSOR WAVES VS MEAN FLOW VELOCITY AT FIXED CONSTRICTION AREA RATIO $\alpha_c \simeq 0.378$

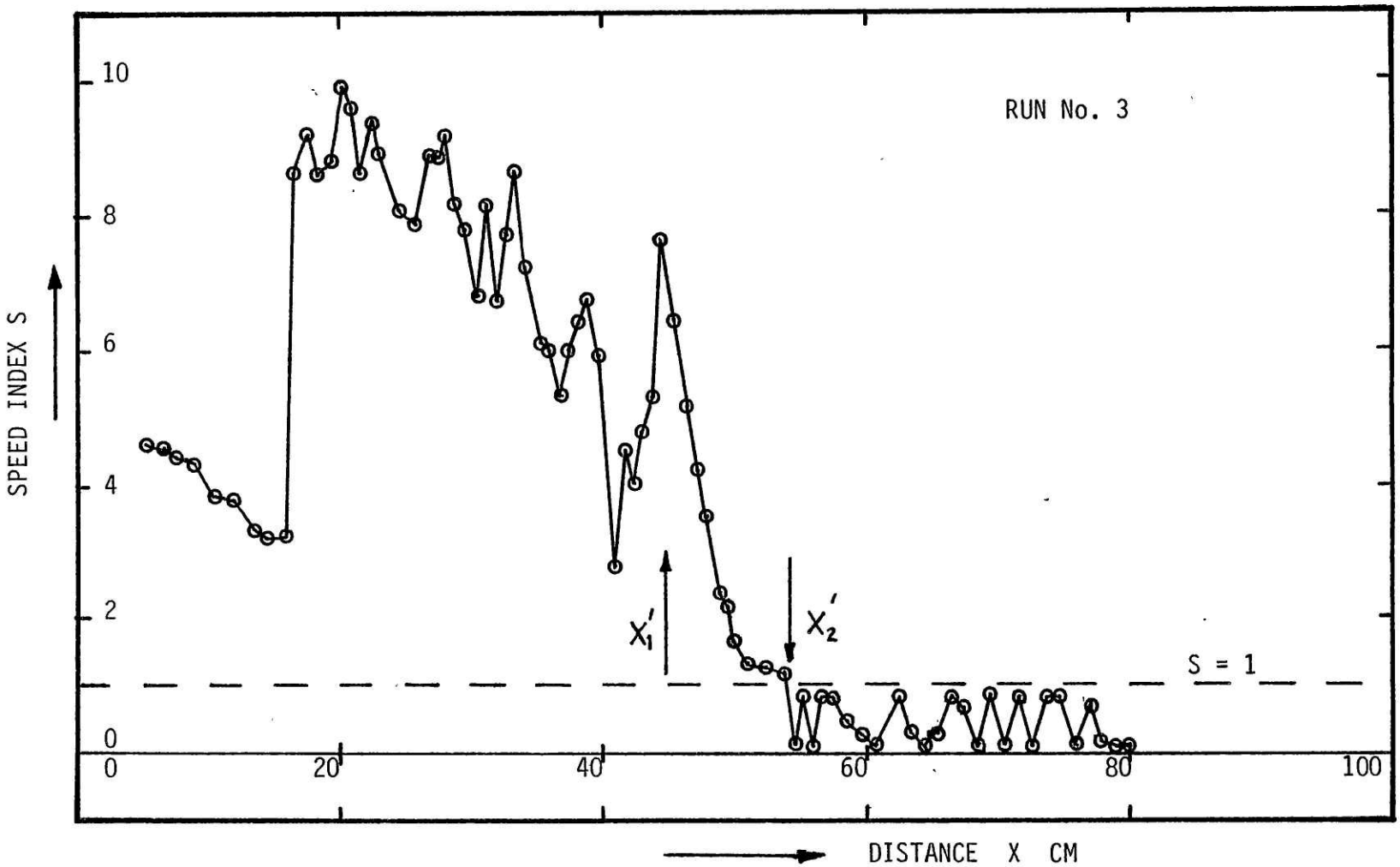

FIG.(55): SPEED INDEX vs DISTANCE FOR RUN NO.3. WAVESPEED OBTAINED FROM TUBE LAW DATA.

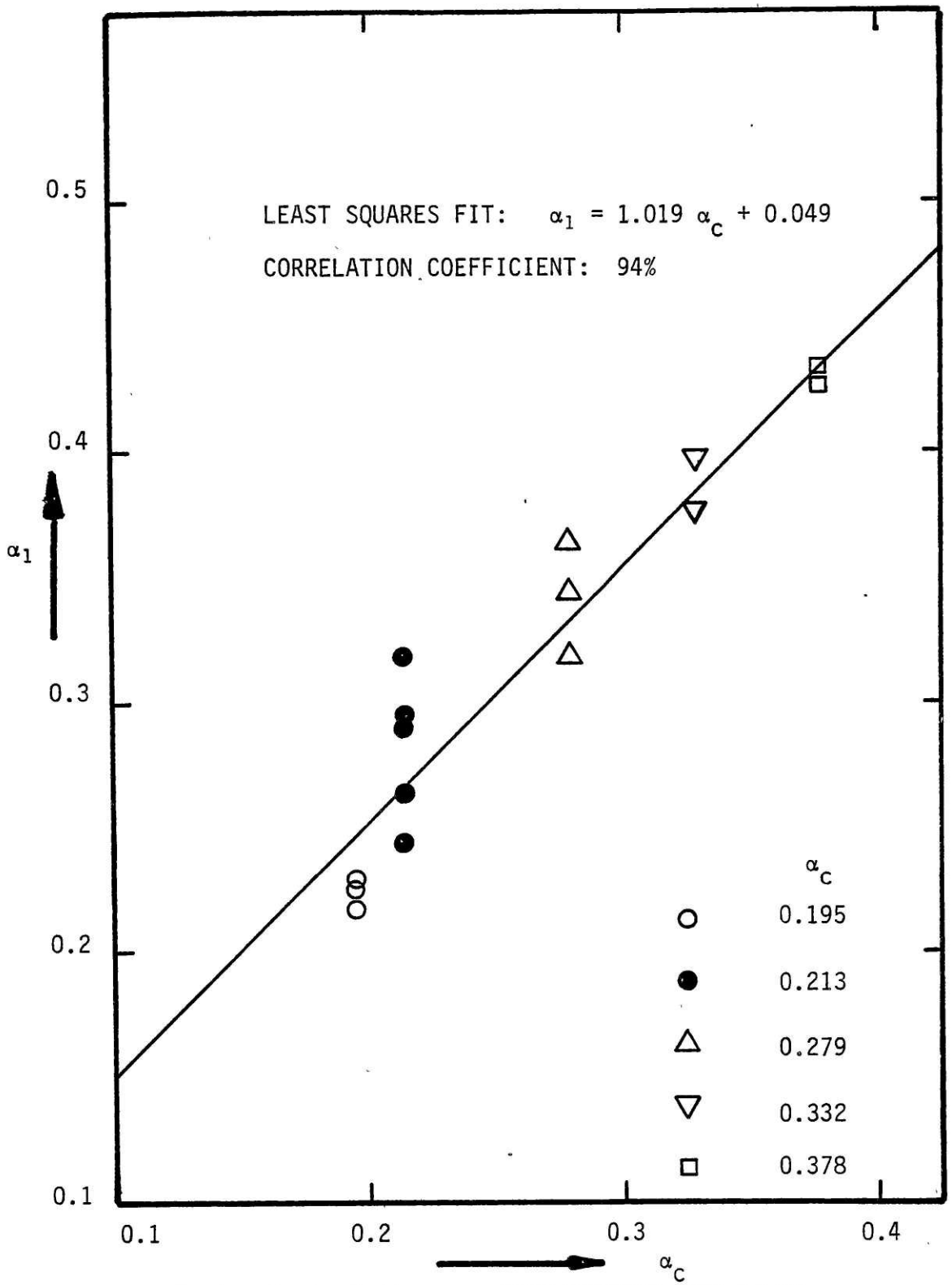

FIG.(56): AREA RATIO α_1 vs CONSTRICTION AREA RATIO α_c.

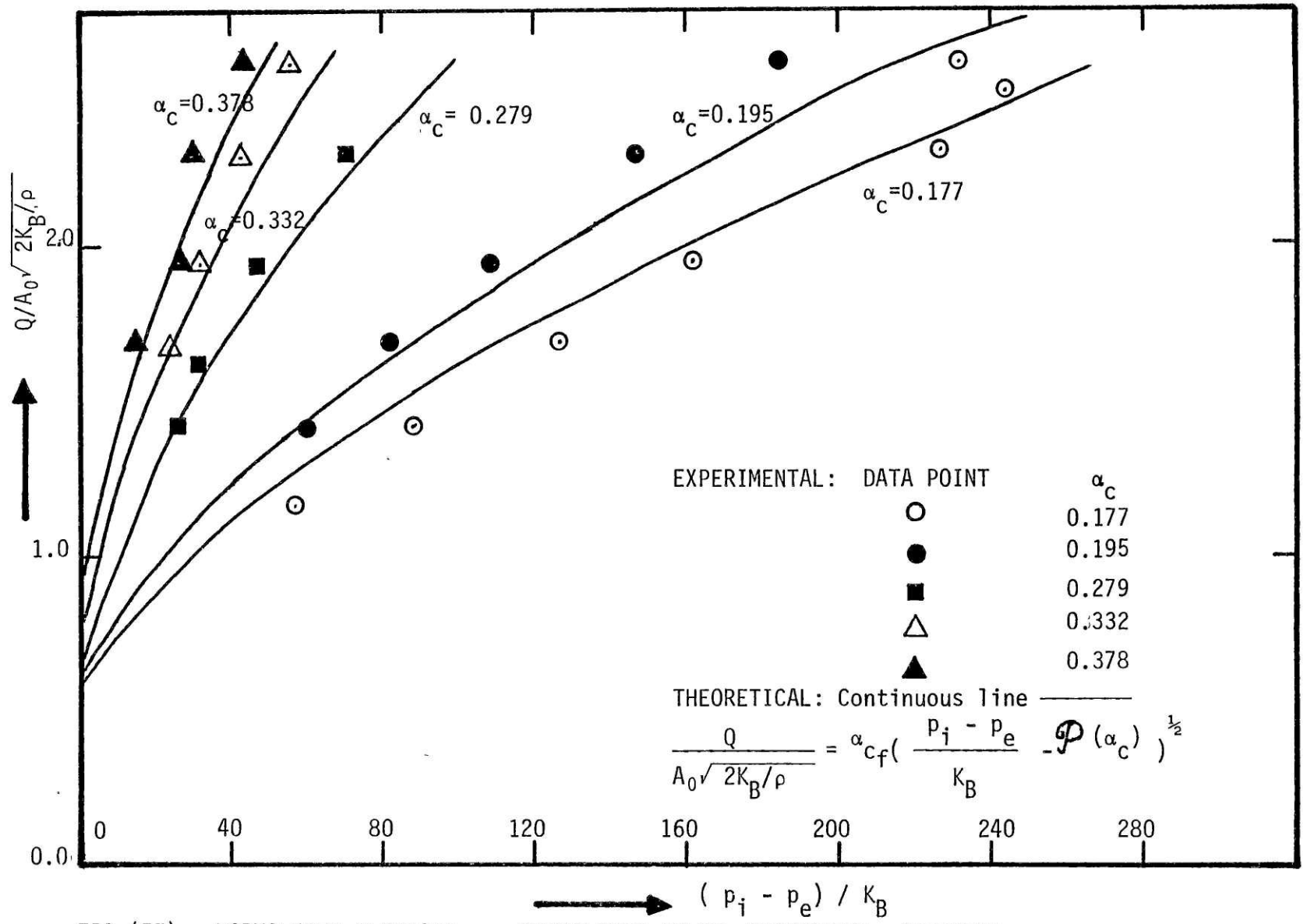

FIG.(57): NORMALIZED FLOWRATE vs NORMALIZED INLET TRANSMURAL PRESSURE.

NOTE : $\mathcal{P}(\alpha_c)$ is the tube law evaluated at α_c.

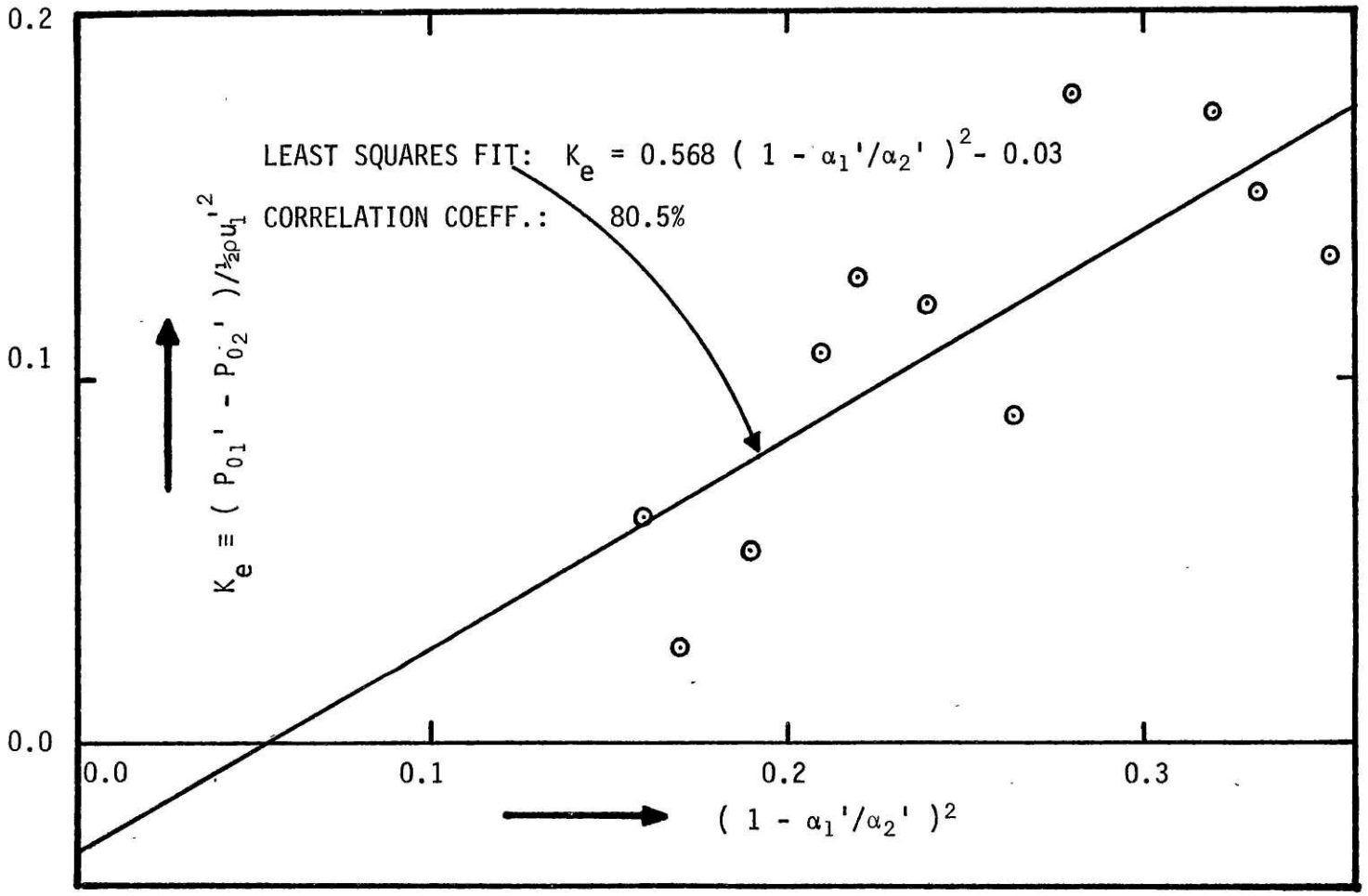

FIG.(58): ACTUAL STAGNATION PRESSURE LOSS K_e ACROSS SHOCK Vs CARNOT STAGNATION PRESSURE LOSS $(\ 1 - \alpha_1'/\alpha_2'\ )^2$.

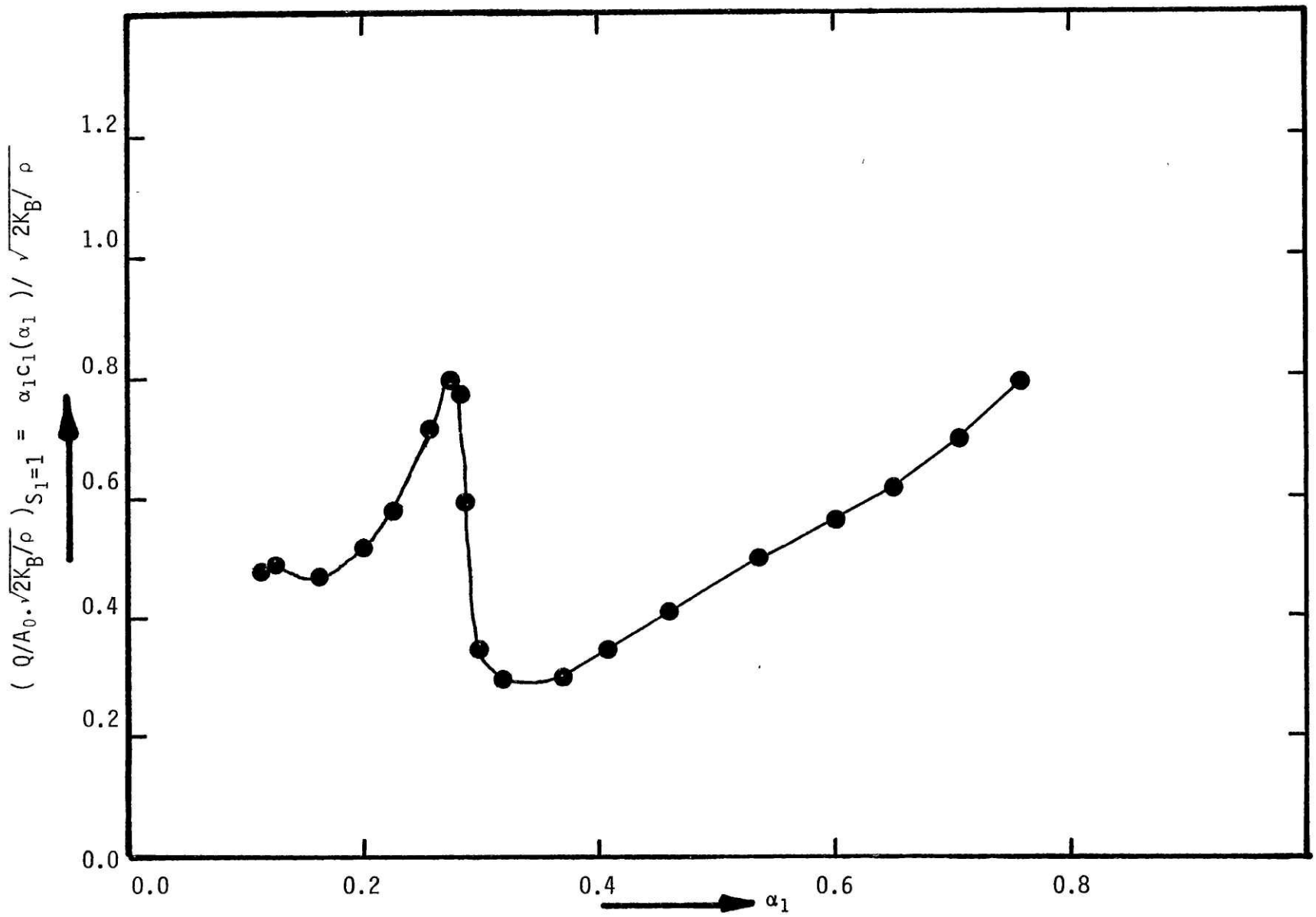

FIG.(59): VARIATION OF NON-DIMENSIONAL FLOWRATE WITH CONSTRICTION EXIT AREA RATIO FOR SONIC CONDITIONS AT CONSTRICTION EXIT. CALCULATED FROM EXPERIMENTAL TUBE LAW DATA.

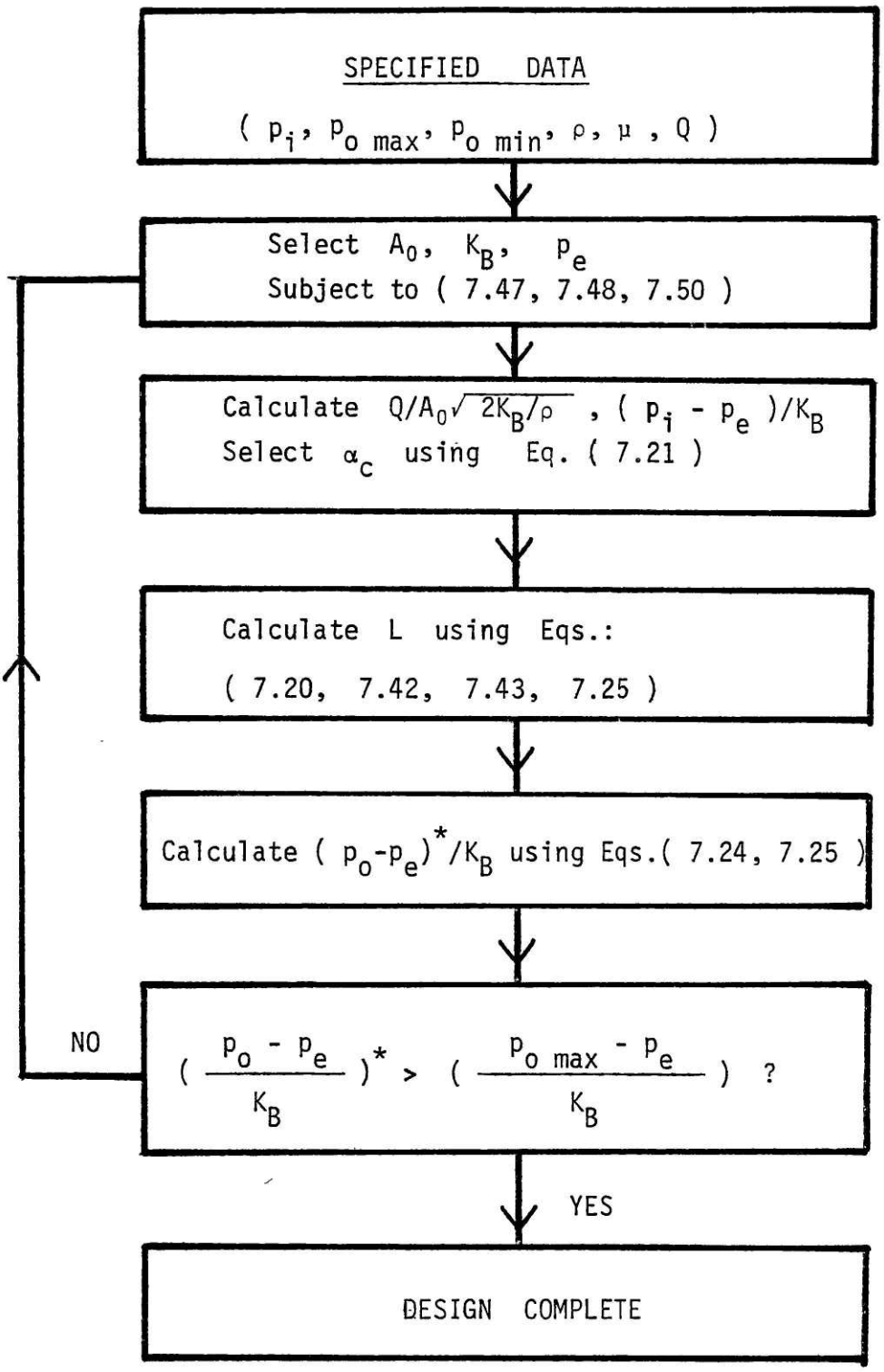

FIG (60): BLOCK DIAGRAM FOR COLLAPSIBLE TUBE FLOW REGULATOR DESIGN.

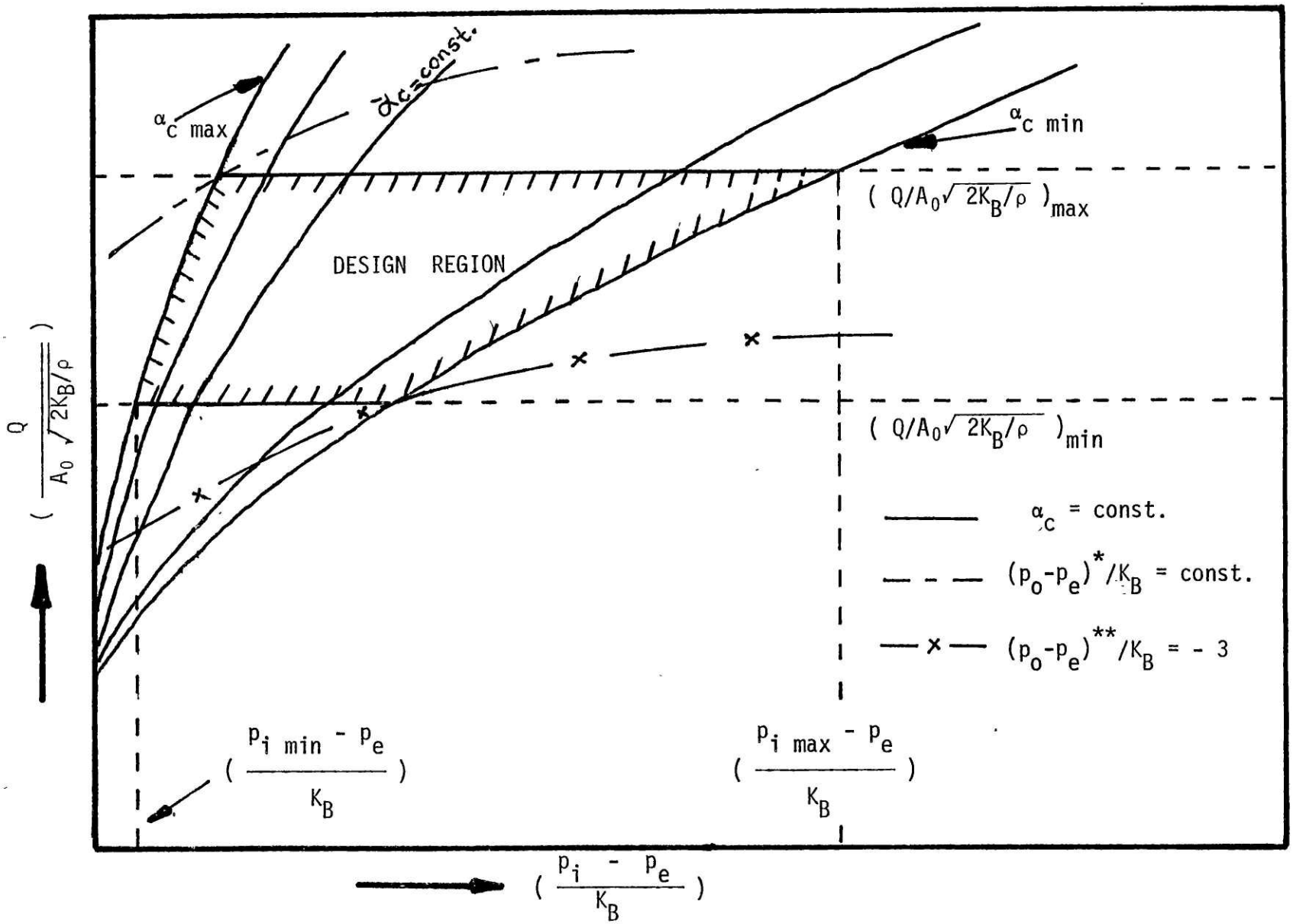

FIG. (61): DESIGN REGION FOR A FLOW REGULATOR REQUIRED TO OPERATE OVER A RANGE OF FLOWRATES AND INLET PRESSURES.

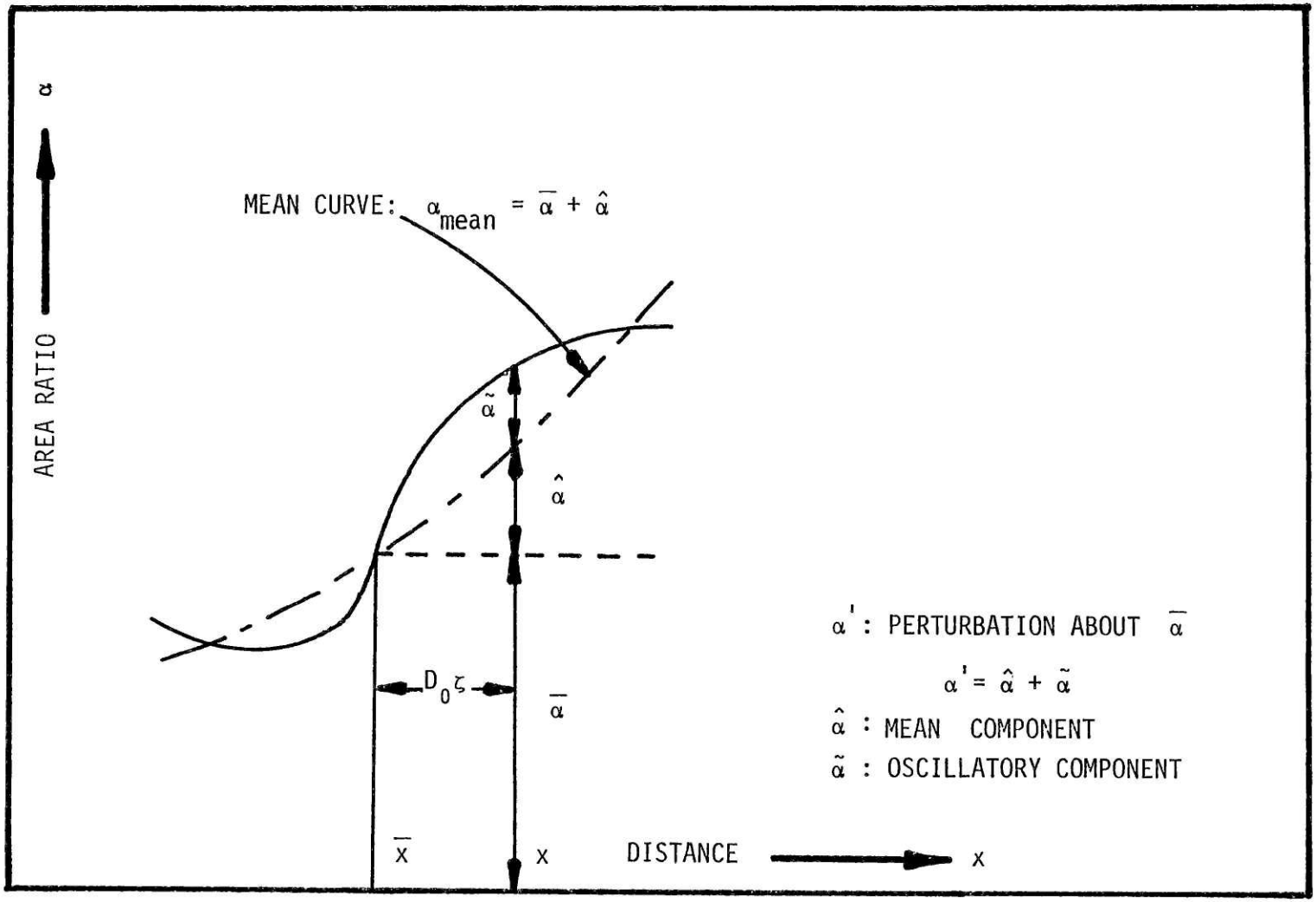

FIG.(62): SPLITTING UP OF THE PERTURBATION QUANTITY α' INTO A MEAN COMPONENT $\hat{\alpha}$ AND AN OSCILLATORY COMPONENT $\tilde{\alpha}$.

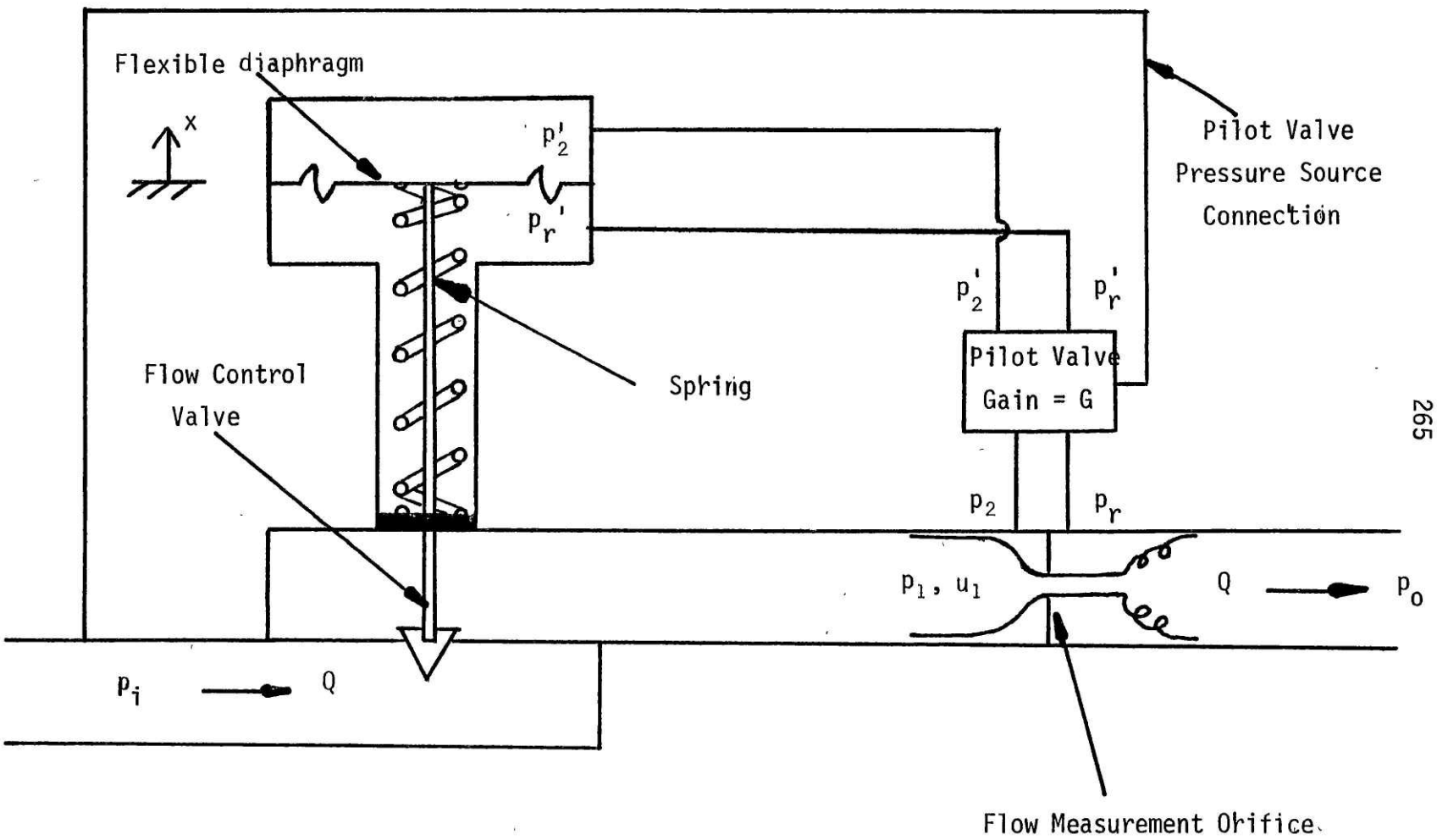

FIG.(63): STANDARD DIAPHRAGM OPERATED FLOW RATE REGULATOR.

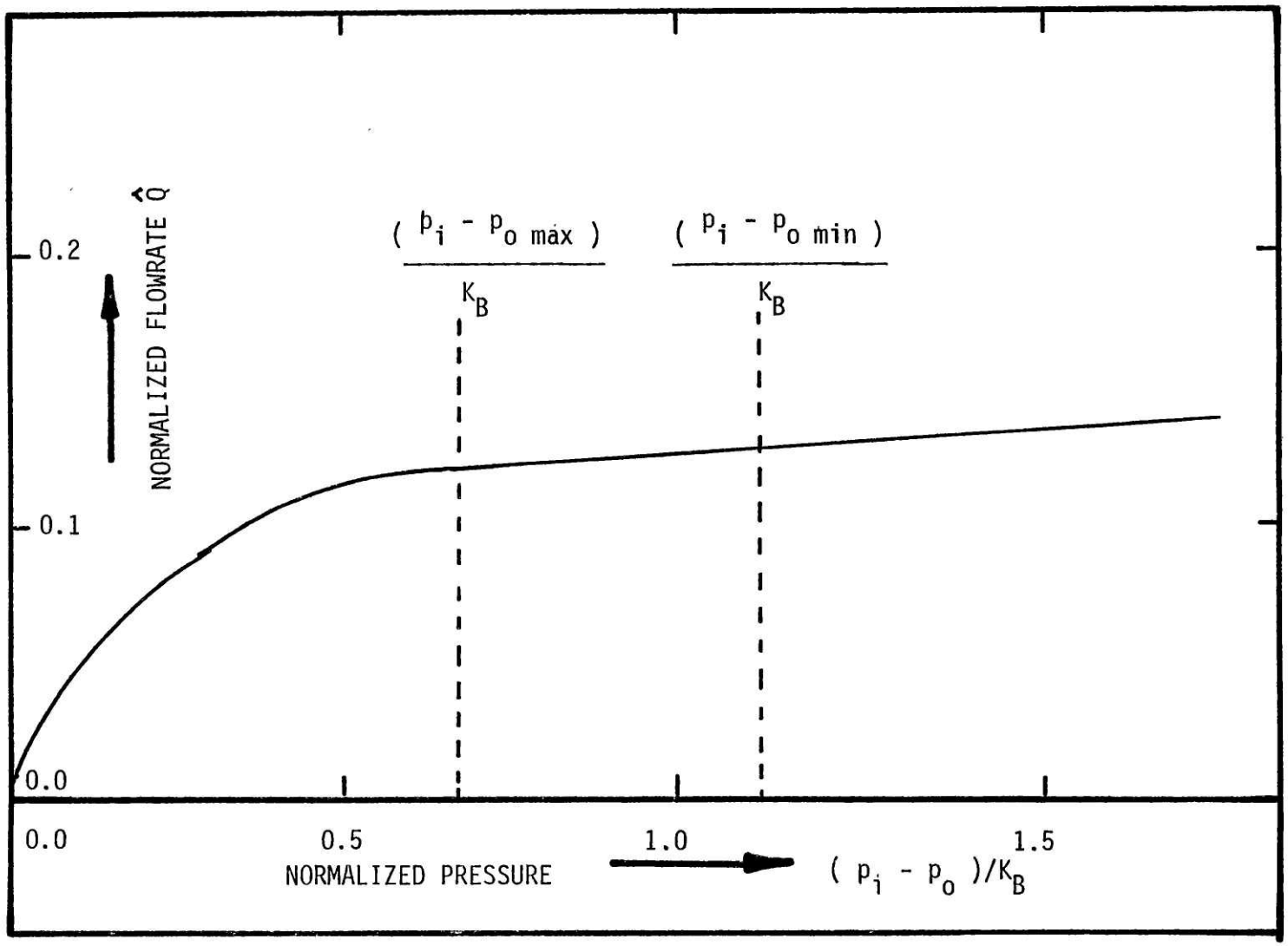

FIG(64): REGULATION CHARACTERISTIC FOR DIAPHRAGM TYPE STANDARD FLOW REGULATOR.

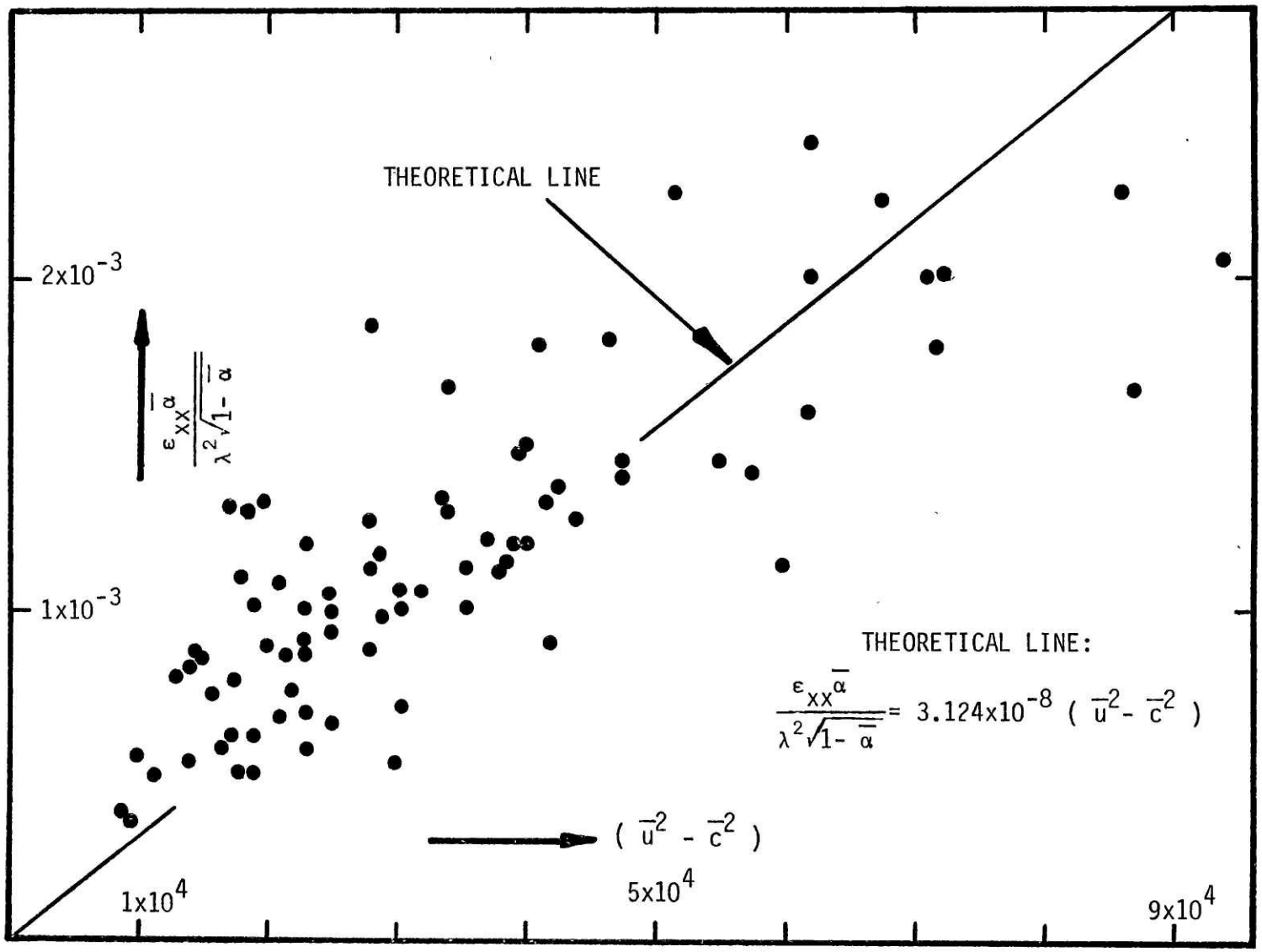

FIG (65): Dispersion relationship for waves in precursor wavetrain.